Decadal variability of the extratropical response to the Madden-Julian Oscillation

A thesis submitted to the School of Mathematics at the University of East Anglia in partial fulfilment of the requirements for the degree of Doctor of Philosophy

Daniel Thomas Skinner

September 2023

Abstract

The Madden—Julian Oscillation (MJO) is the leading mode of intraseasonal variability in the tropics. Though it is a tropical phenomenon, the MJO also excites a response in the extratropics, producing teleconnection patterns. These teleconnections impact on the weather and climate of the extratropics, providing a valuable source of predictability. Whilst MJO teleconnection patterns are predictable, they can be modulated by external factors. The extratropical response to the MJO is sensitive to changes in both MJO forcing and the extratropical background circulation, which in turn can be modulated by various modes of climatic variability. The question of if, and how, the extratropical response to the MJO varies on decadal time scales is yet to be answered.

Here the ability of coupled climate models to simulate MJO teleconnections is assessed, before both reanalysis and model data are used to examine the decadal variability of the extratropical response to the MJO. We find that climate models can capture some of response to the MJO, but cannot represent all of the processes underpinning MJO teleconnections. Evidence is then provided for decadal scale variability of the extratropical response to the MJO over the past 50 years. Finally, a coupled climate model is used to show that both Atlantic Multidecadal Variability (AMV) and the Pacific Decadal Oscillation (PDO) are able to modulate MJO teleconnections on decadal time scales.

Table of Contents

List of Figures

List of Tables

Glossary of Acronyms and Abbreviations

Variables

ψ**200,** ψ**250** . . . . . 200-, 250-hPa streamfunction

K_s . . . . . Stationary Rossby Wavenumber

T**850** . . . . . 850-hPa temperature

U**200,** U**250,** U**850** . . . . . 200-, 250-, 850-hPa zonal wind

Z**50,** Z**100,** Z**500** . . . . . 50-, 100-, 500-hPa geopotential height

Acronyms and abbreviations

AL . . . . . **A**leutian **L**ow

AMO . . . . . **A**tlantic **M**ultidecadal **O**scillation *(See AMV)*

AMV . . . . . **A**tlantic **M**ultidecadal **V**ariability

AO . . . . . **A**rctic **O**scillation *(See NAM)*

AWB . . . . . **A**nticyclonic **W**ave **B**reaking

CMAP . . . . . **C**PC **M**erged **A**nalysis of **P**recipitation

CMIP . . . . . **C**oupled **M**odel **I**ntercomparison **P**roject

CWB . . . . . **C**yclonic **W**ave **B**reaking

DECK . . . . . **D**iagnostic, **E**valuation and **C**haracterization of **K**lima

ENSO . . . . . **E**l **N**iño–**S**outhern **O**scillation

EOF . . . . . **E**mpirical **O**rthogonal **F**unction

EQBO . . . . . **E**asterly **Q**uasi-**B**iennial **O**scillation

ERA . . . . . **E**CMWF **R**e-**A**nalysis

ESM . . . . . **E**arth **S**ystem **M**odel

GCM . . . . . **G**eneral **C**irculation **M**odel

HadGEM . . . . Met Office **Had**ley Centre **G**lobal **E**nvironment **M**odel

HadISST . . . . . Met Office **Had**ley Centre Sea **I**ce and **S**ea **S**urface **T**emperature

IO . . . . . **I**ndian **O**cean

IOD . . . . . **I**ndian **O**cean **D**ipole

KOE . . . . . **K**uroshio–**O**yashio **E**xtension

MC . . . . . **M**aritime **C**ontinent

MJO . . . . . **M**adden–**J**ulian **O**scillation

MSLP . . . . . **M**ean **S**ea **L**evel **P**ressure

NA . . . . . **N**orth **A**tlantic

NAM . . . . . **N**orthern **A**nnular **M**ode

NAO . . . . . **N**orth **A**tlantic **O**scillation

NH . . . . . **N**orthern **H**emisphere

NOAA . . . . . **N**ational **O**ceanic and **A**tmospheric **A**dministration

NP . . . . . **N**orth **P**acific

OLR . . . . . **O**utgoing **L**ongwave **R**adiation

PDO . . . . . **P**acific **D**ecadal **O**scillation

PDV . . . . . **P**acific **D**ecadal **V**ariability *(See PDO)*

piControl . . . . . **P**re-**i**ndustrial **Control** simulation

PNA . . . . . **P**acific–**N**orth **A**merican Pattern

QBO . . . . . **Q**uasi-**B**iennial **O**scillation

RMM . . . . . **R**ealtime **M**ultivariate MJO Index

RWS . . . . . **R**ossby **W**ave **S**ource

S2S . . . . . **S**ubseasonal-**to**-**S**easonal

SACZ . . . . . **S**outh **A**tlantic **C**onvergence **Z**one

SH . . . . . **S**outhern **H**emisphere

SPV . . . . . **S**tratospheric **P**olar **V**ortex

SST . . . . . **S**ea **S**urface **T**emperature

SSW . . . . . **S**udden **S**tratospheric **W**arming

TRMM . . . . . **T**ropical **R**ainfall **M**easuring **M**ission

UKESM . . . . . **UK E**arth **S**ystem **M**odel

WCRP . . . . . **W**orld **C**limate **R**esearch **P**rogramme

WQBO . . . . . **W**esterly **Q**uasi-**B**iennial **O**scillation

List of Incorporated works

Some of the work presented in this thesis has been published in academic journals.

- Chapter 2 is based on Skinner et al. (2022) – 'North Atlantic Oscillation response to the Madden–Julian Oscillation in a coupled climate model'.
- Chapter 3 is based on Skinner et al. (2023) – 'Decadal variability of the extratropical response to the Madden–Julian Oscillation'.

Software

Data analysis and plotting used the following Python packages:

- Matplotlib: A 2D graphics environment (Hunter, 2007)
- Cartopy: a cartographic python library with a matplotlib interface (Met Office, 2016).
- Iris: A Python package for Earth science data, version 2.4.0 (Met Office, 2020).
- Windspharm: A High-Level Library for Global Wind Field Computations Using Spherical Harmonics (Dawson, 2016).
- pandas: Python Data Analysis Library (McKinney, 2010; The pandas development team, 2020).
- cmocean: Beautiful colormaps for oceanography (Thyng et al., 2016).
- cmcrameri: Scientific colour maps (Crameri, 2018*a*,*b*; Crameri et al., 2020).

The research in this thesis was carried out on the High Performance Computing Cluster supported by the Research and Specialist Computing Support service at the University of East Anglia.

This work used JASMIN, the UK's collaborative data analysis environment Lawrence et al. (2013). www.jasmin.ac.uk

Data availability

All data used in this thesis is publicly available at the time of writing.

The following reanalysis data have been used:

- ERA-interim reanalysis – Dee et al. (2011); European Centre for Medium-Range Weather Forecasts (2011)
- ERA5 reanalysis – Hersbach et al. (2018, 2020)
- NOAA OLR interpolated dataset – Liebmann and Smith (1996)
- HadISST reanalysis – Met Office Hadley Centre (2022); Rayner et al. (2003)
- CMAP reanalysis – Xie and Arkin (1997)

Some figures adapted from other sources also reference the TRMM precipitation reanalysis (Tropical Rainfall Measuring Mission, 2011).

Climate models (Table 2.1) and climate indices (Appendix A) used are cited within the text.

Structure of this thesis

This thesis begins with a general introduction (Chapter 1), which gives an overview of the subject and the literature to date. Here you will also find motivation for this study, and the specific research questions to be answered.

The main results of this work are presented in Chapters 2–4. Each of these chapters are designed to be self-contained, with its own introduction, methodology and conclusions. There may, therefore, be some repetition of material between chapter introductions/conclusions and the overall introduction/conclusion. The hope, however, is that this will aid readability.

Finally, a summary and synthesis of the results presented in the three previous chapters is given in Chapter 5. Here, the research questions presented in Chapter 1 are answered and potential avenues for future work are identified.

Acronyms and abbreviations are used throughout for the purposes of readability. A full glossary of acronyms can be found on page 23.

Endnotes are given at the end of each chapter and are marked in the text by numbered superscripts, like this[1].

Acknowledgements

I could fill an entire thesis thanking everyone who has supported me over the past few years and has made this PhD possible. There are a handful of people, though, who deserve special recognition.

Firstly, I would like to thank the Faculty of Science at UEA for funding this PhD project. I would like to thank them also, along with the ARIES Doctoral Training Partnership, for the training I have received as part of my studies.

For the past seven years I have been a part of the School of Mathematics at UEA. It is thanks to the teaching, support and guidance that I have received from the School that I was able to begin, and now finish, this PhD journey.

I have absolutely loved my time as a PhD student, and that is mostly down to my friends and colleagues. Thank you to all of my peers in both Mathematics and Environmental Science for making the experience so enjoyable. In particular, I would like to thank Danny and Beth – I couldn't have asked for better friends to share my PhD with.

My family have been a huge support throughout my studies and along the road to getting here. Thank you to my parents for guiding me and making sure I had the opportunity to follow my dream. Thank you to my grandparents who have always given their support and helped me to believe in my abilities. Thank you to my sister, Kathryn, for all of the laughs. And thank you to my brother, Ben, for keeping me company through sleepless nights and generally keeping me sane!

A PhD can be all-consuming and without an escape can quickly become overwhelming. So, thank you to Maple, Tabasco, Sesame, Treacle, and Custard, for being my escape and for loving me unconditionally.

This PhD would not have been possible without the support of my two supervisors, Adrian and Dave. Their guidance and patience has made me the researcher that I am today and will continue to be an inspiration to me throughout my career.

Finally, thank you to Meg, who has stood by me throughout the whole PhD process. She has been there to celebrate my successes and pick me up when I have fallen, but most importantly, she never stopped believing in me.

This thesis is dedicated to those who have made this journey possible, but who were not able to finish it with me.

For Kimchi, Panko, Noodle, Nori, Miso, and Biscuit – your unconditional love kept me sane when times were tough.
For Nannie – your encouragement and prayers helped me to believe this was possible and reassured me when the path ahead was unclear.
And for Grandad, my biggest cheerleader and my inspiration – you knew what I was capable of long before I did, and inspired me to fulfil that vision. It looks like I might finally be Dr Dan, just as you always said!

Decadal variability of the extratropical response to the Madden–Julian Oscillation

Chapter 1

Introduction

1.1 The Madden–Julian Oscillation

The Madden–Julian Oscillation (MJO; Jiang et al., 2020; Lin, 2022; Madden and Julian, 1971, 1972; Zhang, 2005; Zhang et al., 2020) is the leading mode of intraseasonal variability in the tropics. Through its teleconnections, the MJO modulates atmospheric variability around the world (Section 1.2; Cassou, 2008; Lau and Waliser, 2012; Lin, 2022; Lin et al., 2009, 2010; Matthews et al., 2004; Matthews and Meredith, 2004; Mori and Watanabe, 2008; Seo and Lee, 2017; Stan et al., 2017; Tseng et al., 2020*a*,*b*), and it is therefore a key source of predictability for numerical weather prediction and climate modelling (Kent et al., 2022; Maloney et al., 2019*b*; Nardi et al., 2020).

The MJO is characterised by an eastward-propagating region of enhanced anomalous convection (and corresponding region of suppressed anomalous convection), which initiates off the east coast of Africa and dissipates in the central Pacific (Figure 1.1). The period of the MJO varies between 30 and 60 days, giving a propagation speed of approximately 4–8 ms^{-1}. A number of theories exist around the exact mechanisms behind the formation, propagation and dissipation of the MJO (Jiang et al., 2020, 2018; Lin, 2022), and this is still very much an area of active research. The coupling of dynamics, thermodynamics, and radiative effects make the MJO particularly challenging to pick apart (Ciesielski et al., 2017).

Numerous reviews (e.g. Jiang et al., 2020; Lau and Waliser, 2012; Madden and Julian, 1994; Yang et al., 2020; Zhang, 2005; Zhang et al., 2020) have attempted to summarise the main theories of the MJO and the key processes that govern its initiation, propagation and dissipation. A number of ingredients appear to be essential, but there is still much debate about how exactly the MJO should be defined and studied.

A number of theories categrise the MJO as a moisture mode (Neelin and Yu, 1994; Yu and Neelin, 1994) – that is, a mode of variability in which the

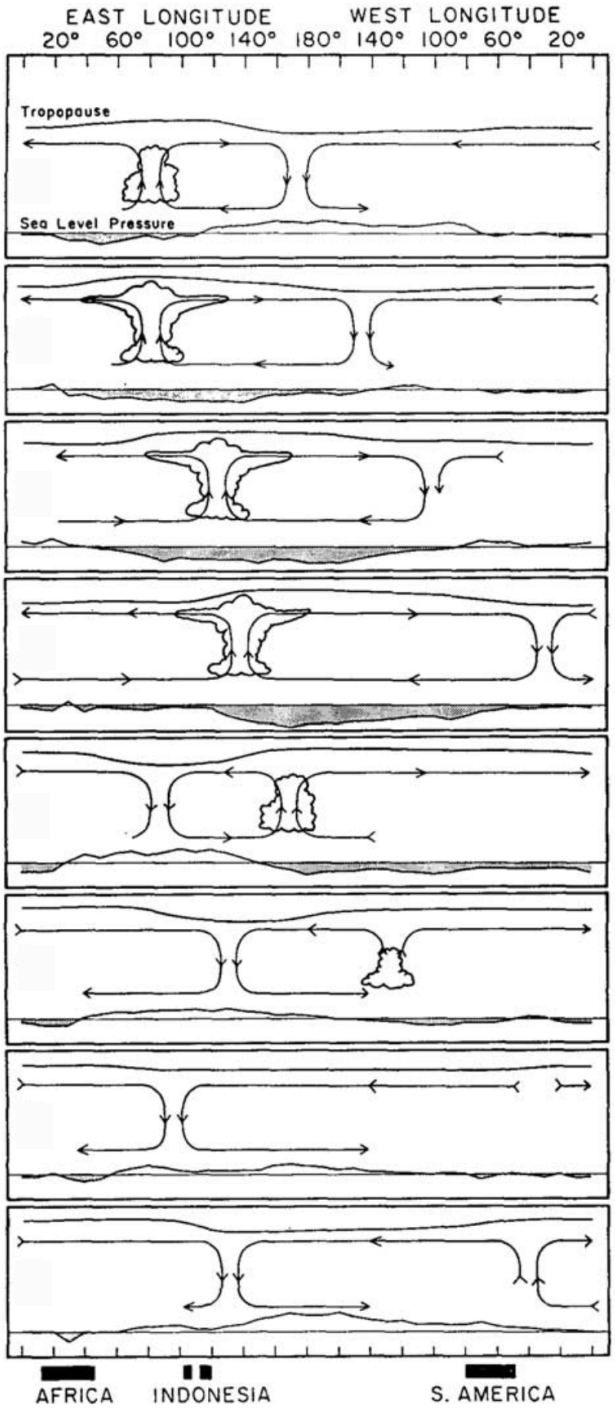

Figure 1.1: Schematic depiction of the time and space (zonal plane) variations of the MJO. The mean pressure disturbance is plotted at the bottom of each chart with negative anomalies shaded. Regions of enhanced large-scale convection are indicated schematically by the cumulus and cumulonimbus clouds. The relative tropopause height is indicated at the top of each chart. Adapted from Figure 16 of Madden and Julian (1972).

dynamics are dominated by the evolution of moisture. The details of this evolution and its impacts on the growth and propagation of the MJO vary between different models, however the importance of moisture–convection feedbacks in the representation of precipitation makes the central role of moisture in the MJO hard to dispute. The eastward propagation of this moisture wave has been attributed to a Matsuno–Gill-like response (Gill, 1980; Matsuno, 1966) to an equatorial heat source which is in weak temperature gradient balance (Adames and Kim, 2016; Sobel and Maloney, 2012, 2013; Sobel et al., 2001), or to wind-induced surface heat exchange (Fuchs and Raymond, 2005, 2017). Both of these models provide an elegant explanation for the MJO, but fail to capture much of its complexity.

Wave activity also appears to be essential to a complete description of the MJO. Convectively coupled equatorial Kelvin waves are very closely linked to the MJO (e.g. Baranowski et al., 2016), contributing to the MJO convective envelope and playing a role in its initiation. Some theories also link the MJO with the propagation of gravity waves (Yang and Ingersoll, 2013, 2014), and there has even been a suggestion that the MJO can be modelled as a nonlinear solitary Rossby wave in a dry framework (Rostami and Zeitlin, 2019; Yano and Tribbia, 2017), removing the need for moisture coupling.

Whilst there is still no 'holy grail' theory which fully describes the MJO, it seems that moisture availability, air–sea fluxes, wave activity (particularly Kelvin waves), and deep convection all play a role.

In order to efficiently describe the state of the MJO at a given point in time, it is common to refer to its phase and amplitude. Whilst many diagnostics and indices are available for the MJO (Waliser et al., 2009), the realtime-multivariate MJO (RMM) index[1] of Wheeler and Hendon (2004) is the most commonly used. The RMM index assigns to the MJO, at each time, a phase and amplitude, which signify the longitudinal position and magnitude of the convective anomalies respectively. MJO phases are given as an integer between 1 and 8, with phases 2–

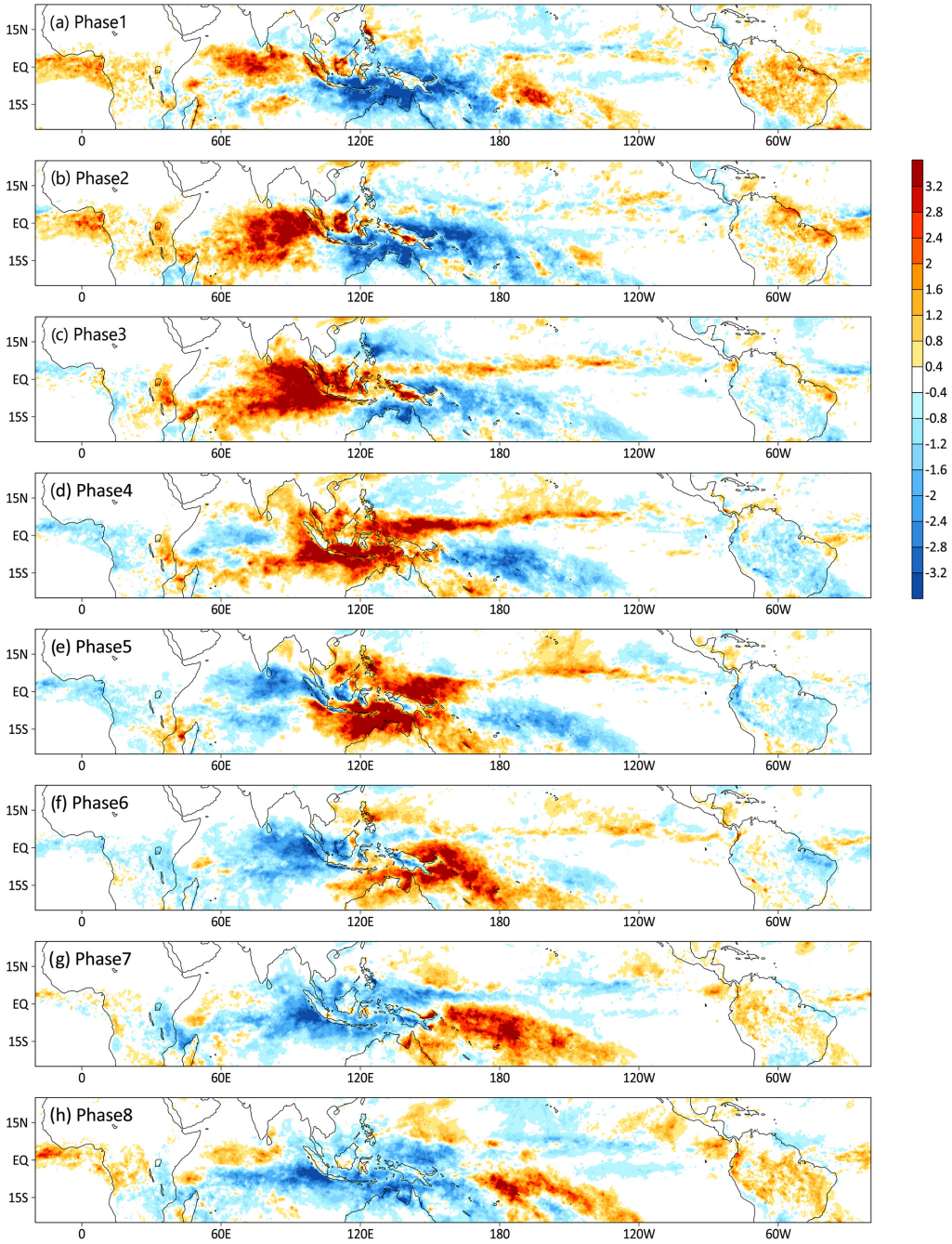

Figure 1.2: Evolution of composite rainfall anomalies (mmday^{-1}) during boreal winter season from November to March for MJO (a–h) Phases 1–8 as defined by Wheeler and Hendon (2004). The rainfall data are based on TRMM from 1998 to 2016. Before used in the composite analysis, daily rainfall anomalies are derived by removing the climatological annual cycle and then applying a 20- to 100-day band-pass filtering. Adapted from Figure 1 of Jiang et al. (2020).

3 corresponding to enhanced convection over the Indian Ocean (IO), phases 4–5 corresponding to enhanced convection over the Maritime Continent (MC), phases 6–7 corresponding to enhanced convection over the western Pacific, and phases 8–1 corresponding to enhanced convection over the central Pacific and western IO (Figure 1.2). The amplitude is scaled so that the MJO may be considered 'active' when its amplitude is greater than one.

The MJO varies on a range of timescales and due to a range of factors, displaying considerable diversity (e.g. Wei et al., 2023). Coupled atmosphere–ocean interactions are a key modulator of the MJO (DeMott et al., 2015), regulating MJO strength (Krishnamurti et al., 1988), propagation (Zhou and Murtugudde, 2020) and initiation (Webber et al., 2010, 2012). The MJO is also modulated by other modes of variability (e.g. Dasgupta et al., 2020; Fu et al., 2022, 2020; Henderson and Maloney, 2018; Marshall et al., 2017; Martin et al., 2021*a*,*b*, 2020, 2019; Nishimoto and Yoden, 2017; Pohl and Matthews, 2007; Son et al., 2017; Suematsu and Miura, 2018; Wei and Ren, 2019; Yoo and Son, 2016), details of which are given in Section 1.4.

The ability of climate models to capture MJO related variability has improved over recent decades (e.g. Ahn et al., 2020, 2017; Fiedler et al., 2020; Hung et al., 2013; Jiang et al., 2015; Kim et al., 2009; Lin et al., 2006; Slingo et al., 1996). A key challenge for climate models is the so-called barrier effect, where MJO propagation tends to stall, slow, or divert over the MC. Whilst the barrier effect appears in observations (Zhou et al., 2023), it is exaggerated in models (Ahn et al., 2020).

Whilst the MJO is, at its core, a tropical system, it also triggers an extratropical response (e.g. Cassou, 2008; Matthews et al., 2004). The predictability obtained through investigation of the MJO and its teleconnections (Kent et al., 2022) motivates the present study. Whilst the MJO is the focus of the following work, a number of other modes of variability are also of import, due to their interactions with the MJO. These will be introduced in Sections 1.3–1.4.

1.2 MJO teleconnection patterns

1.2.1 Tropospheric teleconnection pathway

The primary mechanism by which MJO-induced variability is transferred to the extratropics is through the propagation of extratropical Rossby waves[2] (Barnes et al., 2019; L'Heureux and Higgins, 2008; Matthews et al., 2004; Pedlosky, 2003; Rossby et al., 1938). Extratropical Rossby waves are planetary-scale, quasi-stationary wavetrains which extend across the mid-latitudes, interacting with synoptic-scale weather systems. The propagation, and subsequent breaking (Franzke et al., 2004; Michel and Rivière, 2011; Swenson and Straus, 2017; Woollings et al., 2008), of these Rossby waves in the extratropics leads to changes in blocking (e.g. Henderson et al., 2016), jet dynamics (e.g. Bao and Hartmann, 2014; Kang and Tziperman, 2018), storm tracks (Guo et al., 2017), and weather regimes (e.g. Cassou, 2008; Lin et al., 2009, 2010; Mori and Watanabe, 2008; Riddle et al., 2013; Seo and Lee, 2017), which may be interpreted as teleconnection patterns.

Rossby waves are initiated in the presence of a Rossby Wave Source (RWS; Sardeshmukh and Hoskins, 1988). The RWS is defined as

$$RWS = -\nabla \cdot (\mathbf{v}_\chi \zeta) = -\mathbf{v}_\chi \cdot \nabla\zeta - \zeta\nabla \cdot \mathbf{v}_\chi, \tag{1.1}$$

where $\mathbf{v}_\chi$ is the divergent component of the horizontal wind, and ζ is the absolute vorticity. The first term on the right hand side of Equation 1.1 is the advection of absolute vorticity by the divergent wind. By the conservation of potential vorticity, a meridional displacement of an air parcel produces an anomaly in relative vorticity. This vorticity anomaly induces a circulation, which results in meridional displacement of nearby air parcels and the formation of a wave (Vallis, 2006). The second term is the stretching of absolute vorticity by the divergence of the wind.

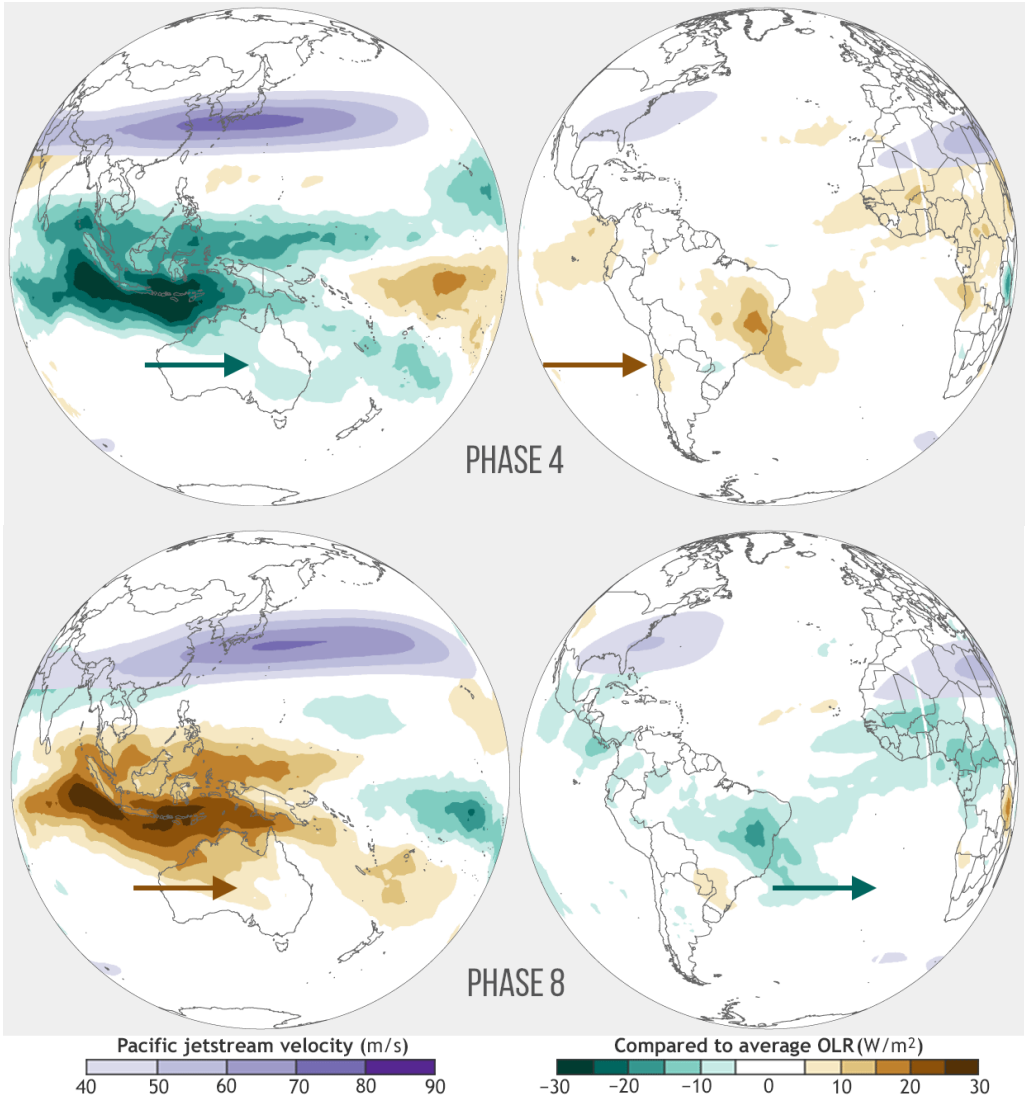

Figure 1.3: Composites of Outgoing Longwave Radiation (OLR) anomaly and jet position for MJO phases 4 and 8. Adapted from NOAA Climate.gov animation (https://www.climate.gov/news-features/blogs/enso/catch-wave-how-waves-mjo-and-enso-impact-us-rainfall).

Enhanced anomalous convection associated with the MJO leads to upper tropospheric divergence, one component of which is an anomalous meridional displacement. By the aforementioned vorticity advection mechanism, the resultant RWS initiates Rossby waves, which propagate northward and eastward across the midlatitudes (Kim et al., 2006; Matthews and Kiladis, 1999*a*; Seo and Son, 2012). The propagation of these waves is governed by the background state through which they move (Lin and Brunet, 2018).

The stationary Rossby wavenumber is defined as

$$K_s = \left(\frac{\beta - \overline{u}_{yy}}{\overline{u}} \right)^{\frac{1}{2}}, \tag{1.2}$$

where $\overline{u}$ is the time-mean zonal wind, β is the meridional gradient of planetary vorticity, and $\overline{u}_{yy}$ is the meridional gradient of time-mean relative vorticity (with the meridional wind component neglected). K_s can be considered an analogue for a refractive index for Rossby waves, such that the waves will tend to follow local maxima in K_s (Dawson et al., 2011; Hoskins and Ambrizzi, 1993; Hoskins and Karoly, 1981; Karoly, 1983). The physical implication of this is that Rossby waves will generally follow the mid-latitude jets (where $-\overline{u}_{yy}$ is large; Matthews and Kiladis, 1999*a*).

Since the mid-latitude jets act as approximate waveguides for Rossby waves, they are a key controller of MJO teleconnections. The position and strength of the jets are sensitive to changes in SSTs (Woollings et al., 2010*b*), providing a mechanism for the modulation of MJO teleconnections by SST variability. Changes in the meridional SST gradient act to strengthen or weaken the jet, leading to zonal shifts in the jet position. If the SST gradient is weakened, then so too is the zonal pressure gradient, allowing the jet to meander. The MJO itself leads to changes in the jets, through the interaction between the jet and Rossby waves, which is in part what leads to the teleconnections we observe. When the MJO is in phases 6–1 (i.e. enhanced convection is over the Pacific), the Asia–Pacific jet extends eastward, whilst in phases 2–5 (i.e. enhanced convection is over the IO and MC) the jet is contracted (Figure 1.3; Matthews and Kiladis, 1999*a*; Molinari and Vollaro, 2012). Similarly, lower-frequency modes of variability such as the El Niño–Southern Oscillation, Atlantic Multidecadal Variability and the Pacific Decadal Oscillation (Section 1.3) can also modulate the jets (e.g. Woollings et al., 2010*b*), and so alter the basic state through which MJO induced Rossby waves propagate.

1.2.2 Stratospheric teleconnection pathway

A secondary teleconnection mechanism from the MJO to the North Atlantic (NA) appears via the Stratospheric Polar Vortex (SPV; Barnes et al., 2019; Green and Furtado, 2019). The SPV is a seasonal phenomenon, in which a cyclonic vortex forms in the stratosphere above the winter pole (Figure 1.4; Butchart, 2022; Mitchell et al., 2021; Palmer, 1959; Waugh and Polvani, 2010). Variations in the strength and/or structure of the SPV can have sizeable effects on the troposphere (e.g. Baldwin et al., 2001). In some instances, the vortex destabilises to the point of breaking down entirely, leading to a sudden stratospheric warming (SSW; Baldwin et al., 2021; Charlton and Polvani, 2007). As a result of large-scale descent, temperatures in the polar stratosphere increase rapidly during an SSW, sometimes by up to 50 K.

During MJO phase 6, the standing Rossby wave response discussed above forms an anomalous low pressure centre over the North Pacific (NP), deepening the Aleutian Low (AL). The enhancement of the AL allows for increased planetary wave activity (Garfinkel et al., 2014), including in the vertical direction. Vertically propagating planetary waves break in the stratosphere, destabilising the SPV, and thus causing it to decelerate (Garfinkel et al., 2014, 2012; Jiang et al., 2017). As the SPV decelerates, the meridional pressure gradient is weakened, favouring the negative phase of the Northern Annular Mode (NAM). This negative shift in the NAM is then propagated downwards to the troposphere (Baldwin and Dunkerton, 1999, 2001; Baldwin et al., 2001; Woollings et al., 2010*a*), pushing the North Atlantic Oscillation (NAO) towards its negative phase.

This weakening of the SPV, as a result of MJO phase 6, also significantly increases the chances of SSW occurrence (Garfinkel and Schwartz, 2017; Kang and Tziperman, 2017, 2018; Liu et al., 2014; Schwartz and Garfinkel, 2017, 2020), which further increases the likelihood of a negative NAM (and hence NAO; Afargan-Gerstman et al., 2022; Furtado et al., 2021; White et al., 2021).

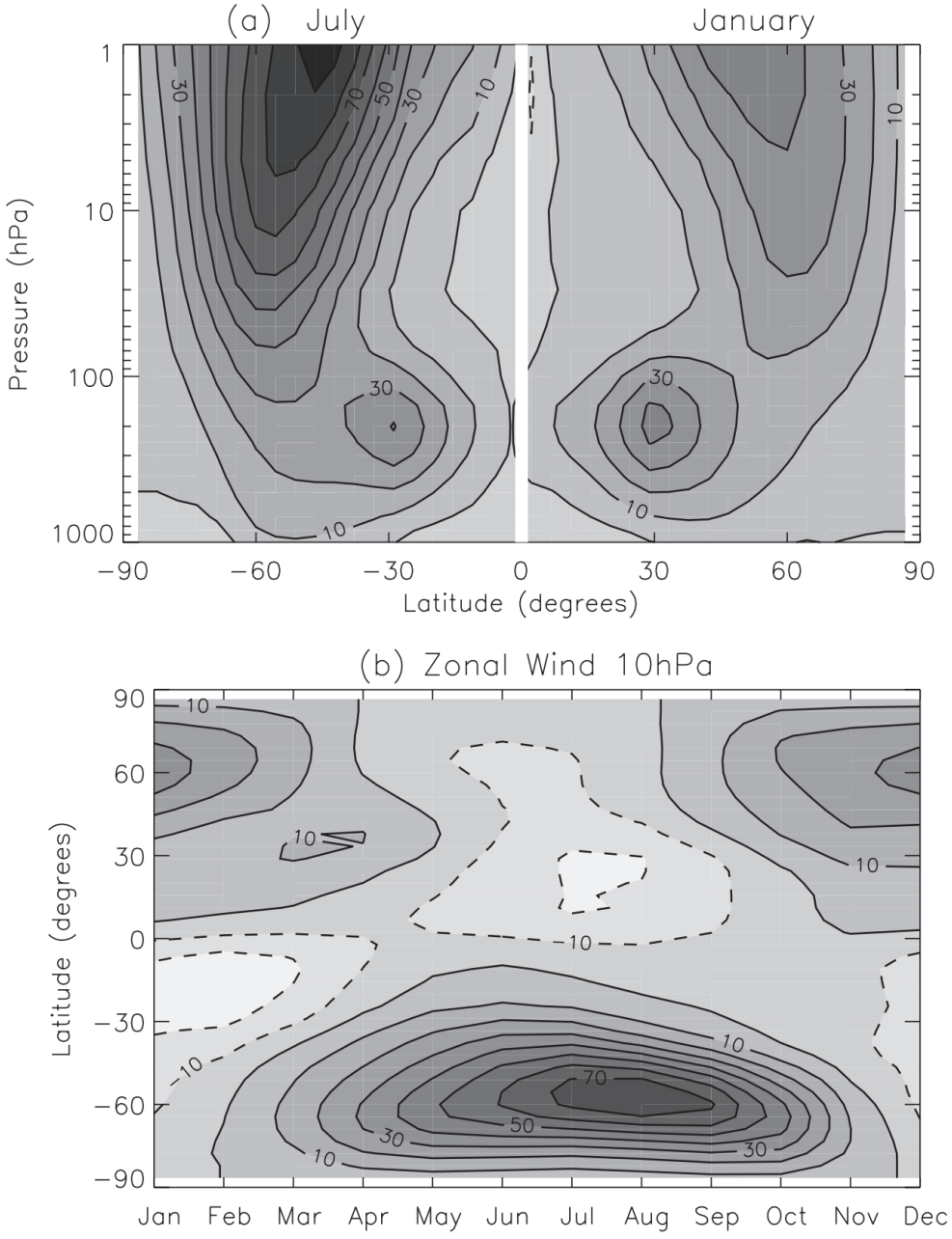

Figure 1.4: (a) Latitude–height variation of climatological mean zonal mean zonal winds for (left) SH in July and (right) NH in January. (b) Latitude–month variation of climatological mean zonal mean zonal winds at 10 hPa. Adapted from Figure 1 of Waugh and Polvani (2010).

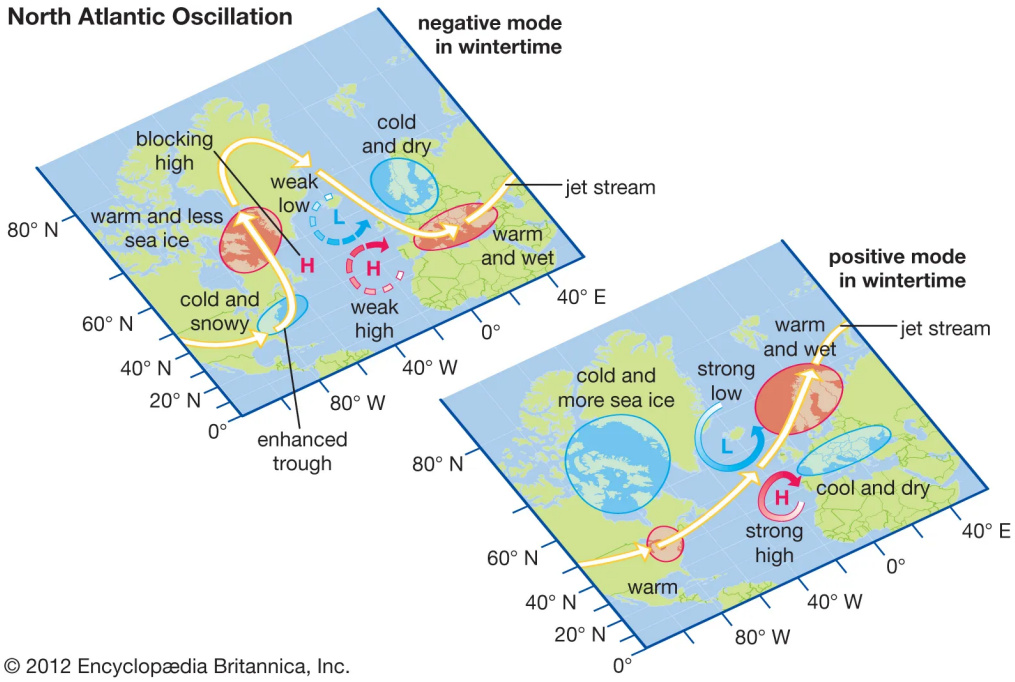

Figure 1.5: The boreal winter NAO in relation to the Icelandic Low, Azores High and Subpolar Jet stream. From Rafferty (2019).

These teleconnections from the MJO to the NA via the stratosphere tend to coincide with those produced via the tropospheric pathway, albeit at a slightly longer lag time (around 10-20 days for the stratospheric pathway, compared with 5-15 days for the tropospheric pathway).

1.2.3 The North Atlantic Oscillation

The North Atlantic Oscillation (NAO; Barnston and Livezey, 1987; Hurrell et al., 2003*a*; Lorenz, 1951; Stephenson et al., 2003; Walker, 1924; Wallace and Gutzler, 1981) is the leading mode of subseasonal variability in the NA (Hurrell et al., 2003*b*; Vautard, 1990) and is central to many climatic processes and impacts throughout the Northern Hemisphere (NH; Hurrell, 1996). Many studies have used the NAO as an indicator of the extratropical response to certain MJO phases (e.g. Cassou, 2008).

The NAO is characterised by a quasi-periodic oscillation in anomalous atmospheric pressure between Iceland and the Azores (Jones et al., 2003;

Walker, 1924; Walker and Bliss, 1932). This corresponds to an oscillation in the strength the climatological Icelandic Low and Azores High, which is directly related to the dynamics of the sub-polar jet (Figure 1.5; Branstator, 2002; Parker et al., 2019; Rafferty, 2019; Visbeck et al., 2001; Woollings et al., 2010*b*). This variability occurs over a range of time scales (Cook et al., 1998; Hurrell and van Loon, 1997; Rogers, 1984), however sub-seasonal variability is of greatest interest to this study.

When the Icelandic Low and Azores High are strengthened (weakened) – that is, when anomalous low (high) pressure is centred over Iceland and anomalous high (low) pressure is centred over the Azores – the NAO is said to be in its positive (negative) phase (NAO+ and NAO−, respectively; Rafferty, 2019). NAO+ leads to a strengthening and poleward shift in the North Atlantic jet, whilst NAO− is associated with a equatorward shift in the jet (Luo and Cha, 2012; Luo et al., 2007; Woollings and Blackburn, 2012; Woollings et al., 2010*b*).

There is a particular interest in the study of the NAO due to its impacts on the weather of North America and Europe (Bliss, 1926; Osborn, 2011). The state of the NAO also has implications for weather forecasting (e.g. Neal et al., 2016), ecology (e.g. Drinkwater et al., 2003; Fromentin and Planque, 1996; Mysterud et al., 2003; Ottersen et al., 2001; Straile et al., 2003), and the economy (e.g. Cherry et al., 2005; Zanardo et al., 2019).

Models and forecasts struggle to fully capture NAO variability (Bracegirdle et al., 2018; Robson et al., 2020; Scaife et al., 2014), meaning that expensive large ensembles are needed to obtain useful predictions (Athanasiadis et al., 2020; Dunstone et al., 2016; Smith et al., 2020). Hence, there is a motivation to study potential sources of NAO predictability, such as the MJO (Kent et al., 2022; Klavans et al., 2021).

Cassou (2008) shows that the NAO is sensitive to MJO forcing at a lag of approximately 10–15 days. In particular, the probability of observing NAO+ increases significantly around 10 days after MJO phase 3 (Figure 1.6).

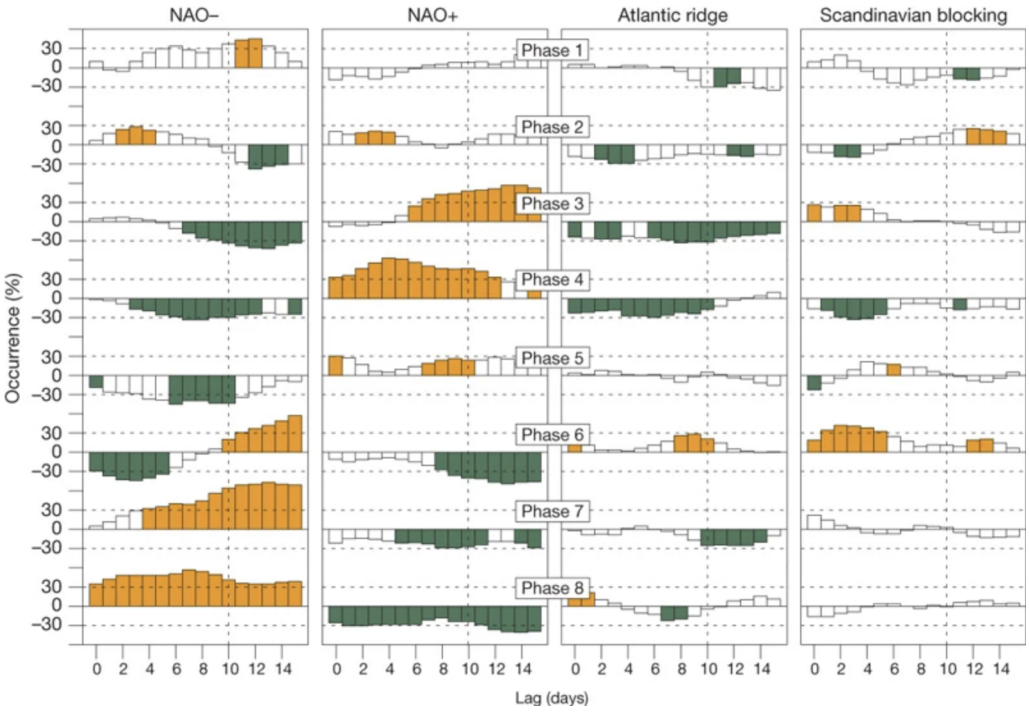

Figure 1.6: Table of contingency between the MJO phases (rows) and the NA weather regimes (columns). For each MJO phase, the anomalous percentage occurrence of a given regime is plotted as a function of lag in days (with regimes lagging MJO phases). The 0% value means that the MJO phase is not discriminative for the regime whose occurrence is climatological. A 100% value would mean that this regime occurs twice as frequently as its climatological mean; -100% means no occurrence of this regime. The presence of a slope as a function of lag is suggestive of the MJO forcing. For white bars, either the change in the distribution between the four regimes is not significant on the basis of χ^2 statistics at the 99% significance level, or the individual anomalous frequency of occurrence is lower than the minimum significant threshold tested at 95% using a Gaussian distribution (approximation for binomial distribution because of the sufficiently large sampling). For orange and green bars, the regimes occur significantly more or, respectively, less frequently than their climatological occurrences. Adapted from Figure 3 of Cassou (2008).

Conversely, the probability of observing NAO− increases significantly around 15 days after MJO phase 6. This is the canonical NAO response to the MJO, and will, hereafter, be referred to as such.

1.2.4 The Northern Annular Mode

The Northern Annular Mode (NAM[3]; Black and McDaniel, 2004; Thompson and Wallace, 1998, 2000; Thompson et al., 2000) is an oscillation in the NH which is closely related to the NAO. Some sources treat the two oscillations as one phenomenon (e.g. Thompson et al., 2003; Thompson and Wallace, 2001), however the two modes have been shown to be distinguishable (Ambaum et al., 2001; Feldstein and Franzke, 2006).

The NAM is characterised by a (approximately) zonally symmetric see-saw in atmospheric mass between the mid- and high-latitudes in the NH, which is also correlated with the strength of the jet. In the troposphere, this variability is strongest in the NA, leading to the similarity with the NAO. The NAM does, however, give a signal in other regions (Wallace and Thompson, 2002).

Whilst the NAO is usually considered a tropospheric phenomenon, the NAM has a stratospheric component which is coupled to the tropospheric variability (Omrani et al., 2022). The NAM in the stratosphere regulates the stratospheric polar vortex, and the NAM index is often used as an analogue for polar vortex strength.

Like the NAO, the NAM impacts on weather and climate across the NH (de Beurs and Henebry, 2008; McAfee and Russell, 2008; Thompson and Wallace, 2001), and is itself modulated by the MJO (Zhou and Miller, 2005). The NAM also varies on decadal time scales (Butler et al., 2023; Schurer et al., 2023), so this could be a potential source of decadal variability in MJO teleconnections.

1.2.5 Pacific–North American Pattern

The Pacific–North American pattern[4] (PNA; Barnston and Livezey, 1987; Wallace and Gutzler, 1981) is a mode of pressure variability with centres over the NP (more specifically, the Aleutian Low) and continental North America.

The pattern is usually described by a 'chequerboard' pattern of four pressure centres located over the eastern NP, central Canada, Hawaii[5] and Florida (Figure 1.7a).

The positive phase of the PNA (PNA+) is defined by anomalous high pressure over Canada and Hawaii with anomalous low pressure over the NP (i.e. a deepening of the AL) and the US Gulf Coast. This also corresponds to a strengthening of the East Asian Jet and an eastward shift in its exit. The negative (PNA−) phase is an approximate mirror of this pattern.

Just as the NAO plays a major role in the weather of the UK, the PNA is key to the weather in the USA and Canada. In PNA+, we observe warmer conditions in Alaska, Canada and the northwestern USA alongside cooler conditions in southeastern USA, the east coast of the USA and Central America (Figure 1.7b). Wetter conditions are found in the Gulf of Mexico and southern coast of Alaska with dry conditions over the Rocky Mountains, Great Lakes and Tennessee Valley (Figure 1.7c). PNA− is associated with a reversal of these states.

The PNA and NAO are linked, with the AL and Icelandic Low anomalies tending to be of opposite sign (Honda et al., 2001). Hence, MJO teleconnections are able to reach the NA via the PNA.

MJO phases 2 and 3 favour PNA−, whilst phases 6 and 7 tend to precede PNA+ (Mori and Watanabe, 2008; Seo and Lee, 2017; Stan et al., 2017; Tseng et al., 2020*a*,*b*).

1.2.6 The Southern Hemisphere

The MJO is known to produce teleconnections in the Southern Hemisphere (SH), impacting on both SH weather regimes (e.g. Grimm, 2019; Matthews et al., 2004; Matthews and Meredith, 2004) and Antarctic sea ice (Lee and Seo, 2019).

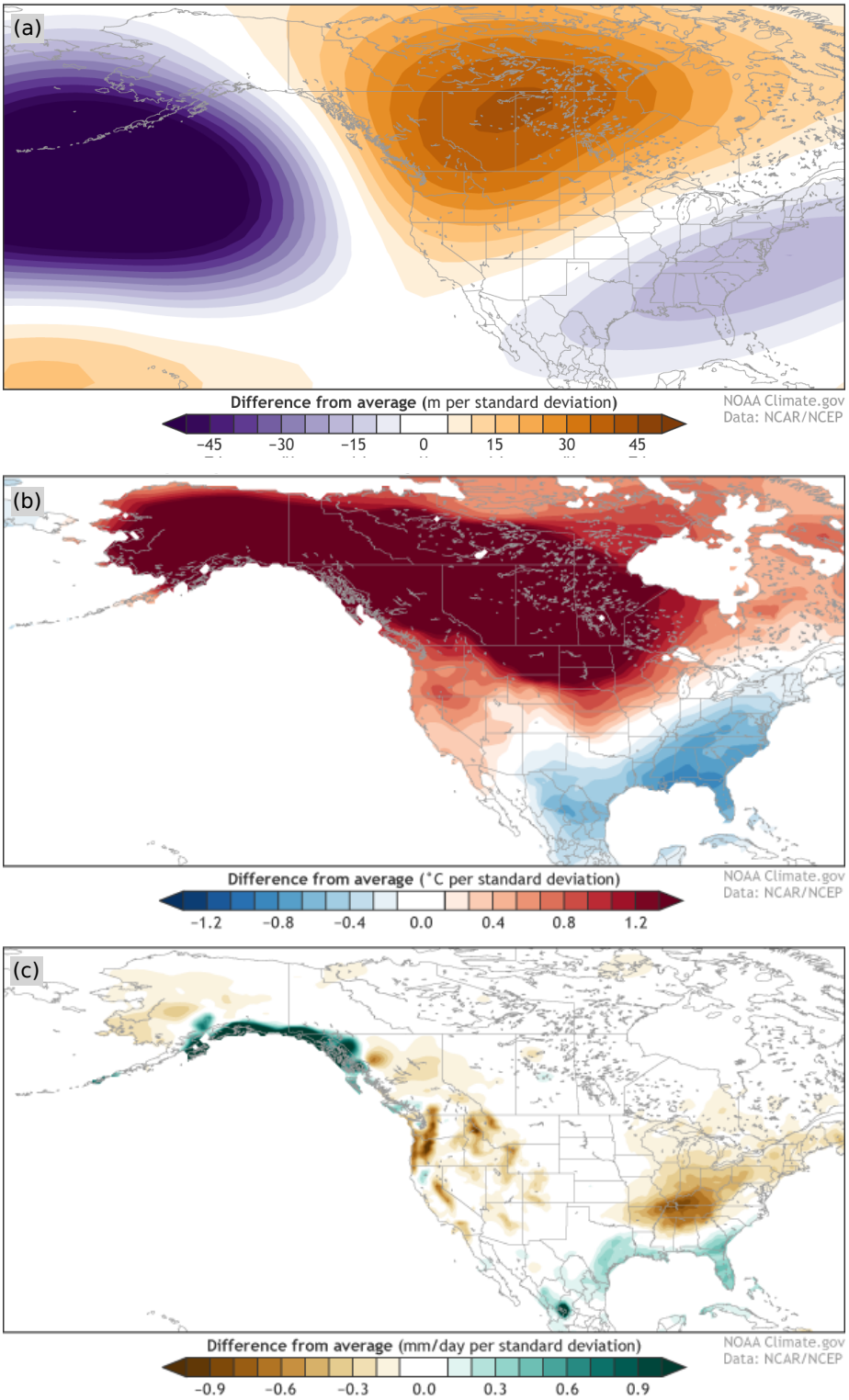

Figure 1.7: (a) 500-hPa geopotential height ($Z500$), (b) surface temperature, and (c) precipitation anomalies over North America, regressed onto the PNA index. Images adapted from L'Heureux (2021).

Whilst these teleconnections are of great importance to SH weather prediction, this thesis will focus on the NH teleconnections from the MJO, which tend to be greater in magnitude and impact.

1.3 Low-frequency modes of climatic variability

The extratropical response to the MJO is dependent on the basic state. Hence, low-frequency changes in the basic state will likely change the extratropical response to the MJO. We introduce three key modes of climatic variability below, so that we may assess their impact on MJO teleconnections.

1.3.1 The El Niño–Southern Oscillation

The El Niño–Southern Oscillation (ENSO; Allan et al., 1996; Neelin et al., 1998; Philander, 1989, 1983; Trenberth, 1997; Wang et al., 2017) is the leading mode of climatic variability on interannual time scales. ENSO is quasi-periodic, with cycles lasting between 2 and 10 years (Figure 1.8). The peak in spectral activity, though, falls between periods of 3 and 7 years (Christensen et al., 2017; Deser and Trenberth, 2016; Rasmusson and Carpenter, 1982; Siqueira et al., 2019).

ENSO is an oscillation in eastern and central Pacific sea surface temperature (SST) anomalies (Figure 1.9). The warm phase, El Niño, is characterised by a 'warm tongue' which stretches from the Peruvian coast across the equatorial Pacific. This warm tongue is flanked by colder SST anomalies in the north, south and west Pacific. The cold phase, La Niña, on the other hand, is characterised by cold SST anomalies in the central and eastern equatorial pacific. Notably, the La Niña SST pattern is not simply the reciprocal of the El Niño SST pattern, instead showing a weaker response in the eastern Pacific, but a stronger response in the central Pacific (Sarachik and Cane, 2010).

ENSO modulates the SST variability in the IO, particularly via the Indian Ocean

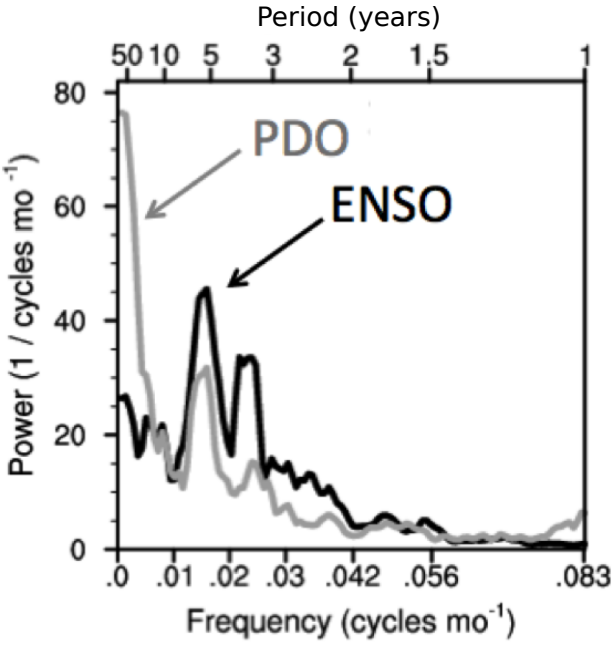

Figure 1.8: Power spectra of the normalised ENSO and PDO indices (Appendix A), based on the HadISST dataset for the period 1870-2014. Adapted from Figure 2 of Deser and Trenberth (2016).

Dipole (IOD; Wang and Wang, 2014; Yu and Lau, 2005). The IOD is an aperiodic meridional oscillation in SST anomalies across the IO, and is the primary mode of variability in the IO (Saji et al., 1999). The IOD itself also impacts on the MJO (e.g. Ajayamohan et al., 2009; Wilson et al., 2013), providing an indirect link between ENSO and the MJO. The importance of ENSO in regulating the IOD is up for debate (Leupold et al., 2021; Wang et al., 2016), however there is certainly a connection between the two modes.

There is a direct link between ENSO SST variability and the Walker circulation (Bjerknes, 1969; Julian and Chervin, 1978; Walker, 1923). El Niño events are associated with a weakened Walker circulation, due to the weakening of the east–west SST gradient. La Niña, however, sees a strengthening of this gradient and hence of the Walker circulation.

ENSO-driven changes in the Walker circulation, and of the associated precipitation patterns, lead to global teleconnection patterns (e.g. Diaz et al., 2001). These changes also modulate the MJO and its teleconnection patterns (Subsection 1.4.2; Arcodia et al., 2020; Hendon et al., 1999; Lee et al., 2019; Ma

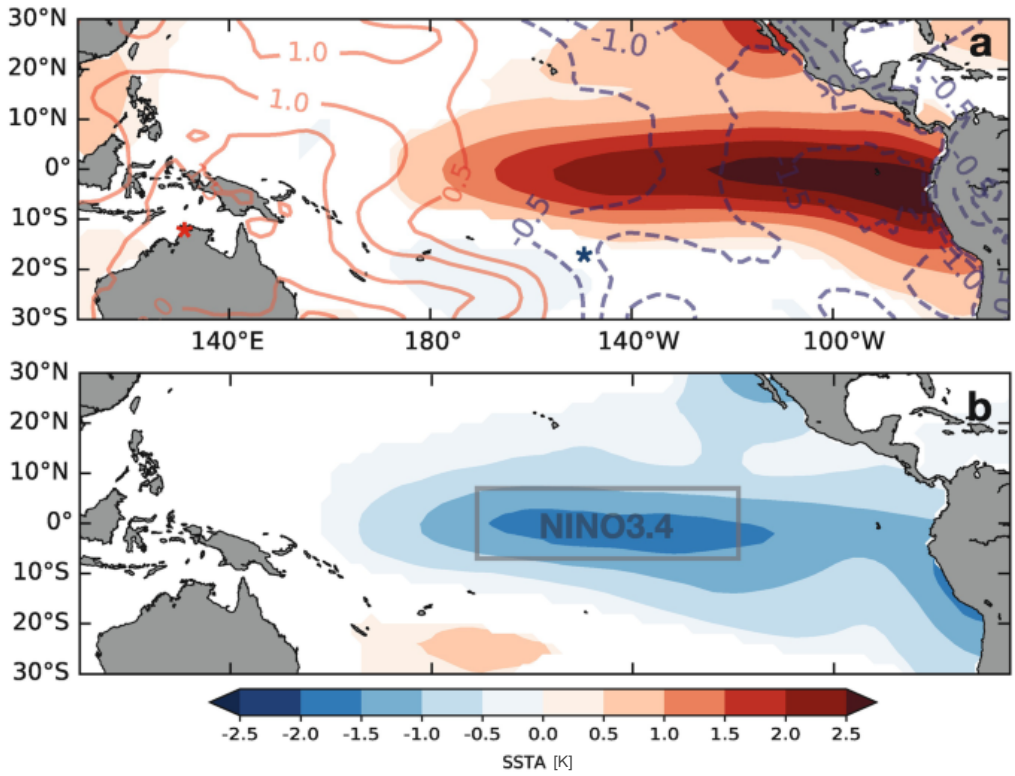

Figure 1.9: Composite tropical Pacific SST anomalies displaying the typical patterns associated with the anomalous peak warming for strong ($\geq$ 1.5) El Niño (a) and La Niña (b); Coloured areas denote regions significant at the 95% level and contours show pressure departures in hPa. Coloured stars show the approximate location of Darwin (red) and Tahiti (blue) from which pressure differences are used to calculate the Southern Oscillation Index. Box in (b) shows the region (NINO3.4) where the largest SST variability occurs on ENSO timescales, typically used for ENSO monitoring. Asymmetry between the location of the maximum anomaly with El Niño peaking farther east and La Niña peaking more toward central Pacific is also noted. Adapted from Figure 1 of Siqueira et al. (2019).

et al., 2020; Moon et al., 2011; Tseng et al., 2020*a*).

1.3.2 Atlantic Multidecadal Variability

The leading mode of decadal and interdecadal variability globally is Atlantic Multidecadal Variability[6] (AMV; Bjerknes, 1964; Grossmann and Klotzbach, 2009; Kavvada et al., 2013; Kerr, 2000; Kushnir, 1994; Lin and Qian, 2022; Trenberth and Shea, 2006; Xie and Tanimoto, 1998). AMV describes an oscillation in North Atlantic SST anomalies over long time scales. The period of

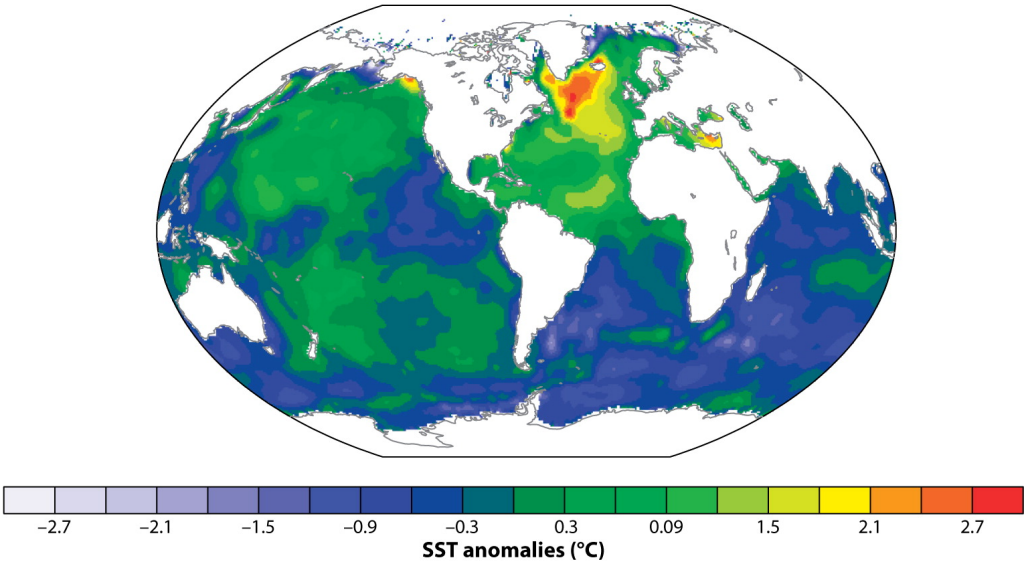

Figure 1.10: Observed SST anomalies projected onto the AMV index (Appendix A), based on HadISST data. Adapted from Figure 11 of Deser et al. (2010).

AMV is on the order of 65–80 years (Enfield et al., 2001), however it is quasi-periodic in nature (Knight et al., 2005).

When AMV is in its positive (or warm) phase (AMV+), North Atlantic SSTs are anomalously warm when compared with the global average (Figure 1.10), whilst in the negative (or cold) phase (AMV−) the reverse is true (Lin and Qian, 2022).

AMV is a driver of the global climate system (Qasmi et al., 2020; Sutton and Hodson, 2005) and regional weather (Ummenhofer et al., 2017) on multidecadal time scales. For example, during AMV+ (AMV−), the NAO (Subsection 1.2.3) tends to favour its negative (positive) phase (Elsbury et al., 2019; Msadek et al., 2011). AMV is also able to modulate ENSO and its teleconnections (Geng et al., 2020, 2017; Ruprich-Robert et al., 2021; Zhao et al., 2022).

1.3.3 The Pacific Decadal Oscillation

The second largest mode of global SST variability on decadal time scales is the Pacific Decadal Oscillation[7] (PDO; Mantua and Hare, 2002; Mantua et al., 1997; Newman et al., 2016). The PDO has a similar spatial SST pattern to

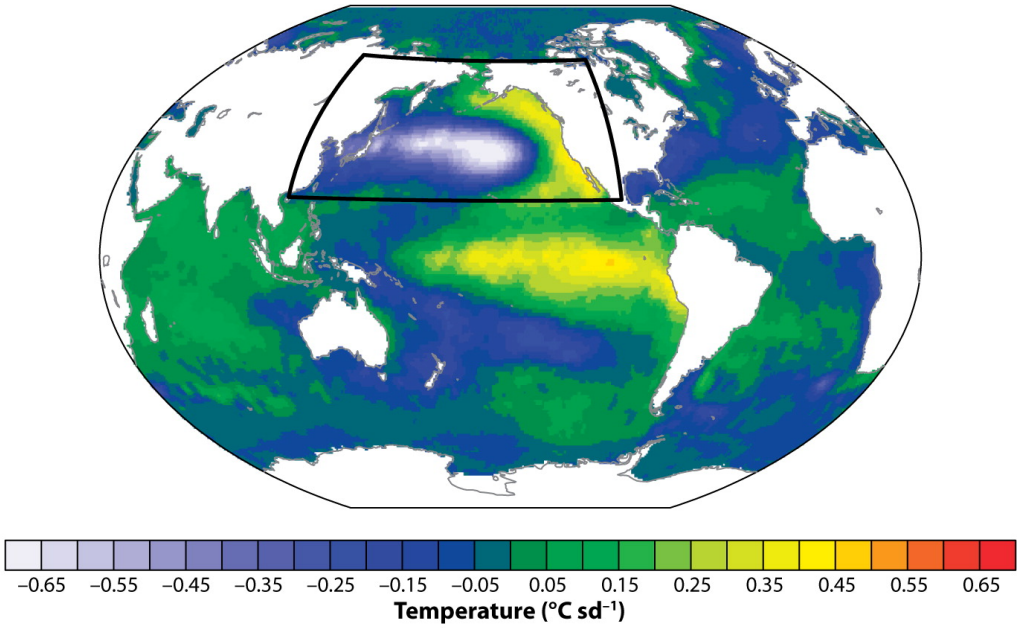

Figure 1.11: Observed SST anomalies projected onto the PDO index (Appendix A), based on HadISST data. Adapted from Figure 10 of Deser et al. (2010).

ENSO, but with greater emphasis on the NP rather than the equatorial Pacific (Figure 1.11). The positive phase (PDO+) is characterised by colder than average SSTs in the western and central NP, with warmer SSTs in the eastern NP and equatorial Pacific (similar to La Niña). The reverse is true of the negative phase (PDO−). The PDO also has a much longer time period than ENSO (Figure 1.8) at approximately 50 years.

During PDO+, the colder SSTs in the NP tend to deepen the Aleutian Low (AL). This in turn produces an atmospheric response similar to the positive phase of the PNA (Taguchi et al., 2012). The PDO is strongly coupled to the atmosphere, though, so care should be taken when discussing the atmospheric response to the PDO.

Since the two modes are so similar in their SST patterns, it is no surprise that the PDO can act as a driver of ENSO. Interestingly, though, the teleconnections produced by Pacific SST variability changes depending on the time scale of the variability (Seabrook et al., 2023). There are also links between the PDO and AMV, with AMV driving low-frequency Pacific variability with an approximately

12 year lag (Wu et al., 2011; Zhang and Delworth, 2007)

1.4 Known modulators of the MJO and its teleconnections

1.4.1 Effects of MJO diversity on teleconnections

Any given MJO event may be described by through a number of different characteristics. Differences in the intensity, propagation speed, periodicity, and various other properties will affect the resultant teleconnection patterns (Chen, 2021; Goss and Feldstein, 2018; Song and Wu, 2020*a*; Yadav and Straus, 2017; Yadav et al., 2019; Zheng and Chang, 2019).

Yadav and Straus (2017) show that the extratropical response to the MJO is sensitive to its propagation speed. The canonical NAO response to the MJO (that is, NAO+ following MJO phase 3 and NAO− following MJO phase 6, as described by Cassou (2008) and discussed in Subsection 1.2.3) is dominated by slowly propagating MJO episodes[8]. The NAO+ response also appears to peak later (around 15 days after MJO phase 4) during slowly propagating MJO events than is observed in overall composites.

The intensity of MJO events is also crucial to the teleconnection produced. Song and Wu (2020*a*) provide evidence of a bimodal distribution in MJO-related OLR anomalies in the IO. Compositing over weak and strong MJO events, they find that stronger MJO events produce a Rossby wave train after MJO phases 2 and 3, which is consistent with the canonical response. The response to weak MJO events, however, is not significant.

1.4.2 Modulation by ENSO

ENSO impacts both on the MJO itself (Pohl and Matthews, 2007), and on its teleconnections (Fernandes and Grimm, 2023; Hood et al., 2020) through alterations in the basic state (Arcodia and Kirtman, 2023).

MJO-related convective anomalies in the Pacific tend to extend further east during El Niño (Hendon et al., 2007, 1999; Kessler, 2001). This relationship, though, seems to be dependent on the spatial structure of the SST pattern associated with a given ENSO event (Chen et al., 2016; Hsu et al., 2018; Hsu and Xiao, 2017; Wang et al., 2018).

During El Niño, the canonical NAO+ response to MJO phase 3, via the tropospheric teleconnection pathway, is enhanced through increased Rossby wave activity (Figure 1.12, upper-left panel; Lee et al., 2019; Moon et al., 2011). Conversely, La Niña tends to enhance the NAO− to MJO phase 6 teleconnection via the stratosphere through deepening of the AL (Figure 1.12, bottom-right panel; Ineson and Scaife, 2009; Lee et al., 2019; Ma et al., 2020).

The effect of ENSO on the Pacific region response to the MJO is more nuanced, with the shift in convective anomalies altering the locations of the circulation anomaly centres. Henderson and Maloney (2018) show that whilst the amplitude of the Rossby wave response to MJO phase 7 is increased during La Niña, producing the enhanced NAO− response discussed above, the path of the teleconnection is altered, leading to destructive interference in the blocking patterns across the Pacific. This work, along with Takahashi et al. (2011), demonstrates the need to consider the alteration of the teleconnection as a whole, rather than focussing just on the impact of the change on a single weather pattern. It is also important to note that whilst ENSO is responsible for changes in MJO teleconnections in the time-averaged sense, it also has an effect on the event-to-event consistency of the teleconnection patterns (Tseng et al., 2020*b*)

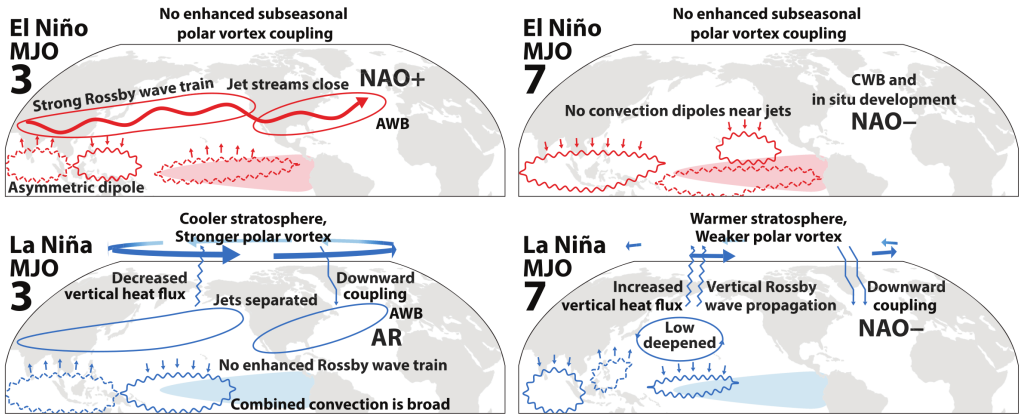

Figure 1.12: Schematic of ENSO modulation of subseasonal teleconnections from the MJO to the NA and Europe. El Niño (upper panels; red) and La Niña (lower panels; blue) states are illustrated following MJO phases 3 (left panels) and 7 (right panels). AWB and CWB refer to anticyclonic wave breaking, and cyclonic wave breaking, respectively. The anomalous convection signals (solid: enhanced; dashed: suppressed) comprise the MJO, in the given phases, as modified by the large-scale ENSO circulation. Adapted from Figure 4 of Lee et al. (2019).

As well as the aforementioned changes in the zonal extent of the MJO convective anomalies, the propagation speed of the MJO is modulated by ENSO (Henderson and Maloney, 2018; Pohl and Matthews, 2007; Suematsu and Miura, 2018; Wei and Ren, 2019). As discussed in Subsection 1.4.1, changes in MJO propagation speed can directly influence the extratropical response to the MJO. Whilst we have separated various modulators of MJO teleconnections here for clarity and ease of understanding, it is important to remember that they are all, in fact, linked and occuring simultaneously.

Although most analyses (including that presented in this thesis) consider modulation of MJO teleconnections as a whole, Arcodia and Kirtman (2023) consider the modulation of the basic state and of the MJO forcing by ENSO as separate phenomena. Using a pair of idealised models, the ENSO conditioned MJO forcing and extratropical mean state are applied independently, so that the effects of ENSO on each stage of the teleconnection mechanism can be assessed. The teleconnection patterns obtained under ENSO conditioning are different depending on the type of modulation applied. These results further strengthen the argument for considering the modulation of MJO teleconnections

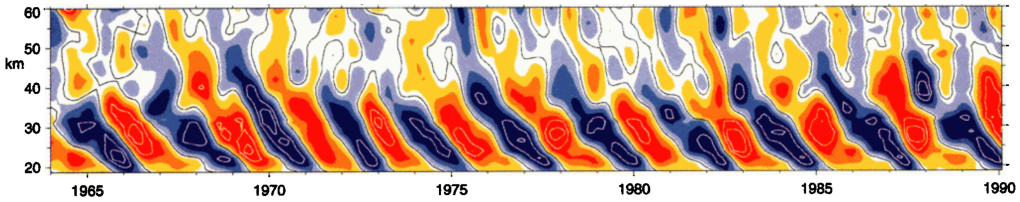

Figure 1.13: Time-height section of the monthly-mean zonal wind component (ms^{-1}), with the seasonal cycle removed, for 1964–1990. Below 31 km, equatorial radiosonde data are used from Canton Island (2.88 °N, January 1964 to August 1967), Gan/Maledive Islands (0.78 °S, September 1967 to December 1975), and Singapore (1.48 °N, January 1976 to February 1990). Above 31 km, rocketsonde data from Kwajalein (8.78 °N) and Ascension Island (8.08 °S) are shown. The contour interval is $6\,\mathrm{ms}^{-1}$, with the band between 23 and 13 unshaded. Red represents positive (westerly) winds. Adapted from Plate 1 of Baldwin et al. (2001).

as a superposition of modulations to both the tropical forcing, and the extratropical teleconnection pathway, rather than as a single process.

It is also worth noting that whilst the effect of ENSO on MJO teleconnections is considered here, there is also evidence of a reciprocal relationship, whereby the MJO can modulate ENSO teleconnections (Hoell et al., 2014).

1.4.3 Modulation by the QBO

The Quasi-Biennial Oscillation (QBO; Baldwin et al., 2001; Lindzen and Holton, 1968; Reed, 1964; Wallace, 1967) is the dominant mode of variability in the tropical stratosphere. It is characterised by an oscillation in anomalous zonal mean winds which propagates downwards and which has a period of approximately two years (Figure 1.13).

The QBO is closely coupled to atmospheric wave activity, with the QBO both being driven by and modulating Rossby wave[9] activity (Andrews et al., 1987; Koval et al., 2022; Yang et al., 2011). It also modulates the sub-polar jets (e.g. Niwano and Takahashi, 1998) and the SPV (e.g. Anstey and Shepherd, 2014; Baldwin and Dunkerton, 1998; Holton and Tan, 1980, 1982; Thompson et al., 2002), both of which are key to MJO teleconnections.

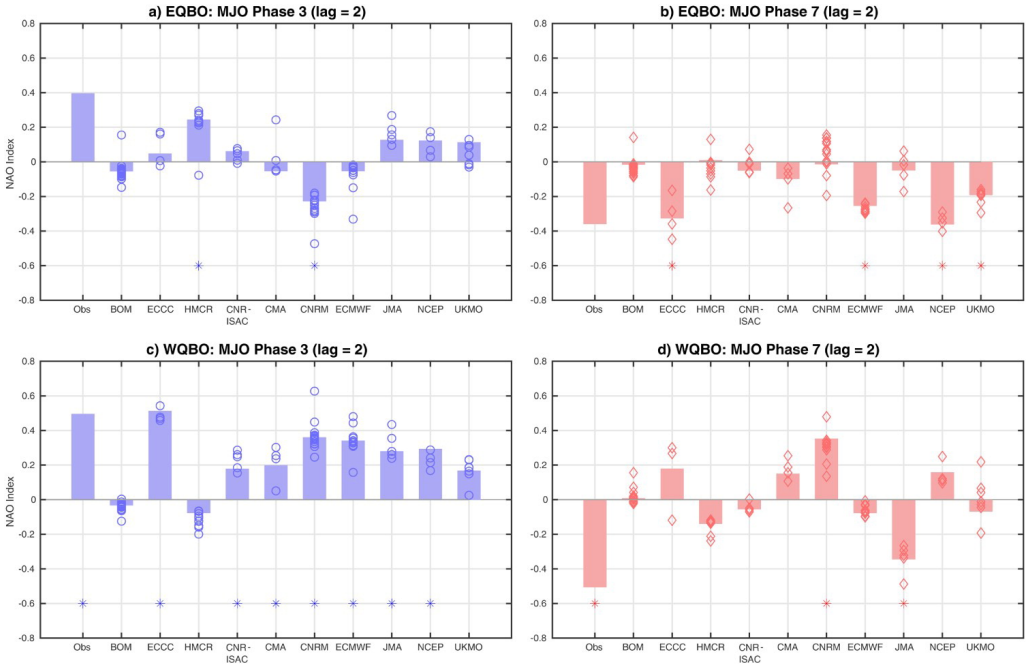

Figure 1.14: Composited NAO indices of the third pentad (11–15 days) for MJO phases 3 and 7 of the EQBO and the WQBO events of observational data and ten S2S[10] simulations. Asterisks indicate those passing the 95% confidence level. The open circles and diamonds are the composited NAO index of individual ensemble members. Adapted from Figure 5 of Feng and Lin (2021).

The QBO alters the MJO directly, with the MJO strengthening (weakening) during the easterly (westerly) phase of the QBO (EQBO and WQBO, respectively; Butler et al., 2019; Klotzbach et al., 2019; Marshall et al., 2017; Martin et al., 2021*a*,*b*, 2020, 2019; Nishimoto and Yoden, 2017; Son et al., 2017; Yoo and Son, 2016). It appears, though, that this strengthening is in fact caused by an increase in the number of active MJO days (due to a weakened maritime continent barrier effect and increased MJO initiation over the IO) rather than an increase in the amplitude of individual MJO events (Zhang and Zhang, 2018).

Evidence of QBO modulation of MJO teleconnections is provided by Toms et al. (2020), however it is not clear whether this modulation is the result of changes to the tropical MJO forcing, the extratropical mean state, or both. Interestingly, although the MJO is strengthened during EQBO, the NAO response to the MJO is stronger during WQBO (Figure 1.14; Feng and Lin, 2019, 2021). This is due

to the strengthening of the Asia-Pacific jet during the westerly phase.

This result is consistent with Song and Wu (2020*b*), who suggest that the QBO may also be modulating the stratospheric teleconnection pathway between MJO phase 6/7 and NAO−[11]. In the Southern Hemisphere (SH) a similar intensification of the extratropical wave train initiated by the MJO is seen during WQBO, however MJO related precipitation anomalies are also intensified in the South Atlantic Convergence Zone (SACZ) during EQBO (Sena et al., 2022).

1.4.4 Modulation on decadal time scales

Fu et al. (2022) show that AMV can alter the location and amplitude of MJO convection. AMV− tends to increase the magnitude of MJO related anomalies, while convective anomalies over the Pacific extend further east during AMV+.

Meanwhile, the PDO influences the distribution of MJO phases, and the location of peak MJO amplitude (Dasgupta et al., 2020), which could in turn affect MJO teleconnection patterns.

Conversely, multiple studies (Suhas and Goswami, 2010; Wang et al., 2021) find evidence of multidecadal variability in the MJO, but state that this variability cannot be attributed to either AMV or PDO modulation.

Whilst there is some evidence (albeit, not a consensus) that the MJO is modulated by AMV and the PDO on decadal time scales, the modulation of MJO teleconnections by decadal SST modes is yet to be thoroughly investigated. Oliver (2015) provide some evidence of a link between the PDO and MJO teleconnections to Alaska, however it is certainly not conclusive.

1.5 Research questions

Having now reviewed the background information and existing literature around MJO teleconnections and decadal climatic variability, we must now define the research questions that will be answered within this thesis. They are as follows:

1. *How well do climate models simulate the extratropical response to the MJO?*

   This question is investigated in Chapter 2. Before using climate models to assess decadal variability of the extratropical response to the MJO, we must first ensure that they are able to properly simulate this response over the observational time period. With the knowledge of any biases in the models and their representation of MJO teleconnections, we can then put further results in context.

2. *Does the extratropical response to the MJO vary on decadal time scales?*

   Whilst the goal of this study is find physical mechanisms for decadal variability of the extratropical response to the MJO, it is important to first check for evidence of this variability in observations. Unfortunately, we have a relatively short (≈50 years) reanalysis dataset to work with, however useful progress can still be made. This work, presented in Chapter 3, will provide the motivation for the following question.

3. *What modulates decadal variability of the extratropical response to the MJO?*

   Since ENSO is a known modulator of MJO teleconnections, we hypothesise that decadal modes of SST variability (AMV and PDO) also modulate the extratropical response to the MJO. A coupled climate model (which provides a much longer dataset) is used in Chapter 4 to examine this hypothesis, within the context of the previous two research questions.

These three questions will be revisited in Section 5.1, having been thoroughly examined in their respective chapters.

Notes for Chapter 1

[1] Further details of the Wheeler and Hendon (2004) RMM index are given in Appendix A.

[2] Rossby waves are sometimes also known as planetary waves.

[3] The NAM is sometimes also known as the Arctic Oscillation (AO).

[4] The PNA's name was coined by Wallace and Gutzler (1981) as the 'Pacific/North American pattern' and is sometimes also stylized as the 'Pacific North American pattern' or 'Pacific–North American Teleconnection Pattern' in other literature. We will continue to use the stylization 'Pacific–North American pattern' in line with the IPCC (e.g. Trenberth et al., 2007).

[5] In some literature the PNA is described as tripolar rather than quadripolar with the Hawaiian pole omitted.

[6] AMV is sometimes also known as the Atlantic Multidecadal Oscillation (AMO).

[7] The PDO is sometimes also known as the Pacific Decadal Variability (PDV).

[8] Slowly propagating MJO episodes are defined by Yadav and Straus (2017) as those in which the OLR minimum takes 20 or more days to propagate from phase 3 to phase 6. For episodes to be counted, they must also exceed an amplitude of 1 for at least 3 consecutive days in phase 3 and, subsequently, 3 consecutive days in phase 6.

[9] Kelvin (Holt et al., 2022; Kawatani et al., 2010; Wallace and Kousky, 1968; Yang et al., 2011), gravity (Kawatani et al., 2010; Lindzen and Holton, 1968) and mixed Rossby–gravity (Holt et al., 2022; Wallace and Kousky, 1968; Yanai and Maruyama, 1966; Yang et al., 2011) waves also impact on the QBO, but we are interested in Rossby waves in the context of MJO teleconnections.

[10] Models displayed in Figure 1.14 taken from the WCRPs subseasonal-to-seasonal (S2S) project (Feng and Lin, 2021).

[11] Song and Wu (2020*b*) analyse the response of the AO to the MJO, rather than the NAO. The result is equivalent, though, since the NAO can be viewed as the Atlantic basin manifestation of the AO.

Chapter 2

Extratropical response to the Madden–Julian Oscillation in a General Circulation Model[1]

2.1 Introduction

The NAO is a key mode of winter variability in northern Europe. Thus, understanding the behaviour of the NAO is key to accurate UK weather prediction. The NAO is characterised by a positive and a negative phase, which bring different types of weather to the UK. During the winter, the NAO+ is associated with warmer, stormier weather, while the reverse relationship is observed for the NAO−.

The PNA, meanwhile, modulates the weather of North America, making it central to weather prediction in the United States and Canada. Like the NAO, the PNA is characterised by a positive and a negative phase. PNA+ brings warmer weather to Canada and the northern United States, with colder weather in the southeastern United States and northern Mexico.

Through observational studies, the NAO (Cassou, 2008; Lin et al., 2010), and PNA (Seo and Lee, 2017), are known to be forced at least in part by the MJO. In this chapter, we will assess the fidelity of these teleconnections in the latest global coupled model from the UK Met Office.

2.2 The HadGEM3–GC3.1 model

We analyse the Met Office Hadley Centre Global Environment Model in the Global Coupled configuration 3.1 with a medium resolution atmosphere and ocean (HadGEM3–GC3.1–MM; HadGEM3 hereafter). For a full description of the model and historical experiment, see Williams et al. (2018) and Andrews et al. (2020), respectively. This model formed part of the sixth phase of the Coupled Model Intercomparison Project (CMIP6) – a collaboration between climate modelling centres from around the globe with the goal of standardising coupled model experiments. In particular, we will focus on the 'historical' experiment runs, which used the CMIP6 defined forcings. This allows for an

assessment of MJO teleconnections in contemporary climate conditions. The historical experiment runs from 1850 to 2014 (inclusive), but we will focus on the final 30 years of this period (1985–2014) to align with the availability of high-quality reanalysis data.

2.3 Methodology

In order to analyse the MJO and its effects, we use the index created by Wheeler and Hendon (2004). This index is constructed from daily mean values of OLR and zonal wind at the 200- and 850-hPa pressure levels ($U200$ and $U850$, respectively). Due to the availability of model wind data in CMIP6, we will use 250-hPa zonal wind ($U250$) instead of $U200$, although analysis has shown that this has little qualitative effect on the outcomes. On each day, the index assigns a value for the MJO amplitude and phase. The amplitude is a positive number which describes the strength of the anomalous convection. On days when the amplitude is greater than one, the MJO is said to be active and this day will be included in our analysis. The phase takes an integer value between one and eight and describes the longitudinal location of the convective centres. Figure 2.1 shows boreal winter (November–April) composites of OLR (which is used as an analogue for convection) in each of the eight phases. For example, phase 1 (Figure 2.1a) represents enhanced convection over the western IO and phase 8 (Figure 2.1h) represents enhanced convection over the mid to eastern Pacific Ocean. RMM indices are calculated separately for the reanalysis and model, using their respective OLR, $U250$ and $U850$ data.

The NAO can be characterised by the difference in anomalous pressure between Iceland and the Azores. Therefore, we define our index as the normalised difference between two area averages of 500-hPa geopotential height ($Z500$) anomaly[2]. The two areas are chosen to suitably encompass the centres of the pressure variation (50–70 °N, 10–50 °W and 30–45 °N, 5–55 °W). This method of calculating the NAO index is similar to that of Cropper et al. (2015).

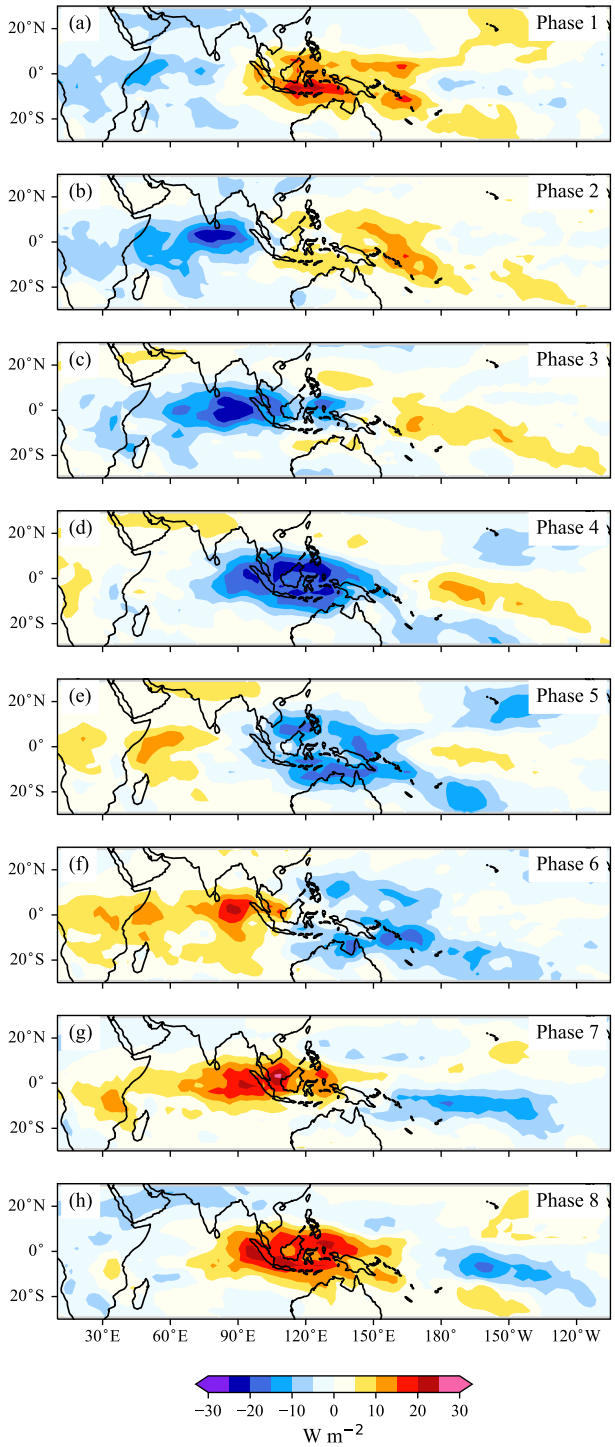

Figure 2.1: Boreal winter Madden–Julian Oscillation phase composites of OLR anomaly over the period 1985–2014 in HadGEM3. Here, a negative anomaly in OLR is analogous to increased anomalous convection.

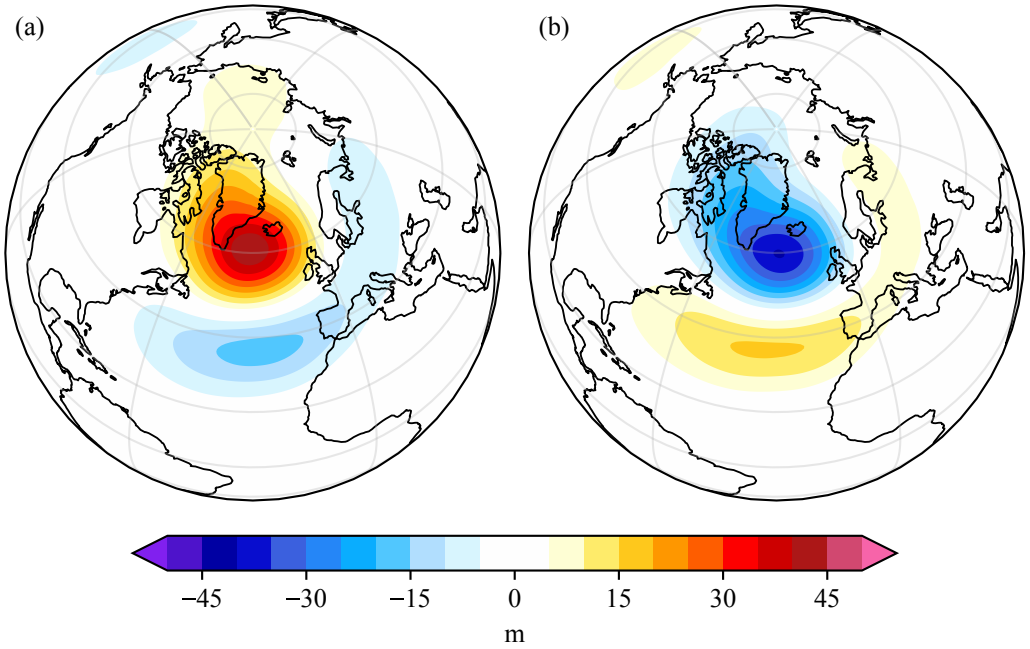

Figure 2.2: Boreal winter (a) NAO− and (b) NAO+ $Z500$ anomaly composites over the period 1985–2014 in HadGEM3.

However, we average the geopotential height anomaly over a larger area to account for the fact that the centres of action can be shifted in models. Our index is a time series, in which each day is either defined to be 'NAO+', 'NAO−' or 'inactive' depending on whether the index exceeds one standard deviation in magnitude and whether its sign is positive or negative. As for the MJO, we can create boreal winter composites to visualise the positive and negative NAO regimes (Figure 2.2). Note that this index is slightly different to that used by Cassou (2008) as we are focussing solely on the NAO in the NA region.

The PNA produces a 'chequerboard' pressure pattern over the NP and North America, with PNA+ characterised by a deepened AL and low pressure over Florida, with corresponding highs over western Canada and Hawaii. The two northernmost nodes (Over western Canada and the Aleutian islands) are dominant, with less variability in the southern nodes. For this reason (and to be consistent with our NAO index), our PNA index is also defined as the normalised difference between two area averages of $Z500$ anomaly (45–70 °N, 80–125 °W and 40–65 °N, 130 °W–150 °E). Positive and negative phases of the

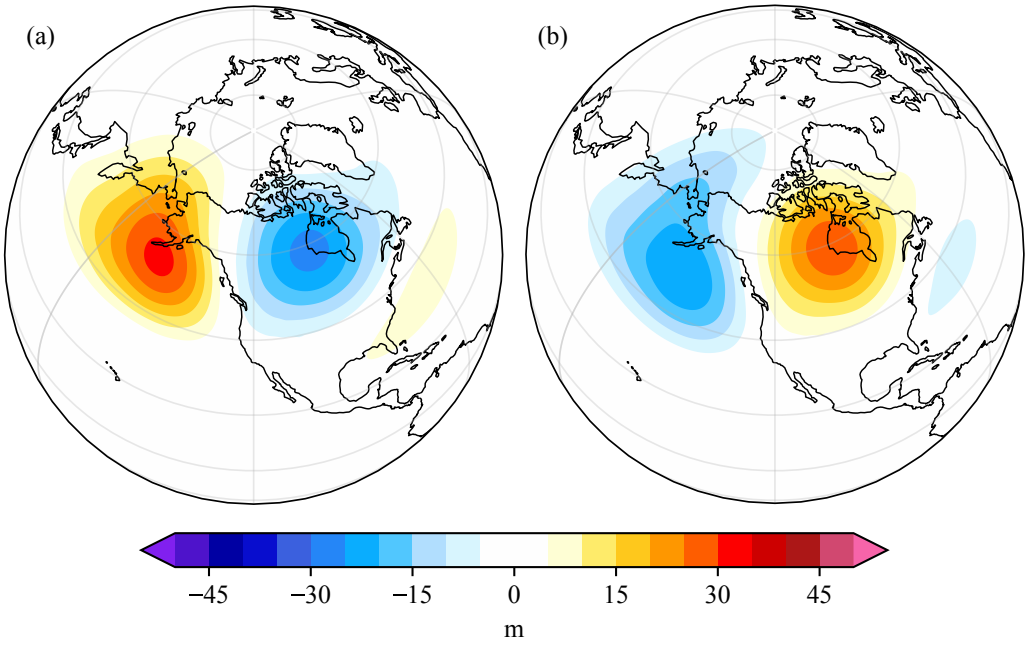

Figure 2.3: Boreal winter (a) PNA− and (b) PNA+ $Z500$ anomaly composites over the period 1985–2014 in HadGEM3.

PNA are classified in the same way as the NAO. $Z500$ composites for PNA− and PNA+ are presented in Figure 2.3.

With time series for both the MJO phase and the states of the NAO and PNA, the link between the tropics and extratropics may then be analysed. Following Cassou (2008), we calculate the frequency of days in which an NAO (or PNA) state is active for each MJO phase in turn. We then obtain a percentage change in the probability of observing each state from the climatological mean probability when a given MJO phase is active. This is then repeated with a lag (MJO leading) of 1–20 days to ascertain how the NAO and PNA respond in the days and weeks following each MJO phase.

To test for statistical significance in the frequency of an NAO or PNA state's occurrence, we employ a Student's t-test at the 95% confidence level. The population dataset is taken to be the value of the normalised extratropical index over the whole time domain, while the sample dataset consists of only the days that fall within the given MJO phase (with some given lag). The relative frequency of each extratropical state is then compared between the population

and sample. This is equivalent to the second of the two significance tests used by Cassou (2008). We have not used the first significance test from Cassou (2008) due to differences in methodology, as we do not assign every day in our analysis to either NAO+ or NAO− (or, in the case of the PNA, PNA+ or PNA−).

The model is compared with reanalysis data taken from the ERA-Interim reanalysis product ($U250$, $U850$ and $Z500$) and the NOAA–interpolated OLR dataset. The above analysis is applied to both the model and reanalysis data so that differences between the two may be assessed. Other reanalysis products provide similar representations of the MJO (Gao et al., 2016).

2.4 Results

The results of our analysis into the NAO response to each MJO phase for both the model and reanalysis data are presented in Figure 2.4. We note that both the magnitude and rate of change of the response are of interest, as the magnitude indicates the strength of the NAO response, while a steep gradient indicates a more direct link between the given MJO phase and NAO state. There are strong responses (over 30% change in probability of observing either NAO+ or NAO−) to a number of MJO phases in the model, which are statistically significant compared to the climatological mean. In general, the NAO response to the MJO in the HadGEM3 model is often of the same sign as the NAO response to the MJO in the reanalysis (Figure 2.4). The model replicates the reanalysis response particularly well in a small number of cases (phases 1 and 8).

However, there are other MJO phases in which the NAO response is either suppressed or even of the wrong sign, particularly at lags of more than one week. Two key teleconnection patterns identified by Cassou (2008), which are visible in the reanalysis data, are the responses of NAO+ and NAO− to MJO phases 3 and 6, respectively (Subsection 1.2.3). Both of these teleconnections

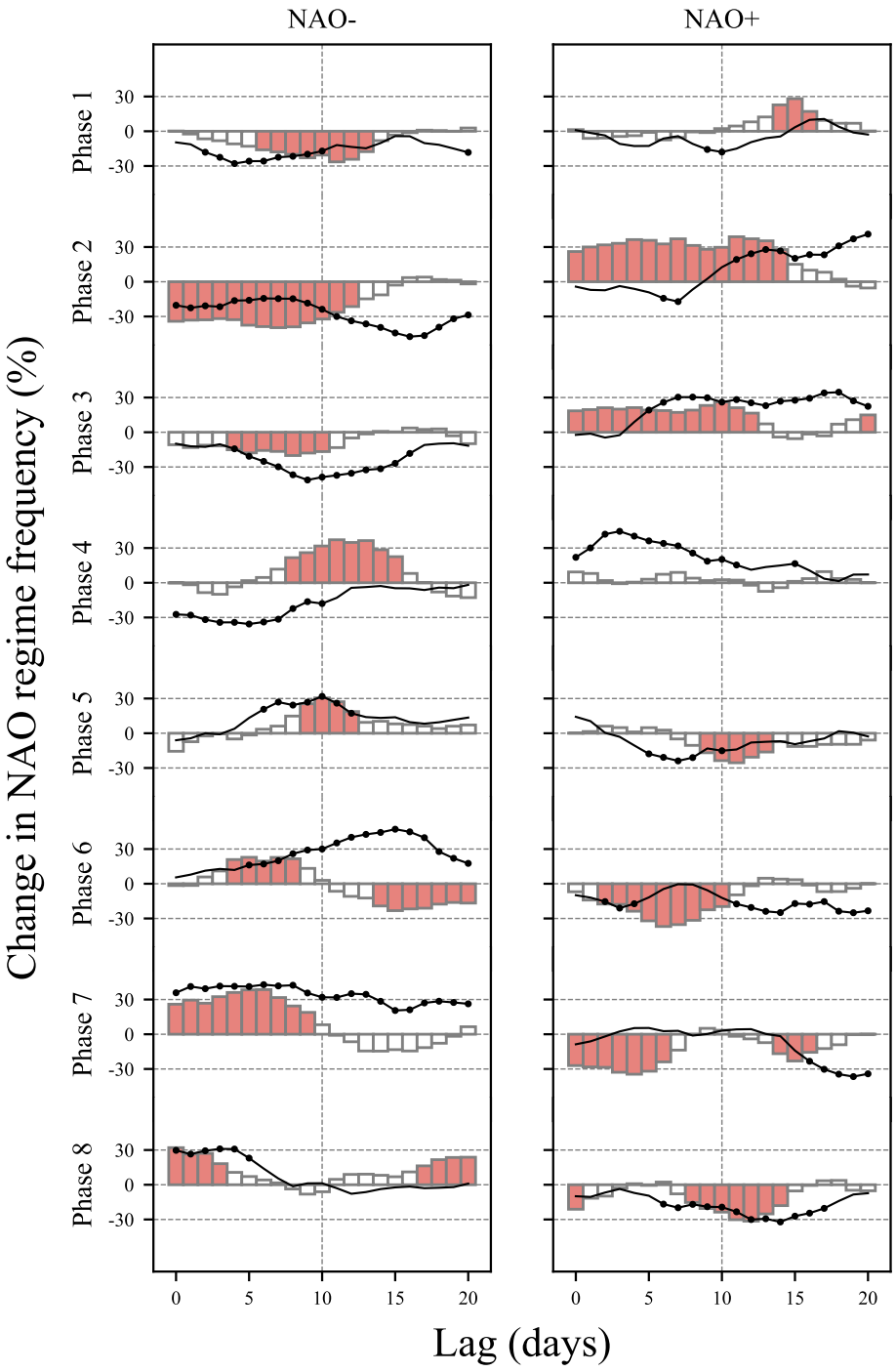

Figure 2.4: NAO response to the MJO. The bars represent the percentage change in the probability of observing a particular NAO state, at a given lag after observing a particular MJO phase, in the HadGEM3 model. Bars which are coloured in red represent a change which is statistically significant at the 95% level. The NAO response to the MJO in the reanalysis data is plotted as the black line, with circular markers to indicate significance.

act as useful predictors for the NAO state and so are the focus of our investigation.

In the reanalysis data, the lag 0 NAO+ response to MJO phase 3 is zero (i.e. climatological probability of observing NAO+). After approximately one week, the probability of occurrence of NAO+ rises by more than 30%, implying predictability of entering an NAO+ regime. However, in the model, the chances of experiencing an NAO+ event are approximately constant from lag 0 onwards, at 20% higher than the climatological mean. It is encouraging that the model at least predicts the correct sign for the response; however, the time dependence of this link is not well reproduced by the HadGEM3 model.

There is a strong NAO− response to MJO phase 6 in the reanalysis data. In this case, the response peaks approximately two weeks after phase 6 and exhibits a 47% increase in NAO− occurrence, suggesting phase 6 as a precursor to an NAO− event. The model replicates the response well for approximately one week. However, at longer lags, it shows a statistically significant decrease in the probability of NAO−. The reasons for the difference should be explored further.

In the reanalysis results we see that, for the most part, the NAO response to one MJO phase approximately follows on from the response to the preceding phase, but lagged by 5–10 days. This indicates that the eight MJO phases are occurring in a sequential manner as we would expect. For example, in MJO phase 4, the NAO+ response peaks at lag 3 days, while in phase 3, it peaks at lag 8 days. In the model, this is not the case, as we see no significant NAO+ response to MJO phase 4. The relationship between these two phases seems to be much weaker, indicating that the model MJO may not be behaving as observed.

MJO events spend less time in each phase in the model than in reanalysis (Figure 2.5a), so we may infer that the MJO propagation is faster in the model. The time-scales over which the MJO propagates are very similar to the timescales over which the extratropics responds to the MJO (that is, the time that the MJO spends in each phase is similar to the lag between changes in the

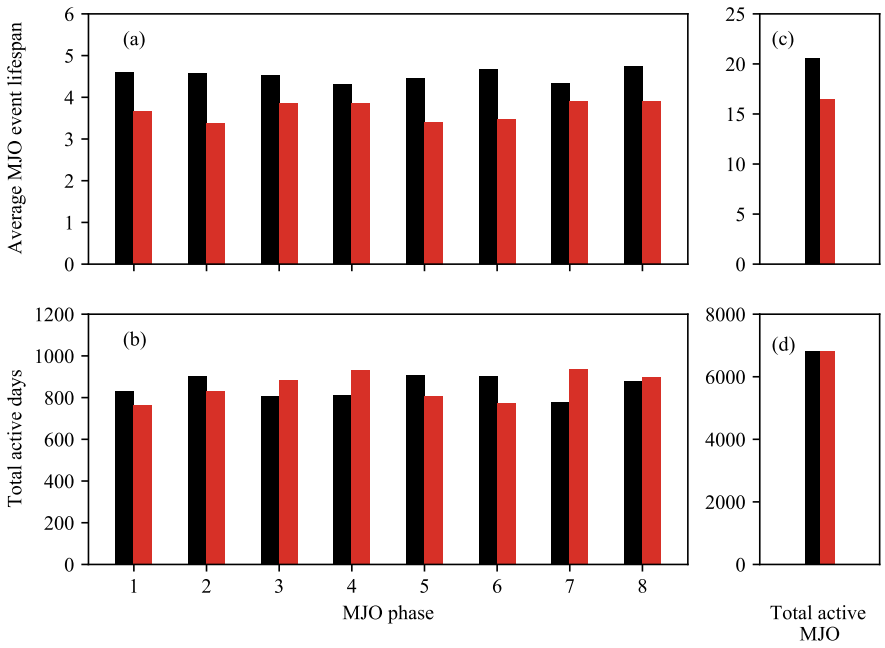

Figure 2.5: Reanalysis (black) and HadGEM3 (red) average MJO event lifespan (a) by phase and (c) overall, and total MJO active days (b) by phase and (d) overall, over the time period 1985–2014. Although the MJO propagates faster in the model (as shown by shorter average event lifetimes), the total number of days spent active in each phase and overall is similar between the model and reanalysis.

MJO and NAO). Therefore, a change to the propagation speed of the MJO means that the NAO response to a given phase will occur within a different atmospheric state. Both Yadav and Straus (2017) and Yadav et al. (2019) have shown that these changes in MJO propagation speed can alter the NAO response to the MJO. They find that both the NAO response to the MJO is predominantly a result of slower moving MJO events, hence this apparently fast moving MJO in the HadGEM model could help to explain the weak teleconnection. It is likely that this is one reason why some of the sequential manner of the NAO response is lost. Interestingly, the total number of days spent in each MJO phase is similar between the model and reanalysis, suggesting that although the MJO is propagating faster, there are also more individual events (Figure 2.5b).

Among other reasons for this seeming lack of continuity is a stalling or dissipation

of the MJO as it propagates over the MC, which can directly impact on the extratropical response observed (Zhou et al., 2023). Ahn et al. (2020) showed that the HadGEM3 model performs well compared to other CMIP6 models in capturing the MJO propagation over the MC, and this has been backed up by our own investigations. We have shown that although the MJO is propagating faster in the model than reanalysis, this difference is approximately the same across all eight MJO phases rather than being confined to those phases in which the MJO is passing over the Maritime Continent. This should be considered when analysing other models.

Turning to the PNA, we again see that the response from HadGEM3 is reasonable in many cases, however there some phases in which the response is less well captured (Figure 2.6). The canonical responses of PNA− after phases 2–3 and PNA+ after phases 6–7 are well represented in the model (in the case of PNA+, even more clearly than in reanalysis).

The response of PNA−, whist smaller in magnitude than the response in PNA+[3], is generally well represented in HadGEM3 (aside from some difficulty with MJO phases 5 and 6). The responses are of reasonable magnitude and are generally of the correct sign (particularly where the responses are significant).

Interestingly, the PNA− response from the model actually seems to be larger than in reanalysis, with the exception of MJO phase 1. This is contrary to our results for the NAO and the consensus around weak tropical–extratropical teleconnections in models.

The PNA+ response to the MJO paints a slightly puzzling picture. The gradients of the response as a function of lag appear to be well modelled, however for some phases we see a positive (phase 6) or negative (phase 2) shift in the response. The fact that the gradients are largely correct suggests that the mechanisms behind the MJO–PNA teleconnection are well modelled, since it is the gradient that points to the direct effect of the MJO on the PNA.

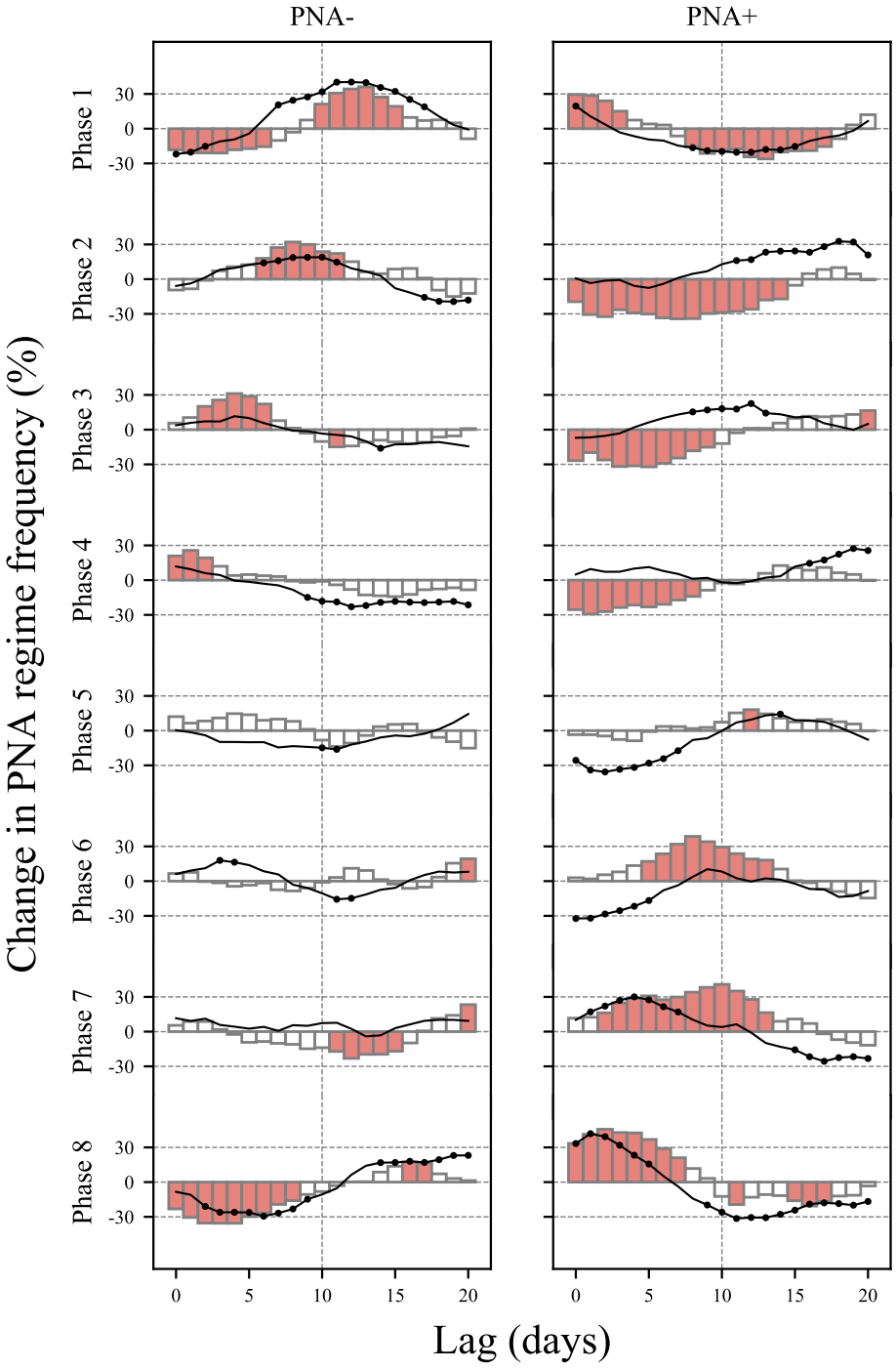

Figure 2.6: PNA response to the MJO. As in Figure 2.4, but for the PNA.

There are many reasons why there may be a shift in the response. In the reanalysis, the likelihood of PNA+ after MJO phase 2 begins at approximately the climatological level at lag 0, before rising to a roughly 30% increase in frequency after two weeks. Meanwhile, in the model, we begin with a 30%-less-than-average chance of observing PNA+ at lag 0. This suggests that some precursor to MJO phase 2 is inhibiting the formation of the PNA+ regime in the model. Looking to phase 1, though, it is clear that the model does a good job of modelling the response. A similar situation is true for phase 6, but this time with the model failing to capture the lower likelihood of PNA+ at lag 0. In this case, the response to the preceding phase (phase 5) is poorly modelled, which would go some way to explaining the error.

It is also possible that our index is not fully capturing response in both the model and reanalysis. The reason for choosing this index (rather than, for example, an EOF analysis) is that it allows for some differences in the exact representation of the PNA pattern, however it does open the possibility that other unwanted signals may also be included. Also, whilst the PNA is a natural mode of variability in the atmosphere, the MJO teleconnection will not necessarily project onto the PNA directly. In fact, Seo and Lee (2017) showed that whilst a PNA-like pattern is observed after MJO phase 2, this pattern does not exactly match the PNA. Differences in how closely the model and reanalysis responses project onto the PNA, even if they are both representing the same mechanisms, could cause the shift we see.

2.5 Discussion

We have shown that HadGEM3 exhibits a significant extratropical response to the MJO, but that this response is not always in line with that seen in reanalysis. This includes NAO responses in some phases which are too weak or the wrong sign, and PNA responses that show the correct gradient, but are positively or negatively shifted. We may, therefore, question the model's ability to predict

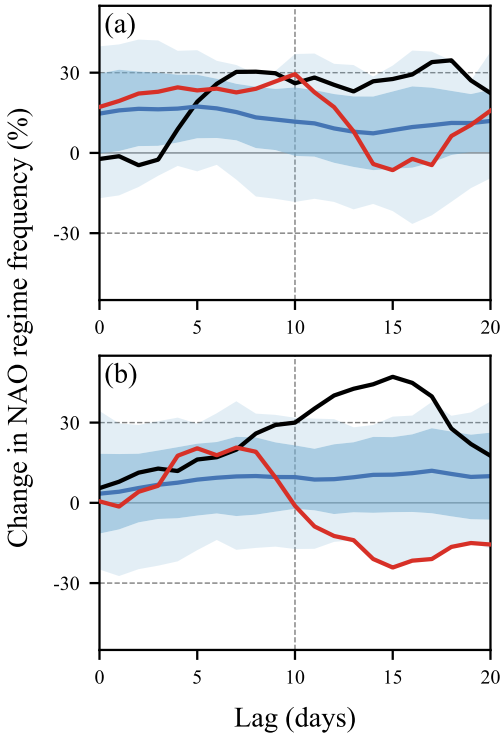

Figure 2.7: (a) NAO+ response to MJO phase 3 and (b) NAO− response to MJO phase 6. The blue line represents the multi-model mean from 25 CMIP6 coupled climate models, with a band of ±1 standard deviation given by the dark blue shading and the multi-model range given by the light blue shaded region. The HadGEM individual model response is shown by the red line and the reanalysis response is shown by the black line.

the extratropical circulation at lead times of more than one week when tropical–extratropical interactions become important, whilst being mindful of the fact that the MJO is only one of many sources of tropical teleconnections to the extratropical NH (Scaife et al., 2017). The results presented above pertain to just one model. However, by analysing an ensemble of models from the CMIP6 project, we may hope to find a more accurate representation of the extratropical response to the MJO.

Figure 2.7 shows the two key teleconnections (NAO+ response to MJO phase 3 and NAO− response to MJO phase 6) discussed above for the reanalysis and HadGEM3 datasets, alongside a summary of 25 CMIP6 models (Table 2.1). The

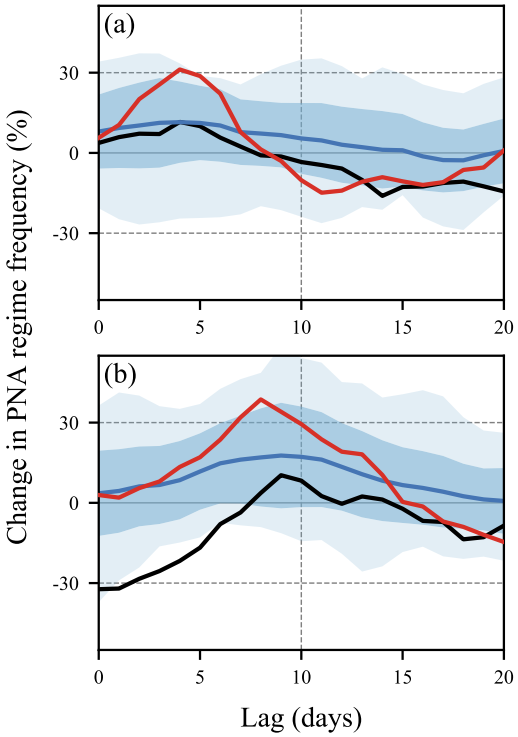

Figure 2.8: (a) PNA− response to MJO phase 3 and (b) PNA+ response to MJO phase 6. The blue line represents the multi-model mean from 25 CMIP6 coupled climate models, with a band of ±1 standard deviation given by the dark blue shading and the multi-model range given by the light blue shaded region. The HadGEM individual model response is shown by the red line and the reanalysis response is shown by the black line.

responses were calculated in the same way for each model as they were for the HadGEM model (see Section 2.3). The MJO and NAO indices are separately calculated for each model and the response in each model is calculated before these responses are then averaged. We find that the majority of the models, including HadGEM3, significantly underestimate the magnitude of the response of the NAO. Even the most extreme response from the models (shown by the light blue shading in Figure 2.7b) cannot simulate the large observed response in NAO− to MJO phase 6. This is in agreement with previous works that have highlighted weakened teleconnections in climate models (Garfinkel et al., 2022; Scaife and Smith, 2018; Vitart, 2017).

The PNA− response to MJO phase 3 is well represented by CMIP6 models (Figure 2.8a), with the reanalysis response falling within one ensemble standard deviation at almost all lags. HadGEM3 tends to overestimate the increase in PNA− frequency in the week after phase 3, producing one of the largest model responses. It does, however, accurately capture the positive-negative switch in likelihood around day 8.

All CMIP6 models appear to show the same positive shift in the PNA+ response to MJO phase 6 that was discussed in Section 2.4. This suggests either a fundamental gap in our ability to model the MJO–PNA teleconnection, or a systematic error produced as a result of our methodology.

2.6 Conclusions

To accurately simulate MJO teleconnection patterns, models must first have accurate representations of the MJO, the climatological mean state (Henderson et al., 2017; Zheng and Chang, 2020), wave trains, and the stratospheric polar vortex (Barnes et al., 2019). The complexity of these processes and linkages between them make the MJO teleconnection problem challenging to model. Even though the HadGEM3 model performs well among CMIP6 models in simulating the MJO propagation over the MC (Ahn et al., 2020), this is countered by the excessive speed of the MJO propagation. Hence, it is still unable to simulate the full range of processes needed to accurately model MJO teleconnections. In this study we examine the extratropical response to the MJO, but the representation of the extratropics will also affect the MJO itself, as discussed in Section 1.4. Biases in the extratropical mean state may also be a source of the discrepancy between the reanalysis and model teleconnections, so in the coming chapters the effect of decadal scale changes in the extratropics will be examined.

It is also clear that whilst the statistical framework used throughout this

Table 2.1: A summary of the CMIP6 models to produce Figures 2.7 and 2.8. The HadGEM3 model used throughout this chapter is shown in bold.

Centre/Institute	**Model**	**Reference(s)**
AS–RCEC	TaiESM1	Lee and Liang (2020); Lee et al. (2020*b*)
AWI	AWI–ESM–1–1–LR	Danek et al. (2020); Semmler et al. (2020)
BCC	BCC–ESM1	Wu et al. (2020); Zhang et al. (2018)
CAS	FGOALS–g3	Li (2019); Li et al. (2020)
CCCma	CanESM5	Swart et al. (2019*a*,*b*)
CCCR–IITM	IITM–ESM	Krishnan et al. (2021); Raghavan and Panickal (2019)
CNRM–CERFACS	CNRM–CM6-1	Centre National de Recherches Météorologiques and Centre Européen de Recherche et Formation Avancée en Calcul Scientifique (2019); Voldoire (2018); Voldoire et al. (2019)
	CNRM–ESM2–1	Séférian (2018); Séférian et al. (2019)
CSIRO–CCSS	ACCESS–CM2	Bi et al. (2020); Dix et al. (2019)
EC–Earth–Consortium	EC–Earth3	Döscher et al. (2021); EC-Earth, (2019)
INM	INM–CM4–8	Volodin et al. (2019*a*, 2018)
	INM–CM5–0	Volodin et al. (2019*b*, 2017)
IPSL	IPSL–CM6A–LR	Boucher et al. (2018, 2020)
MIROC	MIROC6	Tatebe et al. (2019); Tatebe and Watanabe (2018)
MOHC	HadGEM3–GC3.1–LL	Andrews et al. (2020); Kuhlbrodt et al. (2018); Ridley et al. (2019*a*); Williams et al. (2018)
	HadGEM3–GC3.1–MM	Andrews et al. (2020); Ridley et al. (2019*b*); Williams et al. (2018)
	UKESM1.0–LL	O'Connor et al. (2021); Sellar et al. (2019); Tang et al. (2019*a*,*b*)
MPI	MPI–ESM1–2–LR	Mauritsen et al. (2019); Wieners et al. (2019)
	MPI–ESM1–1–HR	Jungclaus et al. (2019); Müller et al. (2018)
MRI	MRI–ESM2–0	Yukimoto et al. (2019*a*,*b*)
NCAR	CESM2	Danabasoglu (2019*b*); Danabasoglu et al. (2020)
	CESM2–FV2	Danabasoglu (2019*a*); Danabasoglu et al. (2020)
	CESM2–WACCM	Danabasoglu (2019*c*); Danabasoglu et al. (2020)
NIMS–KMA	KACE–1–0–G	Byun et al. (2019); Lee et al. (2020*a*)
NOAA–GFDL	GFDL–CM4	Guo et al. (2018); Held et al. (2019)

chapter, which was inspired by Cassou (2008), does not capture the full extent of the extratropical response to the MJO. Whilst the interaction of the MJO with weather regimes such as the NAO and PNA produces a neat and concise representation of MJO teleconnections for prediction purposes, they do not paint the full picture. Hence, when assessing changes in the extratropical response to the MJO, we should take care to assess the whole teleconnection pattern, rather than its projection onto particular regimes.

The goal of this chapter was to answer the question '*How well do climate models simulate the extratropical response to the MJO?*'. We have assessed the ability of the UK Met Office coupled climate model (HadGEM3–GC3.1–MM) to simulate the NAO and PNA responses to the MJO at lead times of 1–2 weeks and show that, whilst elements of the teleconnection are well represented, improvements are needed in the modelling of extratropical response to the MJO.

Notes for Chapter 2

[1] Parts of this chapter are adapted from the published paper 'North Atlantic Oscillation response to the Madden–Julian Oscillation in a coupled climate model' (Skinner et al., 2022).

[2] Both mean sea level pressure (MSLP; e.g. Hurrell, 1995; Visbeck et al., 2001; Walker and Bliss, 1932) and geopotential height (e.g. Cassou, 2008; Vitart, 2017; Wallace and Gutzler, 1981) are commonly used in NAO indices. In Appendix B, we show that the results obtained using $Z500$ are similar to those obtained when using MSLP in our index.

[3] This asymmetry in the responses of PNA+ and PAN− suggests that our PNA index may not be capturing the NP response to the MJO fully.

Chapter 3

Observed decadal variability of the extratropical response to the Madden–Julian Oscillation[1]

3.1 Introduction

In Chapter 2, we showed that General Circulation Models (GCMs) struggle to fully capture MJO teleconnections in their simulations (e.g. Wang et al., 2020*a*,*b*). Though some are able to recreate the patterns of the teleconnections, these responses are almost universally too weak (Lin et al., 2021; Skinner et al., 2022; Vitart, 2017). This is a common feature across tropical–extratropical interactions in climate models and seasonal forecasts (Garfinkel et al., 2022; Williams et al., 2023).

Deterministic weather prediction is skilful up to a lead time of approximately one to two weeks in the extratropics, however this lead time can be extended by considering the effects of modes such as the MJO (Kent et al., 2022; Nardi et al., 2020), QBO (Nardi et al., 2020) and ENSO (Patricola et al., 2020). The signature teleconnection patterns produced by these modes provide predictive skill on sub-seasonal to seasonal time scales. This skill, however, is dependent on the ability of models to reproduce the mechanisms and variability of teleconnections over a range of time scales.

ENSO is able to modulate the MJO (Chen et al., 2016; Hsu and Xiao, 2017; Kessler, 2001) and its teleconnections (Lee et al., 2019; Moon et al., 2011; Tseng et al., 2020*a*) on seasonal to interannual time scales (Subsection 1.4.2). However, there is little understanding of the variability of MJO teleconnections on decadal time scales. Furthermore, the extratropics have been shown to respond differently to remote forcing on interannual and decadal time scales (Seabrook et al., 2023).

In this study, evidence of decadal variability in the extratropical response to the MJO is presented, using ERA5 reanalysis data from 1974 (the start time of reliable MJO indices) to 2018. This variability is then compared with ENSO-modulated interannual variability. Finally, we discuss the impacts of changes in the response on the weather experienced in the extratropics.

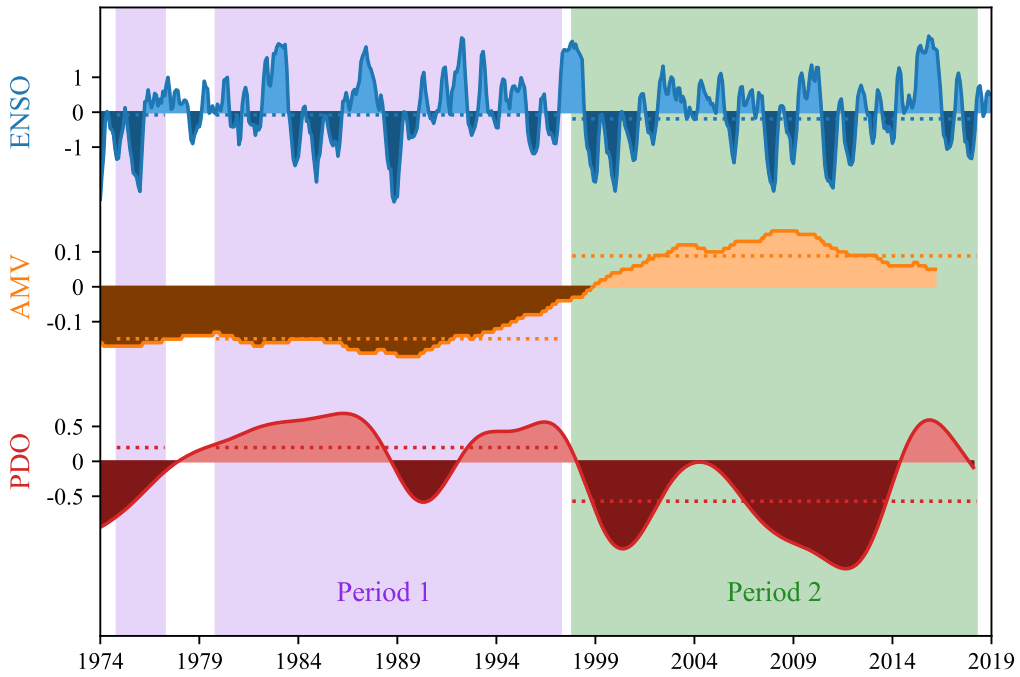

Figure 3.1: Values of ENSO, PDO and AMV indices over our time domain. Periods 1 and 2 are marked. Dotted lines show the average values of indices for each time period. We use the Niño 3.4 index, PDO index (on which we ran a 5 year low-pass filter) and AMO index (10 year low-pass filtered) from the NCAR Climate Data Guide (Appendix A).

3.2 Data and methodology

The MJO varies on interannual (Chen et al., 2016; Hsu and Xiao, 2017; Kessler, 2001) and decadal (Fu et al., 2020; Jones and Carvalho, 2006; Wu et al., 2021) time scales. The extratropical response to the MJO is dependent on the background state of the atmosphere (Henderson et al., 2017), which can also vary on interannual and decadal time scales. These variations can be caused by changes in external forcing or in low-frequency modes of internal variability. Two key modes of variability are AMV (Kerr, 2000; Trenberth and Shea, 2006) and the PDO (Mantua and Hare, 2002; Mantua et al., 1997; Newman et al., 2016). Over the observational time period of 1974–2018, AMV switches from its negative phase to positive phase around 1997 (Figure 3.1, orange line). The PDO displays greater variability but moves from favouring its positive phase to negative phase, also switching around 1997 (Figure 3.1, red line).

This leads us to consider changes in the extratropical response to the MJO between two non-overlapping segments: period one from 1974/75 to 1996/97, and period two from 1997/98 to 2017/18. Subsequent analysis is restricted to boreal winter (November–April) as this is when the MJO (and its teleconnections) are at their strongest (Jenney et al., 2019; Stan et al., 2017), and only considers full winter seasons. Due to an interruption in OLR data availability (Liebmann and Smith, 1996), there is no MJO index for 1978, so the 1977/78 and 1978/79 seasons are omitted. Hence our two time periods are of equal length at 21 winter seasons.

200-hPa streamfunction ($\psi 200^{[2]}$) anomalies are derived from ERA5 wind data. Anomalies are calculated by removing the mean and first three harmonics of the annual cycle from the daily averaged ERA5 data. Annual cycles are calculated and removed separately for each time segment, so that the two periods may be considered independent samples. By removing separate annual cycles, the changes observed in the extratropical response to the MJO are due to changes in the interaction of the MJO with the mean state (i.e., the MJO teleconnection patterns), rather than changes in the mean state itself.

The MJO is diagnosed by the RMM index, described by Wheeler and Hendon (2004), which is available from 1974 to present (Bureau of Meteorology, 2021). The RMM index produces two values: a phase and amplitude. The phase, given by an integer between 1 and 8, signifies the zonal location of the centres of anomalous MJO convection. Phase 1 indicates enhanced convection over the western IO, then, through eastward motion of the MJO, phases 2–3, 4–5, and 6–7 signify enhanced convection over the eastern IO, MC and western Pacific respectively. By phase 8, the enhanced convection has moved into the eastern Pacific and dissipates, whilst simultaneously reforming in the western IO. The amplitude indicates the relative strength of this anomalous convection.

10-day lagged composite maps of $\psi 200$ anomaly are produced for each MJO phase, taking only days in which the MJO is 'active' (defined as amplitude greater

than 1). Note that all active days are included for each MJO event, not just the first day in each phase. The 10-day lag was chosen since the NAO and PNA response to the MJO peaks between 5 and 15 days for most MJO phases (see Figures 2.4 and 2.6). Composites were plotted at a range of lags, with the 10-day lagged composites generally showing the most robust signal, hence that have been displayed below. Statistical significance in the difference between lagged composites in the two periods is assessed using a two-tailed, two-sample t-test at the 95% significance level.

To assess the impact of upper tropospheric circulation changes on meteorological conditions, 10-day lagged MJO composite maps of 850-hPa temperature ($T850$) and precipitation anomalies are also created. $T850$ anomalies are derived from daily-averaged ERA5 data. Precipitation anomalies are derived from CMAP pentad-mean data, which have been interpolated to daily data.

MJO teleconnection patterns are strongest in the winter (Northern) Hemisphere, so results are presented over this domain. Discussion will be made within the context of societal impacts, so will focus on regions which are densely populated, or which impact on key weather patterns such as the NAO.

3.3 Decadal variability of the background state

Period one is characterised by AMV− and PDO+, whilst in period two the reverse is observed. The signatures of AMV and the PDO are visible in November–April mean HadISST SSTs (Figure 3.2a). Whilst the change in AMV state is statistically significant at the 95% confidence level, the PDO SST pattern is only significant in the warm western and central NP but not in the cold eastern NP. There are changes in the upper tropospheric zonal wind (Figure 3.2b), where, as expected, there are changes in the subtropical jets (Matsumura and Horinouchi, 2016; Ruggieri et al., 2021). The northern hemisphere jet exhibits a general poleward shift in period two, particularly over the NP, highlighted by a positive

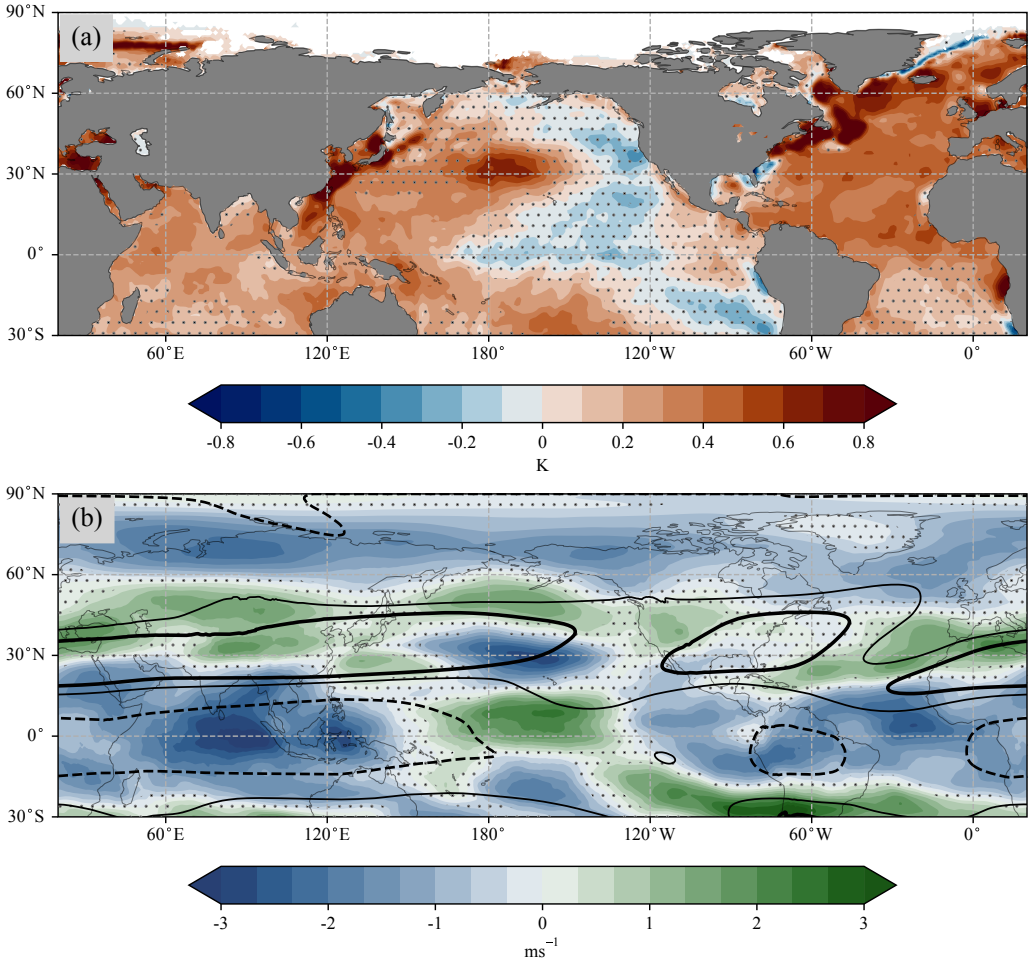

Figure 3.2: Change in boreal winter (November–April) mean (a) SST and (b) $U200$: period two (1997/98–2017/18) minus period one (1974/75–1996/97). Stippling shows the regions in which this difference is not significant at the 95% confidence level, based on a two-sample, two-tailed t-test. Period two mean $U200$ is plotted at $0\,\mathrm{ms}^{-1}$ (dashed black contour), $20\,\mathrm{ms}^{-1}$ (thin black contour), and $30\,\mathrm{ms}^{-1}$ (thick black contour) in panel (b) for reference.

(negative) change in $U200$ to the northern (southern) flank of the mean period two jet position (Figure 3.2b).

Around the MC there is evidence of a strengthened Gill-type response (Gill, 1980, see the negative (positive) shift in $U200$ to the west (east) of the MC in Figure 3.2b) in the period two circulation due to SST warming in the IO and western Pacific, which in turn leads to enhanced convection. This warming is consistent with PDO− (see western Pacific; Mantua and Hare, 2002) and with a global warming signal (see IO; Ruela et al., 2020). To the west of the MC the equatorial

easterly anomalies and off-equatorial westerly anomalies are consistent with twin anticyclones, indicating an enhanced equatorial Rossby wave response, whilst to the east of the MC an enhanced equatorial Kelvin wave response can be seen in amplified westerlies near the equator.

Changes in SST patterns, both in the tropics and extratropics, and the corresponding changes in the upper troposphere together provide a different mean state with which the MJO and its teleconnections will interact. These changes are the combined result of both internal variability (i.e. AMV and the PDO) and long-term trends. In the present study, these changes are treated as a whole, due to the relatively short length of the dataset. Future studies, making use of climate models, may have an opportunity to untangle the effects of individual mean state variations.

We assess changes in the mid-latitude jets by considering the stationary Rossby wavenumber, K_s (Equation 1.2). Since Rossby waves usually propagate in the upper troposphere, K_s is calculated at 200 hPa. Rossby waves are refracted towards regions of high K_s (Dawson et al., 2011; Hoskins and Ambrizzi, 1993), so local maxima in K_s can be approximated as Rossby waveguides. This approximation relies on the crude assumption that the scale of the Rossby waves is much smaller than the scale of changes in the mean state (Hoskins and Ambrizzi, 1993; Hoskins and Karoly, 1981; Karoly, 1983), however it works well in a qualitative sense.

There is relatively little qualitative change in the NA waveguide (Figure 3.3), however a local minimum in K_s around 30 °N, 140 °W in period two diverts the NP waveguide towards British Columbia and central Canada. During period one, however, this waveguide merges into the NA waveguide. The effect of this diversion in the waveguide is an amplified teleconnection over Canada and stronger Rossby wave response passing over Greenland into the NA.

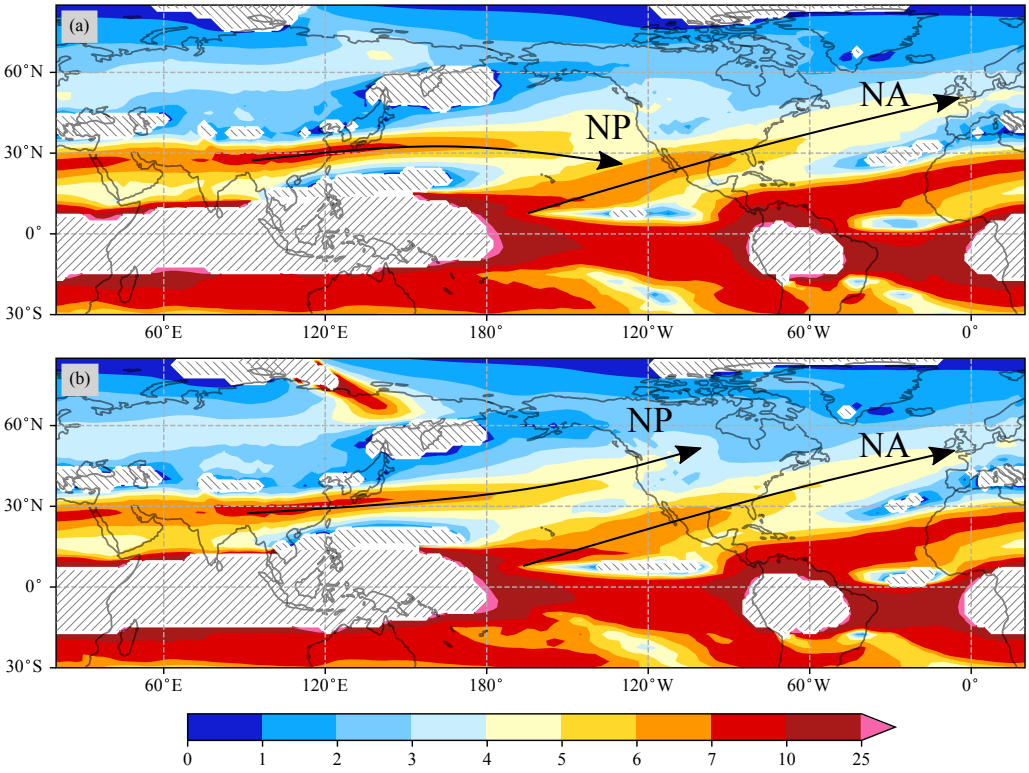

Figure 3.3: Boreal winter (November–April) 200-hPa stationary Rossby wavenumber, K_s, for (a) period one (1974/75–1996/97) and (b) period two (1997/98–2017/18). Regions in which K_s is undefined, and Rossby waves are evanescent – that is, when $\overline{u} < 0$ or $\beta - \overline{u}_{yy} < 0$ – are denoted by hatching (//// and \\\\ respectively). Rossby waves will tend to follow local maxima in K_s, hence these maxima can be qualitatively viewed as Rossby waveguides. Two key Rossby waveguides, the North Pacific (NP), and North Atlantic (NA), are labelled.

3.4 Changes in the upper tropospheric response to the MJO

3.4.1 Decadal changes between periods one (1974/75–1996/7) and two (1997/98–2017/18)

Upper tropospheric divergence associated with anomalous MJO convection forms an anticyclonic anomaly either side of the equator, spanning the convective centre (Figure 3.4). The vorticity perturbation induced by this anticyclonic anomaly produces a stationary Rossby wave, characterised by alternating cyclonic and anticyclonic anomalies across the mid-latitudes. These broad features are visible

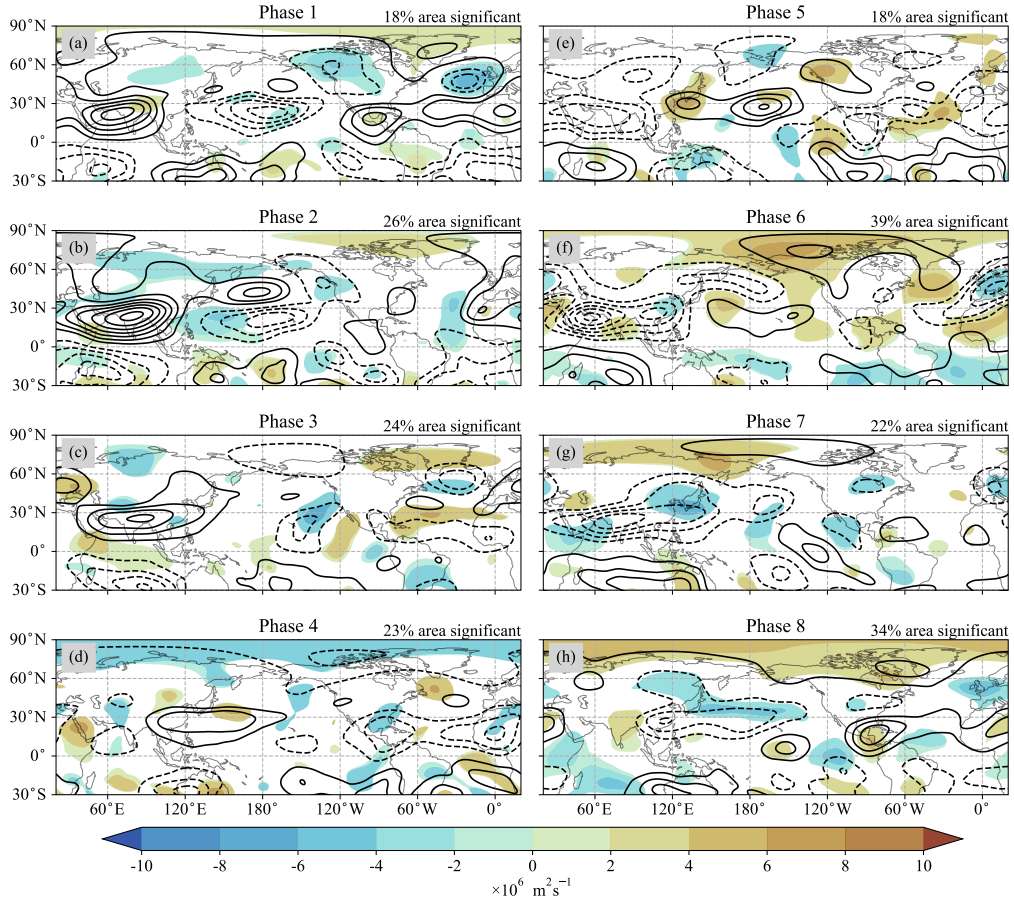

Figure 3.4: Lag 10-day composites of boreal winter (November–April) $\psi 200$ anomaly for each of the eight MJO phases. Thick black contours represent period two, and shading shows the difference – period two (1997/98–2017/18) minus period one (1974/75–1996/7) – wherever this difference is significant at the 95% level. The contour interval for both the line and shaded contours is $2\times10^6\,\mathrm{m^2s^{-1}}$, and dashed contours represent negative values. The zero contour has been omitted. The percentage of the spatial domain in which the difference is significant is stated in the top right of each panel.

in both period one and two; however, the strength and spatial structures of the Rossby wave trains have changed.

Over western North America there are substantial changes to the upper tropospheric circulation 10 days after MJO phases 1–2 and phases 5–6. In period two, the Rossby wave train initiated over the central NP after MJO phases 1–2 extends over Canada, producing an cyclonic (anticyclonic) anomaly over British Columbia after phases 1–2 (5–6). This feature is not observed in

period one. This change may be attributed to the deflection of Rossby waves into Canada as discussed in Section 3.3.

Continuing the Rossby wave train into the NA and Europe, we see the canonical NAO+ and NAO− responses (Subsection 1.2.3; Cassou, 2008) after phases 3 and 6 respectively. Most notably, we see a strengthened anticyclonic anomaly (corresponding to a weakening of the Icelandic Low) in the NA after phase 6. Whilst a broad cyclonic anomaly is present over southern Europe and the NA in period one, a strengthened and tilted cyclonic anomaly covers the entirety of Europe in period two. This anomalous low pressure centre (Figure 3.5) will bring polar air masses across western Europe, which are colder than the air advected from eastern Europe in period one. It also represents a strengthening of the NAO− response that we would expect to see following phase 6 (Cassou, 2008). Period two is characterised by AMV+ in the NA, which weakens the meridional temperature gradient across the NA, favouring NAO− conditions. This compounds and amplifies the NAO− response to MJO phase 6.

Overall, there are a considerable number of changes in the upper tropospheric circulation response to the MJO between periods 1 and 2. Now we compare these decadal variations against known interannual variability (Section 3.4.2) and assess the impacts of these changes (Section 3.5).

3.4.2 Interannual changes associated with ENSO

Whilst the MJO is the leading mode of tropical variability on sub-seasonal timescales, ENSO is the leading mode on interannual time scales. ENSO modulates MJO teleconnection patterns on interannual time scales (Subsection 1.4.2; Lee et al., 2019; Moon et al., 2011; Roundy et al., 2010; Tseng et al., 2020*a*), so it seems natural to compare this variability with the changes observed on decadal time scales. We expect to see some agreement because the ENSO SST pattern projects heavily onto the PDO SST pattern (the key difference being the relative strength of the North and tropical Pacific

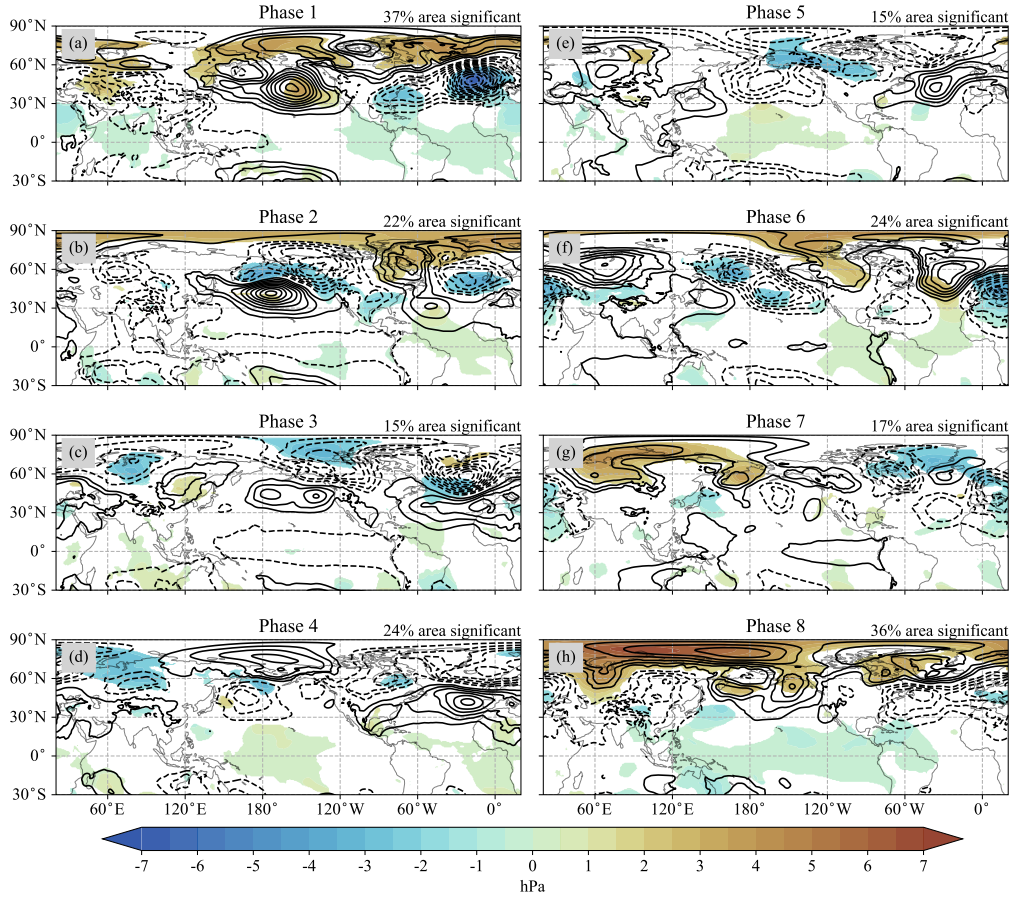

Figure 3.5: As in Figure 3.4, but for mean sea level pressure (MSLP). The contour interval for both the line and shaded contours is 0.5 hPa.

anomalies). On the other hand, there is evidence that the interaction between Pacific SST variability and the extratropics can be dependent on time scale (Seabrook et al., 2023). If the decadal variability discussed in Section 3.4.1 is an aliasing of the interannual ENSO variability, similar changes to the MJO response between El Niño and La Niña as between period one and two might be expected.

A key change to the response to the MJO between periods one and two is the formation of an anticyclonic (cyclonic) anomaly over British Columbia after MJO phase 1–2 (5) (Figure 3.4). A similar shift to a cyclonic anomaly is observed when moving from La Niña to El Niño after MJO phase 5 (Figures 3.6 and 3.7). This shift is in the opposite direction to that expected given the negative PDO tendency in period two. Also, after MJO phases 1 and 2 the circulation changes

over western Canada between La Niña to El Niño, however these changes display a different structure to those between periods one and two.

Over Europe, the largest change to the response to the MJO between periods one and two is the amplification and tilting of the anticyclonic anomaly observed after MJO phase 6. On the other hand, there is little difference between the responses over Europe in El Niño and La Niña years.

However, the spatial patterns of the decadal variability in the extratropical response to the MJO (Figure 3.4) and the interannual variability in the extratropical response to the MJO (Figures 3.6 and 3.7) take different forms. Even with the connection between the PDO and ENSO, there is no evidence that the observed decadal variability is due to aliasing of ENSO-modulated interannual variability.

3.5 Impacts of changes to MJO teleconnections

The observed changes in the upper tropospheric circulation response to the MJO between periods one and two will in turn lead to changes in the weather experienced in the extratropics[3]. 10-day lagged composites of $T850$ anomaly are calculated using ERA5 data (Figure 3.8). Similarly, CMAP precipitation data are used to create 10-day lagged composites of precipitation anomaly (Figure 3.9). Due to the availability of CMAP data, precipitation composites were calculated from 1979/80 to 1996/97 for period one and from 1997/98 to 2015/16 for period two.

The response in lower tropospheric temperature to the MJO in period two (black contours in Figure 3.8) is generally qualitatively consistent with previous studies (e.g. Figure 1 of Seo et al. (2016), and Figure 3 of Zhou et al. (2012), accounting for 1–2 phase shift as a result of the 10-day lag used here). There are some differences between the exact response to each MJO phase in these studies due to differences in the time domains and data sets used; however, our results match

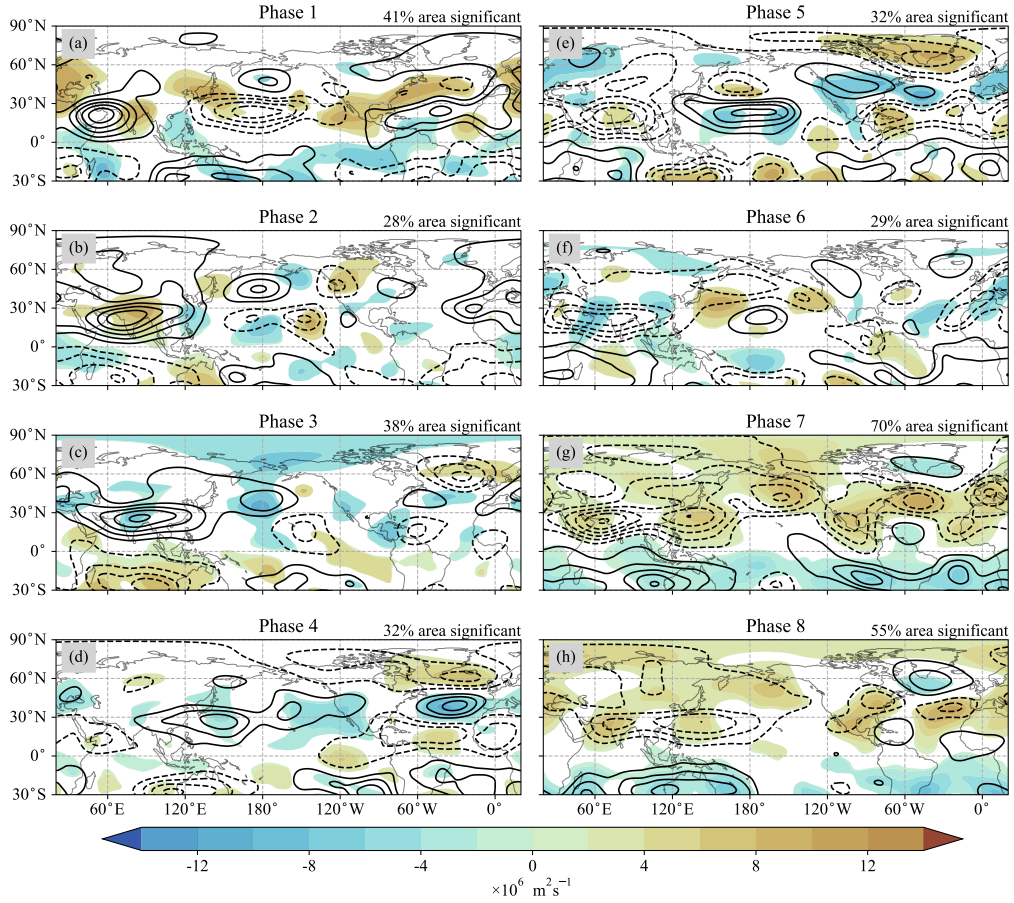

Figure 3.6: Lag 10-day ψ200 anomalies. As in Figure 3.4, but with black contours representing El Niño years, and shaded contours show the difference between El Niño and La Niña years (La Niña minus El Niño).

previous results to leading order.

There are significant and coherent changes in the lower tropospheric temperature response to the MJO from period one to period two. These changes are consistent with the differences observed in the upper tropospheric circulation response[4]. Where responses have changed significantly between periods one and two, this usually corresponds to a strengthening of the teleconnection (since the shaded difference tends to be of the same sign as the black contours for period two).

Changes in the temperature response to the MJO over western Canada after MJO phases 1 and 5 are consistent with the changes in the upper tropospheric circulation and are exacerbated by the presence of the Rocky Mountains. In MJO phase 1 there is a cold shift in the response. In period one there is anomalous

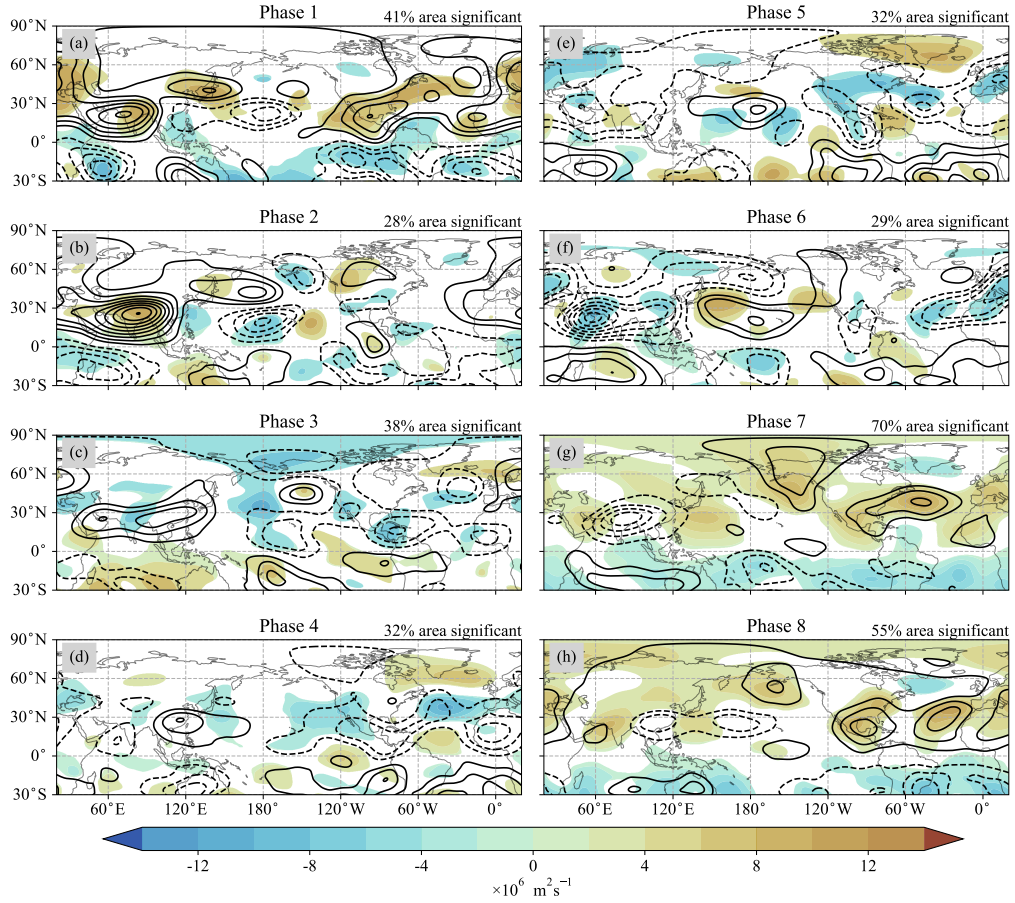

Figure 3.7: Lag 10-day ψ200 anomalies. As in Figure 3.6, but with black contours representing La Niña years.

south-easterly flow from the central United States to western Canada, whereas in period two colder air is advected westward from northern Canada. Conversely, after MJO phase 5 warming is observed over western Canada in period two, as warmer air is transported north-westward from the midwestern United States.

Changes in the response to MJO phase 6 will also have significant impacts on human populations across the NH. Over eastern North America there is a shift to a cold anomaly, from anomalous southward advection from northern Canada rather than westward from the Atlantic. Interestingly, this cold anomaly is more often associated with the response to later MJO phases (specifically MJO phase 8; e.g. Schreck et al., 2013, Figure 2), indicating a shift in the mechanisms of the response.

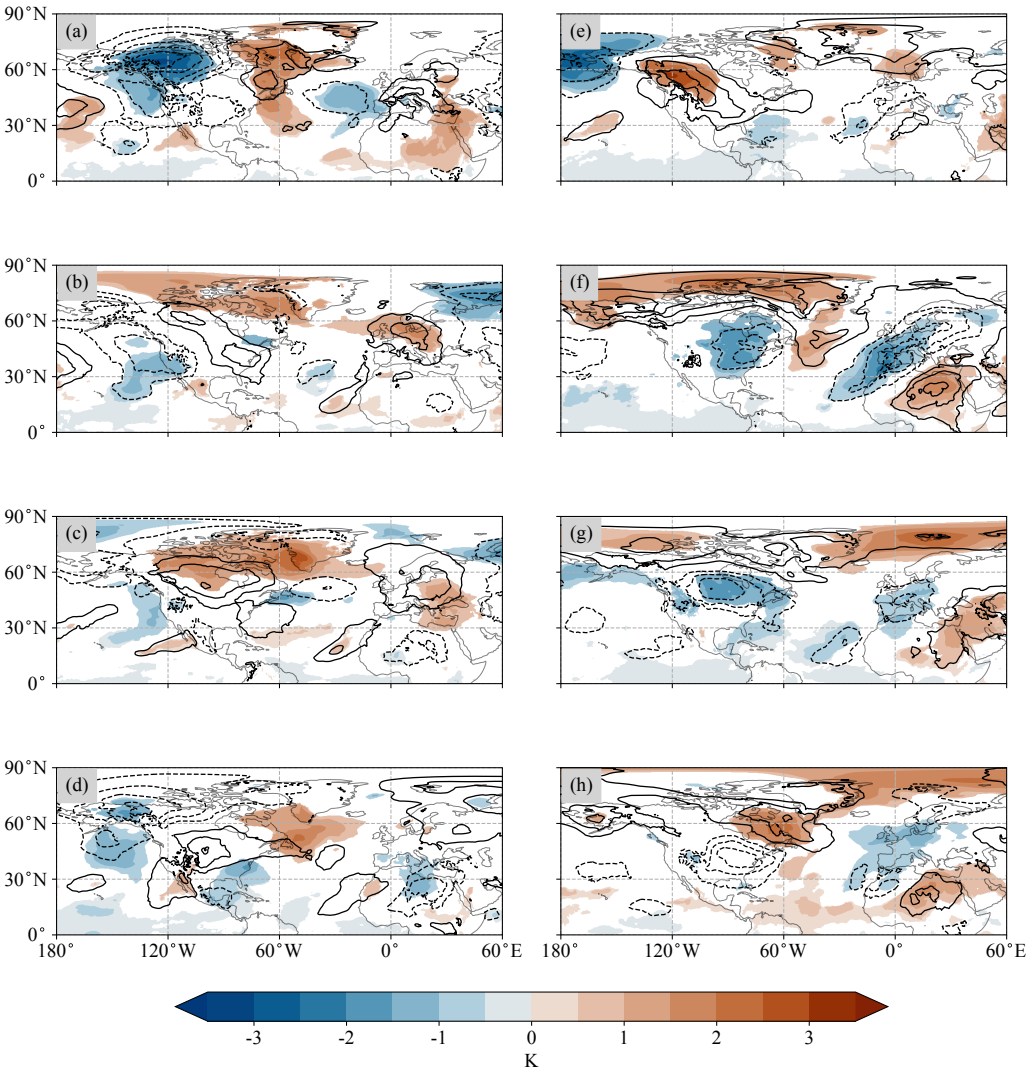

Figure 3.8: As in Figure 3.4, but for $T850$ anomalies

Across Europe, the strengthened and tilted cyclonic anomaly in period two has induced a strong cold anomaly. This feature is not present in period one but has a strength of -1.5 K in period two. The cold anomaly over Europe, paired with the eastern North American cold anomaly and warm anomaly over Greenland and Northern Canada bears considerable resemblance to the temperature pattern associated with NAO− (Wang et al., 2010). Moreover, the average NAO index[5] value at 10-day lag after MJO phase 6 has increased in magnitude (i.e. has become more negative) by approximately 33% in period two, compared to period one. MJO phase 6 is known to precede NAO− (Cassou, 2008; Lin et al., 2009), so the strengthening of these patterns suggests a strengthened link between MJO phase 6 and the NAO− (Figure 3.5).

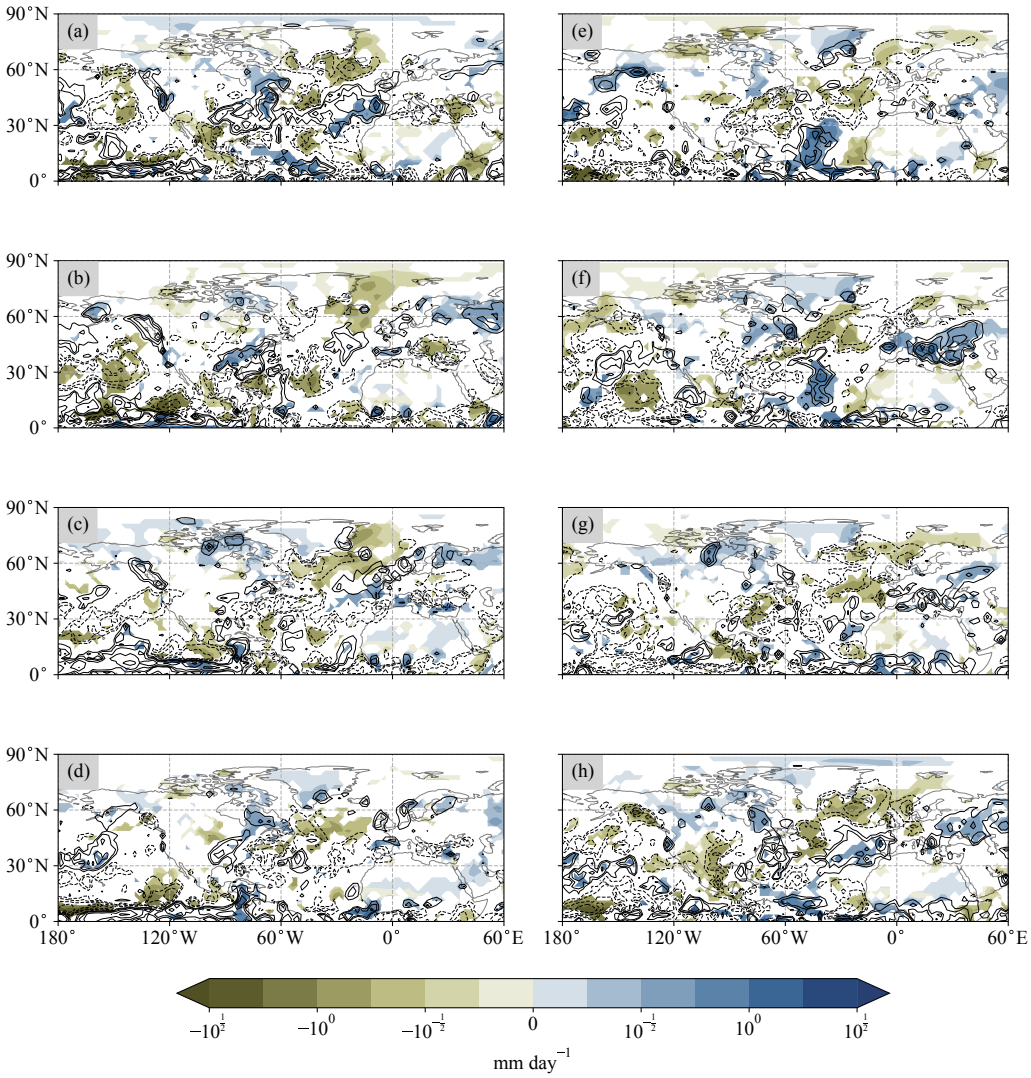

Figure 3.9: As in Figure 3.4, but for precipitation anomaly. Note that anomalies and differences are plotted on a logarithmic scale, and composites were calculated from 1979/80 to 1996/97 for period one and from 1997/98 to 2015/16 for period two.

Precipitation anomalies (Figure 3.9) are less spatially coherent than the corresponding 850-hPa temperature anomalies. Nevertheless, statistically significant changes in the extratropical precipitation response to the MJO from period one to period two are observed in some locations. In particular, the cold shift over central and southern Europe in MJO phase 6 is associated with a wet shift there, which is the opposite of what would usually be expected in boreal winter (Crhová and Holtanová, 2018; Madden and Williams, 1978). Over southern Europe this is due to the formation of a wet anomaly in period two, whereas in central/western Europe this is due to a switch from dry to slightly

wet anomaly. An explanation for the change in southern Europe is that the cyclonic anomaly is associated with a low pressure anomaly. The centre of this low pressure covers southern Europe in period two, whereas in period one the centre is located off the west coast of North Africa. The low pressure over Europe will generally lead to cloudier, wetter weather and hence the positive precipitation anomaly.

3.6 Conclusions

Evidence has been found in ERA5 reanalysis data, showing that the extratropical response to the MJO changes on decadal time scales. ENSO is known to modulate MJO teleconnection patterns on interannual time scales, however the decadal variability we have observed differs from this ENSO-modulated variability and is not an example of aliasing over different time scales.

With only 4 decades of data, however, we are unable to conclusively attribute these changes to either external forcing or internal modes of variability. We hypothesise that low-frequency modes such as AMV the and PDO play a role in modulating MJO teleconnections, and by using climate models to increase our sample size we hope to examine this hypothesis further.

Changes in teleconnection patterns have impacts on meteorological conditions, particularly temperature and precipitation, which will directly affect human populations. These impacts are widespread, covering large portions of the extratropical NH.

Skilful prediction of MJO teleconnections are vital to skilful seasonal forecasting in the extratropics (Kent et al., 2022), which in turn impacts on various industries (Palmer, 2002), including transportation (Karpechko et al., 2015; Palin et al., 2016), agriculture (Cantelaube and Terres, 2005; Challinor et al., 2005) and energy (Bloomfield et al., 2021; Clark et al., 2017). Finding clear evidence of decadal variability in the extratropical response to the MJO is a key

step towards improved MJO-induced predictability in the extratropics and opens exciting opportunities for further refinement.

In Chapter 1 we posed the question '*Does the extratropical response to the MJO vary on decadal time scales?*'. ERA5 reanalysis data have been used to show that the boreal winter MJO teleconnection pattern in the NH has changed in recent decades in line with changes in the PDO and AMV. Changes are seen in the circulation, temperature and precipitation responses. In particular, from 1997, intraseasonal cold anomalies appear over Europe and the eastern United States due to MJO convection over the western Pacific; these were not present 20 years previously. The decadal variability observed is not the product of aliasing of ENSO modulation of the teleconnection.

Notes for Chapter 3

[1] This chapter is adapted from the published paper 'Decadal variability of the extratropical response to the Madden–Julian Oscillation' (Skinner et al., 2023).

[2] Streamfunction is calculated, throughout, in usual way. That is,

$$u = -\frac{\partial \psi}{\partial y}, \qquad v = \frac{\partial \psi}{\partial x}.$$

[3] Also known as "Observed Natural Oscillations Modulating Anomalous Temperature Or Precipitation Over Europe, Iceland and America" (ONOMATOPOEIA)

[4] And hence, are consistent with the lower tropospheric circulation response since we can assume equivalent barotropic behaviour in the extratropics (Figures 3.4 and 3.5)

[5] Here we use the index of the National Oceanic and Atmospheric Administration Earth System Research Laboratories (2023).

Chapter 4

Decadal variability of the extratropical response to the MJO in a General Circulation Model

4.1 Introduction

The MJO influences weather in the extratropics through two teleconnection pathways (Barnes et al., 2019). Upper tropospheric divergence (triggered by anomalous MJO convection) induces a Rossby wave train which extends across the mid-latitudes into the extratropics, providing a tropospheric teleconnection pathway (Subsection 1.2.1; Matthews et al., 2004). A stratospheric teleconnection pathway to the NA is also provided by a deepening of the AL (whilst enhanced MJO convection is centred over the West Pacific) which weakens the SPV (Waugh and Polvani, 2010) through increased vertical wave activity (Garfinkel et al., 2014, 2012; Jiang et al., 2017). The deceleration of the SPV, in turn, favours NAO− (Subsection 1.2.2; Woollings et al., 2010*a*). The tropospheric teleconnection pathway appears to be the dominant mechanism by which the MJO influences the extratropical circulation at lags of up to two weeks, however the stratospheric pathway is still of interest, particularly at longer lead times (Green and Furtado, 2019).

Both the MJO and its teleconnections vary over a range of time scales (Section 1.4). The MJO exhibits variability on interannual (Chen et al., 2016; Hsu and Xiao, 2017; Kessler, 2001; Pohl and Matthews, 2007) and decadal (Fu et al., 2020; Jones and Carvalho, 2006; Wu et al., 2021) time scales. Meanwhile, MJO teleconnections are modulated on sub-seasonal time scales by the propagation speed of the MJO (Yadav and Straus, 2017), on seasonal time scales by the QBO (Feng and Lin, 2019, 2021; Song and Wu, 2020*a*), and on interannual time scales by ENSO (Lee et al., 2019; Moon et al., 2011; Tseng et al., 2020*b*).

The goal of this chapter is to provide mechanisms for decadal variability in MJO teleconnections, having now found evidence of this variability in ERA5 reanalysis data. In Chapter 3, we hypothesised that low-frequency modes of SST variability, such as AMV and the PDO, modulate the extratropical response to the MJO. This chapter will test this hypothesis with the benefit of

the 1,100-year pre-industrial control simulation of the UKESM model. Whilst biases and inaccuracies in the model must be noted, this long-time simulation allows us to robustly interrogate the impact of each SST mode on MJO teleconnections in a way that is not possible using relatively short reanalysis datasets. The pre-industrial control experiment also removes the complication of an anthropogenic global warming signal, which will hopefully mean we see a clearer picture of internal decadal variability.

AMV is the dominant mode of low-frequency variability in the Atlantic (Subsection 1.3.2). It is defined as an oscillation in the average North Atlantic SST anomaly (relative to the global average), with a period of approximately 60–80 years. During AMV+, SST anomalies in the NA are warmer than the global average, whilst AMV− is characterised by cold SST anomalies compared to the global average.

During AMV+, the tropospheric circulation response to the positive SST anomalies projects onto NAO− (Subsection 1.2.3; Elsbury et al., 2019; Msadek et al., 2011).

The PDO is the leading mode of SST variability in the NP (Subsection 1.3.3). It is defined as the first empirical orthogonal function (EOF) of monthly-mean SSTs across the NP basin, and has a period of approximately 20–30 years. PDO+ is characterised by cold SST anomalies in the western and central NP, with warm anomalies in the eastern NP. PDO− displays the opposite SST anomalies. The SST pattern exhibited by the PDO is very similar to that of ENSO. PDO+ and El Niño both show similar cold anomalies in the western North and South Pacific, with warm anomalies in the eastern and tropical Pacific. The PDO differs from ENSO in its time scale (decadal rather than interannual) and in the focus of SST anomalies in the NP rather than the tropical Pacific.

PDO+ tends to induce an atmospheric response which projects onto the PNA+ (Subsection 1.2.5), in turn deepening the AL (Taguchi et al., 2012). The reverse is true for PDO−. The interaction between the PDO and the atmosphere is

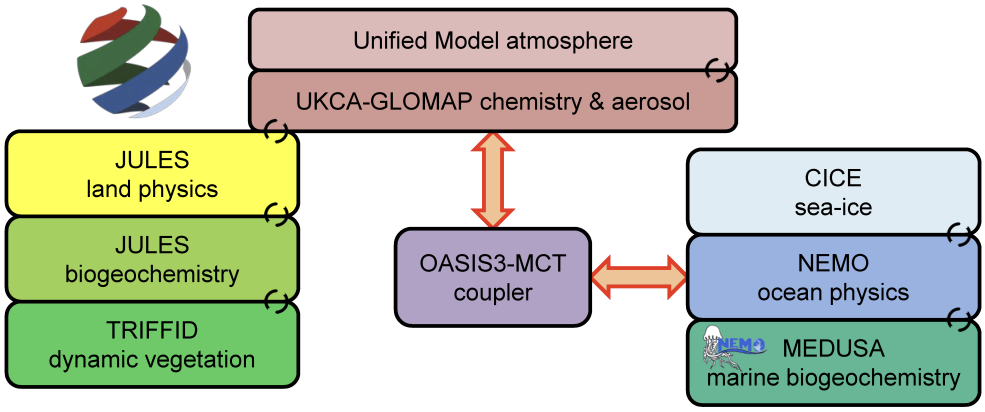

Figure 4.1: Model configuration for UKESM. Image provided by UKESM (https://ukesm.ac.uk/science-of-ukesm/).

non-linear, with atmospheric forcing a major driver of PDO variability (Newman et al., 2016).

The PDO is not entirely independent of AMV, with the latter acting as a driver of low-frequency variability in the Pacific with an observed lag of approximately 12 years (Wu et al., 2011; Zhang and Delworth, 2007). This will be taken into consideration when considering the effect of each mode on MJO teleconnections.

4.2 The UKESM model

The first stage of the UK Earth System Model (UKESM1.0-LL; henceforth simply UKESM) is an earth system model (ESM) developed by the UK Met Office and National Environmental Research Council. For a comprehensive overview of the model, see Sellar et al. (2019).

UKESM is based on the climate model HadGEM3-GC3.1-LL, coupled with additional vegetation and biogeochemistry representations from the JULES, MEDUSA and UKAC models (Figure 4.1). The atmospheric (and land) component of the UKESM model runs on a $1.25° \times 1.875°$ latitude–longitude grid with 85 vertical levels. The ocean component inherits its nominally 1° tripolar horizontal grid and 75 vertical levels from the NEMO model.

Global coupled climate models consistently under-represent tropical–extratropical teleconnections (Skinner et al., 2022; Williams et al., 2023), leading to the so-called "signal-to-noise" paradox, in which individual model realisations display less predictable climate variability than would be expected (Scaife and Smith, 2018). MJO variability is also generally under-predicted in climate models (Le et al., 2021).

A consistent weakness in climate models over recent decades has been the excessive termination of MJO events over the MC, producing a barrier effect (e.g. Ling et al., 2019; Zhou et al., 2023). This phase of MJO propagation is key to skilful prediction of teleconnection patterns (Bao and Hartmann, 2014).

Ahn et al. (2020) assess the ability of climate models from CMIP5 and CMIP6 to simulate MJO propagation across the MC. Whilst UKESM does not have the most skilful representation of trans-MC propagation amongst the CMIP6 models, it does outperform its physics-only counterpart, HadGEM3-GC3.1-LL, and is able display at least some propagation (Figure 4.2).

The UKESM model simulates low frequency SST variability well compared to other ESMs. Coburn and Pryor (2021) show that the model's spatial and temporal representation of AMV are more skilful than the multi-model ensemble mean of eleven ESMs. This result holds regardless of the skill metric used. UKESM has the best spatial PDO representation of the eleven models, whilst the representation of temporal variability is better than average based on two of the three metrics used. Unfortunately, the model has a poor representation of the co-variance between AMV and the PDO, however most of the models struggle to simulate this relationship well.

Robson et al. (2020) found that whilst North Atlantic SST variability is well represented in UKESM when compared against reanalysis data, model AMV explains a smaller proportion of global SST variability than observed AMV. This is likely due to the fact that model AMV is more closely correlated with global mean SST and the AMV spatial pattern is not as tightly confined to the NA.

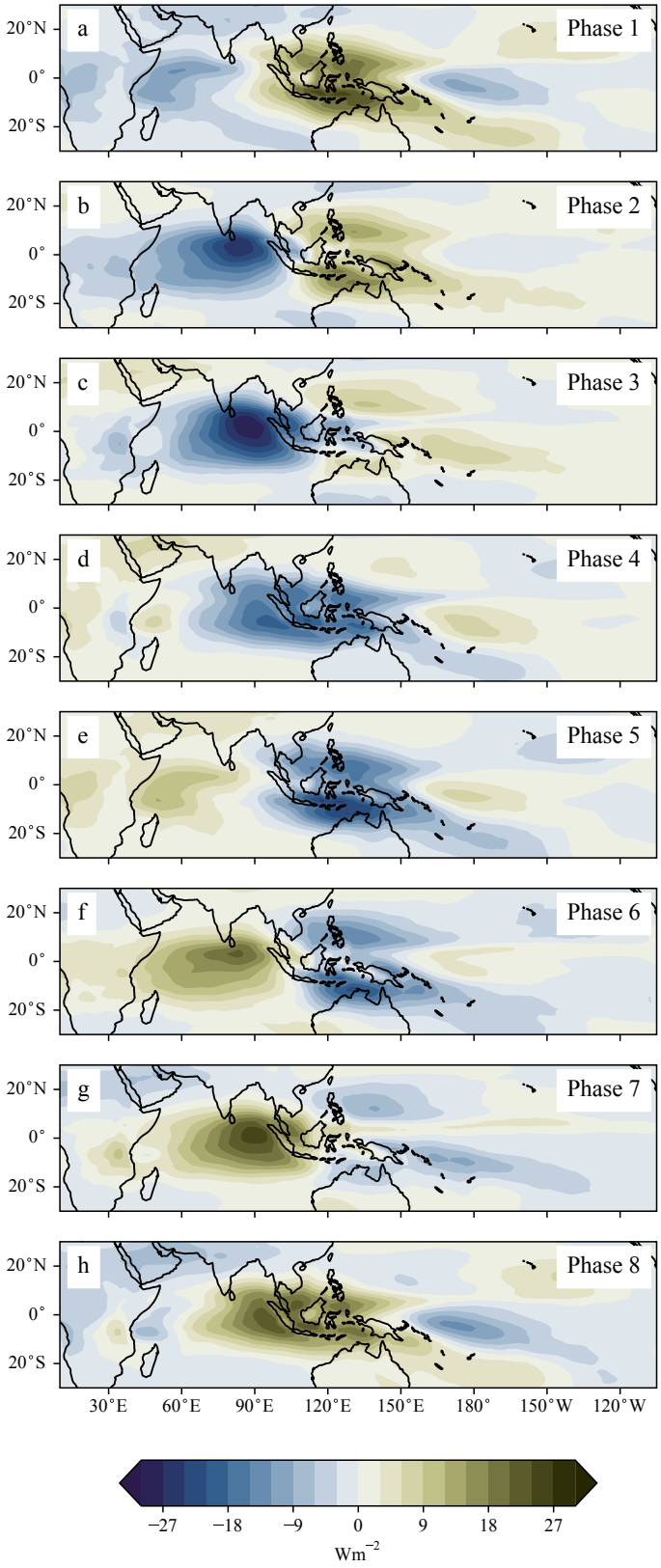

Figure 4.2: November–April OLR anomaly composites for each MJO phase in the UKESM pre-industrial control simulation. Bluer shading (negative OLR) indicates enhanced anomalous convection.

The model SST pattern features larger anomalies in the NP and Arctic (Figure C.1a) than the observed SST pattern.

The North Pacific SST anomalies associated with the PDO are more tightly concentrated around the Kuroshio–Oyashio extension (KOE) region in the model than in observations (Figure C.1b). This difficulty with transporting SST anomalies across the Pacific is a long-standing issue for climate models (e.g. Pierce et al., 2001), particularly at lower resolutions. Zhang and Delworth (2007) also suggest that this concentration of anomalies around the KOE region may help to explain the poor representation of the co-variability of AMV and the PDO.

Overall the model does a relatively good job of representing decadal variability (Sellar et al., 2019), with the exception of the correlation between AMV and theh PDO. We are, however, able to work around this issue (see Section 4.3) by removing instances in which both modes are active simultaneously from our analysis.

The spatial pattern of stationary Rossby wave number (Equation 1.2) displays negligible response to AMV and the PDO in the UKESM model. Since the Rossby wavenumber is used as a qualitative diagnostic of changes in Rossby waveguides, relatively large changes are required in order to reach robust conclusions about its role in modulating teleconnection patterns. The small changes we see in this case are not significant enough to warrant further discussion in the context of these results.

Stratospheric processes such as the SPV and SSWs are represented with a range of accuracy across climate models (Ayarzagüena et al., 2020; Charlton-Perez et al., 2013; Hall et al., 2021; Wu and Reichler, 2020). UKESM has a well resolved stratosphere, compared to many other climate models (Robson et al., 2020; Sellar et al., 2019). When viewed as a whole season average, UKESM represents the SPV and the frequency of SSWs reasonably well. The SPV is slightly too weak (leading to too many SSW events) in early winter and too

strong in late winter, although this is a common feature of climate models (Charlton et al., 2007; Seviour et al., 2016). Also, whilst displacement-type SSWs are well represented in UKESM, split-type SSWs are consistently under-represented (Hall et al., 2021, 2022; Robson et al., 2020). EQBO phases are generally too long in UKESM, however the relationship between the QBO and SPV is better represented in UKESM than most climate models (Rao et al., 2020).

The pre-industrial control (piControl) simulation forms part of the core (DECK) suite of simulations from the CMIP6 project (Eyring et al., 2016). For a full evaluation of the piControl simulation in UKESM, see Section 4.1 of Sellar et al. (2019).

For the piControl simulation, forcings (aerosols, volcanic activity, land use, etc.) are held constant at 1850 levels (or some pre-defined reference level – see Appendix A1.2 of Eyring et al., 2016). Although this is not a true pre-industrial level, the simulation is designed to show natural variability relative to an approximately equilibrium state. The simulation is run for 1,100 years, with a 500 year coupled spin-up which is itself preceded by 5,000 and 1,000 year ocean and land only spin-ups, respectively.

4.3 Methodology

The MJO is described using the RMM index proposed by Wheeler and Hendon (2004). OLR, $U850$, and $U250$[1] anomaly data are projected onto the EOF patterns calculated by Wheeler and Hendon. From the resulting RMM time series, each day is assigned a phase and amplitude. Phases 2–3 signify enhanced convection over the eastern IO, phases 4–5 describe enhanced convection over the MC, phases 6–7 correspond to enhanced convection over the western Pacific, and phases 8–1 denote enhanced convection over the central Pacific and western IO (Figure 4.2).

The index of Trenberth and Shea (2006) is used to describe AMV. SST anomalies are averaged (area weighted) over the NA (0–80°W, 0–80°N), with the global average SST anomaly then subtracted to detrend. This time series is 10-year low-pass filtered, and is normalised so that it has a standard deviation of unity.

The PDO is defined as the first EOF of SST anomalies in the NP (northward of 20°N), as described by Mantua et al. (1997). The EOF loading pattern is provided by the NOAA PSL, and is based on HadISST data (Figure A.2). As with the AMV index, the time series is 10-year low-pass filtered, and is normalised so that it has a standard deviation of unity.

AMV and the PDO are in their positive (negative) phase when their index value is greater than one (less than minus one). When the respective index value has magnitude less than one, AMV and the PDO are said to be in their neutral phase (denoted AMVn and PDOn, respectively).

250-hPa streamfunction (ψ250 hereafter) anomalies are calculated for UKESM piControl simulation data by subtracting the mean, linear trend and first three harmonics from 250-hPa wind data.

We will consider boreal winter (November–April) seasons throughout, since this is when both the MJO and its teleconnections are most active (Jenney et al., 2019; Stan et al., 2017). Only full winter seasons are considered.

Lagged composites of ψ250 are calculated for each MJO phase by averaging over all days in which the MJO is in the given phase and is active (lagged by a given number of days). For different SST states, composites are then calculated by further subsetting on winter seasons which have an average index magnitude greater than one. Since the mean ψ250 field will be different for the particular subset than the whole domain, we subtract this mean from all composites. For example, the lagged composite of ψ250 anomaly for MJO phase 6 with AMV+ and PDOn is the lagged composite of ψ250 anomaly over all days in which, simultaneously, the MJO is in phase 6, AMV is in its positive phase, and the PDO

is neutral, minus the composite of $\psi 250$ anomaly over all days in which AMV is in its positive phase, and the PDO is neutral (regardless of MJO phase). Hence the composites show the anomalous atmospheric response to the MJO, conditional on the given SST state, rather than the combined response to the MJO and the decadal background state changes. For each MJO phase and 'active' SST state (AMV± and PDO±), there are approximately 2000-3000 days out of the 1100 year simulation (November-April only) in which the two are simultaneously active. A full count can be found in Table C.1.

Due to the fact that the model struggles to fully capture the co-variability of AMV and the PDO, we seek to separate the two modes. To achieve this, when compositing over one mode, the other is fixed as neutral. For example, rather than compositing over all AMV+ seasons, we only consider those seasons which are both AMV+ and PDOn. Henceforth, references to, for example, AMV+ will assume PDOn implicitly. SST composites for these regimes, now with the other mode neutral, are displayed in Figure 4.3. Constraining the second mode to neutral decreases the number of days included in each composite by approximately 40% (see Table C.2), however this still leaves well over 1000 days included in each composite.

The strength of the SPV is calculated at both 100 hPa and 50 hPa, in line with Barnes et al. (2019). In each case, boreal winter geopotential height anomalies ($Z100$ and $Z50$, respectively) from 60–90 °N are zonally averaged to assess changes in both the strength and meridional extent of the vortex. These anomalies are then composited by the aforementioned SST regimes and MJO phases to assess the different 10-day lagged responses of the vortex to the MJO, conditioned on SST variability, as a function of latitude. Also calculated are the polar cap (60–90 °N) mean $Z50$ and $Z100$ anomalies as a function of lag, again composited by MJO phase and SST regime.

Statistical significance is assessed throughout through the use of two-tailed t-tests. Unless otherwise stated, significance is tested at the 95% confidence level.

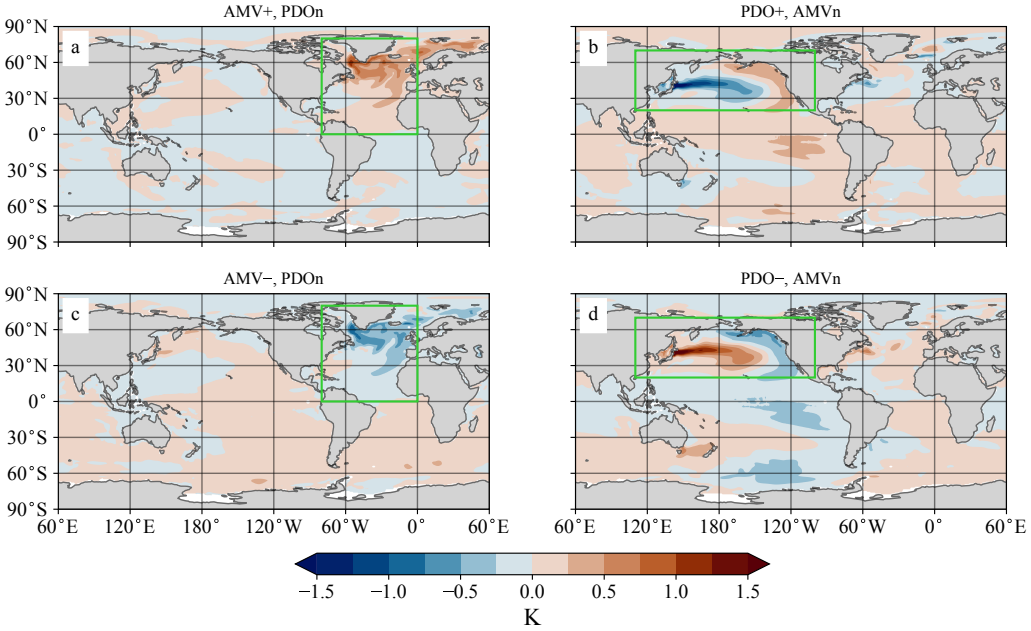

Figure 4.3: November–April composites of SST anomalies for (a) AMV+, PDOn; (b) PDO+, AMVn; (c) AMV−, PDOn; and (d) PDO−, AMVn; in the UKESM pre-industrial control simulation. Composites are taken over all winter seasons in which the respective index has value greater than one. The green box in each panel denotes the region used to calculate the respective index.

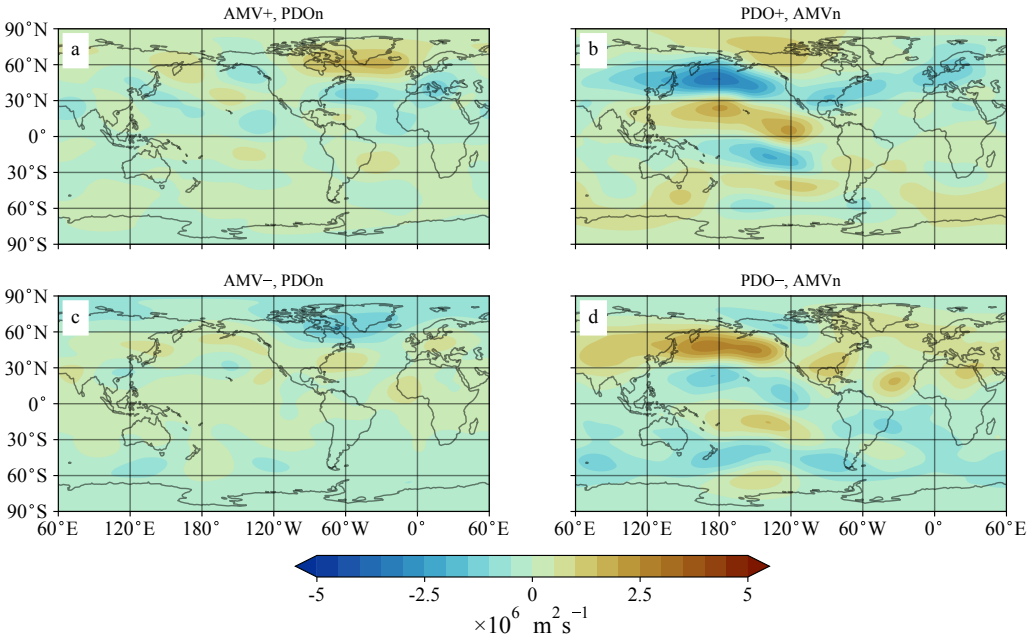

Figure 4.4: As in Figure 4.3, but for ψ250 anomalies.

4.4 Results

MJO phases 3 and 6 produce canonical teleconnections from the MJO to both the NP and NA (e.g. Cassou, 2008). Hence, for the sake of clarity, and for consistency with Chapters 2 and 3, we have focus on these two phases.

4.4.1 Response to MJO phase 6

When the MJO is in phase 6 – that is when enhanced MJO convection is centred over the eastern MC and western Pacific (Figure 4.2f) – a Rossby wavetrain is initiated, deepening the AL and causing a shift to NAO− and PNA+. This is the canonical response to the MJO that has been discussed previously (e.g. Section 1.2).

This canonical response is well represented in the UKESM piControl simulation, with the expected cyclonic and anticyclonic anomalies present[2] in a 10-day lagged composite of winter $\psi 250$ anomaly over the full 1,100 year time domain (Figure 4.5a). Furthermore, the vast majority of the response is statistically significant at the 95% confidence level, suggesting that this is a robust teleconnection pattern from the MJO.

During AMV+ (with PDOn fixed), the response to MJO phase 6 is generally less significant than average (Figure 4.5b). Whilst the AL is still deepened, this response is much smaller in magnitude. Correspondingly, the PNA+ response is almost completely disrupted.

This change in the extratropical response is seen even more clearly when analysing the difference between the AMV+ composite and the overall composite (Figure 4.6b). Note that by subtracting the overall composite from the AMV+ composite, we see the effect that AMV+ has had on the response to the MJO. If MJO teleconnections were independent of AMV modulation, we would expect these differences to be zero (since the lagged $\psi 250$ response to

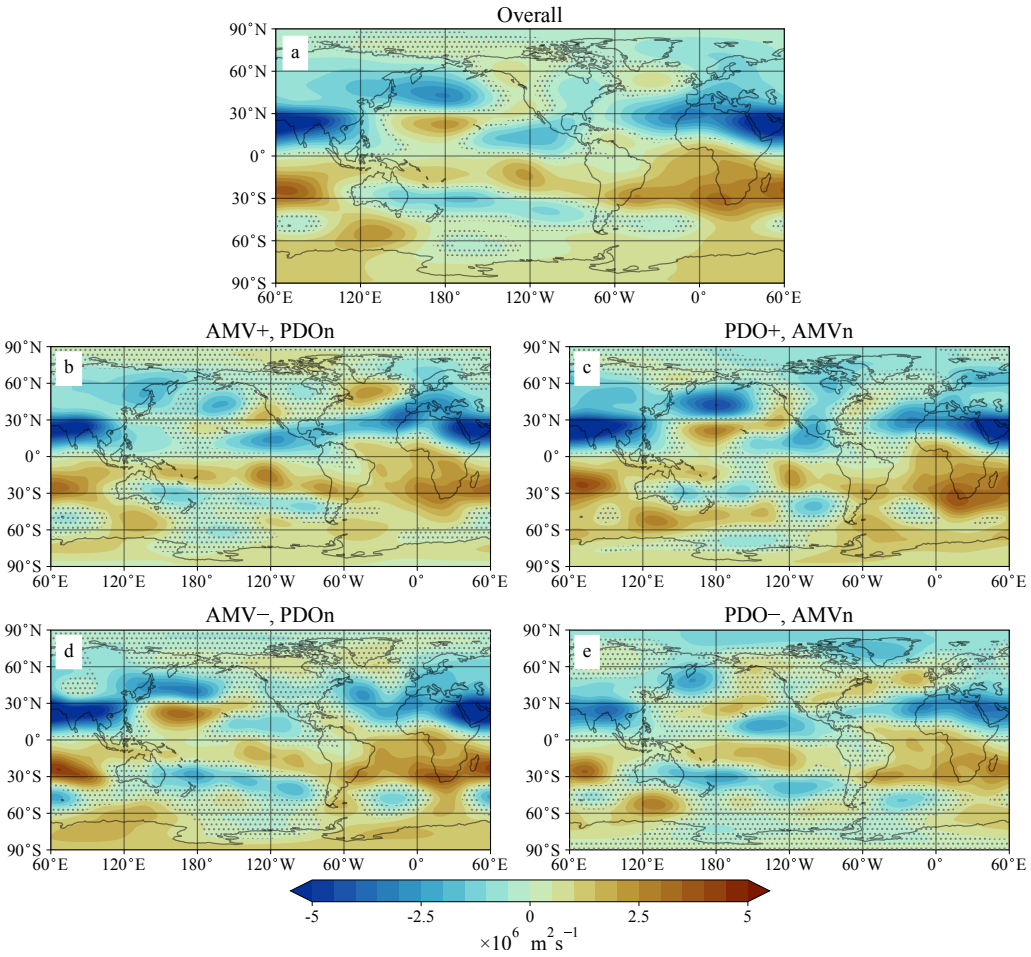

Figure 4.5: (a) 10-day lagged MJO phase 6 composite of ψ250 anomalies. (b–e) 10-day lagged MJO phase 6 composite of ψ250 anomalies when conditioned on the given SST regime. Stippling denotes regions in ψ250 anomalies are not significantly different from zero at the 95% confidence level. In all panels, only November–April seasons are considered.

MJO phase 6 during AMV+ would simply be the linear superposition of the individual responses of ψ250 to the MJO phase 6 and AMV+). Changes in the NP response are of the opposite sign to the overall response, leading to destructive interference.

A considerable change in the response to MJO phase 6 is observed in the NA during AMV+. The canonical NAO− response is strengthened during AMV+, which suggests a nonlinear interaction between the responses to the MJO and AMV (which naturally favours NAO− during AMV+).

The stratospheric MJO–NAO teleconnection pathway may also be responsible

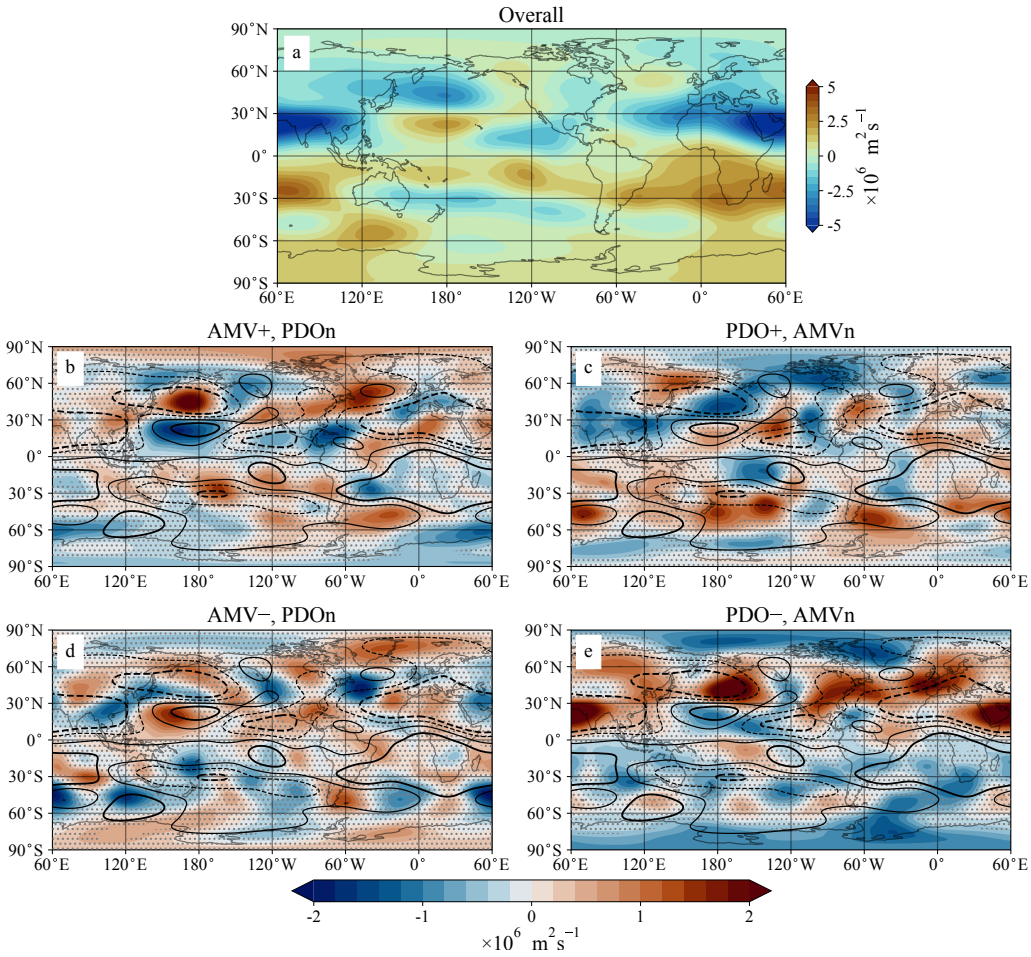

Figure 4.6: (a) 10-day lagged MJO phase 6 composite of ψ250 anomalies, as in panel Figure 4.5a. (b–e) Change in 10-day lagged MJO phase 6 composite of ψ250 anomalies as a result of conditioning on the given SST regime (that is, the response conditioned on the SST regime minus the overall response[3]). Black contours show the overall composite from panel (a), plotted at $\pm 0.5 \times 10^6\,\mathrm{m^2 s^{-1}}$ and $\pm 1.5 \times 10^6\,\mathrm{m^2 s^{-1}}$. Dashed contours represent negative values. Stippling denotes regions in which the SST conditioned response is not significantly different from the overall response at the 95% confidence level. In all panels, only November–April seasons are considered.

for some of change in the response. During AMV+, the SPV is much weaker than usual (Figure 4.7). A weakened SPV would be expected after MJO phase 6, but this response is amplified considerably during AMV+. This result is surprising since the stratospheric MJO–NAO pathway would usually see a weakened SPV associated with a deepened, not weakened, AL. The weakened SPV is, though, consistent with the strengthened NAO− response, suggesting that the stratospheric pathway is indeed important here, however the

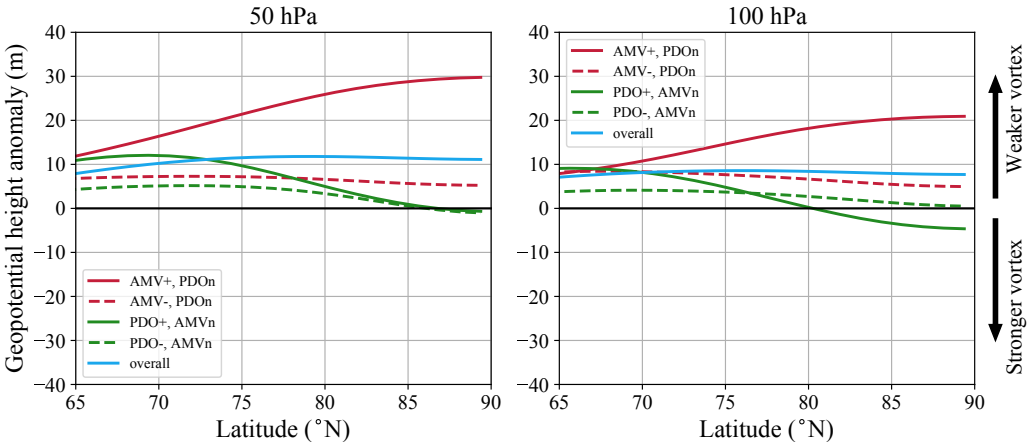

Figure 4.7: 10-day lagged MJO phase 6 composites of zonal mean (a) $Z50$ and (b) $Z100$ anomalies, as a function of latitude, for given SST states. Only November–April seasons are considered.

mechanism by which the MJO is forcing the SPV is not clear.

The weakening of the SPV, appears to happen much earlier during AMV+ (Figure 4.8), which could point to a modified response to an earlier MJO phase. In fact, the tropospheric response to MJO phase 4, which usually features an anticyclonic anomaly across the NP, instead displays a slight deepening of the AL (shown by the cyclonic negative shift in $\psi 250$ anomaly over the NP in Figure C.4a). This shift would not usually occur until MJO phase 6, which may explain the early weakening of the SPV. This modification in the SPV response to the MJO may explain the inconsistency between the expected and observed relationship between the AL and SPV.

Interestingly, the change in the response to MJO phase 6 during AMV− (Figure 4.6d) is not simply a mirror of that seen during AMV+. In this case, the response of the NP remains significant to a greater degree, however the NA response is much weaker.

The change in the response during AMV− resembles a Rossby wave which is slightly out of phase with, and following a lower latitude to, the overall response. In a linear Rossby wave theory[4], this could be interpreted as a shift in the favoured Rossby wave mode (in this case to a higher wavenumber).

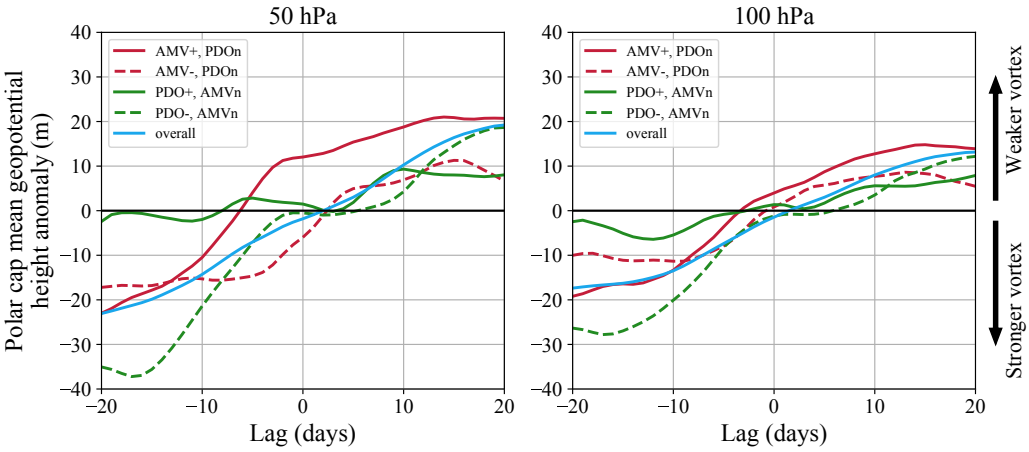

Figure 4.8: Lagged MJO phase 6 composites of mean polar cap (60–90 °N) (a) $Z50$ and (b) $Z100$ anomalies, for given SST states. Only November–April seasons are considered.

The NP response to MJO phase 6 is strengthened during PDO+ (Figure 4.6c), where we observe a considerably deeper AL. PDO+ tends to favour a deeper AL (Figure 4.4b) and corresponding PNA+ (Taguchi et al., 2012), so we again appear to see a nonlinear superposition of the expected responses. Also, the cyclonic anomaly in the AL region is coupled with a strengthened anticyclonic anomaly (RWS) around 20 °N. This is consistent with the strengthening and eastward shift in the MJO convective centre observed during PDO+ (Figure 4.9c).

A wave-like change in the response during PDO+ is visible, extending across Mexico and into the NA (see the alternating positive-negative pattern in $\psi 250$ anomaly change in Figure 4.6c), similar to that observed during AMV−, again pointing to an explaination from linear Rossby wave theory, in which the change in the response is the result of a change in the particular Rossby wave modes being excited by the MJO convection. It is not surprising to see similarities between the AMV− and PDO+ modulation of the MJO teleconnection, since these two SST regimes are correlated with each other. Although the restriction of the second mode to neutral prevents the majority of this aliasing in the signal, we still expect to see some crossover.

The response of the SPV to MJO phase 6 is altered significantly by PDO+ (Figure 4.7). The SPV appears to tighten around the pole, with a weakening

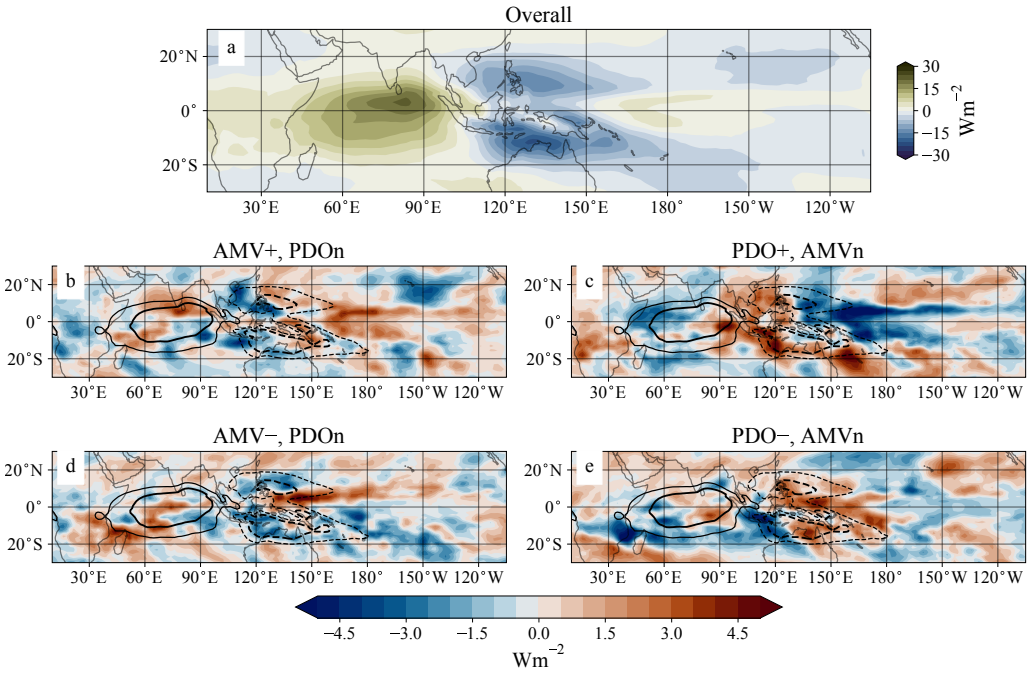

Figure 4.9: (a) MJO phase 6 composite of OLR anomaly, as in panel Figure 4.2f. (b–e) Change in MJO phase 6 composite of OLR as a result of conditioning on the given SST regime. Black contours show the overall composite from panel (a), plotted at $\pm 6\,\mathrm{Wm}^{-2}$ and $\pm 12\,\mathrm{Wm}^{-2}$. Dashed contours represent negative values. In all panels, only November–April seasons are considered.

of the vortex at lower latitudes and a slight strengthening of the vortex in the high latitudes. The SPV also displays suppressed variability as a function of lag relative to MJO phase 6 during PDO+ (Figure 4.8). The mechanisms behind this change, and the effects it has on the NAO, are not yet clear. This does, however, warrant further investigation in a future work.

The effect of PDO− on the extratropical response to MJO phase 6 (Figure 4.6e) is the least clear of the four regimes. Due to a considerable amount of destructive interference, the response is less significant across the NH. The changes in the response are, however, widely significant. Those anomalies that remain significant are shifted in both the NA and NP. One general trend seems to be a positive shift in the NAM[5]. This is consistent with the strengthening (or, more accurately, the reduced weakening) of the SPV during PDO− (Figure 4.7).

Across all SST regimes discussed, changes in the SH response to MJO phase 6 can

be seen, however they are generally less significant, and less spatially coherent, than those changes observed in the NH. One could argue for a Rossby wave-like change in the response across South America during PDO+, however this doesn't have much qualitative impact on the response itself (Figure 4.5c).

4.4.2 Response to MJO phase 3

The other key extratropical response to the MJO is that following MJO phase 3 (e.g. Cassou, 2008). In this case, we expect a teleconnection resembling PNA− (with a weakened AL) and NAO+. Whilst there is a well-defined physical mechanism for the stratospheric teleconnection pathway between MJO phase 6 and the NA, this is not the case for MJO phase 3. Hence the focus of these results will be on the tropospheric circulation response.

The UKESM piControl simulation does a good job of capturing the expected NAO+ response, even if it is weaker than we might expect. That being said, the response is still significant at the 95% confidence level. (Figure 4.10a). The PNA− response is shifted westward. A relatively strong anticyclonic anomaly is visible over the Aleutian Islands, consistent with a weakening of the AL. The eastern nodes of the PNA quadrupole are not clear, though.

AMV provides little modulation to the extratropical response to MJO phase 3 (Figures 4.11b and 4.11d). A statistically significant change is observed during AMV−, with a Rossby wave-like change in the response as previously described. This wave train initiates to the North East of the MC and extends across the mid-latitudes to the NA, however it has a higher frequency than, and is out of phase with, the average response. This change in the Rossby wave mode excited could be due to changes in the MJO convection (Figure 4.12), where the area of suppressed convection appears to shift southward. The precise mechanisms behing this change are not clear, though. Once the wavetrain reaches the NA, it appears to strengthen the NAO+ response, however this change is not statistically significant. AMV− tends to favour NAO+ (Figure 4.4c), so it is slightly surprising

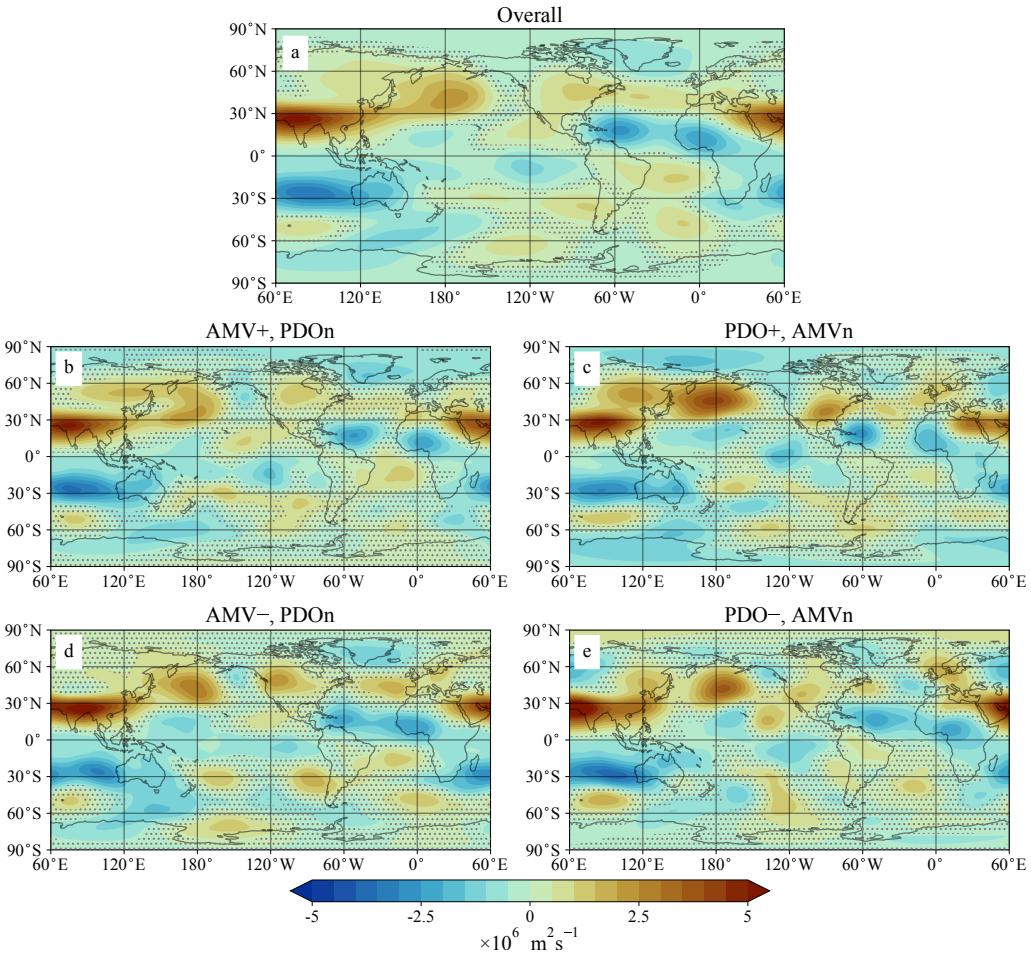

Figure 4.10: Lag 10-day ψ250 anomalies. As in Figure 4.5, but for MJO phase 3.

that a more substantial modification of the teleconnection is not observed given the nonlinear interaction between the responses to AMV and MJO phase 6.

The PDO has a greater impact on the response to MJO phase 3 (compare magnitudes of the change in response between Figure 4.11 panels b–c and d–e). Interestingly, both PDO+ and PDO− appear to amplify the weakening of the AL (albeit with a slight northward shift in the centre of action during PDO+). During PDO− we might expect a strengthening of this response, since a weak AL is already favoured. On the other hand, during PDO+ (when we in fact see the larger modification to the response), a stronger AL would generally be favoured. The exact mechanisms behind this alteration to the NP response are not yet clear, however we hypothesise that an eastward shift in the MJO

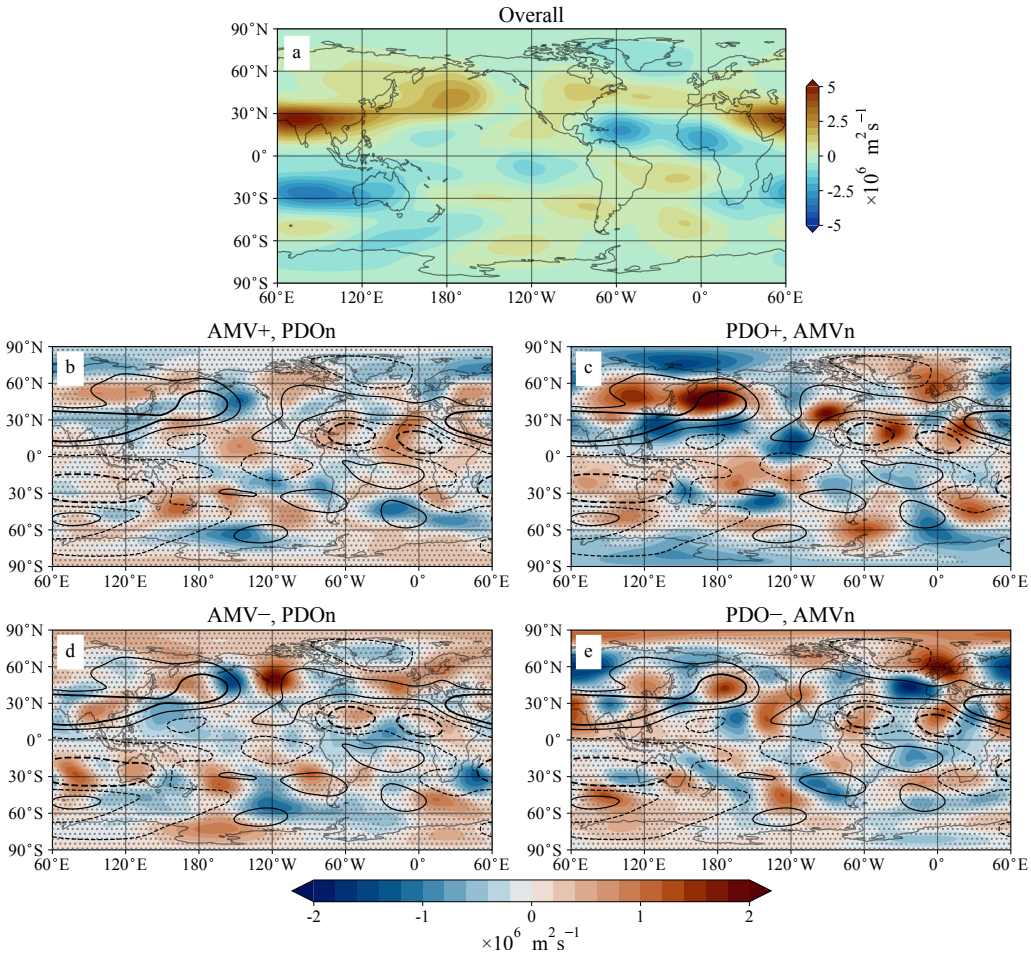

Figure 4.11: Change in lag 10-day ψ250 anomalies. As in Figure 4.6, but for MJO phase 3.

convective centre (Figure 4.12c) may be a factor.

In the NA, both PDO+ and PDO− disrupt the NAO+ response to MJO phase 3. In both cases, the Rossby wavetrain to the NA is modified, however this acts to reduce the significance of the NH response.

In general, the modulation of the extratropical response to MJO phase 3 by AMV and the PDO is, whilst statistically significant in some regions, not well explained by the physical mechanisms studied here. It is also of smaller magnitude than the modulation of the extratropical response to MJO phase 6. Further investigation is required to make more robust conclusions about the effect of decadal SST variability on MJO phase 3 teleconnections.

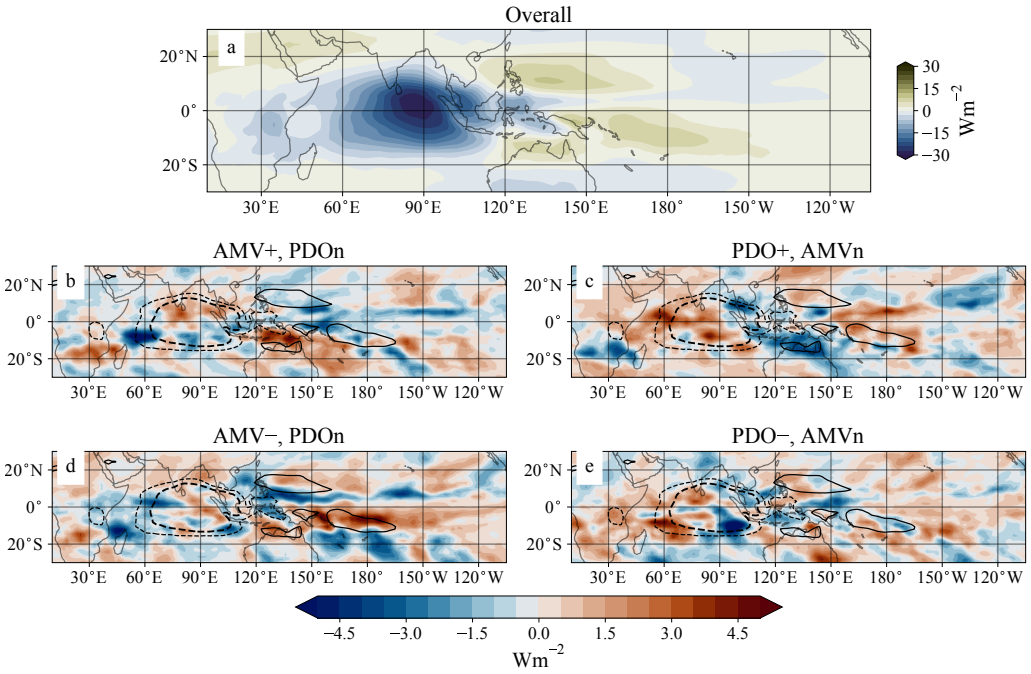

Figure 4.12: Change in OLR anomalies. As in Figure 4.9, but for MJO phase 3.

4.4.3 Response to the remaining MJO phases

The modification of the extratropical response to the remaining phases of the MJO by AMV and the PDO are presented in Figures C.2–C.7. Statistically significant modifications to the MJO teleconnection are observed throughout, providing further confidence in the modulation of the extratropical response to the MJO by decadal SST variability.

As is the case for MJO phase 3, the effects of AMV on the responses to MJO phases 2 and 4 are not clear, since the changes we see, whilst statistically significant in some regions, do not project well onto the teleconnection itself. They also don't appear to project onto common weather regimes, making it difficult to decipher the mechanisms behind the changes. The same is true for MJO phase 5, although there is an argument for a weakening of the Atlantic Ridge pattern during AMV−.

The NAO− response to MJO phase 6 generally persists through phases 7 and 8, however AMV seems to generally disrupt this pattern. In AMV− slighlty

weakens the NOA− response to phase 7, whilst the change as a result of AMV+ doesn't appear to map onto the NAO at all. AMV+, which natually favours NAO−, seems to shift the response to phase 8 closer to a Scandinavian Block regime.

4.5 Conclusions

Both AMV and the PDO cause a statistically significant change in the extratropical response to the MJO, for all MJO phases (Figures 4.6, 4.11, and C.2–C.7).

AMV+ and PDO+ amplify the canonical NAO− and deep AL (PNA+) responses to MJO phase 6, respectively, representing a nonlinear superposition of the responses to the MJO and the decadal mode. The SPV plays a role in the modulation of the teleconnections, however the mechanisms by which the SPV response itself is modulated are not clear.

The amplification of the NAO− response to MJO phase 6 during AMV+ is consistent with results found in Chapter 3 (Skinner et al., 2023), providing further confidence in the result. It is difficult to compare with Chapter 3 too closely, due to the covariance of AMV and the PDO, and the short time domain of the observational analysis. Seeing some agreement is, therefore, a very exciting result.

The response to MJO phase 3 is modulated by both AMV and the PDO, though to a lesser extent than the response to MJO phase 6. There appears to be significant alteration of the Rossby wave response, however some of the changes observed are of the opposite sign to those expected (e.g. Weaker AL during PDO+, which favours a deepening of the AL).

For both MJO phases studied, a linear superposition of Rossby wave responses seems to occur. It is worth reiterating that the differences plotted in panels b–d

of Figures 4.6 and 4.11 are the modification of the MJO teleconnection by the given SST state, not just a superposition of the responses to the MJO and SST variability. Hence, this linear Rossby wave-like change in the teleconnections must occur as a result of different Rossby wave modes being excited by the MJO, depending on the SST state. This could be due to changes in the tropical forcing (Figures 4.9 and 4.12), or changes in the basic state through which these waves propagate.

It is clear that both AMV and the PDO modulate the extratropical response to the MJO on decadal time scales, and some of the mechanisms behind this modulation have been identified. Further study is required to consolidate these results and investigate those mechanisms which are not yet clear. It must also be noted that biases in the model used will also affect the results obtained. Without longer observational datasets, models remain the most effective way to study variability on decadal time scales. Similar studies with other climate models, or the use of idealised modelling experiments, would help to make these results more robust, though.

Since the MJO is used as a source of predictability in the extratropics, these results will have impacts on forecasting over the coming decades. As AMV and the PDO modulate the response to the MJO, so the predictability obtained through these responses will also be modified. Similarly, studies of MJO teleconnections in future climates can now use the context provided by these results to more accurately pick apart the changes in the response as a result of internal an anthropogenically forced variability.

Returning to the research questions posed in Chapter 1, we asked '*What modulates decadal variability of the extratropical response to the MJO?*'. We analysed the effect of two key modes of low-frequency SST variability – AMV and the PDO – on the extratropical response to the MJO in the UKESM climate model. Using the pre-industrial control simulation from the CMIP6 project, we have access to a much longer dataset than would be possible using

observations or reanalysis products. This allowed us to properly assess decadal variability with a robust sample size. Both AMV and the PDO are shown to modulate the extratropical response to all MJO phases, particularly phases 3 and 6. Tropospheric and stratospheric teleconnection pathways, acting through changes in Rossby wave activity and the stratospheric polar vortex respectively, are modified by the decadal SST forcing. Physical mechanisms for a number of these changes are identified, however further investigation is required to fully explain other changes.

Notes for Chapter 4

[1] 250-hPa zonal wind data are used in place of 200-hPa zonal wind for RMM index calculation due to data availability constraints. This has negligible effect on the outcomes.

[2] That is, cyclonic anomalies, corresponding to anomalous pressure lows, over the Aleutian Islands and Florida (PNA+), and the Azores (NAO−). The corresponding anticyclonic (or high pressure) anomalies are observed over Hawaii and Northwest Canada, and (just south of) Iceland.

[3] This is also equivalent to the corresponding panel in Figure 4.5 minus Figure 4.5a.

[4] Whilst Rossby waves in the atmosphere are, of course, not fully linear, it is not unreasonable to make a linearity assumption for conceptual purposes (Deb et al., 2020; Li et al., 2015*a*).

[5] The shift to NAM+ is visible through the large cyclonic anomaly over the pole, with predominantly anticyclonic anomalies present across the mid-latitudes.

Chapter 5

Conclusions

5.1 Review of research questions

We now return to the research questions posed in Section 1.5. Throughout Chapters 2–4, we have attempted to provide some insight into these questions. Whilst each of the three questions has now been answered, they have also raised new questions, promoting further investigation.

1. *How well do climate models simulate the extratropical response to the MJO?*

   In general, climate models under-predict the extratropical response to the MJO. The findings of Chapter 2 are consistent with previous studies and are part of a common theme of under-prediction across many different tropical–extratropical interactions. Whilst some of the broad features of the NAO response to the MJO can be simulated, this response is universally too weak and is, in some cases, of the wrong sign. Of the CMIP6 models examined, the HadGEM3 model performs relatively well, but still struggles to fully capture the teleconnection when compared to ERA-interim reanalysis. We hypothesise that biases in MJO propagation speed may contribute to this under-prediction.

   The predictability provided by MJO teleconnections is key weather forecasting, and so affects everything from the economy, to transport, to energy production. This predictability, though, relies on the ability of models to properly realise the extratropical response to the MJO. Having addressed some shortfalls in the representation of MJO teleconnections in climate models, work can now be undertaken to fill these gaps.

2. *Does the extratropical response to the MJO vary on decadal time scales?*

   By comparing lagged MJO composites of $\psi 200$, $T850$, precipitation, and MSLP across two 21-winter-season time segments, we show, in Chapter 3, that the extratropical response to the MJO has changed on decadal time scales in ERA5 data. These changes are significant and are not a result of aliasing of the ENSO signal.

The two segments chosen coincide with opposite phases of AMV and the PDO, leading to the hypothesis that these modes of SST variability may modulate the MJO teleconnection pattern. Meteorological impacts of these changes in the teleconnection pattern are significant and widespread across the NH.

Further evidence for decadal variability was provided in Chapter 4. Both AMV and the PDO were shown to alter MJO teleconnections on decadal time scales, with the amplification of the NAO− response to MJO phase 6 by AMV+ consistent across both studies. It is difficult to compare the results directly due to the different data, methods and time scales used, however there seems to be some qualitative agreement.

With a fuller understanding of these meteorological impacts, future predictions can account for decadal variability in MJO teleconnections. This result adds to a number our understanding of how the extratropical response to the MJO varies across a range of time scales, taking a step towards greater predictability in the extratropics.

3. *What modulates decadal variability of the extratropical response to the MJO?*

   Our hypothesis that the extratropical response to the MJO is modified by both AMV and the PDO is strengthened by Chapter 3 and confirmed in Chapter 4. Changes in the teleconnections observed in Chapter 3 coincide with changes in AMV and the PDO, whilst statistically significant changes are observed in the response to all MJO phases for both AMV and the PDO in Chapter 4.

   In Chapter 4 we find that both the tropospheric and stratospheric teleconnection pathways from the MJO are altered by decadal SST variability. Nonlinear interactions and alterations in the SPV response to the MJO are key to the modulation of the MJO phase 6 teleconnection. Modification of the Rossby wave response is also central to this modulation, however some of the mechanisms behind the observed

changes in the teleconnection patterns are still to be uncovered.

There are some limitations on the robustness of these results due to known biases in the model used (see Chapter 2), however they still provide exciting insight and an essential first step towards a fuller understanding of the modulation of MJO teleconnections on decadal time scales. In turn, this greater understanding of MJO teleconnections will improve predictions of the extratropical weather and climate.

5.2 Evaluation of data, methodology, and limitations

Whilst care has been taken throughout the work presented to ensure that the data and methods used are up to date, appropriate for the task, and free from unnecessary bias, there are always limitations in science.

In Chapter 2, the limitations in climate models' ability to similulate MJO teleconnections are assessed. Climate models are found to underestimate MJO teleconnections. Taking this result in mind, care should be taken when using climate models to examine the extratropical response to the MJO further. There is certainly an opportunity to use these models to gain insight, but this should be validated using observational/reanalysis-based results where possible. For example, the pairing of a study using renalysis data (Chapter 3) with a model study (Chapter 4) provides additional strength to both pieces of work, especially since they can be put into context using Chapter 2.

On the other hand, the reanalysis data used in Chapter 3 has two key limitations. Since robust OLR observations are necessary to accurately describe the MJO using the RMM index, we have a relatively short observational record to work with. When considering decadal scale variability, this means we are left with a very small sample size and stuggle to make robust conclusions about the mechanisms behind changes in MJO teleconnections. Another limitation of using reanalysis data to study decadal scale variability is the potential presence

of a climate change signal. Whilst the data used has been detrended to remove most of the impacts of climate change, there will also be potential indirect effects on the various modes of variability. Hence, coupling these results with Chapter 4, which uses a pre-industrial control simulation to provide a much larger dataset free from climate change effects, helps to ease these limitations.

The statistical framework presented in Chapter 2 provides a simple way to interpret the differences in the MJO teleconnecton patterns between the reanalysis and model in the context of existing weather patterns. This framework, inspired by Cassou (2008), nicely captures changes in the magnitude of the teleconnections, but (as is shown in Chapters 3 and 4) there is also considerable spatial variability in the teleconnection patterns. As such, there may be more subtle differences between the reanalysis and model that are not picked up. It is for this reason that lagged composites are presented in Chapters 3 and 4, rather than the statistical framework.

Also, the results of Chapters 3 and 4 highlight the dependence of MJO teleconnections on the mean state and its variability on long time scales. If the analysis in Chapter 2 were to be repeated, the state of AMV, the PDO (and ENSO) should be taken into account, as differences in these modes may explain some of the differences in the teleconnection. It is difficult to directly compare the changes in the teleconnctions observed in Chapters Chapters 2 and 4, since they use very different methodologies, however a crude estimate would suggest that the effects are of the same order of magnitude. In Figure 4.5, we see that during AMV+, the NA response to MJO phase 6 is strengthended by a approximately 50–100%. Similarly, in Figure 2.4, we see a difference of around 30% in the likelihood of observing NAO− 10 days after MJO phase 6 between the model and reanalysis. Whilst these metrics cannot be directly compared, this suggests that the differences are at least comparable.

A change in the North Pacific Rossby waveguide, diagnosed using the stationary Rossby wavenumber, plays a key role in altering the MJO teleconnection pattern

seen in Chapter 3. There is scope to explore this further in the future, either by using a ray-tracing analysis (e.g. Barrett, 2019; Li et al., 2015*b*; Zhao et al., 2015), or by using 'E-vectors' (e.g. Hoskins et al., 1983; Matthews and Kiladis, 1999*b*). The stationary wavenumber provides a qualitative description of the Rossby wavefuide in the mean sense, whereas a ray-tracing analysis would directly diagnose the characteristics of individual Rossby waves. This method was avoided due to the time scales involved. Assessing decadal scale variability using ray-tracing would be very computationally expensive and would make drawing robust conclusions very difficult. If used in conjunction with an idealised modelling experiment with much shorter run times, it may be possible, however. E-vector analysis is similar to stationary Rossby wavenumber analysis in that it provides an estimate, based on some assumptions, for the path of Rossby waves. In this case the local group velocity of the Rossby waves can be inferred. The stationary wavenumber analysis provided the clear visualisation of the waveguide that was necessary for Chapter 3, however E-vectors could be used in future analyses as another option.

Significance testing has been used throughout this thesis to solidify arguments and justify conclusions. The effects of autocorrelation have, however, not always been taken into account. In Chapter 2, statistical significance is likely overestimated since each individual day of the analysis was considered an independent event, when in reality there exist autocorrelations in both the MJO and NAO. Each MJO phase is, on average, active for approximately 3–5 days (Figure 2.5), and the NAO has a decorrelation time scale of 5–6 days (Domeisen et al., 2018), so the number of independent samples is likely overestimated by a factor of 3–5 (i.e. the minimum of the two values above). This would mean that the test statistic, which is proportional to the square-root of the number of samples, is likely around twice the size it should be. This, in effect, means that statistical significance was overestimated by a factor of 2 in Chapter 2. Another way to view this, is that rather than the intended 95% threshold, significance is actually tested at the 84% threshold.

5.3 Possible avenues for future work

5.3.1 MJO teleconnections in future climates

Anthropogenic climate change (Mann et al., 1999; Masson-Delmotte et al., 2021; Pörtner et al., 2022) is projected to cause various changes in atmospheric dynamics (e.g. Christensen et al., 2022; Gillett et al., 2003; Gutierrez et al., 2022; Omrani et al., 2022; Woollings et al., 2018), leading to a range of potential impacts (e.g. Wright et al., 2023). These changes are predicted to increase the intensity of MJO-related precipitation anomalies, whilst weakening MJO-related circulation anomalies (e.g. Adames et al., 2017*a*,*b*; Arnold et al., 2014, 2015, 2013; Bui and Maloney, 2018, 2019*a*,*b*; Fu et al., 2020; Jones and Carvalho, 2006; Liu et al., 2013; Maloney et al., 2019*a*; Pritchard and Yang, 2016; Rushley et al., 2019; Takahashi et al., 2011).

MJO teleconnections are generally expected to be amplified in a warming climate (Samarasinghe et al., 2021; Wang et al., 2022; Zhou et al., 2020), which is surprising since these teleconnections are generally regarded as being a result of upper level divergence associate with the MJO (which, as mentioned above, are expected to weaken). These changes will bring greater MJO-induced predictability to the NA, but reduce predictability in the NP (Mayer and Barnes, 2022). There is, though, considerable uncertainty in future model simulations (Jenney et al., 2021; Wang et al., 2022), so further study is needed to solidify these results.

In Chapter 4 we show that low-frequency modes of variability can alter the extratropical response to the MJO, meaning that studies of changes in MJO teleconnections in future climates should be taken in this context. The state of these modes[1] should be accounted for when analysing different time periods, including those in the future.

5.3.2 Causal pathways for MJO teleconnections

As discussed in Section 1.4 and throughout Chapters 3 and 4, there are numerous modes of variability that are able to modulate MJO teleconnection patterns. This forms a complex system of causal relationships and influences, which are difficult to untangle. Through a composite analysis (Chapter 4), we have attempted to isolate the effect of different modes of variability on MJO teleconnections, however in doing this it is easy to lose sight of the system as a whole.

Causal network analysis (Ebert-Uphoff and Deng, 2012; Kretschmer et al., 2021; Nowack et al., 2020; Runge et al., 2019; Su et al., 2023) allows for the many interconnections of the system to be viewed simultaneously, concisely quantifying combined the effects of many different forcings. These methods have been used in various contexts across climate science (e.g. Di Capua et al., 2020; Hannart et al., 2015; Huang et al., 2021; Yessimbet et al., 2022) and allow for neat quantification and visualisation of otherwise complex systems. It would not be unreasonable to apply this type of methodology to MJO teleconnections, however the range of time scales involved, the non-linear nature of some relationships, and the presence of autocorrelations in the system all present challenges. Also, whilst it is possible to infer relationships using causal networks, they are best applied to the analysis of known relationships and systems. Hence studies such as those presented in Chapters 3 and 4 are still a necessary precursor to a causal network approach.

Barnes et al. (2019) used causal networks to consider ENSO modulation of MJO teleconnections, via both the tropospheric and stratospheric teleconnection pathways. Following on from the results presented here, this could now be expanded to include AMV and the PDO[2].

5.3.3 Modelling the simultaneous effects of SST variability on the basic state and MJO forcing

Arcodia and Kirtman (2023) present a very interesting analysis, in which

idealised models are used to pick apart the simultaneous ENSO modulation of MJO forcing and of the extratropical mean state, both of which combine to produce the observed ENSO modulation of the MJO teleconnection. In this way, the mechanisms behind the modulation of the teleconnection can be more clearly assessed. A similar approach could be taken with AMV and the PDO, by separately applying their modulation to the MJO and the extratropics.

An idealised modelling study would also provide greater flexibility and allow for a more indepth analysis of the mechanisms involved in the modulation of the MJO teleconnections. Whilst modelling could present some challenges due to the inability of most models to fully simulate the MJO, an intermediate model might be able to at least provide some insight. In this situation, the SST anomalies associated with the MJO could be artificially induced (in a similar way to Matthews and Kiladis (1999*a*)), whilst the AMV and PDO SST anomalies are also present. Some careful thought would need to go into the length of spinup needed to allow the atmosphere to equilibriate around the new mean SST state, before the MJO anomalies are introduced.

5.4 Summary

The extratropical response to the MJO varies on decadal time scales, and this variability is modulated by AMV and the PDO. Some of the mechanisms behind this modulation have been described, however some still pose open questions.

Climate models have considerable room for improvement when it comes to simulating MJO teleconnections, however they can still provide valuable insight, as long as results are viewed in context.

MJO teleconnections play a valuable role in the prediction of extratropical weather and climate, and these results will help to improve this predictability, especially on longer time scales. With greater knowledge of the decadal variability of MJO teleconnections, further studies can now be put into context

and prediction of extratropical weather can continue to improve.

Notes for Chapter 5

[1] Of course, other known modulators of MJO teleconnections should also be taken into account.

[2] It would also be interesting to include other modulators such as the QBO and IOD in this causal network analysis.

Appendix

Appendix A

Climate indices

Publicly available indices are used throughout, unless stated otherwise.

The RMM index for the MJO (Bureau of Meteorology, 2021; Wheeler and Hendon, 2004) is created projecting $U200$, $U850$, and OLR anomalies (with the ENSO signal filtered out) onto principle components (PCs), calculated from an EOF analysis in the original study (National Center for Atmospheric Research, 2022). This gives two time series – RMM1 and RMM2. The MJO amplitude is then defined as $\sqrt{\mathrm{RMM1}^2 + \mathrm{RMM2}^2}$, and the eight phases are defined as octants of the RMM1–RMM2 plane (Figure A.1).

The AMV index (NCAR Climate Analysis Section et al., 2006; Trenberth and Zhang, 2021; Trenberth and Shea, 2006) is defined by taking the mean of North Atlantic (0–60 °N) SST anomalies, and then subtracting the global mean SST anomaly to detrend. A 10-year low-pass filter is applied to isolate the multidecadal variability.

The PDO (Deser and Trenberth, 2016; Mantua, 1999) is defined as the first EOF of North Pacific (20–70 °N) SST anomalies (Figure A.2). The PDO index is created by projecting SST anomalies onto this EOF pattern.

The Niño 3.4 index (National Oceanic and Atmospheric Administration Earth System Research Laboratories, 2022; Trenberth, 2020) is calculated by taking the mean of equatorial mid-Pacific (5 °S–5 °N, 170–120 °W) SST anomalies. A 5-month running mean is applied to smooth the data.

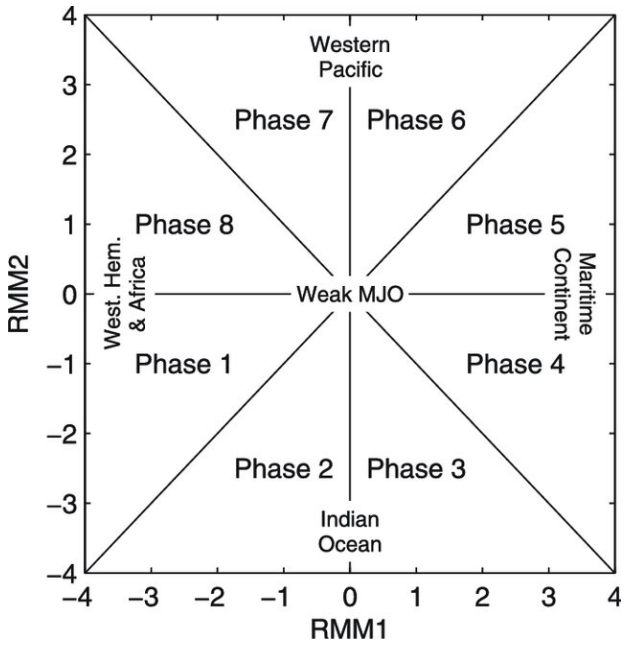

Figure A.1: Phase space of the RMM index (Wheeler and Hendon, 2004). The 8 MJO phases are marked as octants of the plane, whilst MJO amplitude corresponds to the radial distance from the origin. The location of enhanced convection is also marked. Adapted from Figure 1 of Virts and Wallace (2014).

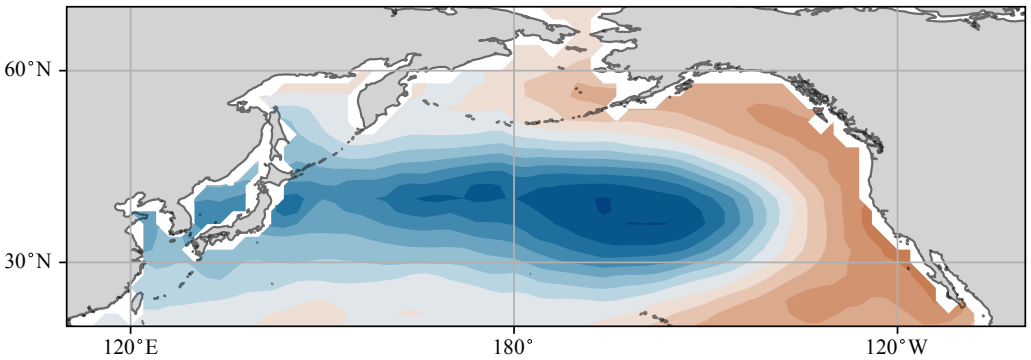

Figure A.2: SST loading pattern for the PDO. Data provided by the NOAA PSL at https://psl.noaa.gov/pdo/.

Appendix B

Further details on the NAO index

As stated in Section 2.3, both geopotential height and sea level pressure are commonly used when defining an index for the NAO. Below we show that within the statistical framework used in Chapter 2, the two indices are qualitatively equivalent.

To compare the response of North Atlantic geopotential height and sea level pressure responses to the MJO, we define two indices to describe the NAO. The first is the index described in Section 2.3, in which we take the difference in $Z500$ anomalies between two area averaged boxes over Iceland and the Azores (50–70 °N, 10–50 °W and 30–45 °N, 5–55 °W). The second index is identical to the first, excpet we take the difference in MSLP anomalies between the same two boxes. The analysis described in Section 2.3 is then performed using each index in turn with the results plotted in Figure B.1.

As we can see, there is little to no qualitative difference in the NAO response between the two regimes, highlighting the barotropic nature of the NAO.

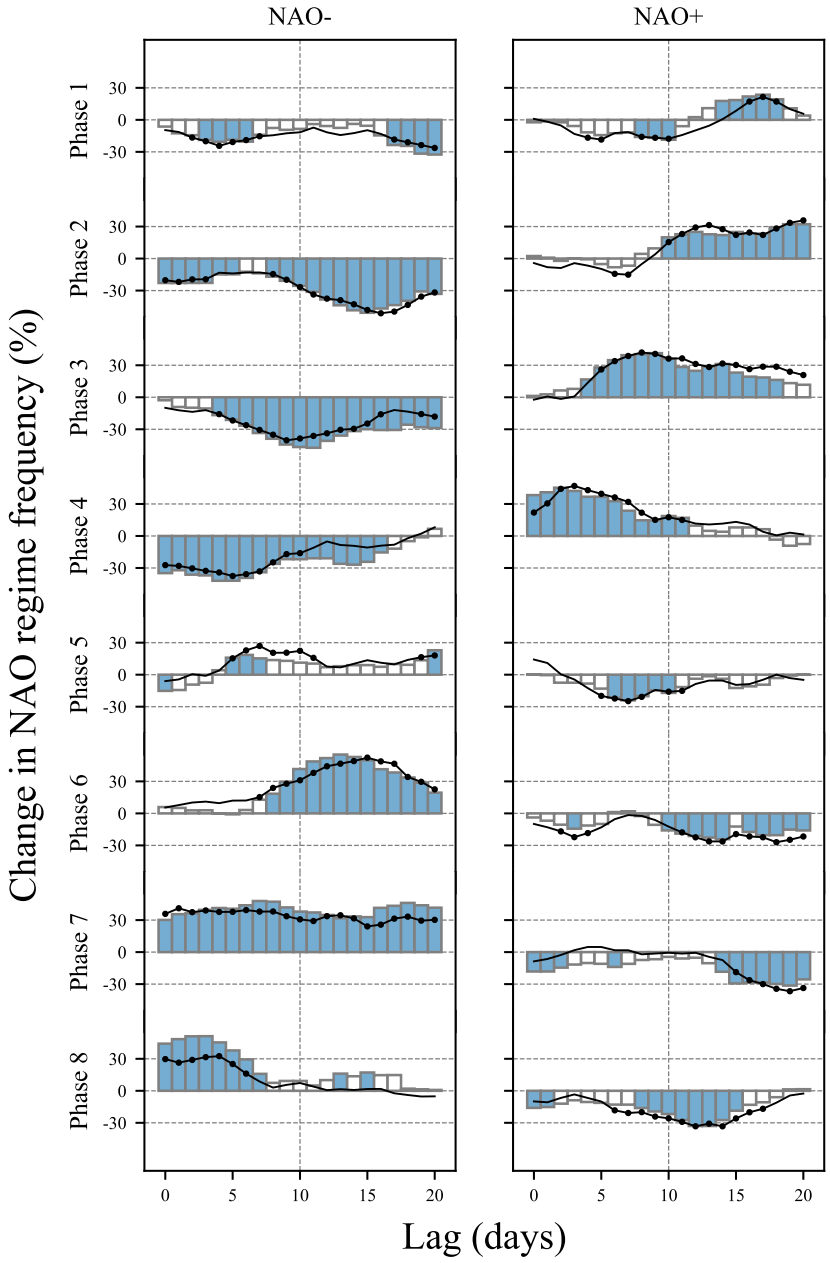

Figure B.1: The NAO response to the MJO in ERA-interim ($Z500$, MSLP, $U250$, $U850$) and NOAA OLR-interpolated (OLR) data using two different NAO indices. The black line represents the response seen when using anomalous $Z500$ data in the NAO index, with markers showing significance at the 95% level. The bars show the response seen when using the same NAO index but with MSLP used instead. Blue shading indicates significance at the 95% level. Qualitatively, the two methods are equivalent.

Appendix C

Supplementary Figures

Supplementary figures and tables for Chapter 4, which have been included here to completeness.

Table C.1: The total number of days in which each MJO phase and SST state are 'active' (see Section 4.3) simultaneously. This is also the number of days included in the creation of relevant composites.

Phase	Overall	AMV+	AMVn	AMV-	PDO+	PDOn	PDO-
1	14773	2225	9924	2370	2114	9812	2593
2	15613	2395	10370	2556	2169	10411	2741
3	16971	2490	11383	2808	2206	11414	3061
4	16360	2408	11099	2518	2346	10908	2771
5	14935	2404	9926	2354	2435	9928	2321
6	15241	2762	9981	2237	2584	10168	2228
7	16391	2935	10845	2329	2625	11098	2386
8	16692	2694	11075	2655	2504	11209	2711

Table C.2: As in Table C.1, but with one decadal mode of variability fixed as neutral. This represents the number of days included in the majority of composites presented in Chapter 4. The numbers shown in brackets are number of days removed by fixing the other mode to neutral (i.e. the upper-left box shows 1599 days in which MJO phase 1, AMV+ and PDO*n* were simultaneously active, however from Table C.1, we see that there were 2225 days in which MJO phase 1 and AMV+ were simultaneously active, giving 2225−1599=626 days lost as a result of constraining PDOn.)

Phase	AMV+, PDOn	AMV-, PDOn	PDO+, AMVn	PDO-, AMVn
1	1599 (626)	1356 (1014)	1441 (673)	1626 (967)
2	1735 (660)	1472 (1084)	1480 (689)	1686 (1055)
3	1783 (707)	1645 (1163)	1495 (711)	1902 (1159)
4	1730 (678)	1543 (975)	1663 (683)	1801 (970)
5	1585 (819)	1472 (882)	1590 (845)	1465 (856)
6	1822 (940)	1408 (829)	1607 (977)	1436 (792)
7	2012 (923)	1518 (811)	1693 (932)	1584 (802)
8	1891 (803)	1697 (958)	1685 (819)	1769 (942)

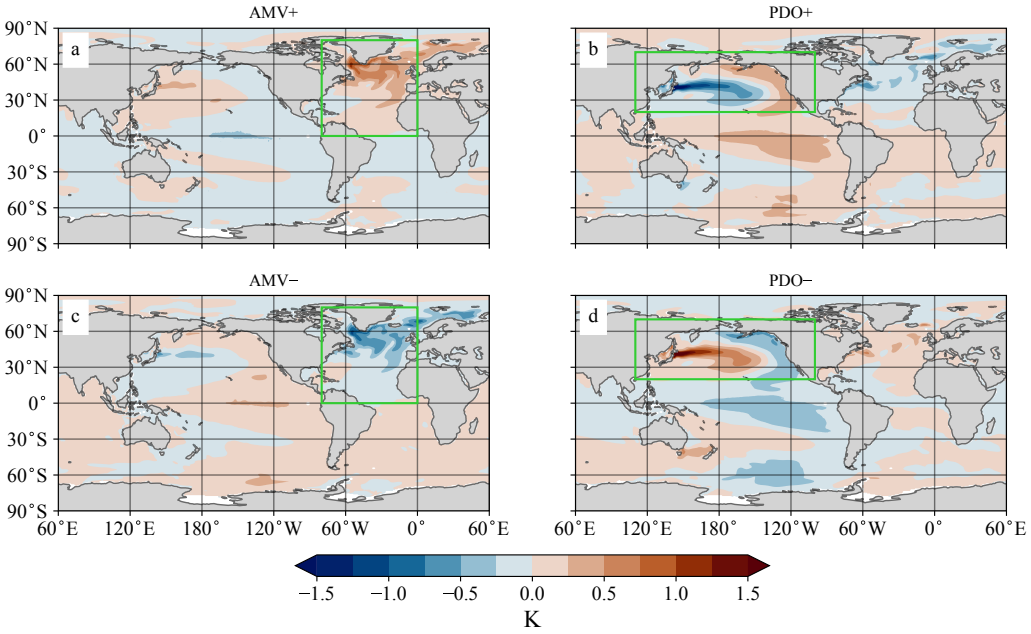

Figure C.1: November–April composites of SST anomalies for (a) AMV+, (b) PDO+, (c) AMV−, and (d) PDO−, in the UKESM pre-industrial control simulation. Composites are taken over all winter seasons in which the respective index has value greater than one. The green box in each panel denotes the region used to calculate the respective index.

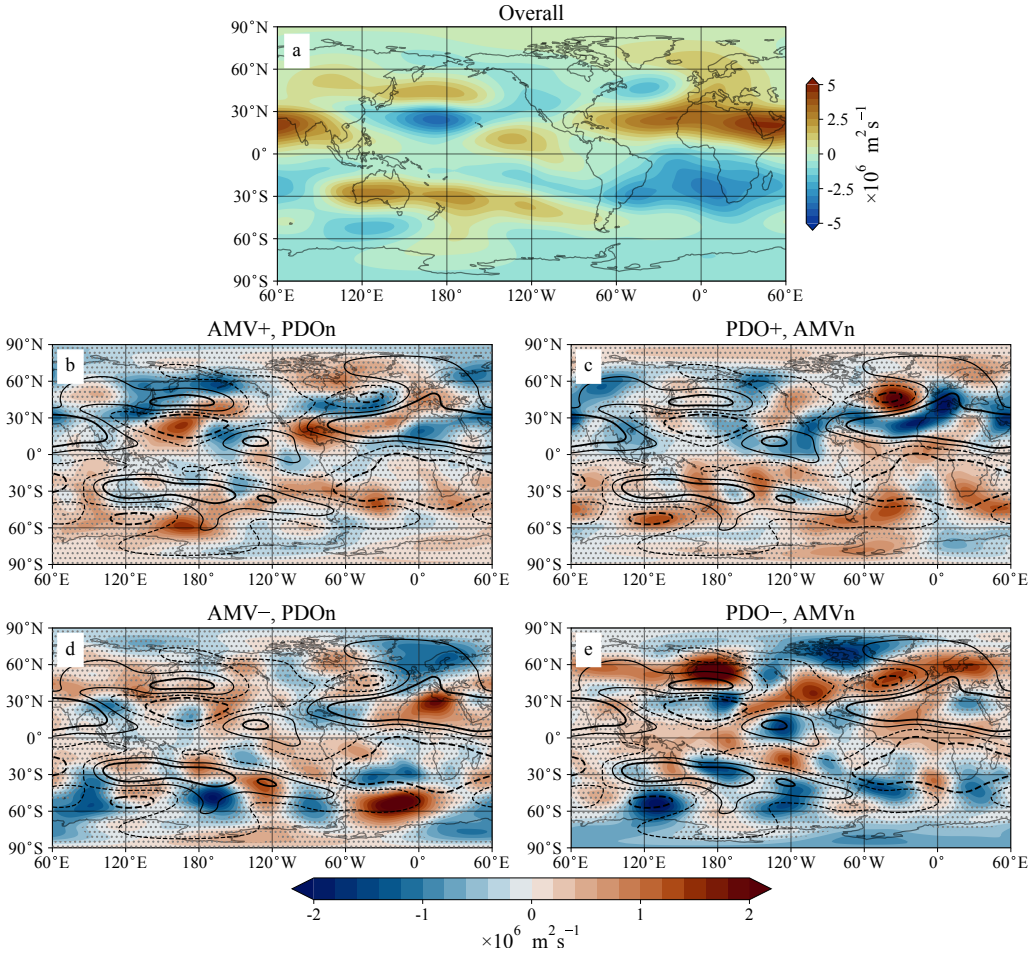

Figure C.2: Change in lag 10-day ψ250 anomalies. As in Figure 4.6, but for MJO phase 1.

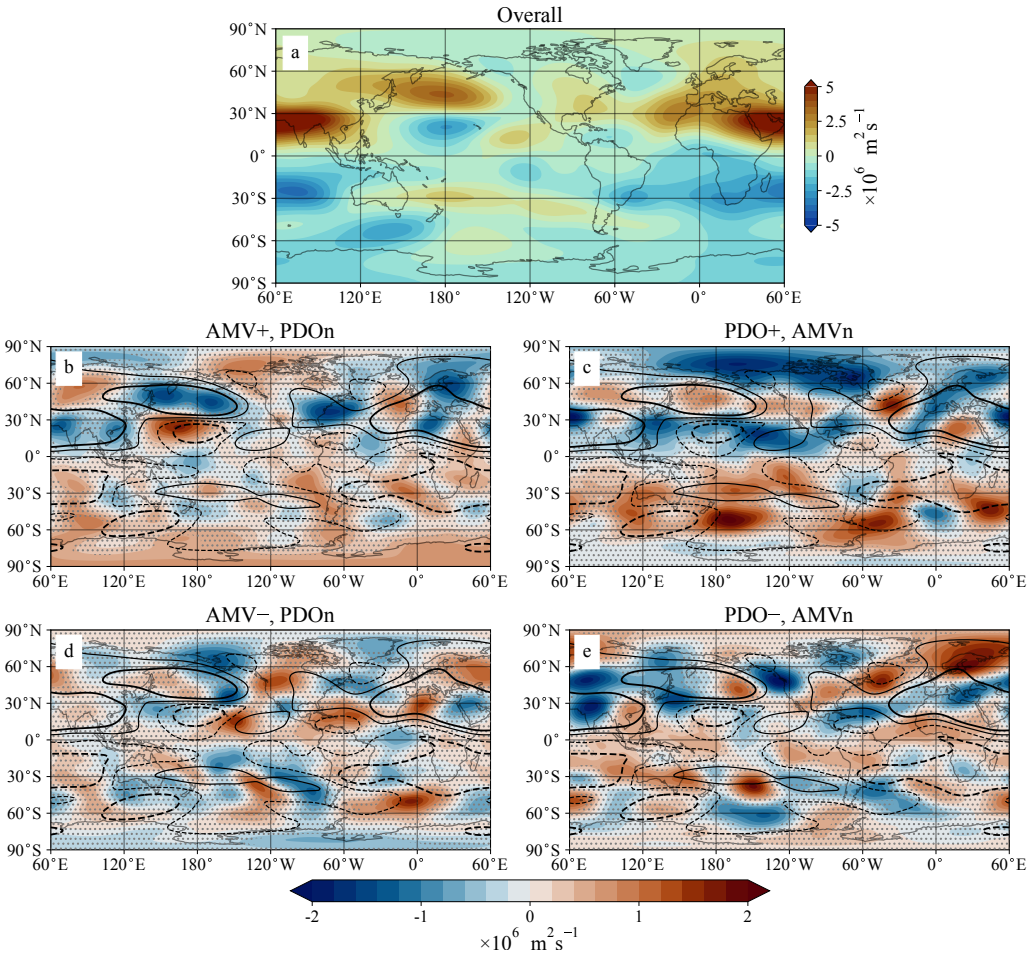

Figure C.3: Change in lag 10-day ψ250 anomalies. As in Figure 4.6, but for MJO phase 2.

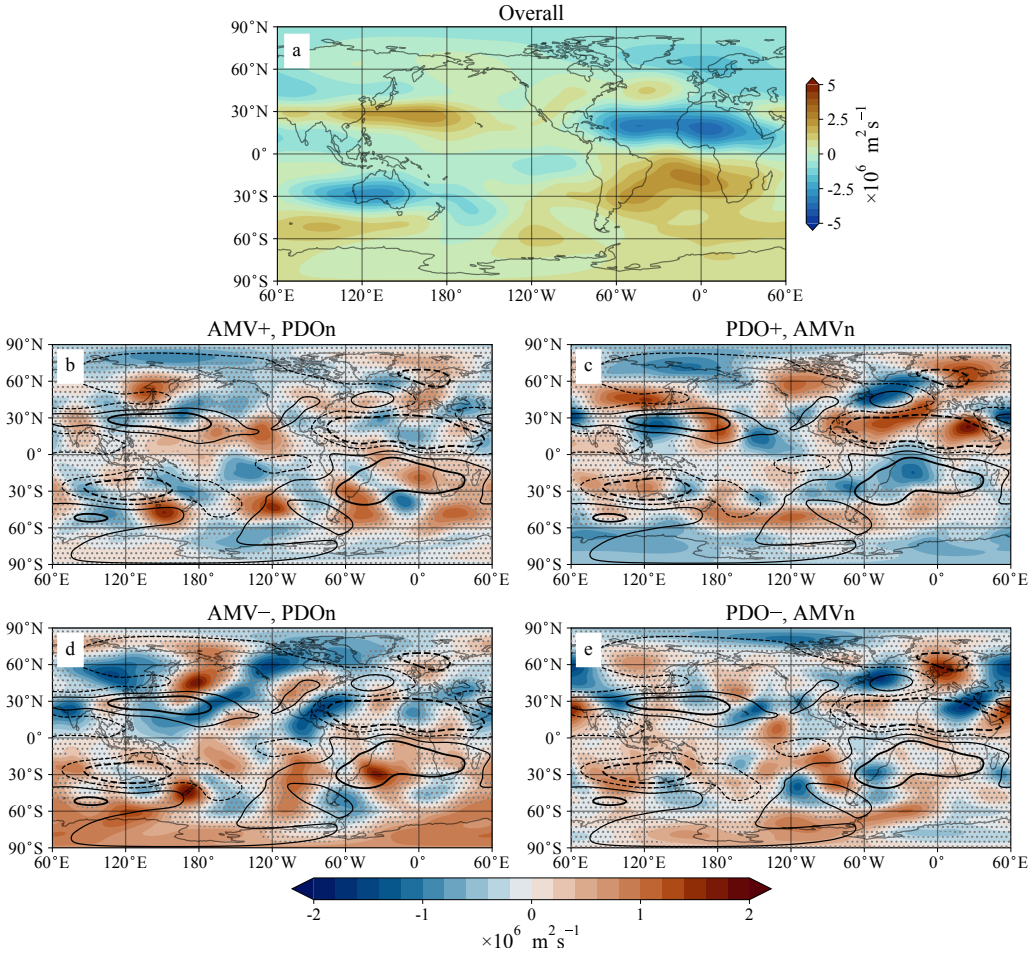

Figure C.4: Change in lag 10-day ψ250 anomalies. As in Figure 4.6, but for MJO phase 4.

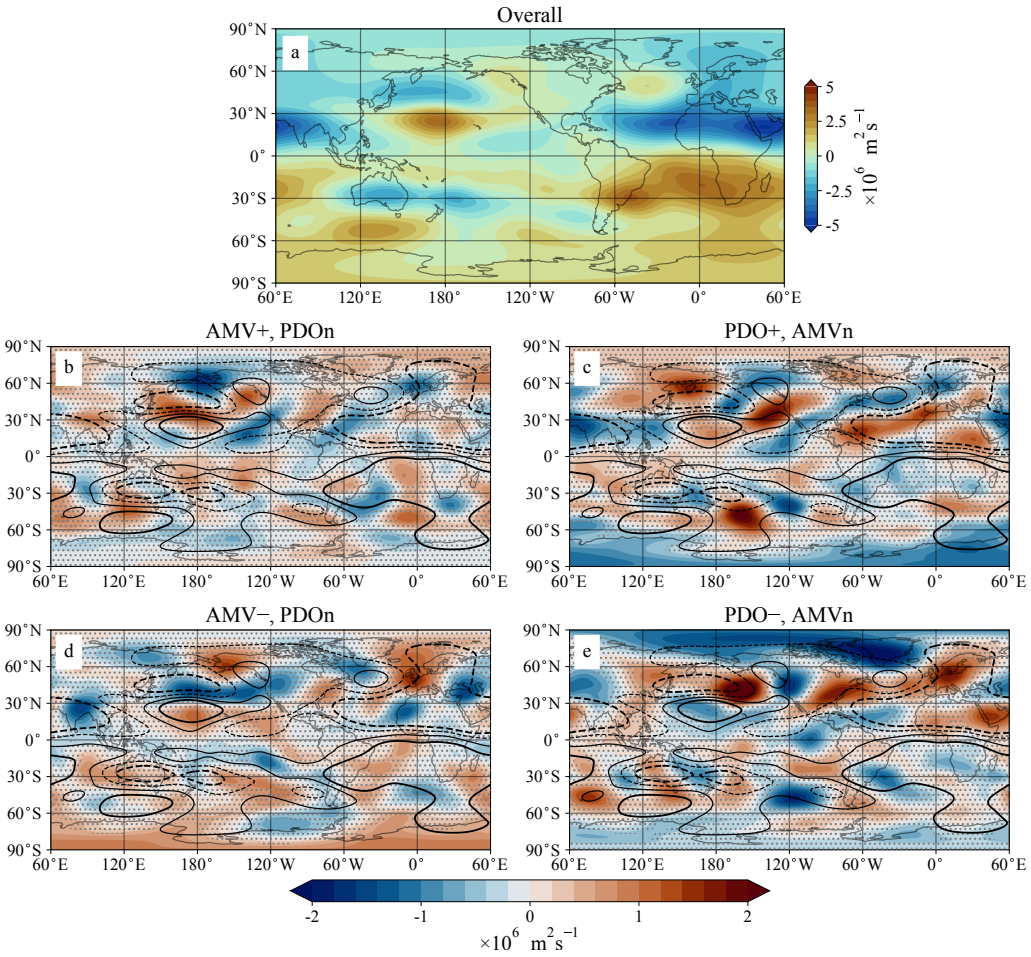

Figure C.5: Change in lag 10-day ψ250 anomalies. As in Figure 4.6, but for MJO phase 5.

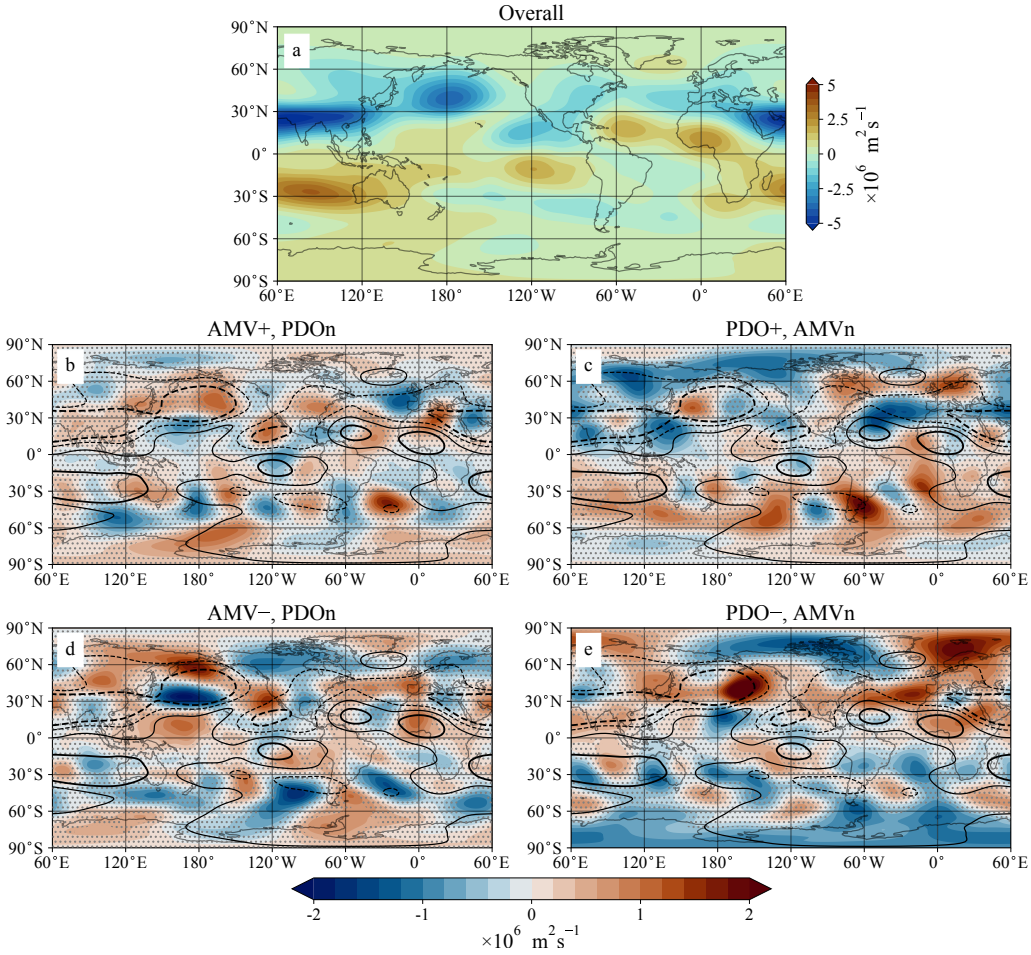

Figure C.6: Change in lag 10-day ψ250 anomalies. As in Figure 4.6, but for MJO phase 7.

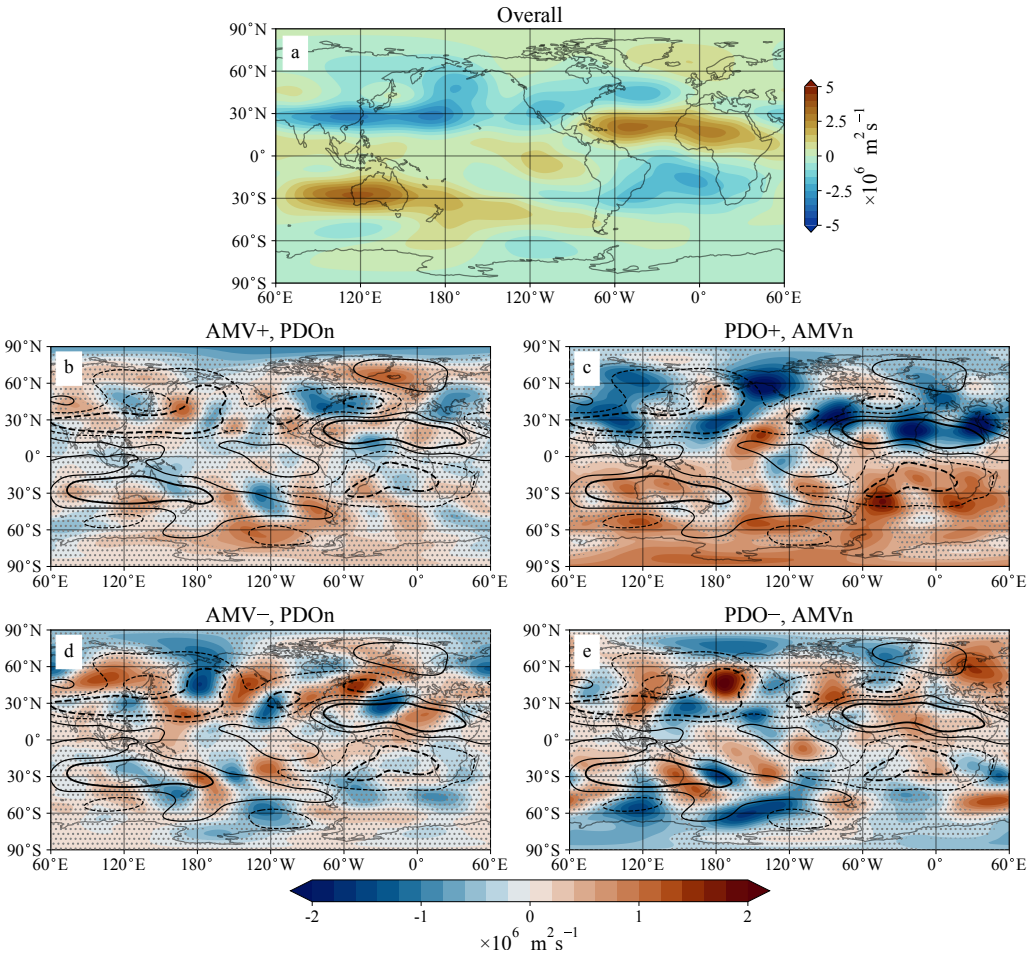

Figure C.7: Change in lag 10-day ψ250 anomalies. As in Figure 4.6, but for MJO phase 8.

Bibliography

Adames, Á. F. and Kim, D. (**2016**) The MJO as a Dispersive, Convectively Coupled Moisture Wave: Theory and Observations. *Journal of the Atmospheric Sciences*, **73**(3): 913 –941. doi.org/10.1175/JAS-D-15-0170.1

Adames, Á. F., Kim, D., Sobel, A. H., Del Genio, A., and Wu, J. (**2017***a*) Changes in the structure and propagation of the MJO with increasing CO2. *Journal of Advances in Modeling Earth Systems*, **9**(2): 1251–1268. doi.org/10.1002/2017MS000913

Adames, Á. F., Kim, D., Sobel, A. H., Del Genio, A., and Wu, J. (**2017***b*) Characterization of Moist Processes Associated With Changes in the Propagation of the MJO With Increasing CO2. *Journal of Advances in Modeling Earth Systems*, **9**(8): 2946–2967. doi.org/10.1002/2017MS001040

Afargan-Gerstman, H., Jiménez-Esteve, B., and Domeisen, D. I. V. (**2022**) On the Relative Importance of Stratospheric and Tropospheric Drivers for the North Atlantic Jet Response to Sudden Stratospheric Warming Events. *Journal of Climate*, **35**(19): 6453–6467. doi.org/10.1175/JCLI-D-21-0680.1

Ahn, M.-S., Kim, D., Kang, D., Lee, J., Sperber, K. R., Gleckler, P. J., Jiang, X., Ham, Y.-G., and Kim, H. (**2020**) MJO Propagation Across the Maritime Continent: Are CMIP6 Models Better Than CMIP5 Models? *Geophysical Research Letters*, **47**(11). doi.org/10.1029/2020GL087250

Ahn, M.-S., Kim, D., Sperber, K. R., Kang, I.-S., Maloney, E., Waliser, D., and Hendon, H. (**2017**) MJO simulation in CMIP5 climate models: MJO skill

metrics and process-oriented diagnosis. *Climate Dynamics*, **49**(11): 4023–4045. doi.org/10.1007/s00382-017-3558-4

Ajayamohan, R. S., Rao, S. A., Luo, J.-J., and Yamagata, T. (**2009**) Influence of Indian Ocean Dipole on boreal summer intraseasonal oscillations in a coupled general circulation model. *Journal of Geophysical Research: Atmospheres*, **114**: D06,119. doi.org/10.1029/2008JD011096

Allan, R., Lindesay, J., Parker, D., et al. (**1996**) *El Niño Southern Oscillation & climatic variability*. CSIRO publishing

Ambaum, M. H. P., Hoskins, B. J., and Stephenson, D. B. (**2001**) Arctic Oscillation or North Atlantic Oscillation? *Journal of Climate*, **14**(16): 3495–3507. doi.org/10.1175/1520-0442(2001)014⟨3495:AOONAO⟩2.0.CO;2

Andrews, D. G., Holton, J. R., and Leovy, C. B. (**1987**) *Middle atmosphere dynamics*. 40. Academic press

Andrews, M. B., Ridley, J. K., Wood, R. A., Andrews, T., Blockley, E. W., Booth, B., Burke, E., Dittus, A. J., Florek, P., Gray, L. J., Haddad, S., Hardiman, S. C., Hermanson, L., Hodson, D., Hogan, E., Jones, G. S., Knight, J. R., Kuhlbrodt, T., Misios, S., Mizielinski, M. S., Ringer, M. A., Robson, J., and Sutton, R. T. (**2020**) Historical Simulations With HadGEM3–GC3.1 for CMIP6. *Journal of Advances in Modeling Earth Systems*, **12**(6). doi.org/10.1029/2019MS001995

Anstey, J. A. and Shepherd, T. G. (**2014**) High-latitude influence of the quasi-biennial oscillation. *Quarterly Journal of the Royal Meteorological Society*, **140**(678): 1–21. doi.org/10.1002/qj.2132

Arcodia, M. and Kirtman, B. (**2023**) Using simplified linear and nonlinear models to assess ENSO-modulated MJO teleconnections. *Climate Dynamics*. doi.org/10.1007/s00382-023-06864-x

Arcodia, M. C., Kirtman, B. P., and Siqueira, L. S. P. (**2020**) How MJO Teleconnections and ENSO Interference Impacts U.S. Precipitation. *Journal of Climate*, **33**(11): 4621–4640. doi.org/10.1175/JCLI-D-19-0448.1

Arnold, N. P., Branson, M., Burt, M. A., Abbot, D. S., Kuang, Z., Randall, D. A., and Tziperman, E. (**2014**) Effects of explicit atmospheric convection at high CO_2. *Proceedings of the National Academy of Sciences*, **111**(30): 10,943–10,948. doi.org/10.1073/pnas.1407175111

Arnold, N. P., Branson, M., Kuang, Z., Randall, D. A., and Tziperman, E. (**2015**) MJO intensification with warming in the superparameterized CESM. *Journal of Climate*, **28**(7): 2706–2724. doi.org/10.1175/JCLI-D-14-00494.1

Arnold, N. P., Kuang, Z., and Tziperman, E. (**2013**) Enhanced MJO-like Variability at High SST. *Journal of Climate*, **26**(3): 988–1001. doi.org/10.1175/JCLI-D-12-00272.1

Athanasiadis, P. J., Yeager, S., Kwon, Y.-O., Bellucci, A., Smith, D. W., and Tibaldi, S. (**2020**) Decadal predictability of North Atlantic blocking and the NAO. *npj Climate and Atmospheric Science*, **3**(20). 10.1038/s41612-020-0120-6

Ayarzagüena, B., Charlton-Perez, A. J., Butler, A. H., Hitchcock, P., Simpson, I. R., Polvani, L. M., Butchart, N., Gerber, E. P., Gray, L., Hassler, B., Lin, P., Lott, F., Manzini, E., Mizuta, R., Orbe, C., Osprey, S., Saint-Martin, D., Sigmond, M., Taguchi, M., Volodin, E. M., and Watanabe, S. (**2020**) Uncertainty in the Response of Sudden Stratospheric Warmings and Stratosphere-Troposphere Coupling to Quadrupled CO2 Concentrations in CMIP6 Models. *Journal of Geophysical Research: Atmospheres*, **125**(6): e2019JD032,345. doi.org/10.1029/2019JD032345

Baldwin, M. P., Ayarzag uena, B., Birner, T., Butchart, N., Butler, A. H., Charlton-Perez, A. J., Domeisen, D. I. V., Garfinkel, C. I., Garny, H., Gerber, E. P., Hegglin, M. I., Langematz, U., and Pedatella, N. M. (**2021**) Sudden Stratospheric Warmings. *Reviews of Geophysics*, **59**(1): e2020RG000,708. doi.org/10.1029/2020RG000708

Baldwin, M. P. and Dunkerton, T. J. (**1998**) Quasi-biennial modulation of the southern hemisphere stratospheric polar vortex. *Geophysical Research*

Letters, **25**(17): 3343–3346. doi.org/10.1029/98GL02445

Baldwin, M. P. and Dunkerton, T. J. (**1999**) Propagation of the Arctic Oscillation from the stratosphere to the troposphere. *Journal of Geophysical Research: Atmospheres*, **104**(D24): 30,937–30,946. doi.org/10.1029/1999JD900445

Baldwin, M. P. and Dunkerton, T. J. (**2001**) Stratospheric Harbingers of Anomalous Weather Regimes. *Science*, **294**(5542): 581–584. doi.org/10.1126/science.1063315

Baldwin, M. P., Gray, L. J., Dunkerton, T. J., Hamilton, K., Haynes, P. H., Randel, W. J., Holton, J. R., Alexander, M. J., Hirota, I., Horinouchi, T., Jones, D. B. A., Kinnersley, J. S., Marquardt, C., Sato, K., and Takahashi, M. (**2001**) The quasi-biennial oscillation. *Reviews of Geophysics*, **39**(2): 179–229. doi.org/10.1029/1999RG000073

Bao, M. and Hartmann, D. L. (**2014**) The response to MJO-like forcing in a nonlinear shallow-water model. *Geophysical Research Letters*, **41**(4): 1322–1328. doi.org/10.1002/2013GL057683

Baranowski, D. B., Flatau, M. K., Flatau, P. J., and Matthews, A. J. (**2016**) Impact of atmospheric convectively coupled equatorial Kelvin waves on upper ocean variability. *Journal of Geophysical Research: Atmospheres*, **121**(5): 2045–2059. doi.org/10.1002/2015JD024150

Barnes, E. A., Samarasinghe, S. M., Ebert-Uphoff, I., and Furtado, J. C. (**2019**) Tropospheric and Stratospheric Causal Pathways Between the MJO and NAO. *Journal of Geophysical Research: Atmospheres*, **124**(16): 9356–9371. doi.org/10.1029/2019JD031024

Barnston, A. G. and Livezey, R. E. (**1987**) Classification, Seasonality and Persistence of Low-Frequency Atmospheric Circulation Patterns. *Monthly Weather Review*, **115**(6): 1083–1126. doi.org/10.1175/1520-0493(1987)115⟨1083:CSAPOL⟩2.0.CO;2

Barrett, B. S. (**2019**) Connections between the Madden–Julian Oscillation and

surface temperatures in winter 2018 over eastern North America. *Atmospheric Science Letters*, **20**(1): e869. doi.org/10.1002/asl.869

Bi, D., Dix, M., Marsland, S., O'Farrell, S., Sullivan, A., Bodman, R., Law, R., Harman, I., Srbinovsky, J., Rashid, H. A., Dobrohotoff, P., Mackallah, C., Yan, H., Hirst, A., Savita, A., Dias, F. B., Woodhouse, M., Fiedler, R., and Heerdegen, A. (**2020**) Configuration and spin-up of ACCESS-CM2, the new generation Australian Community Climate and Earth System Simulator Coupled Model. *Journal of Southern Hemisphere Earth Systems Science*, **70**(1): 225–251. doi.org/10.1071/ES19040

Bjerknes, J. (**1964**) *Atlantic Air-Sea Interaction*, volume 10 of *Advances in Geophysics*. Elsevier. doi.org/10.1016/S0065-2687(08)60005-9

Bjerknes, J. (**1969**) Atmospheric teleconnections from the equatorial Pacific. *Monthly Weather Review*, **97**(3): 163–172. doi.org/10.1175/1520-0493(1969)097⟨0163:ATFTEP⟩2.3.CO;2

Black, R. X. and McDaniel, B. A. (**2004**) Diagnostic Case Studies of the Northern Annular Mode. *Journal of Climate*, **17**(20): 3990–4004. doi.org/10.1175/1520-0442(2004)017⟨3990:DCSOTN⟩2.0.CO;2

Bliss, E. W. (**1926**) British winters in relation to world weather. *Memoirs of the Royal Meteorological Society*, **1**(6): 87–92. https://www.rmets.org/sites/default/files/blissmem1-6.pdf

Bloomfield, H. C., Brayshaw, D. J., Gonzalez, P. L. M., and Charlton-Perez, A. (**2021**) Sub-seasonal forecasts of demand and wind power and solar power generation for 28 European countries. *Earth System Science Data*, **13**(5): 2259–2274. doi.org/10.5194/essd-13-2259-2021

Boucher, O., Denvil, S., Levavasseur, G., Cozic, A., Caubel, A., Foujols, M.-A., Meurdesoif, Y., Cadule, P., Devilliers, M., Ghattas, J., Lebas, N., Lurton, T., Mellul, L., Musat, I., Mignot, J., and Cheruy, F. (**2018**) IPSL IPSL-CM6A-LR model output prepared for CMIP6 CMIP historical. *Earth System Grid Federation*. doi.org/10.22033/ESGF/CMIP6.5195. Accessed

from the Centre for Environmental Data Analysis (CEDA) archive on 11th September 2021

Boucher, O., Servonnat, J., Albright, A. L., Aumont, O., Balkanski, Y., Bastrikov, V., Bekki, S., Bonnet, R., Bony, S., Bopp, L., Braconnot, P., Brockmann, P., Cadule, P., Caubel, A., Cheruy, F., Codron, F., Cozic, A., Cugnet, D., D'Andrea, F., Davini, P., de Lavergne, C., Denvil, S., Deshayes, J., Devilliers, M., Ducharne, A., Dufresne, J.-L., Dupont, E., Éthé, C., Fairhead, L., Falletti, L., Flavoni, S., Foujols, M.-A., Gardoll, S., Gastineau, G., Ghattas, J., Grandpeix, J.-Y., Guenet, B., Guez, Lionel, E., Guilyardi, E., Guimberteau, M., Hauglustaine, D., Hourdin, F., Idelkadi, A., Joussaume, S., Kageyama, M., Khodri, M., Krinner, G., Lebas, N., Levavasseur, G., Lévy, C., Li, L., Lott, F., Lurton, T., Luyssaert, S., Madec, G., Madeleine, J.-B., Maignan, F., Marchand, M., Marti, O., Mellul, L., Meurdesoif, Y., Mignot, J., Musat, I., Ottlé, C., Peylin, P., Planton, Y., Polcher, J., Rio, C., Rochetin, N., Rousset, C., Sepulchre, P., Sima, A., Swingedouw, D., Thiéblemont, R., Traore, A. K., Vancoppenolle, M., Vial, J., Vialard, J., Viovy, N., and Vuichard, N. (**2020**) Presentation and Evaluation of the IPSL-CM6A-LR Climate Model. *Journal of Advances in Modeling Earth Systems*, **12**(7): e2019MS002,010. doi.org/10.1029/2019MS002010

Bracegirdle, T. J., Lu, H., Eade, R., and Woollings, T. (**2018**) Do CMIP5 Models Reproduce Observed Low-Frequency North Atlantic Jet Variability? *Geophysical Research Letters*, **45**(14): 7204–7212. doi.org/10.1029/2018GL078965

Branstator, G. (**2002**) Circumglobal Teleconnections, the Jet Stream Waveguide, and the North Atlantic Oscillation. *Journal of Climate*, **15**(14): 1893–1910. doi.org/10.1175/1520-0442(2002)015⟨1893:CTTJSW⟩2.0.CO;2

Bui, H. X. and Maloney, E. D. (**2018**) Changes in Madden–Julian Oscillation Precipitation and Wind Variance Under Global Warming. *Geophysical Research Letters*, **45**(14): 7148–7155. 10.1029/2018GL078504

Bui, H. X. and Maloney, E. D. (**2019***a*) Mechanisms for Global Warming Impacts on Madden–Julian Oscillation Precipitation Amplitude. *Journal of Climate*, **32**(20): 6961–6975. 10.1175/JCLI-D-19-0051.1

Bui, H. X. and Maloney, E. D. (**2019***b*) Transient Response of MJO Precipitation and Circulation to Greenhouse Gas Forcing. *Geophysical Research Letters*, **46**(22): 13,546–13,555. doi.org/10.1029/2019GL085328

Bureau of Meteorology (**2021**) RMM Data. *Bureau of Meteorology*. http://www.bom.gov.au/climate/mjo. Accessed: 19/07/2021

Butchart, N. (**2022**) The stratosphere: a review of the dynamics and variability. *Weather and Climate Dynamics*, **3**(4): 1237–1272. doi.org/10.5194/wcd-3-1237-2022

Butler, A., Charlton-Perez, A., Domeisen, D. I., Garfinkel, C., Gerber, E. P., Hitchcock, P., Karpechko, A. Y., Maycock, A. C., Sigmond, M., Simpson, I., and Son, S.-W. (**2019**) Chapter 11 - Sub-seasonal Predictability and the Stratosphere. *In* A. W. Robertson and F. Vitart (Editors), *Sub-Seasonal to Seasonal Prediction*, pages 223–241. Elsevier. ISBN 978-0-12-811714-9. doi.org/10.1016/B978-0-12-811714-9.00011-5

Butler, A. H., Karpechko, A. Y., and Garfinkel, C. I. (**2023**) Amplified Decadal Variability of Extratropical Surface Temperatures by Stratosphere-Troposphere Coupling. *Geophysical Research Letters*, **50**(16): e2023GL104,607. doi.org/10.1029/2023GL104607

Byun, Y.-H., Lim, Y.-J., Sung, H. M., Kim, J., Sun, M., and Kim, B.-H. (**2019**) NIMS-KMA KACE1.0-G model output prepared for CMIP6 CMIP historical. *Earth System Grid Federation*. doi.org/10.22033/ESGF/CMIP6.8378. Accessed from the Centre for Environmental Data Analysis (CEDA) archive on 11th September 2021

Cantelaube, P. and Terres, J.-M. (**2005**) Seasonal weather forecasts for crop yield modelling in Europe. *Tellus A: Dynamic Meteorology and Oceanography*, **57**(3): 476–487. doi.org/10.3402/tellusa.v57i3.14669

Cassou, C. (**2008**) Intraseasonal interaction between the Madden-Julian Oscillation and the North Atlantic Oscillation. *Nature*, **455**(7212): 523–527. ISSN 00280836. doi.org/10.1038/nature07286

Centre National de Recherches Météorologiques and Centre Européen de Recherche et Formation Avancée en Calcul Scientifique (**2019**) WCRP CMIP6: the CNRM-CERFACS team CNRM-CM6-1 model output collection. *Centre for Environmental Data Analysis*. http://catalogue.ceda.ac.uk/uuid/a6b405382ac443a7aa26e520f8507e8f. Accessed: 09/09/2021

Challinor, A. J., Slingo, J. M., Wheeler, T. R., and Doblas–Reyes, F. J. (**2005**) Probabilistic simulations of crop yield over western India using the DEMETER seasonal hindcast ensembles. *Tellus A: Dynamic Meteorology and Oceanography*, **57**(3): 498–512. doi.org/10.3402/tellusa.v57i3.14670

Charlton, A. J. and Polvani, L. M. (**2007**) A New Look at Stratospheric Sudden Warmings. Part I: Climatology and Modeling Benchmarks. *Journal of Climate*, **20**(3): 449–469. doi.org/10.1175/JCLI3996.1

Charlton, A. J., Polvani, L. M., Perlwitz, J., Sassi, F., Manzini, E., Shibata, K., Pawson, S., Nielsen, J. E., and Rind, D. (**2007**) A New Look at Stratospheric Sudden Warmings. Part II: Evaluation of Numerical Model Simulations. *Journal of Climate*, **20**(3): 470–488. doi.org/10.1175/JCLI3994.1

Charlton-Perez, A. J., Baldwin, M. P., Birner, T., Black, R. X., Butler, A. H., Calvo, N., Davis, N. A., Gerber, E. P., Gillett, N., Hardiman, S., Kim, J., Krüger, K., Lee, Y.-Y., Manzini, E., McDaniel, B. A., Polvani, L., Reichler, T., Shaw, T. A., Sigmond, M., Son, S.-W., Toohey, M., Wilcox, L., Yoden, S., Christiansen, B., Lott, F., Shindell, D., Yukimoto, S., and Watanabe, S. (**2013**) On the lack of stratospheric dynamical variability in low-top versions of the CMIP5 models. *Journal of Geophysical Research: Atmospheres*, **118**(6): 2494–2505. doi.org/10.1002/jgrd.50125

Chen, G. (**2021**) Diversity of the Global Teleconnections Associated with the

Madden–Julian Oscillation. *Journal of Climate*, **34**(1): 397–414. doi.org/10.1175/JCLI-D-20-0357.1

Chen, X., Ling, J., and Li, C. (**2016**) Evolution of the Madden–Julian Oscillation in Two Types of El Niño. *Journal of Climate*, **29**(5): 1919–1934. doi.org/10.1175/JCLI-D-15-0486.1

Cherry, J., Cullen, H., Visbeck, M., Small, A., and Uvo, C. (**2005**) Impacts of the North Atlantic Oscillation on Scandinavian Hydropower Production and Energy Markets. *Water Resources Management*, **19**: 673–691. doi.org/10.1007/s11269-005-3279-z

Christensen, H. M., Berner, J., Coleman, D. R. B., and Palmer, T. N. (**2017**) Stochastic Parameterization and El Niño–Southern Oscillation. *Journal of Climate*, **30**(1): 17–38. doi.org/10.1175/JCLI-D-16-0122.1

Christensen, O. B., Kjellström, E., Dieterich, C., Gröger, M., and Meier, H. E. M. (**2022**) Atmospheric regional climate projections for the Baltic Sea region until 2100. *Earth System Dynamics*, **13**(1): 133–157. doi.org/10.5194/esd-13-133-2022

Ciesielski, P. E., Johnson, R. H., Jiang, X., Zhang, Y., and Xie, S. (**2017**) Relationships between radiation, clouds, and convection during DYNAMO. *Journal of Geophysical Research: Atmospheres*, **122**(5): 2529–2548. doi.org/10.1002/2016JD025965

Clark, R. T., Bett, P. E., Thornton, H. E., and Scaife, A. A. (**2017**) Skilful seasonal predictions for the European energy industry. *Environmental Research Letters*, **12**(2): 024,002. doi.org/10.1088/1748-9326/aa57ab

Coburn, J. and Pryor, S. C. (**2021**) Differential Credibility of Climate Modes in CMIP6. *Journal of Climate*, **34**(20): 8145–8164. doi.org/10.1175/JCLI-D-21-0359.1

Cook, E. R., D'Arrigo, R. D., and Briffa, K. R. (**1998**) A reconstruction of the North Atlantic Oscillation using tree-ring chronologies from North America and Europe. *The Holocene*, **8**(1): 9–17. doi.org/10.1191/095968398677793725

Crameri, F. (**2018***a*) Geodynamic diagnostics,scientific visualisation and StagLab 3.0. *Geoscientific Model Development*, **11**: 2541–2562. doi.org/10.5194/gmd-11-2541-2018

Crameri, F. (**2018***b*) Scientific colour maps. *Zenodo*. doi.org/10.5281/zenodo.1243862

Crameri, F., Shephard, G. E., and Heron, P. J. (**2020**) The misuse of colour in science communication. *Nature Communications*, **11**: 5444. doi.org/10.1038/s41467-020-19160-7

Crhová, L. and Holtanová, E. (**2018**) Simulated relationship between air temperature and precipitation over Europe: sensitivity to the choice of RCM and GCM. *International Journal of Climatology*, **38**(3): 1595–1604. doi.org/10.1002/joc.5256

Cropper, T. E., Hanna, E., Valente, M. A., and Jónsson, T. (**2015**) A daily Azores–Iceland North Atlantic Oscillation index back to 1850. *Geoscience Data Journal*, **2**(1): 12–24. doi.org/10.1002/gdj3.23

Danabasoglu, G. (**2019***a*) NCAR CESM2-FV2 model output prepared for CMIP6 CMIP historical. *Earth System Grid Federation*. doi.org/10.22033/ESGF/CMIP6.11297. Accessed from the Centre for Environmental Data Analysis (CEDA) archive on 15th September 2021

Danabasoglu, G. (**2019***b*) NCAR CESM2 model output prepared for CMIP6 CMIP historical. *Earth System Grid Federation*. doi.org/10.22033/ESGF/CMIP6.7627. Accessed from the Centre for Environmental Data Analysis (CEDA) archive on 12th September 2021

Danabasoglu, G. (**2019***c*) NCAR CESM2-WACCM model output prepared for CMIP6 CMIP historical. *Earth System Grid Federation*. doi.org/10.22033/ESGF/CMIP6.10071. Accessed from the Centre for Environmental Data Analysis (CEDA) archive on 13th September 2021

Danabasoglu, G., Lamarque, J.-F., Bacmeister, J., Bailey, D. A., DuVivier, A. K., Edwards, J., Emmons, L. K., Fasullo, J., Garcia, R., Gettelman, A.,

Hannay, C., Holland, M. M., Large, W. G., Lauritzen, P. H., Lawrence, D. M., Lenaerts, J. T. M., Lindsay, K., Lipscomb, W. H., Mills, M. J., Neale, R., Oleson, K. W., Otto-Bliesner, B., Phillips, A. S., Sacks, W., Tilmes, S., van Kampenhout, L., Vertenstein, M., Bertini, A., Dennis, J., Deser, C., Fischer, C., Fox-Kemper, B., Kay, J. E., Kinnison, D., Kushner, P. J., Larson, V. E., Long, M. C., Mickelson, S., Moore, J. K., Nienhouse, E., Polvani, L., Rasch, P. J., and Strand, W. G. (**2020**) The Community Earth System Model Version 2 (CESM2). *Journal of Advances in Modeling Earth Systems*, **12**(2): e2019MS001,916. doi.org/10.1029/2019MS001916

Danek, C., Shi, X., Stepanek, C., Yang, H., Barbi, D., Hegewald, J., and Lohmann, G. (**2020**) AWI AWI-ESM1.1LR model output prepared for CMIP6 CMIP historical. *Earth System Grid Federation*. doi.org/10.22033/ESGF/CMIP6.9328. Accessed from the Centre for Environmental Data Analysis (CEDA) archive on 13th September 2021

Dasgupta, P., Metya, A., Naidu, C. V., Singh, M., and Roxy, M. K. (**2020**) Exploring the long-term changes in the Madden Julian Oscillation using machine learning. *Scientific Reports*, **10**: 18,567. 10.1038/s41598-020-75508-5

Dawson, A. (**2016**) Windspharm: A High-Level Library for Global Wind Field Computations Using Spherical Harmonics. *Journal of Open Research Software*, **4**(1): e31. doi.org/10.5334/jors.129

Dawson, A., Matthews, A. J., and Stevens, D. P. (**2011**) Rossby wave dynamics of the North Pacific extra-tropical response to El Niño: Importance of the basic state in coupled GCMs. *Climate dynamics*, **37**(1): 391–405. doi.org/10.1007/s00382-010-0854-7

de Beurs, K. M. and Henebry, G. M. (**2008**) Northern Annular Mode Effects on the Land Surface Phenologies of Northern Eurasia. *Journal of Climate*, **21**(17): 4257–4279. doi.org/10.1175/2008JCLI2074.1

Deb, P., Matthews, A. J., Joshi, M. M., and Senior, N. (**2020**) The Extratropical Linear Step Response to Tropical Precipitation Anomalies and

Its Use in Constraining Projected Circulation Changes under Climate Warming. *Journal of Climate*, **33**(16): 7217–7231. ISSN 0894-8755. doi.org/10.1175/JCLI-D-20-0060.1

Dee, D. P., Uppala, S. M., Simmons, A. J., Berrisford, P., Poli, P., Kobayashi, S., Andrae, U., Balmaseda, M. A., Balsamo, G., Bauer, P., Bechtold, P., Beljaars, A. C. M., van de Berg, L., Bidlot, J., Bormann, N., Delsol, C., Dragani, R., Fuentes, M., Geer, A. J., Haimberger, L., Healy, S. B., Hersbach, H., Hólm, E. V., Isaksen, L., Kållberg, P., Köhler, M., Matricardi, M., McNally, A. P., Monge-Sanz, B. M., Morcrette, J.-J., Park, B.-K., Peubey, C., de Rosnay, P., Tavolato, C., Thépaut, J.-N., and Vitart, F. (**2011**) The ERA-Interim reanalysis: configuration and performance of the data assimilation system. *Quarterly Journal of the Royal Meteorological Society*, **137**(656): 553–597. doi.org/10.1002/qj.828

DeMott, C. A., Klingaman, N. P., and Woolnough, S. J. (**2015**) Atmosphere–ocean coupled processes in the Madden–Julian Oscillation. *Reviews of Geophysics*, **53**(4): 1099–1154. doi.org/10.1002/2014RG000478

Deser, C., Alexander, M. A., Xie, S.-P., and Phillips, A. S. (**2010**) Sea Surface Temperature Variability: Patterns and Mechanisms. *Annual Review of Marine Science*, **2**(1): 115–143. doi.org/10.1146/annurev-marine-120408-151453

Deser, C. and Trenberth, K. and National Center for Atmospheric Research Staff (Editors). (**2016**) The Climate Data Guide: Pacific Decadal Oscillation (PDO): Definition and Indices. https://climatedataguide.ucar.edu/climate-data/pacific-decadal-oscillation-pdo-definition-and-indices. Last modified: 06/01/2016. Accessed: 25/04/2022

Di Capua, G., Kretschmer, M., Donner, R. V., van den Hurk, B., Vellore, R., Krishnan, R., and Coumou, D. (**2020**) Tropical and mid-latitude teleconnections interacting with the Indian summer monsoon rainfall: a theory-guided causal effect network approach. *Earth System Dynamics*,

11(1): 17–34. doi.org/10.5194/esd-11-17-2020

Diaz, H. F., Hoerling, M. P., and Eischeid, J. K. (**2001**) ENSO variability, teleconnections and climate change. *International Journal of Climatology*, **21**(15): 1845–1862. doi.org/10.1002/joc.631

Dix, M., Bi, D., Dobrohotoff, P., Fiedler, R., Harman, I., Law, R., Mackallah, C., Marsland, S., O'Farrell, S., Rashid, H., Srbinovsky, J., Sullivan, A., Trenham, C., Vohralik, P., Watterson, I., Williams, G., Woodhouse, M., Bodman, R., Dias, F. B., Domingues, C., Hannah, N., Heerdegen, A., Savita, A., Wales, S., Allen, C., Druken, K., Evans, B., Richards, C., Ridzwan, S. M., Roberts, D., Smillie, J., Snow, K., Ward, M., and Yang, R. (**2019**) CSIRO-ARCCSS ACCESS-CM2 model output prepared for CMIP6 CMIP historical. *Earth System Grid Federation*. doi.org/10.22033/ESGF/CMIP6.4271. Accessed from the Centre for Environmental Data Analysis (CEDA) archive on 9th September 2021

Domeisen, D. I. V., Badin, G., and Koszalka, I. M. (**2018**) How Predictable Are the Arctic and North Atlantic Oscillations? Exploring the Variability and Predictability of the Northern Hemisphere. *Journal of Climate*, **31**(3): 997–1014. doi.org/10.1175/JCLI-D-17-0226.1

Döscher, R., Acosta, M., Alessandri, A., Anthoni, P., Arneth, A., Arsouze, T., Bergmann, T., Bernadello, R., Bousetta, S., Caron, L.-P., Carver, G., Castrillo, M., Catalano, F., Cvijanovic, I., Davini, P., Dekker, E., Doblas-Reyes, F. J., Docquier, D., Echevarria, P., Fladrich, U., Fuentes-Franco, R., Gröger, M., v. Hardenberg, J., Hieronymus, J., Karami, M. P., Keskinen, J.-P., Koenigk, T., Makkonen, R., Massonnet, F., Ménégoz, M., Miller, P. A., Moreno-Chamarro, E., Nieradzik, L., van Noije, T., Nolan, P., O'Donnell, D., Ollinaho, P., van den Oord, G., Ortega, P., Prims, O. T., Ramos, A., Reerink, T., Rousset, C., Ruprich-Robert, Y., Le Sager, P., Schmith, T., Schrödner, R., Serva, F., Sicardi, V., Sloth Madsen, M., Smith, B., Tian, T., Tourigny, E., Uotila, P., Vancoppenolle, M., Wang, S., Wårlind, D., Willén, U., Wyser, K., Yang, S., Yepes-Arbós, X., and Zhang, Q. (**2021**)

The EC-Earth3 Earth System Model for the Climate Model Intercomparison Project 6. *Geoscientific Model Development Discussions*, pages 1–90. doi.org/10.5194/gmd-2020-446

Drinkwater, K. F., Belgrano, A., Borja, A., Conversi, A., Edwards, M., Greene, C. H., Ottersen, G., Pershing, A. J., and Walker, H. (**2003**) The Response of Marine Ecosystems to Climate Variability Associated with the North Atlantic Oscillation. *In* J. W. Hurrell, Y. Kushnir, G. Ottersen, and M. Visbeck (Editors), *The North Atlantic Oscillation: Climatic Significance and Environmental Impact*, pages 211–234. American Geophysical Union (AGU). ISBN 9781118669037. doi.org/10.1029/134GM10

Dunstone, N., Smith, D., Scaife, A., Hermanson, L., Eade, R., Robinson, N., Andrews, M., and Knight, J. (**2016**) Skilful predictions of the winter North Atlantic Oscillation one year ahead. *Nature Geoscience*, **9**: 809–814. doi.org/10.1038/ngeo2824

Ebert-Uphoff, I. and Deng, Y. (**2012**) Causal Discovery for Climate Research Using Graphical Models. *Journal of Climate*, **25**(17): 5648–5665. doi.org/10.1175/JCLI-D-11-00387.1

EC-Earth Consortium (EC-Earth) (**2019**) EC-Earth-Consortium EC-Earth3 model output prepared for CMIP6 CMIP historical. *Earth System Grid Federation*. doi.org/10.22033/ESGF/CMIP6.4700. Accessed from the Centre for Environmental Data Analysis (CEDA) archive on 9th September 2021

Elsbury, D., Peings, Y., Saint-Martin, D., Douville, H., and Magnusdottir, G. (**2019**) The Atmospheric Response to Positive IPV, Positive AMV, and Their Combination in Boreal Winter. *Journal of Climate*, **32**(14): 4193–4213. doi.org/10.1175/JCLI-D-18-0422.1

Enfield, D. B., Mestas-Nuñez, A. M., and Trimble, P. J. (**2001**) The Atlantic Multidecadal Oscillation and its relation to rainfall and river flows in the continental U.S. *Geophysical Research Letters*, **28**(10): 2077–2080. doi.org/10.1029/2000GL012745

European Centre for Medium-Range Weather Forecasts (**2011**) The ERA-Interim reanalysis dataset. *Copernicus Climate Change Service (C3S).* http://catalogue.ceda.ac.uk/uuid/00f58d1d7b6c8f38993e77c79e72da92. Accessed from the Centre for Environmental Data Analysis (CEDA) archive on 26th May 2021

Eyring, V., Bony, S., Meehl, G. A., Senior, C. A., Stevens, B., Stouffer, R. J., and Taylor, K. E. (**2016**) Overview of the Coupled Model Intercomparison Project Phase 6 (CMIP6) experimental design and organization. *Geoscientific Model Development*, **9**(5): 1937–1958. doi.org/10.5194/gmd-9-1937-2016

Feldstein, S. B. and Franzke, C. (**2006**) Are the North Atlantic Oscillation and the Northern Annular Mode Distinguishable? *Journal of the Atmospheric Sciences*, **63**(11): 2915–2930. doi.org/10.1175/JAS3798.1

Feng, P.-N. and Lin, H. (**2019**) Modulation of the MJO-Related Teleconnections by the QBO. *Journal of Geophysical Research: Atmospheres*, **124**(22): 12,022–12,033. doi.org/10.1029/2019JD030878

Feng, P.-N. and Lin, H. (**2021**) Modulation of the MJO-Related Teleconnection by the QBO in Subseasonal-to-Seasonal Prediction Models. *Atmosphere-Ocean*, **59**(3): 165–177. doi.org/10.1080/07055900.2021.1944045

Fernandes, L. G. and Grimm, A. M. (**2023**) ENSO modulation of global MJO and its impacts on South America. *Journal of Climate*, **36**: 7715–7738. doi.org/10.1175/JCLI-D-22-0781.1

Fiedler, S., Crueger, T., D'Agostino, R., Peters, K., Becker, T., Leutwyler, D., Paccini, L., Burdanowitz, J., Buehler, S. A., Cortes, A. U., Dauhut, T., Dommenget, D., Fraedrich, K., Jungandreas, L., Maher, N., Naumann, A. K., Rugenstein, M., Sakradzija, M., Schmidt, H., Sielmann, F., Stephan, C., Timmreck, C., Zhu, X., and Stevens, B. (**2020**) Simulated Tropical Precipitation Assessed across Three Major Phases of the Coupled Model Intercomparison Project (CMIP). *Monthly Weather Review*, **148**(9): 3653–3680. doi.org/10.1175/MWR-D-19-0404.1

Franzke, C., Lee, S., and Feldstein, S. B. (**2004**) Is the North Atlantic Oscillation a Breaking Wave? *Journal of the Atmospheric Sciences*, **61**(2): 145–160. doi.org/10.1175/1520-0469(2004)061⟨0145:ITNAOA⟩2.0.CO;2

Fromentin, J. M. and Planque, B. (**1996**) Calanus and environment in the eastern North Atlantic. II. Influence of the North Atlantic Oscillation on C. finmarchicus and C. helgolandicus. *Marine Ecology Progress Series*, **134**: 111–118. 10.3354/meps134111

Fu, Z., Hsu, P.-C., Li, J., Cao, J., Yang, Y.-M., and Liu, F. (**2022**) Multidecadal Changes in Zonal Displacement of Tropical Pacific MJO Variability Modulated by North Atlantic SST. *Journal of Climate*, **35**(18): 5951–5966. doi.org/10.1175/JCLI-D-21-0819.1

Fu, Z., Hsu, P.-C., and Liu, F. (**2020**) Factors Regulating the Multidecadal Changes in MJO Amplitude over the Twentieth Century. *Journal of Climate*, **33**(22): 9513–9529. doi.org/10.1175/JCLI-D-20-0111.1

Fuchs, Z. and Raymond, D. J. (**2005**) Large-Scale Modes in a Rotating Atmosphere with Radiative–Convective Instability and WISHE. *Journal of the Atmospheric Sciences*, **62**(11): 4084–4094. doi.org/10.1175/JAS3582.1

Fuchs, Z. and Raymond, D. J. (**2017**) A simple model of intraseasonal oscillations. *Journal of Advances in Modeling Earth Systems*, **9**(2): 1195–1211. doi.org/10.1002/2017MS000963

Furtado, J. C., Cohen, J., Becker, E. J., and Collins, D. C. (**2021**) Evaluating the relationship between sudden stratospheric warmings and tropospheric weather regimes in the NMME phase-2 models. *Climate Dynamics*, **56**: 2321–2338. doi.org/10.1007/s00382-020-05591-x

Gao, Y., Hsu, P.-C., and Hsu, H.-H. (**2016**) Assessments of surface latent heat flux associated with the Madden–Julian oscillation in reanalyses. *Climate Dynamics*, **47**: 1755–1774

Garfinkel, C. I., Benedict, J. J., and Maloney, E. D. (**2014**) Impact of the MJO

on the boreal winter extratropical circulation. *Geophysical Research Letters*, **41**(16): 6055–6062. doi.org/10.1002/2014GL061094

Garfinkel, C. I., Chen, W., Li, Y., Schwartz, C., Yadav, P., and Domeisen, D. (**2022**) The Winter North Pacific Teleconnection in Response to ENSO and the MJO in Operational Subseasonal Forecasting Models Is Too Weak. *Journal of Climate*, **35**(24): 8013–8030. doi.org/10.1175/JCLI-D-22-0179.1

Garfinkel, C. I., Feldstein, S. B., Waugh, D. W., Yoo, C., and Lee, S. (**2012**) Observed connection between stratospheric sudden warmings and the Madden-Julian Oscillation. *Geophysical Research Letters*, **39**(18). doi.org/10.1029/2012GL053144

Garfinkel, C. I. and Schwartz, C. (**2017**) MJO-Related Tropical Convection Anomalies Lead to More Accurate Stratospheric Vortex Variability in Subseasonal Forecast Models. *Geophysical Research Letters*, **44**(19): 10,054–10,062. doi.org/10.1002/2017GL074470

Geng, X., Zhang, W., Jin, F.-F., Stuecker, M. F., and Levine, A. F. Z. (**2020**) Modulation of the Relationship between ENSO and Its Combination Mode by the Atlantic Multidecadal Oscillation. *Journal of Climate*, **33**(11): 4679–4695. doi.org/10.1175/JCLI-D-19-0740.1

Geng, X., Zhang, W., Stuecker, M. F., Liu, P., Jin, F.-F., and Tan, G. (**2017**) Decadal modulation of the ENSO–East Asian winter monsoon relationship by the Atlantic Multidecadal Oscillation. *Climate Dynamics*, **49**: 2531–2544. doi.org/10.1007/s00382-016-3465-0

Gill, A. E. (**1980**) Some simple solutions for heat-induced tropical circulation. *Quarterly Journal of the Royal Meteorological Society*, **106**(449): 447–462. doi.org/10.1002/qj.49710644905

Gillett, N. P., Graf, H. F., and Osborn, T. J. (**2003**) Climate Change and the North Atlantic Oscillation. *In* J. W. Hurrell, Y. Kushnir, G. Ottersen, and M. Visbeck (Editors), *The North Atlantic Oscillation: Climatic Significance*

and Environmental Impact, pages 193–209. American Geophysical Union (AGU). ISBN 9781118669037. doi.org/10.1029/134GM09

Goss, M. and Feldstein, S. B. (**2018**) Testing the Sensitivity of the Extratropical Response to the Location, Amplitude, and Propagation Speed of Tropical Convection. *Journal of the Atmospheric Sciences*, **75**(2): 639–655. doi.org/10.1175/JAS-D-17-0132.1

Green, M. R. and Furtado, J. C. (**2019**) Evaluating the Joint Influence of the Madden–Julian Oscillation and the Stratospheric Polar Vortex on Weather Patterns in the Northern Hemisphere. *Journal of Geophysical Research: Atmospheres*, **124**(22): 11,693–11,709. doi.org/10.1029/2019JD030771

Grimm, A. (**2019**) Madden–Julian Oscillation impacts on South American summer monsoon season: precipitation anomalies, extreme events, teleconnections, and role in the MJO cycle. *Climate Dynamics*, **53**(3-4): 907–932. doi.org/10.1007/s00382-019-04622-6

Grossmann, I. and Klotzbach, P. J. (**2009**) A review of North Atlantic modes of natural variability and their driving mechanisms. *Journal of Geophysical Research: Atmospheres*, **114**(D24). doi.org/10.1029/2009JD012728

Guo, H., John, J. G., Blanton, C., McHugh, C., Nikonov, S., Radhakrishnan, A., Rand, K., Zadeh, N. T., Balaji, V., Durachta, J., Dupuis, C., Menzel, R., Robinson, T., Underwood, S., Vahlenkamp, H., Bushuk, M., Dunne, K. A., Dussin, R., Gauthier, P. P., Ginoux, P., Griffies, S. M., Hallberg, R., Harrison, M., Hurlin, W., Lin, P., Malyshev, S., Naik, V., Paulot, F., Paynter, D. J., Ploshay, J., Reichl, B. G., Schwarzkopf, D. M., Seman, C. J., Shao, A., Silvers, L., Wyman, B., Yan, X., Zeng, Y., Adcroft, A., Dunne, J. P., Held, I. M., Krasting, J. P., Horowitz, L. W., Milly, P., Shevliakova, E., Winton, M., Zhao, M., and Zhang, R. (**2018**) NOAA-GFDL GFDL-CM4 model output historical. *Earth System Grid Federation.* doi.org/10.22033/ESGF/CMIP6.8594. Accessed from the Centre for Environmental Data Analysis (CEDA) archive on 13th September 2021

Guo, Y., Shinoda, T., Lin, J., and Chang, E. K. M. (**2017**) Variations of Northern Hemisphere Storm Track and Extratropical Cyclone Activity Associated with the Madden–Julian Oscillation. *Journal of Climate*, **30**(13): 4790–4818. doi.org/10.1175/JCLI-D-16-0513.1

Gutierrez, C. B. B., de Souza, E. B., and Gutierrez, D. M. G. (**2022**) Global/Regional Impacts on Present and Near-Future Climate Regimes in the Metropolitan Region of Belém, Eastern Amazon. *Atmosphere*, **13**(7): 1077. doi.org/10.3390/atmos13071077

Hall, R. J., Mitchell, D. M., Seviour, W. J. M., and Wright, C. J. (**2021**) Persistent Model Biases in the CMIP6 Representation of Stratospheric Polar Vortex Variability. *Journal of Geophysical Research: Atmospheres*, **126**(12): e2021JD034,759. doi.org/10.1029/2021JD034759

Hall, R. J., Mitchell, D. M., Seviour, W. J. M., and Wright, C. J. (**2022**) How Well Are Sudden Stratospheric Warming Surface Impacts Captured in CMIP6 Climate Models? *Journal of Geophysical Research: Atmospheres*, **127**(7): e2021JD035,725. doi.org/10.1029/2021JD035725

Hannart, A., Vera, C., Cerne, B., and Otto, F. E. L. (**2015**) Causal Influence of Anthropogenic Forcings on the Argentinian Heat Wave of December 2013. *Bulletin of the American Meteorological Society*, **96**(12): S41–S45. doi.org/10.1175/BAMS-D-15-00137.1

Held, I. M., Guo, H., Adcroft, A., Dunne, J. P., Horowitz, L. W., Krasting, J., Shevliakova, E., Winton, M., Zhao, M., Bushuk, M., Wittenberg, A. T., Wyman, B., Xiang, B., Zhang, R., Anderson, W., Balaji, V., Donner, L., Dunne, K., Durachta, J., Gauthier, P. P. G., Ginoux, P., Golaz, J.-C., Griffies, S. M., Hallberg, R., Harris, L., Harrison, M., Hurlin, W., John, J., Lin, P., Lin, S.-J., Malyshev, S., Menzel, R., Milly, P. C. D., Ming, Y., Naik, V., Paynter, D., Paulot, F., Rammaswamy, V., Reichl, B., Robinson, T., Rosati, A., Seman, C., Silvers, L. G., Underwood, S., and Zadeh, N. (**2019**) Structure and Performance of GFDL's CM4.0 Climate Model. *Journal of Advances in*

Modeling Earth Systems, **11**(11): 3691–3727. doi.org/10.1029/2019MS001829

Henderson, S. A. and Maloney, E. D. (**2018**) The Impact of the Madden–Julian Oscillation on High-Latitude Winter Blocking during El Niño–Southern Oscillation Events. *Journal of Climate*, **31**(13): 5293–5318. doi.org/10.1175/JCLI-D-17-0721.1

Henderson, S. A., Maloney, E. D., and Barnes, E. A. (**2016**) The Influence of the Madden–Julian Oscillation on Northern Hemisphere Winter Blocking. *Journal of Climate*, **29**(12): 4597–4616. doi.org/10.1175/JCLI-D-15-0502.1

Henderson, S. A., Maloney, E. D., and Son, S.-W. (**2017**) Madden-Julian Oscillation Pacific Teleconnections: The Impact of the Basic State and MJO Representation in General Circulation Models. *Journal of Climate*, **30**(12): 4567–4587. doi.org/10.1175/JCLI-D-16-0789.1

Hendon, H. H., Wheeler, M. C., and Zhang, C. (**2007**) Seasonal Dependence of the MJO–ENSO Relationship. *Journal of Climate*, **20**(3): 531–543. doi.org/10.1175/JCLI4003.1

Hendon, H. H., Zhang, C., and Glick, J. D. (**1999**) Interannual Variation of the Madden–Julian Oscillation during Austral Summer. *Journal of Climate*, **12**(8): 2538–2550. doi.org/10.1175/1520-0442(1999)012⟨2538:IVOTMJ⟩2.0.CO;2

Hersbach, H., Bell, B., Berrisford, P., Biavati, G., Horányi, A., Muñoz Sabater, J., Nicolas, J., Peubey, C., Radu, R., Rozum, I., Schepers, D., Simmons, A., Soci, C., Dee, D., and Thépaut, J.-N. (**2018**) ERA5 hourly data on pressure levels from 1979 to present. *Copernicus Climate Change Service (C3S).* doi.org/10.24381/cds.bd0915c6. Accessed from the Copernicus Climate Change Service (C3S) Climate Data Store (CDS) on 5th January 2022

Hersbach, H., Bell, B., Berrisford, P., Hirahara, S., Horányi, A., Muñoz Sabater, J., Nicolas, J., Peubey, C., Radu, R., Schepers, D., Simmons, A., Soci, C., Abdalla, S., Abellan, X., Balsamo, G., Bechtold, P., Biavati, G., Bidlot, J., Bonavita, M., De Chiara, G., Dahlgren, P., Dee, D., Diamantakis, M.,

Dragani, R., Flemming, J., Forbes, R., Fuentes, M., Geer, A., Haimberger, L., Healy, S., Hogan, R. J., Hólm, E., Janisková, M., Keeley, S., Laloyaux, P., Lopez, P., Lupu, C., Radnoti, G., de Rosnay, P., Rozum, I., Vamborg, F., Villaume, S., and Thépaut, J.-N. (**2020**) The ERA5 global reanalysis. *Quarterly Journal of the Royal Meteorological Society*, **146**(730): 1999–2049. doi.org/10.1002/qj.3803

Hoell, A., Barlow, M., Wheeler, M. C., and Funk, C. (**2014**) Disruptions of El Niño–Southern Oscillation Teleconnections by the Madden–Julian Oscillation. *Geophysical Research Letters*, **41**(3): 998–1004. doi.org/10.1002/2013GL058648

Holt, L. A., Lott, F., Garcia, R. R., Kiladis, G. N., Cheng, Y.-M., Anstey, J. A., Braesicke, P., Bushell, A. C., Butchart, N., Cagnazzo, C., Chen, C.-C., Chun, H.-Y., Kawatani, Y., Kerzenmacher, T., Kim, Y.-H., McLandress, C., Naoe, H., Osprey, S., Richter, J. H., Scaife, A. A., Scinocca, J., Serva, F., Versick, S., Watanabe, S., Yoshida, K., and Yukimoto, S. (**2022**) An evaluation of tropical waves and wave forcing of the QBO in the QBOi models. *Quarterly Journal of the Royal Meteorological Society*, **148**(744): 1541–1567. doi.org/10.1002/qj.3827

Holton, J. R. and Tan, H.-C. (**1980**) The Influence of the Equatorial Quasi-Biennial Oscillation on the Global Circulation at 50 mb. *Journal of Atmospheric Sciences*, **37**(10): 2200–2208. doi.org/10.1175/1520-0469(1980)037⟨2200:TIOTEQ⟩2.0.CO;2

Holton, J. R. and Tan, H.-C. (**1982**) The Quasi-Biennial Oscillation in the Northern Hemisphere Lower Stratosphere. *Journal of the Meteorological Society of Japan. Ser. II*, **60**(1): 140–148. doi.org/10.2151/jmsj1965.60.1_140

Honda, M., Nakamura, H., Ukita, J., Kousaka, I., and Takeuchi, K. (**2001**) Interannual Seesaw between the Aleutian and Icelandic Lows. Part I: Seasonal Dependence and Life Cycle. *Journal of Climate*, **14**(6): 1029–1042. doi.org/10.1175/1520-0442(2001)014⟨1029:ISBTAA⟩2.0.CO;2

Hood, L. L., Redman, M. A., Johnson, W. L., and Galarneau, T. J. (**2020**) Stratospheric Influences on the MJO-Induced Rossby Wave Train: Effects on Intraseasonal Climate. *Journal of Climate*, **33**(1): 365–389. doi.org/10.1175/JCLI-D-18-0811.1

Hoskins, B. J. and Ambrizzi, T. (**1993**) Rossby Wave Propagation on a Realistic Longitudinally Varying Flow. *Journal of Atmospheric Sciences*, **50**(12): 1661–1671. doi.org/10.1175/1520-0469(1993)050⟨1661:RWPOAR⟩2.0.CO;2

Hoskins, B. J., James, I. N., and White, G. H. (**1983**) The Shape, Propagation and Mean-Flow Interaction of Large-Scale Weather Systems. *Journal of Atmospheric Sciences*, **40**(7): 1595–1612. doi.org/10.1175/1520-0469(1983)040⟨1595:TSPAMF⟩2.0.CO;2

Hoskins, B. J. and Karoly, D. J. (**1981**) The Steady Linear Response of a Spherical Atmosphere to Thermal and Orographic Forcing. *Journal of Atmospheric Sciences*, **38**(6): 1179–1196. doi.org/10.1175/1520-0469(1981)038⟨1179:TSLROA⟩2.0.CO;2

Hsu, P.-C., Fu, Z., and Xiao, T. (**2018**) Energetic processes regulating the strength of MJO circulation over the Maritime Continent during two types of El Niño. *Atmospheric and Oceanic Science Letters*, **11**(2): 112–119. doi.org/10.1080/16742834.2018.1399049

Hsu, P.-C. and Xiao, T. (**2017**) Differences in the Initiation and Development of the Madden–Julian Oscillation over the Indian Ocean Associated with Two Types of El Niño. *Journal of Climate*, **30**(4): 1397–1415. doi.org/10.1175/JCLI-D-16-0336.1

Huang, J., Hitchcock, P., Maycock, A. C., McKenna, C. M., and Tian, W. (**2021**) Northern hemisphere cold air outbreaks are more likely to be severe during weak polar vortex conditions. *Communications Earth & Environment volume*, **2**(147). doi.org/10.1038/s43247-021-00215-6

Hung, M.-P., Lin, J.-L., Wang, W., Kim, D., Shinoda, T., and Weaver, S. J. (**2013**) MJO and Convectively Coupled Equatorial Waves Simulated by

CMIP5 Climate Models. *Journal of Climate*, **26**(17): 6185–6214. doi.org/10.1175/JCLI-D-12-00541.1

Hunter, J. D. (**2007**) Matplotlib: A 2D graphics environment. *Computing in Science and Engineering*, **9**(3): 90–95. doi.org/10.1109/MCSE.2007.55

Hurrell, J. W. (**1995**) Decadal Trends in the North Atlantic Oscillation: Regional Temperatures and Precipitation. *Science*, **269**(5224): 676–679. doi.org/10.1126/science.269.5224.676

Hurrell, J. W. (**1996**) Influence of variations in extratropical wintertime teleconnections on northern hemisphere temperature. *Geophysical Research Letters*, **23**(6): 665–668. doi.org/10.1029/96GL00459

Hurrell, J. W., Kushnir, Y., Ottersen, G., and Visbeck, M. (**2003***a*) *The North Atlantic Oscillation: Climatic Significance and Environmental Impact.* Geophysical monograph: 134. American Geophysical Union. doi.org/10.1029/GM134

Hurrell, J. W., Kushnir, Y., Ottersen, G., and Visbeck, M. (**2003***b*) An Overview of the North Atlantic Oscillation. *In* J. W. Hurrell, Y. Kushnir, G. Ottersen, and M. Visbeck (Editors), *The North Atlantic Oscillation: Climatic Significance and Environmental Impact*, pages 1–35. American Geophysical Union (AGU). ISBN 9781118669037. https://doi.org/10.1029/134GM01

Hurrell, J. W. and van Loon, H. (**1997**) Decadal variations in climate associated with the North Atlantic Oscillation. *Climatic Change*, **36**: 301–326. doi.org/10.1023/A:1005314315270

Ineson, S. and Scaife, A. (**2009**) The role of the stratosphere in the European climate response to El Niño. *Nature Geosciences*, **2**: 32–36. doi.org/10.1038/ngeo381

Jenney, A. M., Nardi, K. M., Barnes, E. A., and Randall, D. A. (**2019**) The Seasonality and Regionality of MJO Impacts on North American

Temperature. *Geophysical Research Letters*, **46**(15): 9193–9202. doi.org/10.1029/2019GL083950

Jenney, A. M., Randall, D. A., and Barnes, E. A. (**2021**) Drivers of uncertainty in future projections of Madden–Julian Oscillation teleconnections. *Weather and Climate Dynamics*, **2**(3): 653–673. doi.org/10.5194/wcd-2-653-2021

Jiang, X., Adames, Á. F., Kim, D., Maloney, E. D., Lin, H., Kim, H., Zhang, C., DeMott, C. A., and Klingaman, N. P. (**2020**) Fifty Years of Research on the Madden-Julian Oscillation: Recent Progress, Challenges, and Perspectives. *Journal of Geophysical Research: Atmospheres*, **125**(17): e2019JD030,911. doi.org/10.1029/2019JD030911

Jiang, X., Adames, A. F., Zhao, M., Waliser, D., and Maloney, E. (**2018**) A Unified Moisture Mode Framework for Seasonality of the Madden–Julian Oscillation. *Journal of Climate*, **31**(11): 4215–4224. doi.org/10.1175/JCLI-D-17-0671.1

Jiang, X., Waliser, D. E., Xavier, P. K., Petch, J., Klingaman, N. P., Woolnough, S. J., Guan, B., Bellon, G., Crueger, T., DeMott, C., Hannay, C., Lin, H., Hu, W., Kim, D., Lappen, C.-L., Lu, M.-M., Ma, H.-Y., Miyakawa, T., Ridout, J. A., Schubert, S. D., Scinocca, J., Seo, K.-H., Shindo, E., Song, X., Stan, C., Tseng, W.-L., Wang, W., Wu, T., Wu, X., Wyser, K., Zhang, G. J., and Zhu, H. (**2015**) Vertical structure and physical processes of the Madden-Julian oscillation: Exploring key model physics in climate simulations. *Journal of Geophysical Research: Atmospheres*, **120**(10): 4718–4748. doi.org/10.1002/2014JD022375

Jiang, Z., Feldstein, S. B., and Lee, S. (**2017**) The relationship between the Madden–Julian Oscillation and the North Atlantic Oscillation. *Quarterly Journal of the Royal Meteorological Society*, **143**(702): 240–250. doi.org/10.1002/qj.2917

Jones, C. and Carvalho, L. M. V. (**2006**) Changes in the Activity of the Madden–Julian Oscillation during 1958–2004. *Journal of Climate*, **19**(24):

6353–6370. doi.org/10.1175/JCLI3972.1

Jones, P. D., Osborn, T. J., and Briffa, K. R. (**2003**) Pressure-Based Measures of the North Atlantic Oscillation (NAO): A Comparison and an Assessment of Changes in the Strength of the NAO and in its Influence on Surface Climate Parameters. *In* J. W. Hurrell, Y. Kushnir, G. Ottersen, and M. Visbeck (Editors), *The North Atlantic Oscillation: Climatic Significance and Environmental Impact*, pages 51–62. American Geophysical Union (AGU). ISBN 9781118669037. doi.org/10.1029/134GM03

Julian, P. R. and Chervin, R. M. (**1978**) A Study of the Southern Oscillation and Walker Circulation Phenomenon. *Monthly Weather Review*, **106**(10): 1433–1451. doi.org/10.1175/1520-0493(1978)106⟨1433:ASOTSO⟩2.0.CO;2

Jungclaus, J., Bittner, M., Wieners, K.-H., Wachsmann, F., Schupfner, M., Legutke, S., Giorgetta, M., Reick, C., Gayler, V., Haak, H., de Vrese, P., Raddatz, T., Esch, M., Mauritsen, T., von Storch, J.-S., Behrens, J., Brovkin, V., Claussen, M., Crueger, T., Fast, I., Fiedler, S., Hagemann, S., Hohenegger, C., Jahns, T., Kloster, S., Kinne, S., Lasslop, G., Kornblueh, L., Marotzke, J., Matei, D., Meraner, K., Mikolajewicz, U., Modali, K., Müller, W., Nabel, J., Notz, D., Peters-von Gehlen, K., Pincus, R., Pohlmann, H., Pongratz, J., Rast, S., Schmidt, H., Schnur, R., Schulzweida, U., Six, K., Stevens, B., Voigt, A., and Roeckner, E. (**2019**) MPI-M MPI-ESM1.2-HR model output prepared for CMIP6 CMIP historical. *Earth System Grid Federation*. doi.org/10.22033/ESGF/CMIP6.6594. Accessed from the Centre for Environmental Data Analysis (CEDA) archive on 14th September 2021

Kang, W. and Tziperman, E. (**2017**) More Frequent Sudden Stratospheric Warming Events due to Enhanced MJO Forcing Expected in a Warmer Climate. *Journal of Climate*, **30**(21): 8727–8743. doi.org/10.1175/JCLI-D-17-0044.1

Kang, W. and Tziperman, E. (**2018**) The MJO-SSW Teleconnection: Interaction Between MJO-Forced Waves and the Midlatitude Jet. *Geophysical*

Research Letters, **45**(9): 4400–4409. doi.org/10.1029/2018GL077937

Karoly, D. J. (**1983**) Rossby wave propagation in a barotropic atmosphere. *Dynamics of Atmospheres and Oceans*, **7**(2): 111–125. ISSN 0377-0265. doi.org/10.1016/0377-0265(83)90013-1

Karpechko, A. Y., Peterson, K. A., Scaife, A. A., Vainio, J., and Gregow, H. (**2015**) Skilful seasonal predictions of Baltic Sea ice cover. *Environmental Research Letters*, **10**(4): 044,007. doi.org/10.1088/1748-9326/10/4/044007

Kavvada, A., Ruiz-Barradas, A., and Nigam, S. (**2013**) AMO's structure and climate footprint in observations and IPCC AR5 climate simulations. *Climate Dynamics*, **41**: 1345–1364. doi.org/10.1007/s00382-013-1712-1

Kawatani, Y., Watanabe, S., Sato, K., Dunkerton, T. J., Miyahara, S., and Takahashi, M. (**2010**) The Roles of Equatorial Trapped Waves and Internal Inertia–Gravity Waves in Driving the Quasi-Biennial Oscillation. Part I: Zonal Mean Wave Forcing. *Journal of the Atmospheric Sciences*, **67**(4): 963–980. doi.org/10.1175/2009JAS3222.1

Kent, C., Scaife, A. A., and Dunstone, N. (**2022**) What potential for improving sub-seasonal predictions of the winter NAO? *Atmospheric Science Letters*, **24**(4): e1146. doi.org/10.1002/asl.1146

Kerr, R. A. (**2000**) A North Atlantic Climate Pacemaker for the Centuries. *Science*, **288**(5473): 1984–1985. doi.org/10.1126/science.288.5473.1984

Kessler, W. S. (**2001**) EOF Representations of the Madden–Julian Oscillation and Its Connection with ENSO. *Journal of Climate*, **14**(13): 3055–3061. doi.org/10.1175/1520-0442(2001)014⟨3055:EROTMJ⟩2.0.CO;2

Kim, B.-M., Lim, G.-H., and Kim, K.-Y. (**2006**) A new look at the midlatitude–MJO teleconnection in the northern hemisphere winter. *Quarterly Journal of the Royal Meteorological Society*, **132**(615): 485–503. doi.org/10.1256/qj.04.87

Kim, D., Sperber, K., Stern, W., Waliser, D., Kang, I.-S., Maloney, E., Wang,

W., Weickmann, K., Benedict, J., Khairoutdinov, M., Lee, M.-I., Neale, R., Suarez, M., Thayer-Calder, K., and Zhang, G. (**2009**) Application of MJO Simulation Diagnostics to Climate Models. *Journal of Climate*, **22**(23): 6413–6436. doi.org/10.1175/2009JCLI3063.1

Klavans, J. M., Cane, M. A., Clement, A. C., and Murphy, L. N. (**2021**) NAO predictability from external forcing in the late 20th century. *npj Climate and Atmospheric Science*, **4**(22). doi.org/10.1038/s41612-021-00177-8

Klotzbach, P., Abhik, S., Hendon, H. H., Bell, M., Lucas, C., Marshall, A. G., and Oliver, E. C. J. (**2019**) On the emerging relationship between the stratospheric Quasi–Biennial oscillation and the Madden–Julian oscillation. *Scientific Reports*, **9**: 2981. doi.org/10.1038/s41598-019-40034-6

Knight, J. R., Allan, R. J., Folland, C. K., Vellinga, M., and Mann, M. E. (**2005**) A signature of persistent natural thermohaline circulation cycles in observed climate. *Geophysical Research Letters*, **32**(20): L20,708. doi.org/10.1029/2005GL024233

Koval, A. V., Gavrilov, N. M., Kandieva, K. K., Ermakova, T. S., and Didenko, K. A. (**2022**) Numerical simulation of stratospheric QBO impact on the planetary waves up to the thermosphere. *Scientific Reports*, **12**: 21,701. doi.org/10.1038/s41598-022-26311-x

Kretschmer, M., Adams, S. V., Arribas, A., Prudden, R., Robinson, N., Saggioro, E., and Shepherd, T. G. (**2021**) Quantifying Causal Pathways of Teleconnections. *Bulletin of the American Meteorological Society*, **102**(12): E2247–E2263. doi.org/10.1175/BAMS-D-20-0117.1

Krishnamurti, T. N., Oosterhof, D. K., and Mehta, A. V. (**1988**) Air–Sea Interaction on the Time Scale of 30 to 50 Days. *Journal of Atmospheric Sciences*, **45**(8): 1304–1322. doi.org/10.1175/1520-0469(1988)045⟨1304:AIOTTS⟩2.0.CO;2

Krishnan, R., Swapna, P., Choudhury, A. D., Narayansetti, S., Prajeesh, A. G., Singh, M., Modi, A., Mathew, R., Vellore, R., Jyoti, J., Sabin, T. P., Sanjay,

J., and Ingle, S. (**2021**) The IITM Earth System Model (IITM ESM) [Preprint]. *arXiv archive*. doi.org/10.48550/arXiv.2101.03410. Accessed: 08/09/2021

Kuhlbrodt, T., Jones, C. G., Sellar, A., Storkey, D., Blockley, E., Stringer, M., Hill, R., Graham, T., Ridley, J., Blaker, A., Calvert, D., Copsey, D., Ellis, R., Hewitt, H., Hyder, P., Ineson, S., Mulcahy, J., Siahaan, A., and Walton, J. (**2018**) The Low-Resolution Version of HadGEM3 GC3.1: Development and Evaluation for Global Climate. *Journal of Advances in Modeling Earth Systems*, **10**(11): 2865–2888. doi.org/10.1029/2018MS001370

Kushnir, Y. (**1994**) Interdecadal Variations in North Atlantic Sea Surface Temperature and Associated Atmospheric Conditions. *Journal of Climate*, **7**(1): 141–157. doi.org/10.1175/1520-0442(1994)007⟨0141:IVINAS⟩2.0.CO;2

Lau, W. K.-M. and Waliser, D. E. (**2012**) *Intraseasonal variability in the atmosphere-ocean climate system*. Springer, 2nd edition

Lawrence, B. N., Bennett, V. L., Churchill, J., Juckes, M., Kershaw, P., Pascoe, S., Pepler, S., Priitchard, M., and Stephens, A. (**2013**) Storing and manipulating environmental big data with JASMIN. *In IEEE Big Data*. doi.org/10.1109/BigData.2013.6691556

Le, P. V. V., Guilloteau, C., Mamalakis, A., and Foufoula-Georgiou, E. (**2021**) Underestimated MJO Variability in CMIP6 Models. *Geophysical Research Letters*, **48**(12): e2020GL092,244. doi.org/10.1029/2020GL092244

Lee, H. and Seo, K. (**2019**) Impact of the Madden–Julian oscillation on Antarctic sea ice and its dynamical mechanism. *Scientific reports*, **9**(1): 10,761. doi.org/10.1038/s41598-019-47150-3

Lee, J., Kim, J., Sun, M.-A., Kim, B.-H., Moon, H., Sung, H. M., Kim, J., and Byun, Y.-H. (**2020***a*) Evaluation of the Korea Meteorological Administration Advanced Community Earth-System model (K-ACE). *Asia-Pacific Journal of Atmospheric Sciences*, **56**: 381–395. doi.org/10.1007/s13143-019-00144-7

Lee, R. W., Woolnough, S. J., Charlton-Perez, A. J., and Vitart, F. (**2019**)

ENSO Modulation of MJO Teleconnections to the North Atlantic and Europe. *Geophysical Research Letters*, **46**(22): 13,535–13,545. doi.org/10.1029/2019GL084683

Lee, W.-L. and Liang, H.-C. (**2020**) AS-RCEC TaiESM1.0 model output prepared for CMIP6 CMIP historical. *Earth System Grid Federation*. doi.org/10.22033/ESGF/CMIP6.9755. Accessed from the Centre for Environmental Data Analysis (CEDA) archive on 13th September 2021

Lee, W.-L., Wang, Y.-C., Shiu, C.-J., Tsai, I., Tu, C.-Y., Lan, Y.-Y., Chen, J.-P., Pan, H.-L., and Hsu, H.-H. (**2020***b*) Taiwan Earth System Model Version 1: description and evaluation of mean state. *Geoscientific Model Development*, **13**(9): 3887–3904. doi.org/10.5194/gmd-13-3887-2020

Leupold, M., Pfeiffer, M., Watanabe, T. K., Reuning, L., Garbe-Schönberg, D., Shen, C.-C., and Brummer, G.-J. A. (**2021**) El Niño–Southern Oscillation and internal sea surface temperature variability in the tropical Indian Ocean since 1675. *Climate of the Past*, **17**(1): 151–170. doi.org/10.5194/cp-17-151-2021

L'Heureux, M. (**2021**) The Pacific-North American Pattern: the stomach sleeper of the atmosphere. https://www.climate.gov/news-features/blogs/enso/pacific-north-american-pattern-stomach-sleeper-atmosphere. Last modified: 26/11/2021. Accessed: 25/04/2022

L'Heureux, M. L. and Higgins, R. W. (**2008**) Boreal Winter Links between the Madden–Julian Oscillation and the Arctic Oscillation. *Journal of Climate*, **21**(12): 3040–3050. doi.org/10.1175/2007JCLI1955.1

Li, L. (**2019**) CAS FGOALS-g3 model output prepared for CMIP6 CMIP historical. *Earth System Grid Federation*. doi.org/10.22033/ESGF/CMIP6.3356. Accessed from the Centre for Environmental Data Analysis (CEDA) archive on 13th September 2021

Li, L., Yu, Y., Tang, Y., Lin, P., Xie, J., Song, M., Dong, L., Zhou, T., Liu, L., Wang, L., Pu, Y., Chen, X., Chen, L., Xie, Z., Liu, H., Zhang, L., Huang, X., Feng, T., Zheng, W., Xia, K., Liu, H., Liu, J., Wang, Y., Wang, L., Jia, B.,

Xie, F., Wang, B., Zhao, S., Yu, Z., Zhao, B., and Wei, J. (**2020**) The Flexible Global Ocean-Atmosphere-Land System Model Grid-Point Version 3 (FGOALS-g3): Description and Evaluation. *Journal of Advances in Modeling Earth Systems*, **12**(9): e2019MS002,012. doi.org/10.1029/2019MS002012

Li, X., Gerber, E. P., Holland, D. M., and Yoo, C. (**2015***a*) A Rossby Wave Bridge from the Tropical Atlantic to West Antarctica. *Journal of Climate*, **28**(6): 2256–2273. doi.org/10.1175/JCLI-D-14-00450.1

Li, Y., Li, J., Jin, F. F., and Zhao, S. (**2015***b*) Interhemispheric Propagation of Stationary Rossby Waves in a Horizontally Nonuniform Background Flow. *Journal of the Atmospheric Sciences*, **72**(8): 3233–3256. doi.org/10.1175/JAS-D-14-0239.1

Liebmann, B. and Smith, C. A. (**1996**) Description of a complete (interpolated) outgoing longwave radiation dataset. *Bulletin of the American Meteorological Society*, **77**(6): 1275–1277. https://www.jstor.org/stable/26233278

Lin, H. (**2022**) The Madden–Julian Oscillation. *Atmosphere-Ocean*, **60**(3–4): 338–359. doi.org/10.1080/07055900.2022.2072267

Lin, H. and Brunet, G. (**2018**) Extratropical Response to the MJO: Nonlinearity and Sensitivity to the Initial State. *Journal of the Atmospheric Sciences*, **75**(1): 219–234. doi.org/10.1175/JAS-D-17-0189.1

Lin, H., Brunet, G., and Derome, J. (**2009**) An Observed Connection between the North Atlantic Oscillation and the Madden–Julian Oscillation. *Journal of Climate*, **22**(2): 364–380. doi.org/10.1175/2008JCLI2515.1

Lin, H., Brunet, G., and Fontecilla, J. S. (**2010**) Impact of the Madden-Julian Oscillation on the intraseasonal forecast skill of the North Atlantic Oscillation. *Geophysical Research Letters*, **37**(19): L19,803. doi.org/10.1029/2010GL044315

Lin, H., Huang, Z., Hendon, H., and Brunet, G. (**2021**) NAO Influence on the MJO and its Prediction Skill in the Subseasonal-to-Seasonal Prediction

Models. *Journal of Climate*, **34**(23): 9425–9442.
doi.org/10.1175/JCLI-D-21-0153.1

Lin, J. and Qian, T. (**2022**) The Atlantic Multi-Decadal Oscillation. *Atmosphere-Ocean*, **60**(3-4): 307–337.
doi.org/10.1080/07055900.2022.2086847

Lin, J.-L., Kiladis, G. N., Mapes, B. E., Weickmann, K. M., Sperber, K. R., Lin, W., Wheeler, M. C., Schubert, S. D., Genio, A. D., Donner, L. J., Emori, S., Gueremy, J.-F., Hourdin, F., Rasch, P. J., Roeckner, E., and Scinocca, J. F. (**2006**) Tropical Intraseasonal Variability in 14 IPCC AR4 Climate Models. Part I: Convective Signals. *Journal of Climate*, **19**(12): 2665–2690.
doi.org/10.1175/JCLI3735.1

Lindzen, R. S. and Holton, J. R. (**1968**) A Theory of the Quasi-Biennial Oscillation. *Journal of Atmospheric Sciences*, **25**(6): 1095–1107.
doi.org/10.1175/1520-0469(1968)025⟨1095:ATOTQB⟩2.0.CO;2

Ling, J., Zhao, Y., and Chen, G. (**2019**) Barrier Effect on MJO Propagation by the Maritime Continent in the MJO Task Force/GEWEX Atmospheric System Study Models. *Journal of Climate*, **32**(17): 5529–5547.
doi.org/10.1175/JCLI-D-18-0870.1

Liu, C., Tian, B., Li, K.-F., Manney, G. L., Livesey, N. J., Yung, Y. L., and Waliser, D. E. (**2014**) Northern Hemisphere mid-winter vortex-displacement and vortex-split stratospheric sudden warmings: Influence of the Madden-Julian Oscillation and Quasi-Biennial Oscillation. *Journal of Geophysical Research: Atmospheres*, **119**(22): 12,599—12,620.
doi.org/10.1002/2014JD021876

Liu, P., Li, T., Wang, B., Zhang, M., jia Luo, J., Masumoto, Y., Wang, X., and Roeckner, E. (**2013**) MJO change with A1B global warming estimated by the 40-km ECHAM5. *Climate Dynamics*, **41**: 1009–1023.
doi.org/10.1007/s00382-012-1532-8

Lorenz, E. N. (**1951**) Seasonal and irregular variations of the Northern

Hemisphere sea-level pressure profile. *Journal of Atmospheric Sciences*, **8**(1): 52–59. doi.org/10.1175/1520-0469(1951)008⟨0052:SAIVOT⟩2.0.CO;2

Luo, D. and Cha, J. (**2012**) The North Atlantic Oscillation and the North Atlantic Jet Variability: Precursors to NAO Regimes and Transitions. *Journal of the Atmospheric Sciences*, **69**(12): 3763–3787. doi.org/10.1175/JAS-D-12-098.1

Luo, D., Gong, T., and Diao, Y. (**2007**) Dynamics of Eddy-Driven Low-Frequency Dipole Modes. Part III: Meridional Displacement of Westerly Jet Anomalies during Two Phases of NAO. *Journal of the Atmospheric Sciences*, **64**(9): 3232–3248. doi.org/10.1175/JAS3998.1

Ma, J., Chen, W., Nath, D., and Lan, X. (**2020**) Modulation by ENSO of the relationship between stratospheric sudden warming and the Madden–Julian Oscillation. *Geophysical Research Letters*, **47**(15): e2020GL088,894. doi.org/10.1029/2020GL088894

Madden, R. A. and Julian, P. R. (**1971**) Detection of a 40-50 Day Oscillation in the Zonal Wind in the Tropical Pacific. *Journal of Atmospheric Sciences*, **28**(5): 702–708. doi.org/10.1175/1520-0469(1971)028⟨0702:DOADOI⟩2.0.CO;2

Madden, R. A. and Julian, P. R. (**1972**) Description of Global-Scale Circulation Cells in the Tropics with a 40-50 Day Period. *Journal of Atmospheric Sciences*, **29**(6): 1109–1123. doi.org/10.1175/1520-0469(1972)029⟨1109:DOGSCC⟩2.0.CO;2

Madden, R. A. and Julian, P. R. (**1994**) Observations of the 40–50-Day Tropical Oscillation – A Review. *Monthly Weather Review*, **122**(5): 814–837. doi.org/10.1175/1520-0493(1994)122⟨0814:OOTDTO⟩2.0.CO;2

Madden, R. A. and Williams, J. (**1978**) The Correlation between Temperature and Precipitation in the United States and Europe. *Monthly Weather Review*, **106**(1): 142–147. doi.org/10.1175/1520-0493(1978)106⟨0142:TCBTAP⟩2.0.CO;2

Maloney, E. D., Adames, A. F., and Bui, H. X. (**2019***a*) Madden–Julian Oscillation changes under anthropogenic warming. *Nature Climate Change*, **9**: 26–33. doi.org/10.1038/s41558-018-0331-6

Maloney, E. D., Gettelman, A., Ming, Y., Neelin, J. D., Barrie, D., Mariotti, A., Chen, C.-C., Coleman, D. R. B., Kuo, Y.-H., Singh, B., Annamalai, H., Berg, A., Booth, J. F., Camargo, S. J., Dai, A., Gonzalez, A., Hafner, J., Jiang, X., Jing, X., Kim, D., Kumar, A., Moon, Y., Naud, C. M., Sobel, A. H., Suzuki, K., Wang, F., Wang, J., Wing, A. A., Xu, X., and Zhao, M. (**2019***b*) Process-Oriented Evaluation of Climate and Weather Forecasting Models. *Bulletin of the American Meteorological Society*, **100**(9): 1665–1686. doi.org/10.1175/BAMS-D-18-0042.1

Mann, M. E., Bradley, R. S., and Hughes, M. K. (**1999**) Northern hemisphere temperatures during the past millennium: Inferences, uncertainties, and limitations. *Geophysical Research Letters*, **26**(6): 759–762. https://doi.org/10.1029/1999GL900070

Mantua, N. J. (**1999**) The Pacific Decadal Oscillation: a brief overview for non-specialists. *Encyclopedia of Environmental Change*

Mantua, N. J. and Hare, S. R. (**2002**) The Pacific Decadal Oscillation. *Journal of Oceanography*, **58**: 35–44. doi.org/10.1023/A:1015820616384

Mantua, N. J., Hare, S. R., Zhang, Y., Wallace, J. M., and Francis, R. C. (**1997**) A Pacific Interdecadal Climate Oscillation with Impacts on Salmon Production. *Bulletin of the American Meteorological Society*, **78**(6): 1069–1080. doi.org/10.1175/1520-0477(1997)078⟨1069:APICOW⟩2.0.CO;2

Marshall, A. G., Hendon, H. H., Son, S.-W., and Lim, Y. (**2017**) Impact of the quasi-biennial oscillation on predictability of the Madden–Julian oscillation. *Climate Dynamics*, **49**: 1365–1377. doi.org/10.1007/s00382-016-3392-0

Martin, Z., Orbe, C., Wang, S., and Sobel, A. (**2021***a*) The MJO–QBO Relationship in a GCM with Stratospheric Nudging. *Journal of Climate*, **34**(11): 4603–4624. doi.org/10.1175/JCLI-D-20-0636.1

Martin, Z., Son, S.-W., Butler, A., Hendon, H., Kim, H., Sobel, A., Yoden, S., and Zhang, C. (**2021***b*) The influence of the quasi-biennial oscillation on the Madden–Julian oscillation. *Nature Reviews Earth and Environment*, **2**: 477–489. doi.org/10.1038/s43017-021-00173-9

Martin, Z., Vitart, F., Wang, S., and Sobel, A. (**2020**) The Impact of the Stratosphere on the MJO in a Forecast Model. *Journal of Geophysical Research: Atmospheres*, **125**(4): e2019JD032,106. doi.org/10.1029/2019JD032106

Martin, Z., Wang, S., Nie, J., and Sobel, A. (**2019**) The Impact of the QBO on MJO Convection in Cloud-Resolving Simulations. *Journal of the Atmospheric Sciences*, **76**(3): 669–688. doi.org/10.1175/JAS-D-18-0179.1

Masson-Delmotte, V., Zhai, P., Pirani, A., Connors, S., Péan, C., Berger, S., Caud, N., Chen, Y., Goldfarb, L., Gomis, M., Huang, M., Leitzell, K., Lonnoy, E., Matthews, J., Maycock, T., Waterfield, T., Yelekçi, O., Yu, R., and Zhou, B. (**2021**) Climate Change 2021: The Physical Science Basis. *In* IPCC (Editor), *Sixth Assessment Report of the Intergovernmental Panel on Climate Change*. Cambridge University Press, Cambridge, UK and New York, USA. doi.org/10.1017/9781009157896

Matsumura, S. and Horinouchi, T. (**2016**) Pacific Ocean decadal forcing of long-term changes in the western Pacific subtropical high. *Scientific Reports*, **6**: 37,765. doi.org/10.1038/srep37765

Matsuno, T. (**1966**) Quasi-geostrophic motions in the equatorial area. *Journal of the Meteorological Society of Japan. Ser. II*, **44**(1): 25–43

Matthews, A. J., Hoskins, B. J., and Masutani, M. (**2004**) The global response to tropical heating in the Madden–Julian oscillation during the northern winter. *Quarterly Journal of the Royal Meteorological Society*, **130**(601): 1991–2011. doi.org/10.1256/qj.02.123

Matthews, A. J. and Kiladis, G. N. (**1999***a*) Interactions between ENSO, Transient Circulation, and Tropical Convectionover the Pacific. *Journal of*

Climate, **12**(10): 3062–3086.
doi.org/10.1175/1520-0442(1999)012⟨3062:IBETCA⟩2.0.CO;2

Matthews, A. J. and Kiladis, G. N. (**1999***b*) The Tropical–Extratropical Interaction between High-Frequency Transients and the Madden–Julian Oscillation. *Monthly Weather Review*, **127**(5): 661–677.
doi.org/10.1175/1520-0493(1999)127⟨0661:TTEIBH⟩2.0.CO;2

Matthews, A. J. and Meredith, M. P. (**2004**) Variability of Antarctic circumpolar transport and the Southern Annular Mode associated with the Madden-Julian Oscillation. *Geophysical Research Letters*, **31**(24): L24,312.
doi.org/10.1029/2004GL021666

Mauritsen, T., Bader, J., Becker, T., Behrens, J., Bittner, M., Brokopf, R., Brovkin, V., Claussen, M., Crueger, T., Esch, M., Fast, I., Fiedler, S., Fläschner, D., Gayler, V., Giorgetta, M., Goll, D. S., Haak, H., Hagemann, S., Hedemann, C., Hohenegger, C., Ilyina, T., Jahns, T., Jimenéz-de-la Cuesta, D., Jungclaus, J., Kleinen, T., Kloster, S., Kracher, D., Kinne, S., Kleberg, D., Lasslop, G., Kornblueh, L., Marotzke, J., Matei, D., Meraner, K., Mikolajewicz, U., Modali, K., Möbis, B., Müller, W. A., Nabel, J. E. M. S., Nam, C. C. W., Notz, D., Nyawira, S.-S., Paulsen, H., Peters, K., Pincus, R., Pohlmann, H., Pongratz, J., Popp, M., Raddatz, T. J., Rast, S., Redler, R., Reick, C. H., Rohrschneider, T., Schemann, V., Schmidt, H., Schnur, R., Schulzweida, U., Six, K. D., Stein, L., Stemmler, I., Stevens, B., von Storch, J.-S., Tian, F., Voigt, A., Vrese, P., Wieners, K.-H., Wilkenskjeld, S., Winkler, A., and Roeckner, E. (**2019**) Developments in the MPI-M Earth System Model version 1.2 (MPI-ESM1.2) and Its Response to Increasing CO2. *Journal of Advances in Modeling Earth Systems*, **11**(4): 998–1038.
doi.org/10.1029/2018MS001400

Mayer, K. J. and Barnes, E. A. (**2022**) Quantifying the Effect of Climate Change on Midlatitude Subseasonal Prediction Skill Provided by the Tropics. *Geophysical Research Letters*, **49**(14): e2022GL098,663.
doi.org/10.1029/2022GL098663. E2022GL098663 2022GL098663

McAfee, S. A. and Russell, J. L. (**2008**) Northern Annular Mode impact on spring climate in the western United States. *Geophysical Research Letters*, **35**(17): L17,701. doi.org/10.1029/2008GL034828

McKinney, W. (**2010**) Data Structures for Statistical Computing in Python. *In* Stéfan van der Walt and Jarrod Millman (Editors), *Proceedings of the 9th Python in Science Conference*, pages 56–61. doi.org/10.25080/Majora-92bf1922-00a

Met Office (**2016**) Cartopy: a cartographic python library with a matplotlib interface. http://scitools.org.uk/cartopy

Met Office (**2020**) Iris: A Python library for analysing and visualising meteorological and oceanographic data sets. http://scitools.org.uk/iris

Met Office Hadley Centre (**2022**) Met Office Hadley Centre observations datasets. https://www.metoffice.gov.uk/hadobs/hadisst/data/download.html. Accessed on 27th April 2022

Michel, C. and Rivière, G. (**2011**) The Link between Rossby Wave Breakings and Weather Regime Transitions. *Journal of the Atmospheric Sciences*, **68**(8): 1730–1748. doi.org/10.1175/2011JAS3635.1

Mitchell, D. M., Scott, R. K., Seviour, W. J. M., Thomson, S. I., Waugh, D. W., Teanby, N. A., and Ball, E. R. (**2021**) Polar Vortices in Planetary Atmospheres. *Reviews of Geophysics*, **59**(4): e2020RG000,723. doi.org/10.1029/2020RG000723

Molinari, J. and Vollaro, D. (**2012**) A Subtropical Cyclonic Gyre Associated with Interactions of the MJO and the Midlatitude Jet. *Monthly Weather Review*, **140**(2): 343–357. doi.org/10.1175/MWR-D-11-00049.1

Moon, J. Y., Wang, B., and Ha, K. J. (**2011**) ENSO regulation of MJO teleconnection. *Climate Dynamics*, **37**: 1133–1149. doi.org/10.1007/s00382-010-0902-3

Mori, M. and Watanabe, M. (**2008**) The Growth and Triggering Mechanisms of

the PNA: A MJO-PNA Coherence. *Journal of the Meteorological Society of Japan*, **86**(1): 213–236. doi.org/10.2151/jmsj.86.213

Msadek, R., Frankignoul, C., and Li, L. (**2011**) Mechanisms of the atmospheric response to North Atlantic multidecadal variability: a model study. *Climate Dynamics*, **36**: 1255–1276. doi.org/10.1007/s00382-010-0958-0

Müller, W. A., Jungclaus, J. H., Mauritsen, T., Baehr, J., Bittner, M., Budich, R., Bunzel, F., Esch, M., Ghosh, R., Haak, H., Ilyina, T., Kleine, T., Kornblueh, L., Li, H., Modali, K., Notz, D., Pohlmann, H., Roeckner, E., Stemmler, I., Tian, F., and Marotzke, J. (**2018**) A Higher-resolution Version of the Max Planck Institute Earth System Model (MPI-ESM1.2-HR). *Journal of Advances in Modeling Earth Systems*, **10**(7): 1383–1413. doi.org/10.1029/2017MS001217

Mysterud, A., Stenseth, N. C., Yoccoz, N. G., Ottersen, G., and Langvatn, R. (**2003**) The Response of Terrestrial Ecosystems to Climate Variability Associated with the North Atlantic Oscillation. *In* J. W. Hurrell, Y. Kushnir, G. Ottersen, and M. Visbeck (Editors), *The North Atlantic Oscillation: Climatic Significance and Environmental Impact*, pages 235–262. American Geophysical Union (AGU). ISBN 9781118669037. doi.org/10.1029/134GM11

Nardi, K. M., Baggett, C. F., Barnes, E. A., Maloney, E. D., Harnos, D. S., and Ciasto, L. M. (**2020**) Skillful All-Season S2S Prediction of U.S. Precipitation Using the MJO and QBO. *Weather and Forecasting*, **35**(5): 2179–2198. doi.org/10.1175/WAF-D-19-0232.1

National Center for Atmospheric Research (**2022**) NCL: Madden Julian Oscillation Climate Variability. *NCAR - Climate Data Guide*. https://www.ncl.ucar.edu/Applications/mjoclivar.shtml. Accessed: 20/04/2022

National Oceanic and Atmospheric Administration Earth System Research Laboratories (**2022**) Niño 3.4 SST Index. https://psl.noaa.gov/gcos_wgsp/Timeseries/Data/nino34.long.data

National Oceanic and Atmospheric Administration Earth System Research Laboratories (**2023**) North Atlantic Oscillation (NAO). https://psl.noaa.gov/data/timeseries/daily/NAO/

NCAR Climate Analysis Section, Trenberth, K. E., and Shea, D. J. (**2006**) AMO Index Data. https://climatedataguide.ucar.edu/climate-data/atlantic-multi-decadal-oscillation-amo. Updated yearly. Accessed 22/04/2022

Neal, R., Fereday, D., Crocker, R., and Comer, R. E. (**2016**) A flexible approach to defining weather patterns and their application in weather forecasting over Europe. *Meteorological Applications*, **23**(3): 389–400. doi.org/10.1002/met.1563

Neelin, J. D., Battisti, D. S., Hirst, A. C., Jin, F.-F., Wakata, Y., Yamagata, T., and Zebiak, S. E. (**1998**) ENSO theory. *Journal of Geophysical Research: Oceans*, **103**(C7): 14,261–14,290. doi.org/10.1029/97JC03424

Neelin, J. D. and Yu, J.-Y. (**1994**) Modes of Tropical Variability under Convective Adjustment and the Madden–Julian Oscillation. Part I: Analytical Theory. *Journal of Atmospheric Sciences*, **51**(13): 1876–1894. doi.org/10.1175/1520-0469(1994)051⟨1876:MOTVUC⟩2.0.CO;2

Newman, M., Alexander, M. A., Ault, T. R., Cobb, K. M., Deser, C., Lorenzo, E. D., Mantua, N. J., Miller, A. J., Minobe, S., Nakamura, H., Schneider, N., Vimont, D. J., Phillips, A. S., Scott, J. D., and Smith, C. A. (**2016**) The Pacific Decadal Oscillation, Revisited. *Journal of Climate*, **29**(12): 4399–4427. doi.org/10.1175/JCLI-D-15-0508.1

Nishimoto, E. and Yoden, S. (**2017**) Influence of the Stratospheric Quasi-Biennial Oscillation on the Madden–Julian Oscillation during Austral Summer. *Journal of the Atmospheric Sciences*, **74**(4): 1105–125. doi.org/10.1175/JAS-D-16-0205.1

Niwano, M. and Takahashi, M. (**1998**) The Influence of the Equatorial QBO on the Northern Hemisphere Winter Circulation of a GCM. *Journal of the*

Meteorological Society of Japan. Ser. II, **76**(3): 453–461. doi.org/10.2151/jmsj1965.76.3_453

Nowack, P., Runge, J., Eyring, V., and Haigh, J. D. (**2020**) Causal networks for climate model evaluation and constrained projections. *Nature Communications*, **11**(1415). doi.org/10.1038/s41467-020-15195-y

O'Connor, F. M., Abraham, N. L., Dalvi, M., Folberth, G. A., Griffiths, P. T., Hardacre, C., Johnson, B. T., Kahana, R., Keeble, J., Kim, B., Morgenstern, O., Mulcahy, J. P., Richardson, M., Robertson, E., Seo, J., Shim, S., Teixeira, J. C., Turnock, S. T., Williams, J., Wiltshire, A. J., Woodward, S., and Zeng, G. (**2021**) Assessment of pre-industrial to present-day anthropogenic climate forcing in UKESM1. *Atmospheric Chemistry and Physics*, **21**(2): 1211–1243. doi.org/10.5194/acp-21-1211-2021

Oliver, E. (**2015**) Multidecadal variations in the modulation of Alaska wintertime air temperature by the Madden–Julian Oscillation. *Theoretical and Applied Climatology*, **121**: 1–11. doi.org/10.1007/s00704-014-1215-y

Omrani, N.-E., Keenlyside, N., Matthes, K., Boljka, L., Zanchettin, D., Jungclaus, J. H., and Lubis, S. W. (**2022**) Coupled stratosphere-troposphere-Atlantic multidecadal oscillation and its importance for near-future climate projection. *npj Climate and Atmospheric Science*, **5**(59). doi.org/10.1038/s41612-022-00275-1

Osborn, T. J. (**2011**) Winter 2009/2010 temperatures and a record-breaking North Atlantic Oscillation index. *Weather*, **66**(1): 19–21. doi.org/10.1002/wea.660

Ottersen, G., Planque, B., Belgrano, A., Post, E., Reid, P. C., and Stenseth, N. C. (**2001**) Ecological effects of the North Atlantic Oscillation. *Oecologia*, **128**(1): 1–14. ISSN 1432-1939. doi.org/10.1007/s004420100655

Palin, E. J., Scaife, A. A., Wallace, E., Pope, E. C. D., Arribas, A., and Brookshaw, A. (**2016**) Skillful Seasonal Forecasts of Winter Disruption to the

U.K. Transport System. *Journal of Applied Meteorology and Climatology*, **55**(2): 325–344. doi.org/10.1175/JAMC-D-15-0102.1

Palmer, C. E. (**1959**) The stratospheric polar vortex in winter. *Journal of Geophysical Research*, **64**(7): 749–764. doi.org/10.1029/JZ064i007p00749

Palmer, T. N. (**2002**) The economic value of ensemble forecasts as a tool for risk assessment: From days to decades. *Quarterly Journal of the Royal Meteorological Society*, **128**(581): 747–774. doi.org/10.1256/0035900021643593

Parker, T., Woollings, T., Weisheimer, A., O'Reilly, C., Baker, L., and Shaffrey, L. (**2019**) Seasonal Predictability of the Winter North Atlantic Oscillation From a Jet Stream Perspective. *Geophysical Research Letters*, **46**(16): 10,159–10,167. doi.org/10.1029/2019GL084402

Patricola, C. M., O'Brien, J. P., Risser, M. D., Rhoades, A. M., amd Paul A. Ullrich, T. A. O., Stone, D. A., and Collins, W. D. (**2020**) Maximizing ENSO as a source of western US hydroclimate predictability. *Climate Dynamics*, **54**: 351–372. doi.org/10.1007/s00382-019-05004-8

Pedlosky, J. (**2003**) *Rossby Waves*, pages 149–158. Springer Berlin Heidelberg, Berlin, Heidelberg. ISBN 978-3-662-05131-3. doi.org/10.1007/978-3-662-05131-3_14

Philander, S. (**1989**) *El Niño, La Niña, and the Southern Oscillation.* International geophysics series. Academic Press. ISBN 9780125532358

Philander, S. G. H. (**1983**) El Niño Southern Oscillation phenomena. *Nature*, **302**: 295–301. doi.org/10.1038/302295a0

Pierce, D. W., Barnett, T. P., Schneider, N., Saravanan, R., Dommenget, D., and Latif, M. (**2001**) The role of ocean dynamics in producing decadal climate variability in the North Pacific. *Climate Dynamics*, **18**: 51–70. doi.org/10.1007/s003820100158

Pohl, B. and Matthews, A. J. (**2007**) Observed Changes in the Lifetime and

Amplitude of the Madden–Julian Oscillation Associated with Interannual ENSO Sea Surface Temperature Anomalies. *Journal of Climate*, **20**(11): 2659–2674. doi.org/10.1175/JCLI4230.1

Pritchard, M. S. and Yang, D. (**2016**) Response of the Superparameterized Madden-Julian Oscillation to Extreme Climate and Basic-State Variation Challenges a Moisture Mode View. *Journal of Climate*, **29**(13): 4995–5008. 10.1175/JCLI-D-15-0790.1

Pörtner, H.-O., Roberts, D., Adams, H., Adelekan, I., Adler, C., Adrian, R., Aldunce, P., Ali, E., Begum, R. A., Friedl, B. B., Kerr, R. B., Biesbroek, R., Birkmann, J., Bowen, K., Caretta, M., Carnicer, J., Castellanos, E., Cheong, T., Chow, W., G. Cissé, G. C., and Ibrahim, Z. Z. (**2022**) Climate Change 2022: Impacts, Adaptation and Vulnerability. *In* IPCC (Editor), *Sixth Assessment Report of the Intergovernmental Panel on Climate Change*. Cambridge University Press, Cambridge, UK and New York, USA. doi.org/10.1017/9781009325844

Qasmi, S., Cassou, C., and Boé, J. (**2020**) Teleconnection Processes Linking the Intensity of the Atlantic Multidecadal Variability to the Climate Impacts over Europe in Boreal Winter. *Journal of Climate*, **33**(7): 2681–2700. doi.org/10.1175/JCLI-D-19-0428.1

Rafferty, J. P. (**2019**) The North Atlantic Oscillation. *Encyclopedia Britannica*. https://www.britannica.com/science/North-Atlantic-Oscillation. Accessed on 17th March 2022

Raghavan, K. and Panickal, S. (**2019**) CCCR-IITM IITM-ESM model output prepared for CMIP6 CMIP historical. *Earth System Grid Federation*. doi.org/10.22033/ESGF/CMIP6.3708. Accessed from the Centre for Environmental Data Analysis (CEDA) archive on 11th September 2021

Rao, J., Garfinkel, C. I., and White, I. P. (**2020**) Impact of the Quasi-Biennial Oscillation on the Northern Winter Stratospheric Polar Vortex in CMIP5/6 Models. *Journal of Climate*, **33**(11): 4787–4813.

doi.org/10.1175/JCLI-D-19-0663.1

Rasmusson, E. M. and Carpenter, T. H. (**1982**) Variations in Tropical Sea Surface Temperature and Surface Wind Fields Associated with the Southern Oscillation/El Niño. *Monthly Weather Review*, **110**(5): 354–384. doi.org/10.1175/1520-0493(1982)110⟨0354:VITSST⟩2.0.CO;2

Rayner, N. A., Parker, D. E., Horton, E. B., Folland, C. K., Alexander, L. V., Rowell, D. P., Kent, E. C., and Kaplan, A. (**2003**) Global analyses of sea surface temperature, sea ice, and night marine air temperature since the late nineteenth century. *Journal of Geophysical Research: Atmospheres*, **108**(D14). doi.org/10.1029/2002JD002670

Reed, R. J. (**1964**) A tentative model of the 26-month oscillation in tropical latitudes. *Quarterly Journal of the Royal Meteorological Society*, **90**(386): 441–466. doi.org/10.1002/qj.49709038607

Riddle, E. E., Stoner, M. B., Johnson, N. C., L'Heureux, M. L., Collins, D. C., and Feldstein, S. B. (**2013**) The impact of the MJO on clusters of wintertime circulation anomalies over the North American region. *Climate Dynamics*, **40**: 1749–1766. doi.org/10.1007/s00382-012-1493-y

Ridley, J., Menary, M., Kuhlbrodt, T., Andrews, M., and Andrews, T. (**2019***a*) MOHC HadGEM3-GC31-LL model output prepared for CMIP6 CMIP historical. *Earth System Grid Federation*. doi.org/10.22033/ESGF/CMIP6.6109. Accessed from the Centre for Environmental Data Analysis (CEDA) archive on 8th September 2021

Ridley, J., Menary, M., Kuhlbrodt, T., Andrews, M., and Andrews, T. (**2019***b*) MOHC HadGEM3-GC31-MM model output prepared for CMIP6 CMIP historical. *Earth System Grid Federation*. doi.org/10.22033/ESGF/CMIP6.6109. Accessed from the Centre for Environmental Data Analysis (CEDA) archive on 8th September 2021

Robson, J., Aksenov, Y., Bracegirdle, T. J., Dimdore-Miles, O., Griffiths, P. T., Grosvenor, D. P., Hodson, D. L. R., Keeble, J., MacIntosh, C., Megann, A.,

Osprey, S., Povey, A. C., Schröder, D., Yang, M., Archibald, A. T., Carslaw, K. S., Gray, L., Jones, C., Kerridge, B., Knappett, D., Kuhlbrodt, T., Russo, M., Sellar, A., Siddans, R., Sinha, B., Sutton, R., Walton, J., and Wilcox, L. J. (**2020**) The Evaluation of the North Atlantic Climate System in UKESM1 Historical Simulations for CMIP6. *Journal of Advances in Modeling Earth Systems*, **12**(9): e2020MS002,126. doi.org/10.1029/2020MS002126

Rogers, J. C. (**1984**) The Association between the North Atlantic Oscillation and the Southern Oscillation in the Northern Hemisphere. *Monthly Weather Review*, **112**(10): 1999–2015. doi.org/10.1175/1520-0493(1984)112⟨1999:TABTNA⟩2.0.CO;2

Rossby, C.-G., Willett, H. C., Holmboe, J., Namias, J., Page, L., and Allen, R. (**1938**) Relation between variations in the intensity of the zonal circulation of the atmosphere and the displacements of the permanent centers of action atmosphere and the displacements of the permanent centers of action. *Journal of Marine Research*, **2**(1): 38–55. https://elischolar.library.yale.edu/journal_of_marine_research/544/

Rostami, M. and Zeitlin, V. (**2019**) Eastward-moving convection-enhanced modons in shallow water in the equatorial tangent plane. *Physics of Fluids*, **31**(2): 021,701. ISSN 1070-6631. doi.org/10.1063/1.5080415

Roundy, P. E., MacRitchie, K., Asuma, J., and Melino, T. (**2010**) Modulation of the Global Atmospheric Circulation by Combined Activity in the Madden–Julian Oscillation and the El Niño–Southern Oscillation during Boreal Winter. *Journal of Climate*, **23**(15): 4045–4059. doi.org/10.1175/2010JCLI3446.1

Ruela, R., Sousa, M., deCastro, M., and Dias, J. (**2020**) Global and regional evolution of sea surface temperature under climate change. *Global and Planetary Change*, **190**: 103,190. ISSN 0921-8181. doi.org/10.1016/j.gloplacha.2020.103190

Ruggieri, P., Bellucci, A., Nicolí, D., Athanasiadis, P. J., Gualdi, S., Cassou, C.,

Castruccio, F., Danabasoglu, G., Davini, P., Dunstone, N., Eade, R., Gastineau, G., Harvey, B., Hermanson, L., Qasmi, S., Ruprich-Robert, Y., Sanchez-Gomez, E., Smith, D., Wild, S., and Zampieri, M. (**2021**) Atlantic Multidecadal Variability and North Atlantic Jet: A Multimodel View from the Decadal Climate Prediction Project. *Journal of Climate*, **34**(1): 347–360. doi.org/10.1175/JCLI-D-19-0981.1

Runge, J., Bathiany, S., Bollt, E., Camps-Valls, G., Coumou, D., Deyle, E., Glymour, C., Kretschmer, M., Mahecha, M. D., Muñoz-Marí, J., van Nes, E. H., Peters, J., Quax, R., Reichstein, M., Scheffer, M., Schölkopf, B., Spirtes, P., Sugihara, G., Sun, J., Zhang, K., and Zscheischler, J. (**2019**) Inferring causation from time series in Earth system sciences. *Nature Communications*, **10**(2553). doi.org/10.1038/s41467-019-10105-3

Ruprich-Robert, Y., Moreno-Chamarro, E., Levine, X., Bellucci, A., Cassou, C., Castruccio, F., Davini, P., Eade, R., Gastineau, G., Hermanson, L., Hodson, D., Lohmann, K., Lopez-Parages, J., Monerie, P.-A., Nicolì, D., Qasmi, S., Roberts, C. D., Sanchez-Gomez, E., Danabasoglu, G., Dunstone, N., Martin-Rey, M., Msadek, R., Robson, J., Smith, D., and Tourigny, E. (**2021**) Impacts of Atlantic multidecadal variability on the tropical Pacific: a multi-model study. *npj climate and atmospheric science*, **4**(1): 33. doi.org/10.1038/s41612-021-00188-5

Rushley, S. S., Kim, D., and Ángel F. Adames (**2019**) Changes in the MJO under Greenhouse Gas–Induced Warming in CMIP5 Models. *Journal of Climate*, **32**(3): 803–821. doi.org/10.1175/JCLI-D-18-0437.1

Saji, N., Goswami, B., Vinayachandran, P., and et al. (**1999**) A dipole mode in the tropical Indian Ocean. *Nature*, **401**(6751): 360–363. doi.org/10.1038/43854

Samarasinghe, S. M., Connolly, C., Barnes, E. A., Ebert-Uphoff, I., and Sun, L. (**2021**) Strengthened Causal Connections Between the MJO and the North Atlantic With Climate Warming. *Geophysical Research Letters*, **48**(5):

e2020GL091,168. doi.org/10.1029/2020GL091168

Sarachik, E. S. and Cane, M. A. (**2010**) *The El Niño-Southern Oscillation Phenomenon.* Cambridge University Press. ISBN 9780521847865. https://search.ebscohost.com/login.aspx?direct=true&AuthType=sso&db=nlebk&AN=317662&authtype=sso&custid=s8993828&site=eds-live&scope=site

Sardeshmukh, P. D. and Hoskins, B. J. (**1988**) The Generation of Global Rotational Flow by Steady Idealized Tropical Divergence. *Journal of Atmospheric Sciences*, **45**(7): 1228–1251. doi.org/10.1175/1520-0469(1988)045⟨1228:TGOGRF⟩2.0.CO;2

Scaife, A. A., Arribas, A., Blockley, E., Brookshaw, A., Clark, R. T., Dunstone, N., Eade, R., Fereday, D., Folland, C. K., Gordon, M., Hermanson, L., Knight, J. R., Lea, D. J., MacLachlan, C., Maidens, A., Martin, M., Peterson, A. K., Smith, D., Vellinga, M., Wallace, E., Waters, J., and Williams, A. (**2014**) Skillful long-range prediction of European and North American winters. *Geophysical Research Letters*, **41**(7): 2514–2519. doi.org/10.1002/2014GL059637

Scaife, A. A., Comer, R. E., Dunstone, N. J., Knight, J. R., Smith, D. M., MacLachlan, C., Martin, N., Peterson, K. A., Rowlands, D., Carroll, E. B., Belcher, S., and Slingo, J. (**2017**) Tropical rainfall, Rossby waves and regional winter climate predictions. *Quarterly Journal of the Royal Meteorological Society*, **143**(702): 1–11. doi.org/10.1002/qj.2910

Scaife, A. A. and Smith, D. (**2018**) A signal-to-noise paradox in climate science. *npj Climate and Atmospheric Science*, **1**(28). doi.org/10.1038/s41612-018-0038-4

Schreck, C. J., Cordeira, J. M., and Margolin, D. (**2013**) Which MJO Events Affect North American Temperatures? *Monthly Weather Review*, **141**(11): 3840–3850. doi.org/10.1175/MWR-D-13-00118.1

Schurer, A. P., Hegerl, G. C., Goosse, H., Bollasina, M. A., England, M. H., Smith, D. M., and Tett, S. F. B. (**2023**) Role of multi-decadal variability of

the winter North Atlantic Oscillation on Northern Hemisphere climate. *Environmental Research Letters*, **18**(4): 044,046. doi.org/10.1088/1748-9326/acc477

Schwartz, C. and Garfinkel, C. I. (**2017**) Relative roles of the MJO and stratospheric variability in North Atlantic and European winter climate. *Journal of Geophysical Research: Atmospheres*, **122**(8): 4184–4201. doi.org/10.1002/2016JD025829

Schwartz, C. and Garfinkel, C. I. (**2020**) Troposphere-Stratosphere Coupling in Subseasonal-to-Seasonal Models and Its Importance for a Realistic Extratropical Response to the Madden-Julian Oscillation. *Journal of Geophysical Research: Atmospheres*, **125**(10): e2019JD032,043. doi.org/10.1029/2019JD032043

Seabrook, M., Smith, D. M., Dunstone, N. J., Eade, R., Hermanson, L., Scaife, A. A., and Hardiman, S. C. (**2023**) Opposite Impacts of Interannual and Decadal Pacific Variability in the Extratropics. *Geophysical Research Letters*, **50**(2): e2022GL101,226. doi.org/10.1029/2022GL101226

Séférian, R. (**2018**) CNRM-CERFACS CNRM-ESM2-1 model output prepared for CMIP6 CMIP historical. *Earth System Grid Federation*. doi.org/10.22033/ESGF/CMIP6.4068. Accessed from the Centre for Environmental Data Analysis (CEDA) archive on 13th September 2021

Séférian, R., Nabat, P., Michou, M., Saint-Martin, D., Voldoire, A., Colin, J., Decharme, B., Delire, C., Berthet, S., Chevallier, M., Sénési, S., Franchisteguy, L., Vial, J., Mallet, M., Joetzjer, E., Geoffroy, O., Guérémy, J.-F., Moine, M.-P., Msadek, R., Ribes, A., Rocher, M., Roehrig, R., Salas-y Mélia, D., Sanchez, E., Terray, L., Valcke, S., Waldman, R., Aumont, O., Bopp, L., Deshayes, J., Éthé, C., and Madec, G. (**2019**) Evaluation of CNRM Earth System Model, CNRM-ESM2-1: Role of Earth System Processes in Present-Day and Future Climate. *Journal of Advances in Modeling Earth Systems*, **11**(12): 4182–4227. doi.org/10.1029/2019MS001791

Sellar, A. A., Jones, C. G., Mulcahy, J. P., Tang, Y., Yool, A., Wiltshire, A., O'Connor, F. M., Stringer, M., Hill, R., Palmieri, J., Woodward, S., de Mora, L., Kuhlbrodt, T., Rumbold, S. T., Kelley, D. I., Ellis, R., Johnson, C. E., Walton, J., Abraham, N. L., Andrews, M. B., Andrews, T., Archibald, A. T., Berthou, S., Burke, E., Blockley, E., Carslaw, K., Dalvi, M., Edwards, J., Folberth, G. A., Gedney, N., Griffiths, P. T., Harper, A. B., Hendry, M. A., Hewitt, A. J., Johnson, B., Jones, A., Jones, C. D., Keeble, J., Liddicoat, S., Morgenstern, O., Parker, R. J., Predoi, V., Robertson, E., Siahaan, A., Smith, R. S., Swaminathan, R., Woodhouse, M. T., Zeng, G., and Zerroukat, M. (**2019**) UKESM1: Description and Evaluation of the U.K. Earth System Model. *Journal of Advances in Modeling Earth Systems*, **11**(12): 4513–4558. doi.org/10.1029/2019MS001739

Semmler, T., Danilov, S., Gierz, P., Goessling, H. F., Hegewald, J., Hinrichs, C., Koldunov, N., Khosravi, N., Mu, L., Rackow, T., Sein, D. V., Sidorenko, D., Wang, Q., and Jung, T. (**2020**) Simulations for CMIP6 With the AWI Climate Model AWI-CM-1-1. *Journal of Advances in Modeling Earth Systems*, **12**(9): e2019MS002,009. doi.org/10.1029/2019MS002009

Sena, A. C. T., Peings, Y., and Magnusdottir, G. (**2022**) Effect of the Quasi-Biennial Oscillation on the Madden Julian Oscillation Teleconnections in the Southern Hemisphere. *Geophysical Research Letters*, **49**(6): e2021GL096,105. doi.org/10.1029/2021GL096105

Seo, K.-H. and Lee, H.-J. (**2017**) Mechanisms for a PNA-Like Teleconnection Pattern in Response to the MJO. *Journal of the Atmospheric Sciences*, **74**(6): 1767–1781. doi.org/10.1175/JAS-D-16-0343.1

Seo, K.-H., Lee, H.-J., and Frierson, D. M. W. (**2016**) Unraveling the Teleconnection Mechanisms that Induce Wintertime Temperature Anomalies over the Northern Hemisphere Continents in Response to the MJO. *Journal of the Atmospheric Sciences*, **73**(9): 3557–3571. doi.org/10.1175/JAS-D-16-0036.1

Seo, K.-H. and Son, S.-W. (**2012**) The Global Atmospheric Circulation Response to Tropical Diabatic Heating Associated with the Madden–Julian Oscillation during Northern Winter. *Journal of the Atmospheric Sciences*, **69**(1): 79–96. doi.org/10.1175/2011JAS3686.1

Seviour, W. J. M., Gray, L. J., and Mitchell, D. M. (**2016**) Stratospheric polar vortex splits and displacements in the high-top CMIP5 climate models. *Journal of Geophysical Research: Atmospheres*, **121**(4): 1400–1413. doi.org/10.1002/2015JD024178

Siqueira, L., Ramírez, E., and Camayo, R. (**2019**) An Overview of the El Niño, La Niña, and the Southern Oscillation Phenomena: Theory, Observations, and Modeling Links. *In* L. Bacelar Lima Santos, R. Galante Negri, and T. J. de Carvalho (Editors), *Towards Mathematics, Computers and Environment: A Disasters Perspective*, pages 1–18. Springer International Publishing, Cham. ISBN 978-3-030-21205-6. doi.org/10.1007/978-3-030-21205-6_1

Skinner, D. T., Matthews, A. J., and Stevens, D. P. (**2022**) North Atlantic Oscillation response to the Madden–Julian Oscillation in a coupled climate model. *Weather*, **77**(6): 201–205. doi.org/10.1002/wea.4215

Skinner, D. T., Matthews, A. J., and Stevens, D. P. (**2023**) Decadal variability of the extratropical response to the Madden–Julian Oscillation. *Geophysical Research Letters*, **50**(17): e2023GL104,576. doi.org/10.1029/2023GL104576

Slingo, J., Sperber, K., Boyle, J., Ceron, J.-P., Dix, M., Dugas, B., Ebisuzaki, W., Fyfe, J., Gregory, D., Gueremy, J., Hack, J., Harzallah, A., Inness, P., Kitoh, A., Lau, W. K.-M., McAvaney, B., Madden, R., Matthews, A., Palmer, T., Park, C.-K., Randall, D., and Renno, N. (**1996**) Intraseasonal oscillations in 15 atmospheric general circulation models: results from an AMIP diagnostic subproject. *Climate Dynamics*, **12**(5): 325–358. doi.org/10.1007/BF00231106

Smith, D. M., Scaife, A. A., Eade, R., Athanasiadis, P., Bellucci, A., Bethke, I., Bilbao, R., Borchert, L. F., Caron, L.-P., Counillon, F., Danabasoglu, G.,

Delworth, T., Doblas-Reyes, F. J., Dunstone, N. J., Estella-Perez, V., Flavoni, S., Hermanson, L., Keenlyside, N., Kharin, V., Kimoto, M., Merryfield, W. J., Mignot, J., Mochizuki, T., Modali, K., Monerie, P.-A., M uller, W. A., Nicolí, D., Ortega, P., Pankatz, K., Pohlmann, H., Robson, J., Ruggieri, P., Sospedra-Alfonso, R., Swingedouw, D., Wang, Y., Wild, S., Yeager, S., Yang, X., and Zhang, L. (**2020**) North Atlantic climate far more predictable than models imply. *Nature*, **583**: 796–800. doi.org/10.1038/s41586-020-2525-0

Sobel, A. and Maloney, E. (**2012**) An Idealized Semi-Empirical Framework for Modeling the Madden–Julian Oscillation. *Journal of the Atmospheric Sciences*, **69**(5): 1691–1705. doi.org/10.1175/JAS-D-11-0118.1

Sobel, A. and Maloney, E. (**2013**) Moisture Modes and the Eastward Propagation of the MJO. *Journal of the Atmospheric Sciences*, **70**(1): 187–192. doi.org/10.1175/JAS-D-12-0189.1

Sobel, A. H., Nilsson, J., and Polvani, L. M. (**2001**) The Weak Temperature Gradient Approximation and Balanced Tropical Moisture Waves. *Journal of the Atmospheric Sciences*, **58**(23): 3650–3665. doi.org/10.1175/1520-0469(2001)058⟨3650:TWTGAA⟩2.0.CO;2

Son, S.-W., Lim, Y., Yoo, C., Hendon, H. H., and Kim, J. (**2017**) Stratospheric Control of the Madden–Julian Oscillation. *Journal of Climate*, **30**(6): 1909–1922. doi.org/10.1175/JCLI-D-16-0620.1

Song, L. and Wu, R. (**2020***a*) Distinct Eurasian climate anomalies associated with strong and weak MJO events. *International Journal of Climatology*, **40**(15): 6666–6674. doi.org/10.1002/joc.6630

Song, L. and Wu, R. (**2020***b*) Modulation of the Westerly and Easterly Quasi-Biennial Oscillation Phases on the Connection between the Madden–Julian Oscillation and the Arctic Oscillation. *Atmosphere*, **11**(2). ISSN 2073–4433. doi.org/10.3390/atmos11020175

Stan, C., Straus, D. M., Frederiksen, J. S., Lin, H., Maloney, E. D., and Schumacher, C. (**2017**) Review of Tropical-Extratropical Teleconnections on

Intraseasonal Time Scales. *Reviews of Geophysics*, **55**(4): 902–937. doi.org/10.1002/2016RG000538

Stephenson, D. B., Wanner, H., Brönnimann, S., and Luterbacher, J. (**2003**) The History of Scientific Research on the North Atlantic Oscillation. *In* J. W. Hurrell, Y. Kushnir, G. Ottersen, and M. Visbeck (Editors), *The North Atlantic Oscillation: Climatic Significance and Environmental Impact*, pages 37–50. American Geophysical Union (AGU). ISBN 9781118669037. doi.org/10.1029/134GM02

Straile, D., Livingstone, D. M., Weyhenmeyer, G. A., and George, D. G. (**2003**) The Response of Freshwater Ecosystems to Climate Variability Associated with the North Atlantic Oscillation. *In* J. W. Hurrell, Y. Kushnir, G. Ottersen, and M. Visbeck (Editors), *The North Atlantic Oscillation: Climatic Significance and Environmental Impact*, pages 263–279. American Geophysical Union (AGU). ISBN 9781118669037. doi.org/10.1029/134GM12

Su, J., Chen, D., Zheng, D., Su, Y., and Li, X. (**2023**) The insight of why: Causal inference in Earth system science. *Science China Earth Sciences*. doi.org/10.1007/s11430-023-1148-7

Suematsu, T. and Miura, H. (**2018**) Zonal SST Difference as a Potential Environmental Factor Supporting the Longevity of the Madden–Julian Oscillation. *Journal of Climate*, **31**(18): 7549–7564. doi.org/10.1175/JCLI-D-17-0822.1

Suhas, E. and Goswami, B. N. (**2010**) Loss of Significance and Multidecadal Variability of the Madden–Julian Oscillation. *Journal of Climate*, **23**(13): 3739–3751. doi.org/10.1175/2010JCLI3180.1

Sutton, R. T. and Hodson, D. L. R. (**2005**) Atlantic Ocean Forcing of North American and European Summer Climate. *Science*, **309**(5731): 115–118. doi.org/10.1126/science.1109496

Swart, N. C., Cole, J. N., Kharin, V. V., Lazare, M., Scinocca, J. F., Gillett, N. P., Anstey, J., Arora, V., Christian, J. R., Jiao, Y., Lee, W. G., Majaess,

F., Saenko, O. A., Seiler, C., Seinen, C., Shao, A., Solheim, L., von Salzen, K., Yang, D., Winter, B., and Sigmond, M. (**2019***a*) CCCma CanESM5 model output prepared for CMIP6 CMIP historical. *Earth System Grid Federation*. doi.org/10.22033/ESGF/CMIP6.3610. Accessed from the Centre for Environmental Data Analysis (CEDA) archive on 11th September 2021

Swart, N. C., Cole, J. N. S., Kharin, V. V., Lazare, M., Scinocca, J. F., Gillett, N. P., Anstey, J., Arora, V., Christian, J. R., Hanna, S., Jiao, Y., Lee, W. G., Majaess, F., Saenko, O. A., Seiler, C., Seinen, C., Shao, A., Sigmond, M., Solheim, L., von Salzen, K., Yang, D., and Winter, B. (**2019***b*) The Canadian Earth System Model version 5 (CanESM5.0.3). *Geoscientific Model Development*, **12**(11): 4823–4873. doi.org/10.5194/gmd-12-4823-2019

Swenson, E. T. and Straus, D. M. (**2017**) Rossby Wave Breaking and Transient Eddy Forcing during Euro-Atlantic Circulation Regimes. *Journal of the Atmospheric Sciences*, **74**(6): 1735–1755. doi.org/10.1175/JAS-D-16-0263.1

Taguchi, B., Nakamura, H., Nonaka, M., Komori, N., Kuwano-Yoshida, A., Takaya, K., and Goto, A. (**2012**) Seasonal Evolutions of Atmospheric Response to Decadal SST Anomalies in the North Pacific Subarctic Frontal Zone: Observations and a Coupled Model Simulation. *Journal of Climate*, **25**(1): 111–139. doi.org/10.1175/JCLI-D-11-00046.1

Takahashi, C., Sato, N., Seiki, A., Yoneyama, K., and Shirooka, R. (**2011**) Projected future change of MJO and its extratropical teleconnection in East Asia during the northern winter simulated in IPCC AR4 models. *Sola*, **7**: 201–204. doi.org/10.2151/sola.2011-051

Tang, Y., Rumbold, S., Ellis, R., Kelley, D., Mulcahy, J., Sellar, A., Walton, J., and Jones, C. (**2019***a*) MOHC UKESM1.0-LL model output prepared for CMIP6 CMIP historical. *Earth System Grid Federation*. doi.org/10.22033/ESGF/CMIP6.6113. Accessed from the Centre for Environmental Data Analysis (CEDA) archive on 9th September 2021

Tang, Y., Rumbold, S., Ellis, R., Kelley, D., Mulcahy, J., Sellar, A., Walton, J.,

and Jones, C. (**2019***b*) MOHC UKESM1.0-LL model output prepared for CMIP6 CMIP piControl. *Earth System Grid Federation*. doi.org/10.22033/ESGF/CMIP6.6298. Accessed from the Centre for Environmental Data Analysis (CEDA) archive on 6th October 2021

Tatebe, H., Ogura, T., Nitta, T., Komuro, Y., Ogochi, K., Takemura, T., Sudo, K., Sekiguchi, M., Abe, M., Saito, F., Chikira, M., Watanabe, S., Mori, M., Hirota, N., Kawatani, Y., Mochizuki, T., Yoshimura, K., Takata, K., O'ishi, R., Yamazaki, D., Suzuki, T., Kurogi, M., Kataoka, T., Watanabe, M., and Kimoto, M. (**2019**) Description and basic evaluation of simulated mean state, internal variability, and climate sensitivity in MIROC6. *Geoscientific Model Development*, **12**(7): 2727–2765. doi.org/10.5194/gmd-12-2727-2019

Tatebe, H. and Watanabe, M. (**2018**) MIROC MIROC6 model output prepared for CMIP6 CMIP historical. *Earth System Grid Federation*. doi.org/10.22033/ESGF/CMIP6.5603. Accessed from Centre for Environmental Data Analysis (CEDA) archive on 11th September 2021

The pandas development team (**2020**) pandas (version 1.4.4). *Zenodo*. doi.org/10.5281/zenodo.3509134

Thompson, D. W. J., Baldwin, M. P., and Wallace, J. M. (**2002**) Stratospheric Connection to Northern Hemisphere Wintertime Weather: Implications for Prediction. *Journal of Climate*, **15**(12): 1421–1428. doi.org/10.1175/1520-0442(2002)015⟨1421:SCTNHW⟩2.0.CO;2

Thompson, D. W. J., Lee, S., and Baldwin, M. P. (**2003**) Atmospheric Processes Governing the Northern Hemisphere Annular Mode/North Atlantic Oscillation. *In* J. Hurrell, Y. Kushnir, G. Ottersen, and M. Visbeck (Editors), *The North Atlantic Oscillation: Climatic Significance and Environmental Impact*, pages 81–112. American Geophysical Union (AGU). ISBN 9781118669037. doi.org/10.1029/134GM05

Thompson, D. W. J. and Wallace, J. M. (**1998**) The Arctic oscillation signature in the wintertime geopotential height and temperature fields. *Geophysical*

Research Letters, **25**(9): 1297–1300. https://doi.org/10.1029/98GL00950

Thompson, D. W. J. and Wallace, J. M. (**2000**) Annular Modes in the Extratropical Circulation. Part I: Month-to-Month Variability. *Journal of Climate*, **13**(5): 1000 – 1016. https://doi.org/10.1175/1520-0442(2000)013⟨1000:AMITEC⟩2.0.CO;2

Thompson, D. W. J. and Wallace, J. M. (**2001**) Regional Climate Impacts of the Northern Hemisphere Annular Mode. *Science*, **293**(5527): 85–89. https://doi.org/10.1126/science.1058958

Thompson, D. W. J., Wallace, J. M., and Hegerl, G. C. (**2000**) Annular Modes in the Extratropical Circulation. Part II: Trends. *Journal of Climate*, **13**(5): 1018 – 1036. https://doi.org/10.1175/1520-0442(2000)013⟨1018:AMITEC⟩2.0.CO;2

Thyng, K., Greene, C., Hetland, R., Zimmerle, H., and DiMarco, S. (**2016**) True colors of oceanography: Guidelines for effective and accurate colormap selection. *Oceanography*, **29**(3): 9–13. doi.org/10.5670/oceanog.2016.66

Toms, B. A., Barnes, E. A., Maloney, E. D., and van den Heever, S. C. (**2020**) The Global Teleconnection Signature of the Madden-Julian Oscillation and Its Modulation by the Quasi-Biennial Oscillation. *Journal of Geophysical Research: Atmospheres*, **125**(7): e2020JD032,653. doi.org/10.1029/2020JD032653

Trenberth, K., Jones, P., Ambenje, P., Bojariu, R., Easterling, D., Tank, A. K., Parker, D., Rahimzadeh, F., Renwick, J., Rusticucci, M., Soden, B., and Zhai, P. (**2007**) Observations: Surface and Atmospheric Climate Change. *In* S. Solomon, D. Qin, M. Manning, Z. Chen, M. Marquis, K. Averyt, M. Tignor, and H. Miller (Editors), *Climate Change 2007: The Physical Science Basis. Contribution of Working Group I to the Fourth Assessment Report of the Intergovernmental Panel on Climate Change*. Cambridge University Press

Trenberth, K. and Zhang, R. and National Center for Atmospheric Research

Staff (Editors). (**2021**) The Climate Data Guide: Atlantic Multi-decadal Oscillation (AMO) *[WEBSITE]*. https://climatedataguide.ucar.edu/climate-data/atlantic-multi-decadal-oscillation-amo. Last modified: 05/06/2021. Accessed: 22/04/2022

Trenberth, K. and National Center for Atmospheric Research Staff (Editors). (**2020**) The Climate Data Guide: Nino SST Indices (Nino 1+2, 3, 3.4, 4; ONI and TNI). https://climatedataguide.ucar.edu/climate-data/nino-sst-indices-nino-12-3-34-4-oni-and-tni. Last modified: 21/01/2020. Accessed: 25/04/2022

Trenberth, K. E. (**1997**) The Definition of El Niño. *Bulletin of the American Meteorological Society*, **78**(12): 2771–2778. doi.org/10.1175/1520-0477(1997)078⟨2771:TDOENO⟩2.0.CO;2

Trenberth, K. E. and Shea, D. J. (**2006**) Atlantic hurricanes and natural variability in 2005. *Geophysical Research Letters*, **33**(12): L12,704. doi.org/10.1029/2006GL026894

Tropical Rainfall Measuring Mission (**2011**) TRMM (TMPA) Rainfall Estimate L3 3 hour 0.25 degree × 0.25 degree V7. *Goddard Earth Sciences Data and Information Services Center (GES DISC)*. doi.org/10.5067/TRMM/TMPA/3H/7

Tseng, K.-C., Barnes, E. A., and Maloney, E. (**2020***a*) The Importance of Past MJO Activity in Determining the Future State of the Midlatitude Circulation. *Journal of Climate*, **33**(6): 2131–2147. doi.org/10.1175/JCLI-D-19-0512.1

Tseng, K.-C., Maloney, E., and Barnes, E. A. (**2020***b*) The Consistency of MJO Teleconnection Patterns on Interannual Time Scales. *Journal of Climate*, **33**(9): 3471–3486. doi.org/10.1175/JCLI-D-19-0510.1

Ummenhofer, C. C., Seo, H., Kwon, Y.-O., Parfitt, R., Brands, S., and Joyce, T. M. (**2017**) Emerging European winter precipitation pattern linked to atmospheric circulation changes over the North Atlantic region in recent

decades. *Geophysical Research Letters*, **44**(16): 8557–8566. doi.org/10.1002/2017GL074188

Vallis, G. K. (**2006**) *Atmospheric and Oceanic Fluid Dynamics: Fundamentals and Large-scale Circulation.* Cambridge University Press. doi.org/10.1017/CBO9780511790447

Vautard, R. (**1990**) Multiple Weather Regimes over the North Atlantic: Analysis of Precursors and Successors. *Monthly Weather Review*, **118**(10): 2056–2081. doi.org/10.1175/1520-0493(1990)118⟨2056:MWROTN⟩2.0.CO;2

Virts, K. S. and Wallace, J. M. (**2014**) Observations of Temperature, Wind, Cirrus, and Trace Gases in the Tropical Tropopause Transition Layer during the MJO. *Journal of the Atmospheric Sciences*, **71**(3): 1143–1157. doi.org/10.1175/JAS-D-13-0178.1

Visbeck, M. H., Hurrell, J. W., Polvani, L., and Cullen, H. M. (**2001**) The North Atlantic Oscillation: Past, present, and future. *Proceedings of the National Academy of Sciences*, **98**(23): 12,876–12,877. doi.org/10.1073/pnas.231391598

Vitart, F. (**2017**) Madden–Julian Oscillation prediction and teleconnections in the S2S database. *Quarterly Journal of the Royal Meteorological Society*, **143**(706): 2210–2220. doi.org/10.1002/qj.3079

Voldoire, A. (**2018**) CMIP6 simulations of the CNRM-CERFACS based on CNRM-CM6-1 model for CMIP experiment historical. *Earth System Grid Federation.* doi.org/10.22033/ESGF/CMIP6.4066. Accessed from the Centre for Environmental Data Analysis (CEDA) archive on 9th September 2021

Voldoire, A., Saint-Martin, D., Sénési, S., Decharme, B., Alias, A., Chevallier, M., Colin, J., Guérémy, J.-F., Michou, M., Moine, M.-P., Nabat, P., Roehrig, R., Salas y Mélia, D., Séférian, R., Valcke, S., Beau, I., Belamari, S., Berthet, S., Cassou, C., Cattiaux, J., Deshayes, J., Douville, H., Ethé, C., Franchistéguy, L., Geoffroy, O., Lévy, C., Madec, G., Meurdesoif, Y., Msadek, R., Ribes, A., Sanchez-Gomez, E., Terray, L., and Waldman, R. (**2019**)

Evaluation of CMIP6 DECK Experiments With CNRM-CM6-1. *Journal of Advances in Modeling Earth Systems*, **11**(7): 2177–2213. doi.org/10.1029/2019MS001683

Volodin, E., Mortikov, E., Gritsun, A., Lykossov, V., Galin, V., Diansky, N., Gusev, A., Kostrykin, S., Iakovlev, N., Shestakova, A., and Emelina, S. (**2019***a*) INM INM-CM4-8 model output prepared for CMIP6 CMIP historical. *Earth System Grid Federation*. doi.org/10.22033/ESGF/CMIP6.5069. Accessed from the Centre for Environmental Data Analysis (CEDA) archive on 12th September 2021

Volodin, E., Mortikov, E., Gritsun, A., Lykossov, V., Galin, V., Diansky, N., Gusev, A., Kostrykin, S., Iakovlev, N., Shestakova, A., and Emelina, S. (**2019***b*) INM INM-CM5-0 model output prepared for CMIP6 CMIP historical. *Earth System Grid Federation*. doi.org/10.22033/ESGF/CMIP6.5070. Accessed from the Centre for Environmental Data Analysis (CEDA) archive on 12th September 2021

Volodin, E. M., Mortikov, E. V., Kostrykin, S. V., Galin, V. Y., Lykossov, V. N., Gritsun, A. S., Diansky, N. A., Gusev, A. V., and Iakovlev, N. G. (**2017**) Simulation of the present-day climate with the climate model INMCM5. *Climate Dynamics*, **49**: 3715–3734. doi.org/10.1007/s00382-017-3539-7

Volodin, E. M., Mortikov, E. V., Kostrykin, S. V., Galin, V. Y., Lykossov, V. N., Gritsun, A. S., Diansky, N. A., Gusev, A. V., Iakovlev, N. G., Shestakova, A. A., and Emelina, S. V. (**2018**) Simulation of the modern climate using the INM-CM48 climate model:. *Russian Journal of Numerical Analysis and Mathematical Modelling*, **33**(6): 367–374. doi.org/10.1515/rnam-2018-0032

Waliser, D., Sperber, K., Hendon, H., Kim, D., Maloney, E., Wheeler, M., Weickmann, K., Zhang, C., Donner, L., Gottschalck, J., Higgins, W., Kang, I.-S., Legler, D., Moncrieff, M., Schubert, S., Stern, W., Vitart, F., Wang, B.,

Wang, W., and Woolnough, S. (**2009**) MJO Simulation Diagnostics. *Journal of Climate*, **22**(11): 3006–3030. ISSN 08948755, 15200442. doi.org/10.1175/2008JCLI2731.1

Walker, G. T. (**1923**) Correlation in seasonal variations of weather, VIII. A preliminary study of world weather. *Memoirs of the India Meteorological Department*, **24**(4): 75–131. https://www.rmets.org/sites/default/files/papers/classicindia1.pdf

Walker, G. T. (**1924**) Correlation in seasonal variations of weather, IX. A further study of world weather. *Memoirs of the India Meteorological Department*, **24**(9): 275–333. https://www.rmets.org/sites/default/files/papers/classicindia2.pdf

Walker, G. T. and Bliss, E. W. (**1932**) World Weather V. *Memoirs of the Royal Meteorological Society*, **4**: 53–84. https://www.rmets.org/sites/default/files/ww5.pdf

Wallace, J. M. (**1967**) On the role of mean meridional motions in the biennial wind oscillation. *Quarterly Journal of the Royal Meteorological Society*, **93**(396): 176–185. doi.org/10.1002/qj.49709339604

Wallace, J. M. and Gutzler, D. S. (**1981**) Teleconnections in the Geopotential Height Field during the Northern Hemisphere Winter. *Monthly Weather Review*, **109**(4): 784–812. doi.org/10.1175/1520-0493(1981)109⟨0784:TITGHF⟩2.0.CO;2

Wallace, J. M. and Kousky, V. E. (**1968**) Observational Evidence of Kelvin Waves in the Tropical Stratosphere. *Journal of Atmospheric Sciences*, **25**(5): 900–907. doi.org/10.1175/1520-0469(1968)025⟨0900:OEOKWI⟩2.0.CO;2

Wallace, J. M. and Thompson, D. W. J. (**2002**) The Pacific Center of Action of the Northern Hemisphere Annular Mode: Real or Artifact? *Journal of Climate*, **15**(14): 1987–1991. doi.org/10.1175/1520-0442(2002)015⟨1987:TPCOAO⟩2.0.CO;2

Wang, C., Deser, C., Yu, J.-Y., DiNezio, P., and Clement, A. (**2017**) El Niño

and Southern Oscillation (ENSO): A Review. *In* P. W. Glynn, D. P. Manzello, and I. C. Enochs (Editors), *Coral Reefs of the Eastern Tropical Pacific: Persistence and Loss in a Dynamic Environment*, pages 85–106. Springer Netherlands, Dordrecht. ISBN 978-94-017-7499-4. doi.org/10.1007/978-94-017-7499-4_4

Wang, C., Liu, H., and Lee, S.-K. (**2010**) The record-breaking cold temperatures during the winter of 2009/2010 in the Northern Hemisphere. *Atmospheric Science Letters*, **11**(3): 161–168. doi.org/10.1002/asl.278

Wang, H., Murtugudde, R., and Kumar, A. (**2016**) Evolution of Indian Ocean dipole and its forcing mechanisms in the absence of ENSO. *Climate Dynamics*, **47**(7-8): 2481–2500. doi.org/10.1007/s00382-016-2977-y

Wang, J., Kim, H., and DeFlorio, M. J. (**2022**) Future Changes of PNA-like MJO Teleconnections in CMIP6 Models: Underlying Mechanisms and Uncertainty. *Journal of Climate*, **35**(11): 3459–3478. doi.org/10.1175/JCLI-D-21-0445.1

Wang, J., Kim, H., Kim, D., Henderson, S. A., Stan, C., and Maloney, E. D. (**2020***a*) MJO Teleconnections over the PNA Region in Climate Models. Part I: Performance- and Process-Based Skill Metrics. *Journal of Climate*, **33**(3): 1051–1067. doi.org/10.1175/JCLI-D-19-0253.1

Wang, J., Kim, H., Kim, D., Henderson, S. A., Stan, C., and Maloney, E. D. (**2020***b*) MJO Teleconnections over the PNA Region in Climate Models. Part II: Impacts of the MJO and Basic State. *Journal of Climate*, **33**(12): 5081–5101. doi.org/10.1175/JCLI-D-19-0865.1

Wang, L., Li, T., Chen, L., Behera, S. K., and Nasuno, T. (**2018**) Modulation of the MJO intensity over the equatorial western Pacific by two types of El Niño. *Climate Dynamics*, **51**: 687–700. doi.org/10.1007/s00382-017-3949-6

Wang, X. and Wang, C. (**2014**) Different impacts of various El Niño events on the Indian Ocean Dipole. *Climate Dynamics*, **42**(3-4): 991–1005. doi.org/10.1007/s00382-013-1711-2

Wang, Z., Li, T., and Sun, Y. (**2021**) Interdecadal variability of intensity of the Madden–Julian oscillation. *Atmospheric Science Letters*, **22**(5): e1027. doi.org/10.1002/asl.1027

Waugh, D. W. and Polvani, L. M. (**2010**) Stratospheric polar vortices. *In* L. M. Polvani, A. H. Sobel, and D. W. Waugh (Editors), *The stratosphere: dynamics, transport and chemistry*, volume 190 of *Geophysical monograph series*, pages 43–58. American Geophysical Union. doi.org/10.1029/2009GM000887

Webber, B. G. M., Matthews, A. J., and Heywood, K. J. (**2010**) A dynamical ocean feedback mechanism for the Madden–Julian Oscillation. *Quarterly Journal of the Royal Meteorological Society*, **136**(648): 740–754. doi.org/10.1002/qj.604

Webber, B. G. M., Matthews, A. J., Heywood, K. J., and Stevens, D. P. (**2012**) Ocean Rossby waves as a triggering mechanism for primary Madden–Julian events. *Quarterly Journal of the Royal Meteorological Society*, **138**(663): 514–527. doi.org/10.1002/qj.936

Wei, Y. and Ren, H.-L. (**2019**) Modulation of ENSO on Fast and Slow MJO Modes during Boreal Winter. *Journal of Climate*, **32**(21): 7483–7506. doi.org/10.1175/JCLI-D-19-0013.1

Wei, Y., Ren, H.-L., Duan, W., and Sun, G. (**2023**) Westward-Propagating Disturbances Shape Diverse MJO Propagation. *Geophysical Research Letters*, **50**(17): e2023GL104,778. doi.org/10.1029/2023GL104778

Wheeler, M. C. and Hendon, H. H. (**2004**) An All-Season Real-Time Multivariate MJO Index: Development of an Index for Monitoring and Prediction. *Monthly Weather Review*, **132**(8): 1917–1932. doi.org/10.1175/1520-0493(2004)132⟨1917:AARMMI⟩2.0.CO;2

White, I. P., Garfinkel, C. I., Cohen, J., Jucker, M., and Rao, J. (**2021**) The Impact of Split and Displacement Sudden Stratospheric Warmings on the

Troposphere. *Journal of Geophysical Research: Atmospheres*, **126**(8): e2020JD033,989. doi.org/10.1029/2020JD033989

Wieners, K.-H., Giorgetta, M., Jungclaus, J., Reick, C., Esch, M., Bittner, M., Legutke, S., Schupfner, M., Wachsmann, F., Gayler, V., Haak, H., de Vrese, P., Raddatz, T., Mauritsen, T., von Storch, J.-S., Behrens, J., Brovkin, V., Claussen, M., Crueger, T., Fast, I., Fiedler, S., Hagemann, S., Hohenegger, C., Jahns, T., Kloster, S., Kinne, S., Lasslop, G., Kornblueh, L., Marotzke, J., Matei, D., Meraner, K., Mikolajewicz, U., Modali, K., Müller, W., Nabel, J., Notz, D., Peters-von Gehlen, K., Pincus, R., Pohlmann, H., Pongratz, J., Rast, S., Schmidt, H., Schnur, R., Schulzweida, U., Six, K., Stevens, B., Voigt, A., and Roeckner, E. (**2019**) MPI-M MPI-ESM1.2-LR model output prepared for CMIP6 CMIP historical. *Earth System Grid Federation*. doi.org/10.22033/ESGF/CMIP6.6595. Accessed from the Centre for Environmental Data Analysis (CEDA) archive on 11th September 2021

Williams, K. D., Copsey, D., Blockley, E. W., Bodas-Salcedo, A., Calvert, D., Comer, R., Davis, P., Graham, T., Hewitt, H. T., Hill, R., Hyder, P., Ineson, S., Johns, T. C., Keen, A. B., Lee, R. W., Megann, A., Milton, S. F., Rae, J. G. L., Roberts, M. J., Scaife, A. A., Schiemann, R., Storkey, D., Thorpe, L., Watterson, I. G., Walters, D. N., West, A., Wood, R. A., Woollings, T., and Xavier, P. K. (**2018**) The Met Office Global Coupled Model 3.0 and 3.1 (GC3.0 and GC3.1) Configurations. *Journal of Advances in Modeling Earth Systems*, **10**(2): 357–380. doi.org/10.1002/2017MS001115

Williams, N. C., Scaife, A. A., and Screen, J. A. (**2023**) Underpredicted ENSO Teleconnections in Seasonal Forecasts. *Geophysical Research Letters*, **50**(5): e2022GL101,689. doi.org/10.1029/2022GL101689

Wilson, E. A., Gordon, A. L., and Kim, D. (**2013**) Observations of the Madden Julian Oscillation during Indian Ocean Dipole events. *Journal of Geophysical Research: Atmospheres*, **118**(6): 2588–2599. doi.org/10.1002/jgrd.50241

Woollings, T., Barriopedro, D., Methven, J., Son, S.-W., Martius, O., Harvey,

B., Sillmann, J., Lupo, A. R., and Seneviratne, S. (**2018**) Blocking and its Response to Climate Change. *Current Climate Change Reports*, **4**: 287–300. doi.org/10.1007/s40641-018-0108-z

Woollings, T. and Blackburn, M. (**2012**) The North Atlantic Jet Stream under Climate Change and Its Relation to the NAO and EA Patterns. *Journal of Climate*, **25**(3): 886–902. doi.org/10.1175/JCLI-D-11-00087.1

Woollings, T., Charlton-Perez, A., Ineson, S., Marshall, A. G., and Masato, G. (**2010***a*) Associations between stratospheric variability and tropospheric blocking. *Journal of Geophysical Research: Atmospheres*, **115**(D6). doi.org/10.1029/2009JD012742

Woollings, T., Hannachi, A., and Hoskins, B. (**2010***b*) Variability of the North Atlantic eddy-driven jet stream. *Quarterly Journal of the Royal Meteorological Society*, **136**(649): 856–868. doi.org/10.1002/qj.625

Woollings, T., Hoskins, B., Blackburn, M., and Berrisford, P. (**2008**) A New Rossby Wave–Breaking Interpretation of the North Atlantic Oscillation. *Journal of the Atmospheric Sciences*, **65**(2): 609–626. doi.org/10.1175/2007JAS2347.1

Wright, M., Skinner, D., Bloomfield, H., and Mallinson, H. (**2023**) Meeting Report – RMetS Climate Change Forum 2022: A Vision for 2050 and Implications for Action. *Weather*, **78**: 117–119. doi.org/10.1002/wea.4372

Wu, N., Li, Y., Li, J., Feng, L.-C., and Liu, F. (**2021**) Decadal changes of the intraseasonal oscillation during 1979-–2016. *Advances in Climate Change Research*, **12**(6): 772–782. ISSN 1674-9278. doi.org/10.1016/j.accre.2021.10.001

Wu, S., Liu, Z., Zhang, R., and Delworth, T. L. (**2011**) On the observed relationship between the Pacific Decadal Oscillation and the Atlantic Multi-decadal Oscillation. *Journal of Oceanography*, **67**: 27–35. doi.org/10.1007/s10872-011-0003-x

Wu, T., Zhang, F., Zhang, J., Jie, W., Zhang, Y., Wu, F., Li, L., Yan, J., Liu,

X., Lu, X., Tan, H., Zhang, L., Wang, J., and Hu, A. (**2020**) Beijing Climate Center Earth System Model version 1 (BCC-ESM1): model description and evaluation of aerosol simulations. *Geoscientific Model Development*, **13**(3): 977–1005. doi.org/10.5194/gmd-13-977-2020

Wu, Z. and Reichler, T. (**2020**) Variations in the Frequency of Stratospheric Sudden Warmings in CMIP5 and CMIP6 and Possible Causes. *Journal of Climate*, **33**(23): 10,305–10,320. doi.org/10.1175/JCLI-D-20-0104.1

Xie, P. and Arkin, P. A. (**1997**) Global Precipitation: A 17-Year Monthly Analysis Based on Gauge Observations, Satellite Estimates, and Numerical Model Outputs. *Bulletin of the American Meteorological Society*, **78**(11): 2539–2558. doi.org/10.1175/1520-0477(1997)078⟨2539:GPAYMA⟩2.0.CO;2

Xie, S.-P. and Tanimoto, Y. (**1998**) A pan-Atlantic decadal climate oscillation. *Geophysical Research Letters*, **25**(12): 2185–2188. doi.org/10.1029/98GL01525

Yadav, P. and Straus, D. M. (**2017**) Circulation Response to Fast and Slow MJO Episodes. *Monthly Weather Review*, **145**(5): 1577–1596. doi.org/10.1175/MWR-D-16-0352.1

Yadav, P., Straus, D. M., and Swenson, E. T. (**2019**) The Euro-Atlantic Circulation Response to the Madden-Julian Oscillation Cycle of Tropical Heating: Coupled GCM Intervention Experiments. *Atmosphere-Ocean*, **57**(3): 161–181. doi.org/10.1080/07055900.2019.1626214

Yanai, M. and Maruyama, Y. (**1966**) Stratospheric wave disturbances propagating over the equatorial Pacific. *Journal of the Meteorological Society of Japan. Ser. II*, **44**(5): 291–294. doi.org/10.2151/jmsj1965.44.5_291

Yang, D. and Ingersoll, A. P. (**2013**) Triggered Convection, Gravity Waves, and the MJO: A Shallow-Water Model. *Journal of the Atmospheric Sciences*, **70**(8): 2476–2486. doi.org/10.1175/JAS-D-12-0255.1

Yang, D. and Ingersoll, A. P. (**2014**) A theory of the MJO horizontal scale.

Geophysical Research Letters, **41**(3): 1059–1064. doi.org/10.1002/2013GL058542

Yang, D., Ángel F. Adames, Khouider, B., Wang, B., and Zhang, C. (**2020**) A Review of Contemporary MJO Theories. *In* C.-P. Chang, K.-J. Ha, R. H. Johnson, D. Kim, G. N. C. Lau, and B. Wang (Editors), *The Multiscale Global Monsoon System*, chapter Chapter 19, pages 233–247. World Scientific. doi.org/10.1142/9789811216602_0019

Yang, G.-Y., Hoskins, B. J., and Slingo, J. M. (**2011**) Equatorial Waves in Opposite QBO Phases. *Journal of the Atmospheric Sciences*, **68**(4): 839–862. doi.org/10.1175/2010JAS3514.1

Yano, J.-I. and Tribbia, J. J. (**2017**) Tropical Atmospheric Madden–Julian Oscillation: A Strongly Nonlinear Free Solitary Rossby Wave? *Journal of the Atmospheric Sciences*, **74**(10): 3473–3489. doi.org/10.1175/JAS-D-16-0319.1

Yessimbet, K., Shepherd, T. G., Ossó, A. C., and Steiner, A. K. (**2022**) Pathways of Influence Between Northern Hemisphere Blocking and Stratospheric Polar Vortex Variability. *Geophysical Research Letters*, **49**(23): e2022GL100,895. doi.org/10.1029/2022GL100895

Yoo, C. and Son, S.-W. (**2016**) Modulation of the boreal wintertime Madden-Julian oscillation by the stratospheric quasi-biennial oscillation. *Geophysical Research Letters*, **43**(3): 1392–1398. doi.org/10.1002/2016GL067762

Yu, J. Y. and Lau, K. (**2005**) Contrasting Indian Ocean SST variability with and without ENSO influence: A coupled atmosphere-ocean GCM study. *Meteorology and Atmospheric Physics*, **90**(3-4): 179–191. doi.org/10.1007/s00703-004-0094-7

Yu, J.-Y. and Neelin, J. D. (**1994**) Modes of Tropical Variability under Convective Adjustment and the Madden–Julian Oscillation. Part II: Numerical Results. *Journal of Atmospheric Sciences*, **51**(13): 1895–1914. doi.org/10.1175/1520-0469(1994)051⟨1895:MOTVUC⟩2.0.CO;2

Yukimoto, S., Kawai, H., Koshiro, T., Oshima, N., Yoshida, K., Urakawa, S., Tsujino, H., Deushi, M., Tanaka, T., Hosaka, M., Yabu, S., Yoshimura, H., Shindo, E., Mizuta, R., Obata, A., Adachi, Y., and Ishii, M. (**2019***a*) The Meteorological Research Institute Earth System Model Version 2.0, MRI-ESM2.0: Description and Basic Evaluation of the Physical Component. *Journal of the Meteorological Society of Japan*, (2). doi.org/10.2151/jmsj.2019-051

Yukimoto, S., Koshiro, T., Kawai, H., Oshima, N., Yoshida, K., Urakawa, S., Tsujino, H., Deushi, M., Tanaka, T., Hosaka, M., Yoshimura, H., Shindo, E., Mizuta, R., Ishii, M., Obata, A., and Adachi, Y. (**2019***b*) MRI MRI-ESM2.0 model output prepared for CMIP6 CMIP historical. *Earth System Grid Federation*. doi.org/10.22033/ESGF/CMIP6.6842. Accessed from the Centre for Environmental Data Analysis (CEDA) archive on 11th September 2021

Zanardo, S., Nicotina, L., Hilberts, A. G. J., and Jewson, S. P. (**2019**) Modulation of Economic Losses From European Floods by the North Atlantic Oscillation. *Geophysical Research Letters*, **46**(5): 2563–2572. doi.org/10.1029/2019GL081956

Zhang, C. (**2005**) Madden–Julian Oscillation. *Reviews of Geophysics*, **43**(2). doi.org/10.1029/2004RG000158

Zhang, C., Adames, A. F., Khouider, B., Wang, B., and Yang, D. (**2020**) Four Theories of the Madden–Julian Oscillation. *Reviews of Geophysics*, **58**(3): e2019RG000,685. doi.org/10.1029/2019RG000685

Zhang, C. and Zhang, B. (**2018**) QBO-MJO Connection. *Journal of Geophysical Research: Atmospheres*, **123**(6): 2957–2967. doi.org/10.1002/2017JD028171

Zhang, J., Wu, T., Shi, X., Zhang, F., Li, J., Chu, M., Liu, Q., Yan, J., Ma, Q., and Wei, M. (**2018**) BCC BCC-ESM1 model output prepared for CMIP6 CMIP historical. *Earth System Grid Federation*. doi.org/10.22033/ESGF/CMIP6.2949. Accessed from the Centre for Environmental Data Analysis (CEDA) archive on 13th September 2021

Zhang, R. and Delworth, T. L. (**2007**) Impact of the Atlantic Multidecadal Oscillation on North Pacific climate variability. *Geophysical Research Letters*, **34**(23). doi.org/10.1029/2007GL031601

Zhao, C., Geng, X., and Qi, L. (**2022**) Atlantic Multidecadal Oscillation Modulates the Relation of ENSO With the Precipitation in the Central-Western Indian Ocean. *Frontiers in Earth Science*, **10**. ISSN 2296–6463. doi.org/10.3389/feart.2022.866241

Zhao, S., Li, J., and Li, Y. (**2015**) Dynamics of an Interhemispheric Teleconnection across the Critical Latitude through a Southerly Duct during Boreal Winter. *Journal of Climate*, **28**(19): 7437–7456. doi.org/10.1175/JCLI-D-14-00425.1

Zheng, C. and Chang, E. K. M. (**2019**) The Role of MJO Propagation, Lifetime, and Intensity on Modulating the Temporal Evolution of the MJO Extratropical Response. *Journal of Geophysical Research: Atmospheres*, **124**(10): 5352–5378. doi.org/10.1029/2019JD030258

Zheng, C. and Chang, E. K.-M. (**2020**) The Role of Extratropical Background Flow in Modulating the MJO Extratropical Response. *Journal of Climate*, **33**(11): 4513–4536. doi.org/10.1175/JCLI-D-19-0708.1

Zhou, L. and Murtugudde, R. (**2020**) Oceanic Impacts on MJOs Detouring near the Maritime Continent. *Journal of Climate*, **33**(6): 2371–2388. doi.org/10.1175/JCLI-D-19-0505.1

Zhou, S., L'Heureux, M., Weaver, S., and Kumar, A. (**2012**) A composite study of the MJO influence on the surface air temperature and precipitation over the Continental United States. *Climate Dynamics*, **38**(7-8): 1459–1471. doi.org/10.1007/s00382-011-1001-9

Zhou, S. and Miller, A. J. (**2005**) The Interaction of the Madden–Julian Oscillation and the Arctic Oscillation. *Journal of Climate*, **18**(1): 143–159. doi.org/10.1175/JCLI3251.1

Zhou, W., Yang, D., Xie, S.-P., and Ma, J. (**2020**) Amplified Madden–Julian

oscillation impacts in the Pacific–North America region. *Nature Climate Change*, **10**: 654–660. doi.org/10.1038/s41558-020-0814-0

Zhou, Y., Wang, S., Fang, J., and Yang, D. (**2023**) The Maritime Continent Barrier Effect on the MJO Teleconnections during the Boreal Winter Seasons in the Northern Hemisphere. *Journal of Climate*, **36**(1): 171–192. doi.org/10.1175/JCLI-D-21-0492.1